Characterising Land Cover Changes in the Niger Delta Caused by Oil Production

By

Abdullahi Ahmed Kuta

(B. Tech. Surv. & Geoinformatics, MSc GIS)

A thesis submitted to the University of Nottingham for the degree of Doctor of Philosophy in Engineering Surveying and Space Geodesy

Under the supervision of

Dr Stephen Grebby

Prof Doreen Sandra Boyd

Nottingham Geospatial Institute, Department of Civil Engineering,

Faculty of Engineering, University of Nottingham

September 2023

Abstract

In recent decades, oil extraction activities have particularly affected land cover in the Niger Delta region, subsequently increasing or reducing the extent of certain land cover types. Where complete change has not occurred, the quality of the land cover may have still been affected and degraded. However, the extent to which oil activities have affected the landscape is not fully understood. This thesis presents an integrated multiscale land cover change characterisation using geospatial analyses to determine the impact of oil extraction activities on the land cover. Firstly, a spatiotemporal hotspot analysis of oil spills from 2007- 2019 and oil facilities shows that the area around Omuko-Ahoada in the north-eastern and around Ijaw-South in the southern part of the study area are the most impacted by the oil extraction activities. Secondly, from analysis of the impact of soil hydrocarbon parameters (SHP) on the health of different types of vegetation at the leaf scale from field spectrometer data, the mangrove is the most impacted by total petroleum hydrocarbon (TPH) and soil toxicity by showing a decrease in chlorophyll content and low spectral reflectance. At the same time, the mango shows the most tolerance to TPH, while oil palm is the most tolerant to toxicity (EC50). Thirdly, from the analysis of the impact of the oil spill volume and time gap after the occurrence of oil spills on the health of dense, sparse and mangrove vegetation even many years after the occurrence of spills by way of normalised difference vegetation index (NDVI) show that the dense vegetation is only impacted at volumes 1000 barrels and sparse vegetation between 400 and 1000 barrels. However, the mangrove vegetation is not impacted at any volume. Additionally, the impact of oil spills was more visible within 90 days of the spill for sparse and mangrove vegetation than for dense vegetation, which can withstand the oil spill due to its size. Also, the result shows that the health condition of vegetation on spill sites is impacted by oil spills when compared with those on none spill sites for all vegetation types. Finally, land cover change detection at the landscape scale was performed using a Bayesian classifier from 1987-2016 and NDVI map. The results show that the oil extraction activities have affected the land cover, especially the vegetation, with many conversions from vegetation to non-vegetation and degradation occurring near oil extraction activities. The results from this thesis could help address the environmental problems in the Niger Delta, such as land pollution, degradation and land cover change, by prioritising programs such as oil spill cleans up or remediation and the restoration of the vegetation using some plants that have shown some resistance to the impact oil spills to ensure the sustainability of the natural environment in the Niger Delta.

Dedication

This work is dedicated to God the Father, God the Son and God the Holy Spirit.

Acknowledgement

I would like to acknowledge my supervisors Dr Stephen Grebby, who has been supportive from the beginning of my PhD, and Professor Doreen Boyd for her support during this PhD. They gave me constructive feedback, criticisms, insight, support, and courage. I am also grateful to Professor Sturt Mash, my internal examiner, for his contributions. My gratitude also goes to the National Oil Spill Detection and Response Agency (NOSDRA) for making the oil spill data available online and the USGS for providing free Landsat image data for the study.

I would also like to appreciate Dr Bolaji Bernard Babatunde of the Department of Animal and Environmental Biology, Faculty of Applied Science Nwipie, Goodluck Nakaima Nwipie of the Department of Fisheries and Science, Faculty of Agriculture, University of Port Harcourt, Nigeria, for contacting the people and the communities during my field data collection and for the soil sample collection. Additionally, I would like to thank Dr Salamatu Kassah, Dr Gbenga Ajayi, and Dr Sa'ad Ibrahim. My thanks to Dr Abimbola M. Ayeni for being a "good" neighbour and taking the time to read through my thesis. Additionally, I thank the entire staff of the Department of Surveying & Geoinformatics, Federal University of Technology, Minna, for their support. Thanks to Dr. Yusuf D. Opaluwa and Surv. Hassan Samaila A. Ija of the Department of Surveying and Geoinformatics, Federal University Technology, Minna, Niger State, Nigeria, and Prof Lazarus M Ojigi, Director of Mission Planning and Satellite Data Management, National Space Research and Development Agency, Abuja, Nigeria, for their contribution towards my academic journey. Time and space will not permit me to mention others who contributed to this success in one way or another. I say thanks for your support, prayers, and encouragement to my mother-in-law, Mrs Adama Gozie Wakaso and the entire Wakaso family.

I respectfully acknowledge the Petroleum Technology Development Fund (PTDF), Nigeria, for sponsoring me for this PhD; without their support, I might not have been able to come for this programme. My colleagues at Nottingham Geospatial Institute, Jubilee Campus, University of Nottingham, you made my PhD enjoyable.

Additionally, to Pastor Vincent and Pastor Ann Ibikunle and the entire RCCG CRA Nottingham for your prayer and fellowship, and my parents, Mr and Mrs Ahmed Waziri Kuta, for their concern, love and prayers.

Finally, I am grateful to Semiratu Abdullahi and my “girls”, Shelomith and Shemariah, for their patience and understanding during my PhD. I appreciate your support, encouragement, love and care.

List of Abbreviations.

AG	Awolowo grass
AH	Appeared hotspot
AHNS	Annual-Monthly highest number of spills
ALNS	Annual-monthly lowest number of spills
AMT	Annual monthly total
AN	Annual spill
ASD	Analytical spectral devices
CAH	Combined annual hotspot
CH	Consistent hotspot
CS	Corrosion of oil pipeline,
DAS	Days after a spill
DH	Disappeared hotspot and
DSS	Dense vegetation spill sites,
DV	Dense vegetation
DV	Dense vegetation
EF	Equipment failures
EG	Elephant grass
ETM+	Enhanced Thematic Mapper Plus and
HD	High density
HVIs	Hyperspectral vegetation indices
LD	Low density
MD	Medium density
MG	Mangrove
MS	Monthly spills
MSS	Mangrove Vegetation Spill Sites
MT	Mango tree
MV	Mangrove vegetation
NDVI	Normalised difference vegetation index
NOSDRA	National Oil Spill Detection and Response Agency
OLI	Operational Land Imager
OP	Oil palm tree
REP	Red edge position
SHP	Soil hydrocarbon property
SP	Soil properties

SSS	sparse vegetation spill sites
ST	Sabotage.
SV	Spare Vegetation
SV	Sparse vegetation
TH	Total hotspot
TIRS	Thermal Infrared Sensor
TM	Thematic Mapper
TOC	Total organic carbon
TPH	Total petroleum hydrocarbons
VLD	Very low density

List of Conferences Attended

AfricaGIS 2019 Innovations in Geospatial Technologies for Achieving Sustainable Development Goals in Africa, Kigali, Rwanda, 18 - 22 November 2019, Kigali Conference an Exhibition Village (KCEV).

National Association of Surveying and Geoinformatics Lecturers

1ST AGM/Conference Maiden Edition, 4th-7th February 2019, Federal University of Technology, Minna, Niger State, Nigeria.

UK National Earth Observation Conference, 7 -8th September 2018, University of Birmingham.

Wavelength Conference by RSPSoc, 12th -14th 2018, University of Sheffield.

Remote Sensing & Photogrammetry Society (RSPSoc) conference, 5th -8th 2017, Imperial College London.

Table of Contents

List of Figures

List of Tables

Chapter 1 Introduction

1.1 Background

Land cover is a physical characteristic of the Earth's surface, such as the distribution of vegetation, water, soil and other physical and manmade features. Comprehensive and precise knowledge of land cover is crucial for many scientific and operational applications (Inglada et al., 2017). Over the years, human activities and some natural processes have led to land cover changes. Land cover change (LCC) is the conversion of different land-cover types (Liping et al., 2018), which results from complex human-environmental interactions with high interdependencies on social-ecological systems, making it difficult to identify the main drivers (Kleemann et al., 2017). Land cover change detection identifies differences in the state of land cover types at different points in time (Ridd & Liu, 1998). Land cover change information is important in global environmental change research (Chen et al., 2003). Inventories and monitoring of land-use/land-cover changes are essential for further understanding the change mechanisms and modelling the impact of change on the environment and associated ecosystems at different scales (Chen et al., 2003; Turner et al., 1995). The main manifestations of land cover change involve the complete conversion or more subtle modification of land cover or subtle alterations (Joshi et al., 2016).

The Niger Delta has undergone a land cover change in the form of both conversion and degradation. Historically, the quantity and degradation (specifically vegetation) of land cover change have not been well documented. However, it is well-known that one of the major causes of land cover change in the Niger Delta is oil extraction activities: oil spills onto the land and water and gas flares into the air. Ultimately, the responsibility lies with the multinational oil and gas companies, whose activities lead to oil spills from their facilities, e.g. from oil pipelines, due to negligence and ageing pipelines or sabotage. Oil spill affects the water and vegetation, causing land cover changes, especially to the health of vegetation. For more than four decades, oil exploration and production activities have left a severely degraded environment in the Niger Delta region (Okoye & Okunrobo, 2014). Several studies have revealed apparent environmental contamination on land, groundwater, surface water and sediments, with severe impacts on vegetation, air quality and public health (Agbonifo, 2016). This has led to farming and fishing becoming impossible or extremely difficult in oil-affected areas. Drinking water has become scarce, and about 90% of water is not safe because of contamination (Okoye & Okunrobo, 2014).

Despite the threat of land cover change in the Niger Delta, there has not been much effort to comprehensively characterise the land cover changes that have occurred due to oil extraction activities, especially using a geospatial approach, remote sensing and spatial analysis. Most published studies focus on geology, geochemistry and environmental toxicology, while studies employing Earth observation (EO) satellite data to assess Niger Delta dynamics are scarce (Kuenzer et al., 2014). Nonetheless, the data available from satellite remote sensing missions can immensely aid efforts to accurately determine land cover/use and quantify changes in land cover/use management (Joshi et al., 2016), such as urban planning, and to prevent further destruction of land cover by introducing policies to help mitigate land cover changes, especially the destruction of natural environments.

In a predominantly mangrove vegetation ecosystem such as the Niger Delta, there is a need for techniques that will afford the mapping of such land cover types over large geographical areas and with high temporal frequency. Traditional remote sensing classification methods have failed to map mangrove-dominated species due to relatively coarse spatial data resolution and spectral confusion with other land cover types (Heumann, 2011). Generally, image classification methods are grouped as per-pixel (hard) and sub-pixel (soft) classification (Lu & Weng, 2007). The hard image classification methods classify the remotely sensed data into a single map where each pixel belongs to a single land cover class. In contrast, the soft classification methods simultaneously categorize each pixel into several classes (Lu & Weng, 2007). While a mixed pixel cannot be appropriately represented by hard classification, the soft classification can overcome the problem of mixed pixel to some extent by indicating the class composition (Ling et al., 2016).

Mapping fringe mangroves using remote sensing data remains a challenge due to the spectral similarity of mangroves and associated species, lack of clear zonation between species, and mixed pixel effects, especially when vegetation is sparse or degraded (Heumann, 2011). Innovative remote sensing techniques, such as soft spectral classifiers and geographic object-based image analysis, can offer a more effective approach for mapping land cover and utilising ancillary environmental data for vegetative land cover classifications (Gudex-Cross et al., 2017).

Understanding the relationship between the spatiotemporal dynamics of LULCC scenarios will assist planners/decision-makers in formulating sustainable urban development and environmental protection plans and will remain a scientific asset for

future generations (Rimal et al., 2017). Advances in geographic information systems (GIS) have significantly improved the spatial representation and analysis of all kinds of information and data (Mohamadi et al., 2015). Change detection methods using satellite imagery and the analytical functions of distance and size in the GIS environment can help to monitor and map land cover change (Mirkatouli et al., 2015; Rawat & Kumar, 2015), as well as to understand spatial and temporal land cover change dynamics (Gyawali et al., 2004).

The effect of oil extraction activities in the Niger Delta region is no longer contestable; what remains contestable is the amount of change that has taken place across space and time due to oil extraction activities, which this research aims to address.

1.2 Problem statement

In recent decades, the oil industry has undoubtedly contributed significantly to land cover change in the Niger Delta, due to the impact of oil extraction activities. However, the extent and severity of land cover change due to oil extraction activities remains unclear. The Niger Delta is characterised by contaminated streams, rivers, forest destruction and loss of biodiversity, leading to ecological wasteland due to oil pollution from oil spills, gas flares, effluent and waste discharges for over four decades (Agbonifo, 2016; Kadafa, 2012a; Twumasi & Merem, 2006). The greatest problem is that the soils absorb oil like sponges and re-release them every rainy season. Therefore, oil is taken up by the roots of plants, making mangrove forests particularly vulnerable to oil spills (Pyagbara, 2007). One of the major problems facing the Niger Delta region is a lack of adequate forest and vegetation monitoring capacity (Ochege et al., 2017). The lack of spatiotemporal data on the evolution of oil spill hotspots and oil extraction activities and their relationship with land cover changes in the Niger Delta, especially vegetation, means that there is a limited understanding of the effect of oil extraction activities on land cover change. Although several studies have examined various problems of environmental degradation in the Niger Delta, there is still a need for improved understanding, monitoring, and management of the ecosystems because there are limited in-depth studies that employ geospatial technology to better understand land-use changes in the Niger Delta (Ohimain, 2007)

1.3 Research gap

The land cover, especially the vegetation in the Niger Delta, has been affected by oil extraction activities in the form of destruction or degradation due to the construction of oil facilities and oil spills. However, a comprehensive multiscale-level land cover characterisation of the change, and the impact of oil extraction activities on the land cover, especially the vegetation in the Niger Delta, has not been carried out. Understanding the spatial and temporal pattern of oil extraction facilities and oil spill is important in characterising their impact on the land cover changes. Previous work on oil spill-related spatial statistics in the Niger Delta is limited.

Firstly, no study has attempted to conduct an annual spatiotemporal analysis of oil spills to show the hotspot trends over time and oil facilities hotspots and integrate them with land cover change data. For example, Obida et al. (2017) and Obida et al. (2018) Identified human and environmental exposure to hotspots of oil spills along the oil pipeline networks, and Whanda et al. (2016) assessed the geographical distribution of oil-spill clusters. Also, Rowland (2010) analysed hotspots and cold spots of oil spill clusters to explain incident patterns related to third-party interference via oil pipeline vandalism.

Secondly, in the Niger Delta, to the best of my knowledge from the available literature, there has not been a study on the impact of soil hydrocarbon parameters on different types of plant species at the leaf scale using hyperspectral remote sensing to capture subtle changes in the health of vegetation that cannot be captured from the satellite.

Thirdly, the impact of oil spills on different vegetation types at plot scale using satellite images has not been carried out. The first study that assessed the impact of oil spills on vegetation at plot scale was conducted by Adamu (2016); Adamu et al. (2015, 2016, 2018) and focused only on the mangrove vegetation.

Fourthly, concerning the use of remote sensing to map and detect a land cover change in the Niger Delta, previous land cover mapping and change detection employed pixel-based, hard classification techniques (Eyoh & Okwuashi (2016)**;** Nababa et al. (2020), which are unsuitable because of the nature and complexity of the study area.

Combining object-based analysis and soft classification could help overcome pixel and object-based land cover classification limitations in areas such as the Niger Delta. Integrating land cover change data with oil extraction activities data (e.g., oil spill

hotspots) to characterise their impact on the land cover using a multi-scale approach will produce results for a better understanding of the interaction between land cover changes and oil extraction activities in the Niger Delta.

1.4 Aim and Objectives.

1.4.1 Aim.

This research aims to comprehensively characterise the impact of oil extraction activities on the land cover change in the Niger Delta at different scales using multispectral and hyperspectral remote sensing data. This study analysed the spatiotemporal oil spill hotspot and oil facilities hotspot, the relationships between oil extraction activities/facilities and the observed land cover changes in quality (degradation) and quantity (conversions from one land cover type to another) by integrating oil spill and facilities data with land cover change information derived from remote sensing data. To achieve the aim of this research, the following research questions and objectives were identified. The objectives are also shown in Figure 1.1

Research questions 1:

- Where are the oil facilities located in the Niger Delta?
- Where and how frequently have oil spills occurred over the past 13 years?

Objective 1: To map and examine the spatiotemporal evolution of oil spill hotspots, oil facilities hotspots and the spatial distributions of oil facilities in the Niger Delta using spatial statistics.

Research question 2:

- What are the responses of plant types to various concentrations of soil hydrocarbon properties?

Objective 2: To determine the impact of soil hydrocarbon parameters (SHP) on the health of plant types at the leaf scale using hyperspectral vegetation indices (HVIs) in the Niger Delta.

Research question 3:

- What are the effects of oil on the health of different types of vegetation and plants?

Objective 3: To determine the effect of oil spills on vegetation health at the plot scale using satellite imagery.

Research question 4:

- What are the observed general patterns of land cover changes, and what land cover types are more affected by extraction activities in the Niger Delta?
- At what scale (i.e., leaf, plot, and landscape) are these effects manifested?

Objective 4: To map land cover changes at the landscape scale and the effect of oil extraction activities on the observed changes using the best performing land cover mapping classifier.

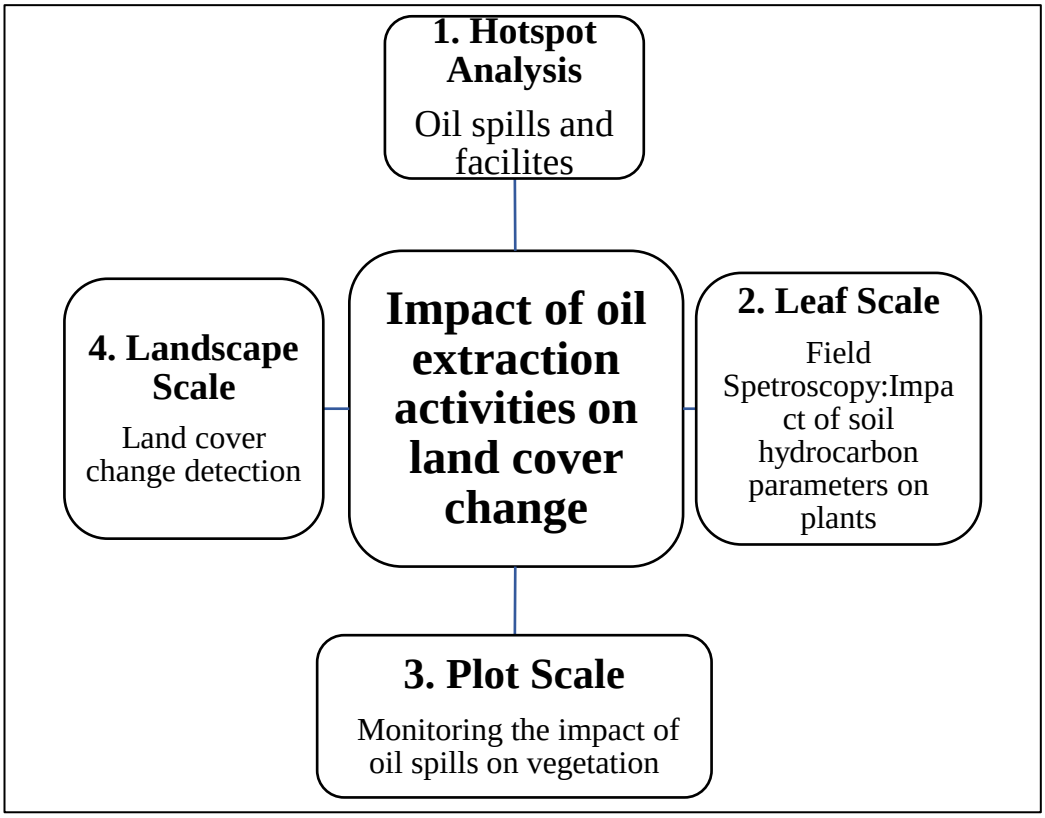

Figure 1.1: Structure of the thesis: multiscale characterisations of the impact of oil extraction activities on the land cover in the Niger Delta.

1.5 Thesis structure

This thesis consists of 8 chapters, including an introduction, literature review, general methodology, analysis associated with each of the four objectives, and a discussion and conclusion.

Chapter 1 provides a background for the study of land cover change mapping. The introduction highlights the importance of mapping land cover change to assess the impact of oil extraction activities in the Niger Delta. The chapter also discusses the problem this research attempts to solve by revealing the true extent and severity of the land cover change due to oil production and exploration, which is currently unclear. The knowledge gaps, aim and objectives, and research questions have also been presented in this chapter.

Chapter 2 provides a review of the existing literature associated with the study area, land cover change, the physiographical overview of the Niger Delta, oil extraction activities both present and past. It also review the previous studies looking at land cover change associated with the oil industry, the methodology for spatial analysis of oil spills and land cover change monitoring, and mapping using earth observation. This chapter also reviews optical and hyperspectral data for monitoring vegetation health.

Chapter 3 provides an overview of the general methodology employed in this thesis. The first part describes the study area and data sources used for the analysis. The general approach to spatiotemporal hotspot analysis, field spectroscopy, soil hydrocarbon analysis, and land cover change detections are also presented.

Chapter 4 analyses the spatiotemporal evolution of oil spills and oil facilities hotspots in the Niger Delta region using spatial statistics from 2007-2019. The hotspot results were used with land cover change information to determine the impact of oil extraction activities on land cover changes.

Chapter 5 seeks to determine the effect of soil hydrocarbon properties on vegetation at the leaf scale using the data obtained from field spectrometer. This chapter discussed the methods for field data collection (soil and leaf samples from different plant species) in the Niger Delta to extract hydrocarbons and other soil parameters and corresponding spectral measurements from the leaf samples using an ASD FieldSpec Pro instrument. The spectral characteristics of the leaves were correlated with the soil hydrocarbon analysis to investigate the effect of soil hydrocarbon properties on the health of plants.

Chapter 6 focuses on monitoring the impact of oil spills on vegetation at the plot scale using the satellite-derived normalised difference vegetation index (NDVI). The effect of oil spill volume and time gap after spills on different types of vegetation, temporal analysis of the impact of oil spills on vegetation condition by observing changes in NDVI before the spill and many years after spills and comparing them with their corresponding control site (non-spill) sites were determined to help in understanding the effect of time on vegetation health recovery.

Chapter 7 reveals the land cover changes in the Niger Delta from 1987-2016. Land cover mapping was performed using six different classifiers, and the most accurate classifier was used as the basis for land cover change detection. The degradation of vegetation was analysed based on the NDVI. Oil extraction data were overlaid to determine the impact of oil activities on the land cover changes.

Chapter 8 discusses the key findings of each objective covered in chapters 4 to 7. Some overall conclusions are derived, and recommendations for for future studies are proposed.

Chapter 2 Literature Review

2.1 Introduction.

This chapter provides a general literature review describing an overview of the Niger Delta's geography and geology, land use/land cover, oil extraction activities, and the related impact on land cover. It also provides a review of the current methodologies for land cover change mapping, monitoring and spatial statistics.

2.2 Physiographical overview of the Niger Delta

The Niger Delta is the largest river delta on the African continent and the most densely populated river delta globally and has the third-largest mangrove forest in the world. It is a major biodiversity hotspot of our planet (Kuenzer, van Beijma, Gessner, & Dech, 2014). The River Niger drains a large part of West Africa. It discharges its waters, sediments, and other loads, including exotic species, into the Niger Delta and its extensions into the Atlantic Ocean, resulting in a complex and fragile delta with rich biodiversity (Abam, 2001). The delta's surface is separated by a dense network of rivers and creeks, which creates a condition of delta-wide hydrological continuity (Abam, 2001). Historically and cartographically, the Niger Delta consists of present-day Bayelsa, Delta, and Rivers States. The Niger Delta, as officially defined by the Nigerian government in 2000, extends over approximately 70,000 km^2 and makes up 7.5% of Nigeria's land mass and includes Abia, Akwa-Ibom, Cross River, Edo, Imo and Ondo states, with 185 Local Government Council Areas making a total of nine coastal southern Nigerian states (Asanebi, 2016).

2.2.1 Geography of Niger Delta.

The Niger Delta area lies within the wet equatorial climate; high cloud cover and fewer sunshine hours cause damp weather conditions throughout most parts of the year (Shittu, 2014). The Niger Delta consists of the most extensive freshwater swamp, coastal ridges, fertile-dry land forest, immeasurable creeks and streams, and tropical rainforest characterised by great biological diversity providing habitat for an abundance of fish and marine wildlife. Over thousands of years, seasonal flooding and sediment deposits have made the land fertile. It is located in the central part of southern Nigeria between latitudes 5°33'49"N and 6°'31'38"E in the north. Its western boundary is given as Benin 5° 44'11"N and 5°03'49"E, and its eastern boundary is Imo River 4°27'16" N and 7°35'27"E. The Niger Delta is located along the Atlantic coast, which forms the southern boundary of

Nigeria, as shown in Figure 2.1. It is the entrance of the Niger and Benue Rivers into the ocean through a network of rivers, creeks, and estuaries (Alagoa, 2005).

Figure 2.1: Map of Niger showing the location of Niger Delta states.

A semi-hot, humid equatorial climate characterises the Niger Delta with wide variations from one part of the region. The temperature is uniformly high throughout the year, with high relative humidity and intense rainfall occurring virtually year-round in the core delta but becoming more seasonal further inland with an increase in distance from the ocean. Mean yearly rainfall ranges from over 4,000 mm in the coastal towns of Bonny and Brass in Rivers and Bayelsa States, respectively, and decreases inland to 3,000 mm in the mid-delta around Ahoada, Yenagoa, and Warri in Rivers, Bayelsa and Delta States, respectively (The historical Niger Delta), and slightly less than 2,400 mm in the northern parts of the region, such as Imo and Abia States. The annual rainfall ranges from 1,500 to 2,000 mm in the north-western portions of the Niger Delta, including Edo and Ondo

states (NDRDMP, 2006). The average monthly temperature for the warmest months (February to April) ranges from 28–33 °C, while the average monthly temperature for the coolest months (June to September) ranges from 21–23 °C (UNDP, 2006).

2.2.2 Geology and petroleum of Niger Delta

The Nigerian coastal geology is sedimentary and is dominated by the geology of the arcuate Niger Delta (Egberongbe, Nwilo, & Badejo, 2006). The large amount of sediment carried by the river system over the centuries has resulted in a vast, relatively flat basin (Abam, 1999a). The river Niger forms a complex network of channels that drain into the Gulf of Guinea characterised by rain-fed deltaic vegetation. The area is formed of both fluvial and marine sediments built-up over the past 50 million years since the upper Cretaceous period (Adamu et al., 2016). The natural delta of the Niger River is a vast sedimentary basin with deltaic deposits comprised mainly of medium to coarse unconsolidated sands, silt, clay, shale and peat (UNDP, 2006).

The Niger Delta is among the most abundant petroleum basins in the world, with about 25 billion barrels of oil and 256 trillion cubic feet of natural gas deposits. The three lithostratic units in the Niger Delta were developed from Akata Formation, Agbada Formation and Benin Formation (Deng et al.,2008). Petroleum in the Niger Delta is produced from sandstone and unconsolidated sands predominantly in the Agbada Formation (Tuttle et al., 1999). The Hydrocarbons have been in good-quality sandstone reservoirs, with the larger accumulations occurring in roll-over anticlines in the hanging walls of growth faults (Doust, 1990). Three petroleum systems are present in the Niger Delta and delta frame: Lower Cretaceous (lacustrine), Upper Cretaceous-lower Paleocene (marine), and Tertiary (deltaic)(Haack et al., 2000).

The Crude oil from the Niger Delta basin comes in two types: light (Bonny light crude oil) and comparatively heavy. The lighter has around 36 gravity while the heavier has 20–25 gravity. Bonny light is a highly demanded high-quality crude oil produced in the Niger Delta due to its low sulfur content.

2.2.3 The population and ethnic groups in the Niger Delta

The Niger Delta has a very dense population of approximately 31 million, projected to be approximately 45 million people by 2020. A dominant feature of the structure of the population of the Niger Delta region is its significant level of young people, with over 62% of the population below the age of 30 years, while the age group 30-69 years makeup

only 36% and those aged 70 years and above just 2% (NDRDMP, 2006). The high populations are concentrated in the two major urban cities of Port Harcourt and Warri, which is attributed to the rapid growth in the oil and gas industries (Abam, 2001). The dominant ethnic group in the traditional Niger Delta is the Ijaw, while the Isoko, Itsekiri, Kwale, and Urhobo are located in the Western Delta. In the eastern Niger Delta, the main ethnic groups include the Ekpeye, Andoni, Ikwerre, Ndoni and Ogoni (Akujuru, 2014). However, with the inclusion of other states in 2000, the ethnic groups have increased to include groups such as Igbos, Yorubas, and Benis, making approximately 40 different ethnic groups speaking 250 languages and dialects ("Niger Delta Region: Land and People," n.d.). Table 2.1 shows the population of the nine states that make up the Niger Delta.

Table 2.1: Projected population of the Niger Delta. Source: GTZ projections (2004) based on national population commission data.

State	2005	2010	2015	2020
Abia	3,230,000	3,763,000	4,383,000	5,106,000
Akwa Ibom	3,343,000	3,895,000	4,537,000	5,285,000
Bayelsa	1,710,000	1,992,000	2,320,000	2,703,000
Cross River	2,736,000	3,187,000	3,712,000	4,325,000
Delta	3,594,000	4,186,000	4,877,000	5,681,000
Edo	3,018,000	3,516,000	4,096,000	4,871,000
Imo	3,342,000	3,894,000	4,535,000	5,283,000
Ondo	3,025,000	3524,000	4,105,000	4,782,000
River	4,858,000	5,659,000	6,592,000	7,679,000
Total	28,856,000	33,616,000	39,157,000	45,715,000

2.2.4 Land use/land cover and ecology

Land cover is the physical characteristic of the Earth's surface, such as the distribution of vegetation, water, soil and other physical and manmade features, e.g., settlements and tarred roads. At the same time, land use is the way humans use the land and its habitat, usually for economic activities (Ramachandra & Kumar, 2004). The major land cover types in the region are vegetation, predominantly forest type with 8600 km^2 of swamp forest and approximately 1900 km^2 of mangrove forests (Alagoa, 2005). Others are water bodies and built-up areas in the core Niger Delta. The major land-use types in the Niger Delta could be grouped into two categories: traditional and modern. The traditional economic activities of the Niger Delta communities can also be categorised as land-based type on the drier parts of the northern end of the Delta, which includes farming, fishing,

collecting and processing of palm fruits and hunting, and water-based type of economy at the southern parts of the Niger Delta, including fishing, gathering of seafood, and trading, with a less diversified economy. The Niger Delta region produces a variety of cash crops and food crops. The economically important crops are palm fruits from which palm oil and palm kernels are derived, rubber, cocoa, groundnuts and pineapples. The modern land use is largely associated with oil and gas extraction (e.g., pipelines, refineries, transportation).

A variety of vegetation characterises the ecology of the Niger Delta (Ayanlade & Howard, 2017). The Niger Delta ecology and diversity of estuarine and coastal communities are very understudied and poorly understood (Akani, Luiselli, & Politano, 1999; Igu, 2016; Luiselli, Amori, Akani, & Eniang, 2015; Zabbey & Malaquias, 2013). The larger part of West Africa, which has been draining and discharging its water and sediment into the Niger Delta, and its extension into the Atlantic Ocean over the years, has given rise to the formation of a complex and fragile delta with rich biodiversity. This has subsequently resulted in the development of dry flat land ecological zones, dry land with abundant swamp zones and freshwater swamps. Other ecological zones are mangrove swamps, beach ridges, and bars (Abam, 1999b). However, Ogon (2003) stated that the above statement was in relation to the pre-crude oil Niger Delta because today's Niger Delta Wetland is well-known more for the large deposit of crude oil and gas and little of its endowed natural resources, which are being devastated. The five main ecological zones with a summary of their characteristics are shown in Table 2.2, while Figure 2.3 shows the area of ecological zones by states in the Niger Delta. Oil and gas activities have led to the reduction and fragmentation of habitats and conversion of biodiversity-rich and productive ecosystems to one form of development, and pollution constitutes a major threat to eco-sustainability and biodiversity in the Niger Delta (Zabbey & Malaquias, 2013). The impact of joint oil multinational and government operations on the environment and ecology are laregely associated with three main aspects of oil production; namely, gas flaring, oil spillage and pipeline networks (Takon, 2014). The shrinking of the floodplain has gradually engineered a change in the soil moisture conditions, with a corresponding change in plant speciation. Several of the fish-spawning areas within the freshwater swamps have been lost due to low flood levels. Varieties of wildlife species intolerant of ecological change in the Niger Delta are bound to suffer stress and eventually extinction. For instance, ecologists have reported the disappearance

of some species of fish, birds and other wildlife downstream of dammed rivers (Crisp, 1985; Abam, 1999).

Table 2.2: Ecological zones in the Niger Delta. Source:(NDRDMP, 2006)

Ecological Zone	**Characteristic**
Mangrove Forest and Coastal Vegetation.	A chain of low sandy barrier islands protects the coast of the Niger Delta, between Benin and Imo estuaries, less than a meter above high-tide level. The dominant vegetation is freshwater swamp forest with occasional small salt marshes,where seawater washes over beaches. As the poorly drained and sandy soils are not conducive for farming, there is little direct conversion of forest to agricultural land.
Fresh Water Swamp Forest.	The Swamp forests, which are subject to the silt-laden 'white water' of the Niger floods, have a very high fishery and agricultural potential. Within this white water sector, there are two broad zones: (a) the Upper Delta or Flood Forest zone and (b) the Swampy Tidal Freshwater zone. The 'Upper Delta' or 'Flood Forest' zone (Aboh to Bomadi and Oporoma)has large sandy river channels, high flood levels, and numerous floodplain lakes.
Lowland Rainforest Zone.	This zone occupies the non-riverine or 'upland' areas, which flank the delta. The natural rainforest of the area has been largely cleared for agriculture, and the dominant vegetation types are now farmed bush, a mosaic of cropped and fallow areas, usually with many oil palms, and plantations, mainly oil palm and rubber. Open farmed areas lead to the entry of invasive grassland or 'savannah' species. Some forest species can survive in the old fallow land but most have disappeared due to shorter fallow periods attributable to the demands of an increasing population.
Derived Savannah Zone.	This is found in the northern parts of the Niger Delta Region.The vegetation type in this zone appears as regrowth after the original rainforest has been cleared for agriculture. It comprises of Savannah type grasses and shrub, with a few scattered trees. Due to constant human pressure, it is virtually impossible for trees to grow to maturity.
The Montane Zone.	The zone is confined to the north eastern part of Cross River State around Obudu/Sankwala area. The high altitude location of the zone – approximately 900 to 1500 m above sea level means that species diversity is not as great as in the other tropical high forest although floristic diversity is enhanced by the presence of many species of herbs and shrubs.

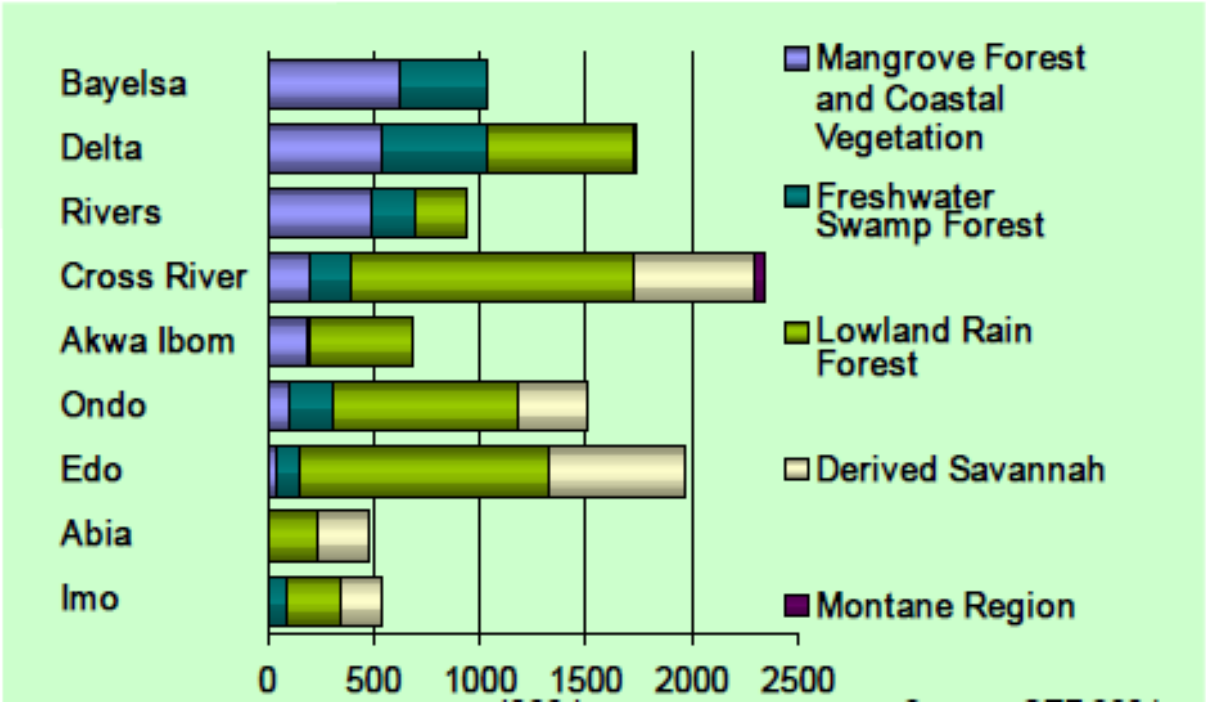

Figure 2.2: Areas of ecological zones (in Hectares) by states in the Niger Delta region (NDRDMP, 2006).

2.3 Oil exploration activities in the Niger Delta region: past and present

Petroleum exploration and production in the Niger Delta region and the export of oil and gas resources have greatly improved the economy of Nigeria over the past five decades (Ite, Ibok, Ite, & Petters, 2013). The discovery of commercially viable oil resources in Nigeria was a long, drawn-out process, much to the disappointment of early oil ventures. The Nigerian environment proved to be the most challenging obstacle, requiring more advanced technology than the petroleum industry possessed at the time (Steyn, 2009). Oil and gas exploration activities started in Nigeria when German surveyors for the Nigerian Bitumen Corporation began exploration in the Araromi area of western Nigeria in 1908 (Anejionu et al., 2015; Ite, Ibok, Ite, & Petters, 2013)**,** which ended shortly with the start of World War I in 1914 and later resumed in 1938 when Shell D'Arcy, a consortium of Iranian Oil Company (later British Petroleum and Royal Dutch Shell) was granted an exclusive concessionary right over the whole of Nigeria (Ite et al., 2013). The first commercial oil discovery dates back to 1956 when Shell British Petroleum (now Shell plc) discovered crude oil at Oloibiri, a village in Bayelsa state situated within the Niger Delta of Nigeria (Abbas, 2012; Egwu, 2012; Okoye & Okunrobo, 2014)**.** By 1958,

Shell/D'Arcy had discovered oil in twelve areas, of which Oloibiri, Afam and Bomu were the most promising. Oil production started at Oloibiri in early 1958 at 3,000 barrels per day (Steyn, 2009). The first shipment of Nigerian crude oil exports (8,500 tons of crude oil) arrived at Rotterdam on 8 March 1958 (Steyn, 2009). The daily output of crude oil increased to 12,000 barrels per day by the end of 1959 and 900,000 barrels per day from the late 1960s to the early 1970s (Shittu, 2014) but it did not play a significant role in the Nigerian economy (Ugochukwu & Ertel, 2008).

Oil and natural gas exploration has increased significantly in recent years in Nigeria due to increased demand and technological improvements that allow access to geologic strata once considered impractical to pursue petroleum from (Unger et al., 2015). By the late 1970s to 1980s, Nigeria reached a production level of over 2 million barrels per day, but the year 2004 saw significant improvement as production reached a record level of 2.5 million barrels per day (Shittu, 2014). By 2006, Nigeria became the largest oil producer in Africa and the sixth-largest globally, averaging 2.7 million barrels per day (bbl/d) (Egberongbe et al., 2006). This has led to oil companies requiring land for oil wells, flow stations, oil and gas pipelines and a flurry of oil and gas-related developments, which has led to several spillages, bulldozing of farmlands and economic trees to create rights of way and exploitation of oil wells (Odudu, 2017).

2.3.1 Oil spills in the Niger Delta

Oil spills – the uncontrolled release of crude oil into the environment can have considerable economic, human and environmental consequences (Rim-rukeh, 2015). Oil spillage resulting from oil extraction activities has been a global problem since the discovery of crude oil (Kadafa, 2012b). Oil-related activities and their impact on the environment remain a quarrelsome issue that has affected the bond between oil communities, oil companies and governments, especially in developing countries, and less so in advanced economies with oil resources and vibrant civil societies (Takon, 2014)**.** Globally, oil spills are the price that must be paid whenever oil exploration activities occur. Rim-rukeh (2015) stated that *"oil spill therefore, is an inevitable consequence of the ever-increasing demand for exploration, production, transportation, and use of oil*". In the Niger Delta, 77% of oil spills into the environment between 1976 and 1996 were not recovered from the environment they were spilt into (Abbas, 2012).

2.3.2 Causes of oil spills and attacks on oil facilities

The causes and circumstances of oil spills are many and vary from one region to another. The main causes of oil spills in the Niger Delta are equipment failure, operational errors, or wilful damage to oil facilities (Okoye & Okunrobo, 2014; Rim-rukeh, 2015). The driving force behind attacks on oil facilities and pipelines in the Niger Delta are socio-economic and political deprivation (Shittu, 2014), shallow pipeline laying, insecurity and corruption, and bad governance across the communities (Chika & Ndidi, 2022). The reason for the attack on oil facilities in the Niger Delta is grouped into two: economic gain (bunkers) and agitation (vandals). The bunkers illegally obtain oil from pipelines with collaborations with security agents and oil workers to siphon crude oil directly from pipelines that supply the various refineries. While the agitators, saboteurs and vandals of oil facilities use explosives and break pipelines that supply oil to various companies and refineries to show their grievances towards the government and multinational oil companies (Umar et al., 2021). In most cases, the vandals have the blessing and support of the communities, making it difficult for them to be arrested by security personnel.

In recent times, the issue of oil spills in the Niger Delta was aggravated due to militants' activities in early 2006. A substantial amount of crude oil pipeline vandalism in the Niger Delta was carried out by the militant groups with the excuse of fighting for better environmental management and development of the region (Umar & Hajj Othman, 2017). The activities of the militants, which include blowing up/shutting down oil installations and facilities, setting off car bombs, and illegal oil bunkering (estimated at between 80,000 and 300 000 bbl/day) valued at six billion US dollars, is caused by years of political and economic marginalization, environmental degradation, bad governance and policy inconsistency by the government and the divide-and-rule policy of the oil companies in the region (Nwogwugwu et al, 2012). For instance, nearly 14,000 tons of crude oil flowed into the creeks of the Niger Delta from the Royal Dutch Shell plc oil facilities in 2009 due to the activities of oil thieves and militants, which was more than double the amount spilt into the delta in 2008 and quadruple what was spilt in 2007 (Press, 2010).

To address the militancy issues in the region, the late President Umaru Yar'Adua offered an unconditional pardon and cash (amnesty) on 6 August 2009 to militants willing to lay down their arms. However, at the beginning of 2016, militants in the Niger Delta region once again declared war on the Federal Government of Nigeria and international oil

companies (IOCs) to press home their demands by resuming attacks on oil pipelines, bringing oil production to its lowest rate in more than two decades with nine attacks a month on average (Amevor, 2016). However, due to a series of dialogues and consultations with stakeholders, the activities of the militants were reduced to a minimum. However, large-scale illegal oil bunkering in the region through breaking pipelines both offshore and onshore to steal oil to either refine them locally or sell them on the black market has been on the increase unabated. The oil typically spills into the environment, affecting the land cover. However, oil pipelines are not blown using an explosive, recently. The illegal oil refinery activity started with oil bunkering and vandalism in 2003 but later transformed into stealing and selling crude oil and illegal oil refinery activities in 2012 after the militants were offered amnesty (Olujobi, Olarinde, & Yebisi, 2022). The issue of pipeline vandals has become worrisome to the Federal government of Nigeria. According to Mr Kyari, the Nigeria National Petroleum Company Limited (NNPCL) chief, "*the pipeline taps are so sophisticated that they ran for 3-4 kilometres and would have involved cranes, industrial equipment and at least 40 workers with 295 illegal connections in one line of less than 200 kilometres*" (Yusuf, 2022). By September 2022, the large-scale attacks on oil pipelines have caused Nigeria to lose 95% of its oil output to criminals at the oil hub Bonny. Only 3000 out of 239,000 barrels injected into the pipeline from the Bonny Terminal oil hub, a key export point for Nigeria, was recovered, while the remainder was lost to criminals.

2.3.3 Effect of oil extraction activities on land cover

Crude oil has had a profound impact on world civilization compared to any other single natural resource in the history of humankind and has become a very significant constituent in defining the politics, rhetoric and diplomacy of the nation (Pyagbara, 2007)**,** affecting the lives and destinies of many people and countries around the world both negatively and positively. The oil and gas industry is global, with operations conducted in every part of the world, from Alaska to Australia, from Peru to China, and in every habitat, including desert, tropical rainforest, temperate woodland, mangrove, etc. (E&P Forum/UNEP, 1997). Exploration, drilling, extraction, transportation and refining of oil always leads to clearing of vegetation, waste discharge, accidental spills and operational failures combined with sabotage, pipeline bunkering and illegal refining, contributing to serious environmental pollution (Langeveld & Delany, 2014), which may be regional or global in scale (Kharaka & Dorsey, 2005). Some ecological side effects of oil extraction are

damaged land, fire accidents, incidents of air and water pollution, contamination of local streams/rivers, farmlands, forest resources and biodiversity in oil-producing areas (E&P Forum/UNEP, 1997; Whanda, Adekola, Adamu, Yahaya, & Pandey, 2016). The increase in oil and gas activities in the Niger Delta has led to the conversion of land cover, such as forest or agricultural land, to oil and gas wells (Unger et al., 2015).

The way communities in the Niger Delta interacted with their environment in pre-oil exploration greatly enhanced the natural resource base. The environment is more of a heritage than something to be conquered for the people (Ogon, 2003)**.** With an extensive network of more than 900 oil wells, 100 flow stations and gas plants, over 1,500 km of trunk lines and some 45,000 km of oil and gas flow lines, the Niger Delta has become synonymous with oil pollution, recording an average number of 221 oil spills per year (Ugochukwu & Ertel, 2008).

The Niger Delta is now characterised by contaminated streams and rivers (i.e., sources of water for domestic uses), forest destruction and biodiversity loss and has become an ecological wasteland due to oil pollution for over four decades (Agbonifo, 2016; Kadafa, 2012a; Twumasi & Merem, 2006). The fact that soils absorb oil like sponges and re-release it every rainy season and it is therefore taken up by the roots of plants makes mangrove forests particularly vulnerable to oil spills (Pyagbara, 2007). Pyagbara (2007) also stated that oil prevents the lenticels of mangroves from absorbing oxygen; hence, oxygen starvation results in withering and the death of large numbers of mangroves, lowers soil fertility and causes poor growth of other plants. A total area of dead mangrove forests has been estimated at 25,000, 80,000 and 190,000 hectares, for the Low, Probable and High Damage scenarios, respectively (Langeveld & Delany, 2014). The impact of oil exploration and extraction on land cover can be devastating, and it is not always easy to completely clean up oil that is spilt into the environment. Figure 2.3 is the typical Niger Delta oil spills sites showing some dead mangroves due to oil spills and residual oil spills along/in water and on land along the oil pipeline.

Additionally, between 1970 and 2004, Nigeria flared an average of 76% of the total gas produced at approximately 70 million/m^3 per day (Akpoborie & Akporhonor, 2008), equivalent to 40% of African natural gas consumption. The flared gas generates tremendous heat, thereby causing thermal pollution and increasing the temperature by 40°C at an average distance of 43.8 m from flare sites, having negative effects on vegetation growth, animal life and ecological equilibrium in the Niger Delta area

(Alakpodia, 1989; Akpoborie & Akporhonor, 2008). Aside from oil exploration/exploitation activities, other causes of land cover change include clearing forests and mangroves for farming, lumbering, road construction, and industrial development.

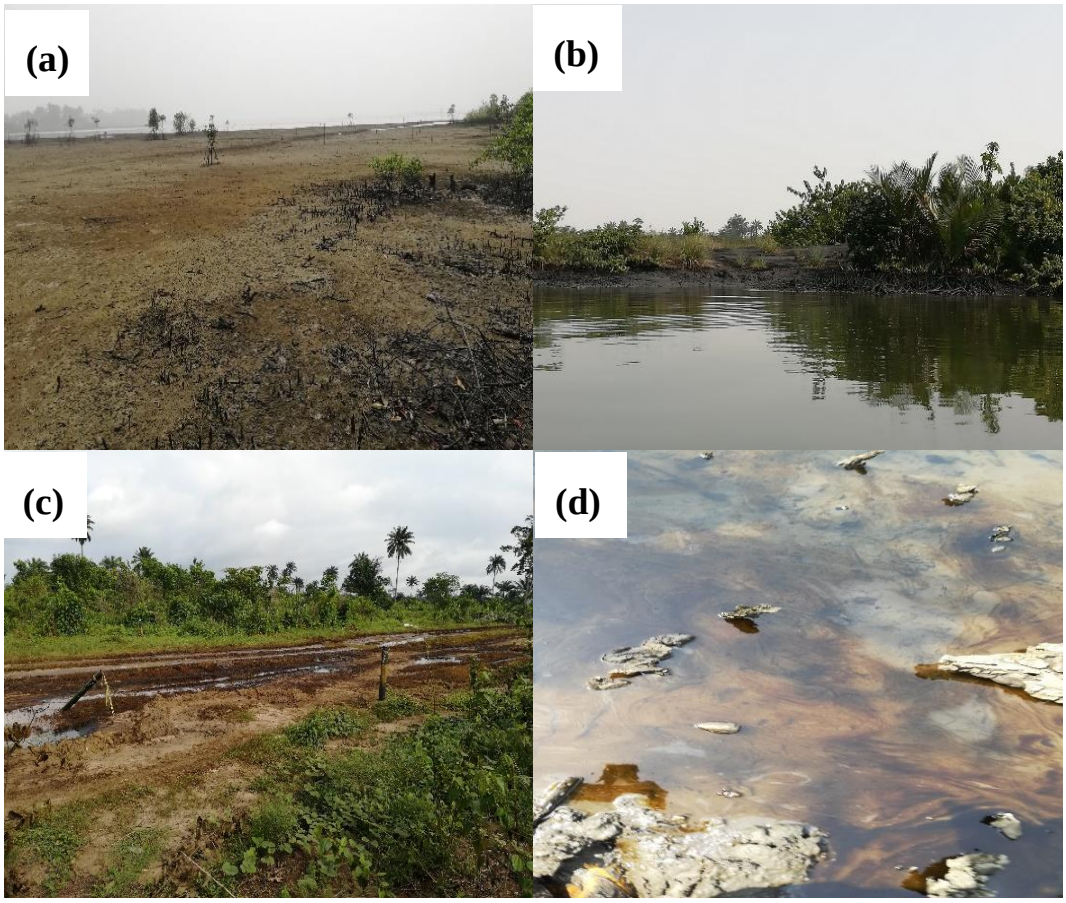

Figure 2.3: (a) Dead mangrove due to the oil spill, (b) residual oil along the water, (c) oil spill on land along the oil pipeline and (d) oil spill on water observed during field work.

2.4 Land cover change associated with the oil industry in the Niger Delta

The Niger Delta region has become a hotspot for numerous researchers investigating various issues relating to oil exploration from different perspectives, such as social economy, environmental and engineering aspects. Many have attempted to study the impact of oil on land cover changes using both geospatial and non-geospatial techniques. One of the major problems facing the whole Niger Delta region is inadequate forest and vegetation monitoring capacity (Ochege, George, Dike, & Okpala-Okaka, 2017). Although several studies have examined the problems of environmental degradation in the Niger Delta, there is still a need for improved understanding, monitoring, and

management of the ecosystems because there are only a few in-depth studies that employ geospatial technology to understand land-use changes in coastal ecosystems in the Niger Delta (Ohimain, 2007).

Abbas (2012) used remote sensing and GIS to detect land use/land cover changes using Landsat TM satellite imagery for 1986 and 2008 to generate the magnitude, trend, and annual rate of change from the classified land cover map and then used the annual rate of change as the basis for the projection of land cover change through to 2050. Kuenzer et al. (2014) detected and analysed land cover changes in the Niger Delta caused by socio-economic factors and oil exploration and discovered serious impacts on the ecological system in the Niger Delta from 1986 to 2013 using remote sensing. Ochege et al. (2017) also used remote sensing and GIS – specifically, the NDVI and the maximum likelihood classifier (MLC) supervised methods – to detect significant transformations of forests due to the impacts of oil and gas exploration and production in the Sagbama oil field environment in the Niger Delta region. Omo-Irabor & Oduyemi (2007) combined unsupervised and supervised image classification for detecting land cover classes in the Niger Delta using Landsat TM and ETM+ images from 1987 - 2002 and detected the depletion of forests and mangroves by 9.21 % and 0.82 % respectively which they attributed to logging and the creation of land for farming and oil activities. Another study by Eyoh & Okwuashi (2016) examined the spatial and temporal dynamics of land use/land cover in the Niger Delta region from 1986-2016 using remote sensing and GIS techniques with Landsat TM 1986, ETM+ 2002 and OLI Landsat 8 2016 images to evaluate the LULC spatial distribution/magnitude, change trend, gains and losses, net change, and rate of change of each LULC class.

A study carried out by Adamu, Tansey, & Ogutu (2016) used remote sensing to determine how the length of the time gap between the oil spill and image acquisition date influences the detectability of impacts of oil spill on vegetation; the number of days between oil spill events and image acquisition date on normalised difference vegetation index (NDVI) and normalised difference water index (NDWI). The result based on regression analysis shows that an increase in the volume of oil spills resulted in increased deterioration of vegetation conditions in the study site, and the longer the time between the date of image acquisition and the oil spill event, the lower the detectability of the impacts of oil spills on vegetation conditions. Another study by Adamu et al. (2015) investigated the potential for using broadband multispectral vegetation indices to detect the impacts of oil pollution

on vegetation conditions by exploring and evaluating twenty broadband multispectral vegetation indices computed using the visible, near-infrared and shortwave infrared wavelengths of Landsat TM and ETM. The results show that five spectral indices, namely normalised difference vegetation index (NDVI), soil-adjusted vegetation index (SAVI), adjusted resistant vegetation index (ARVI2), green near-infrared (G/NIR) and green shortwave infrared (G/SWIR) were consistently sensitive to the effects of oil pollution on vegetation and could be used to map and monitor oil pollution in vegetated areas.

There have been several geospatial-based land studies focused on the Niger Delta and studies assessing the impact of oil on the environment (Akpoborie & Akporhonor, 2008; Akujuru, 2014; Kadafa, 2012a; Ogon, 2003; Sam, Coulon, & Prpich, 2017; Zabbey, Sam, & Onyebuchi, 2017). In addition, several other studies discuss hydrology, flooding and sea-level rise (Dim, 2017; Ite et al., 2013; Musa, Popescu, & Mynett, 2016a, 2016b; Obi, 2014).

From the literature reviewed, no studies currently focus on mapping land cover changes in the Niger Delta region by providing maps showing where the changes have occurred. This is important as it can reveal the locations of changes that policymakers could then use to take action in solving specific environmental problems. The Niger Delta land cover consists of mangroves, freshwater swamps, and a mixture of water with oil, which gives rise to a mixed pixel that cannot be appropriately represented using hard classification techniques. Additionally, the classification techniques might not be appropriate for quantifying the land cover charges and showing the intensity or severity of changes in the study area since land cover changes are unlikely to occur spatially at the same magnitude.

2.5 Hotspot analysis.

Many researchers have been concerned about environmental pollution and have carried out wide-ranging research on environmental pollution incidents (Ding et al., 2015). The primary goal of oil spill risk appraisals and impact assessments is to characterise and quantitatively estimate the amount of potential harm that a spill may cause for a particular location (Nelson & Grubesic, 2017). GIS techniques have been used for oil spill response planning because they support the integration and preparation of geospatial information on the location, nature and sensitivities of different resources with rapid access (Giziakis et al., 2013). Hotspot mapping is used to help identify where pollution exists and its source (Lin et al., 2011). Hotspots are concentrations of incidents within a limited

geographical space that appear over time (Levine, 2007). Spatial-temporal hotspot pattern analysis of environmental pollution incidents provides a vital source of information for the further development of incident prevention measures (Ding et al., 2015). The method to use for hotspot analysis depends on the type of data (i.e. point, line and polygon) and the objectives of the study. The hotspot analysis detection methods can be grouped into three categories: spatial analysis, interpolation and spatial autocorrelation, as shown in Figure 2.4.

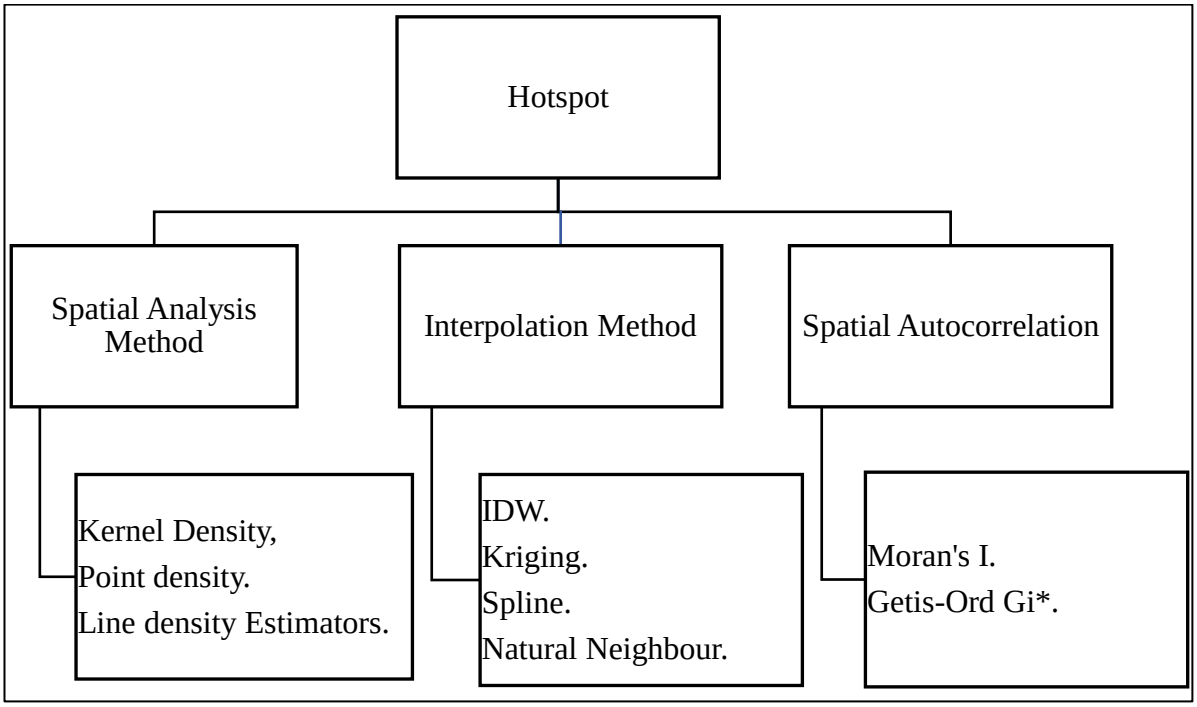

Figure 2.4: Hotspot analysis methods.

2.5.1 Spatial analysis method

Many spatial analysis techniques are used to identify hotspots (Chainey, 2013). The three spatial analysis methods are Kernel Density Estimation (KDE), Point Density Estimator (PDE) and Line Density Estimator (LDE). Spatial Analysis with KDE, PDE, and LDE techniques process checks the locations, attributes, and connection of features in spatial data among overlay and other analytical techniques, which is used for acquiring knowledge that can be used in a different aspect (Amiri, Imaninasab, & Nadimi, 2018). KDE is specifically useful in detecting hotspots due to the series of estimations made over a grid placed over the entire point pattern, with each estimation showing the intensity at a certain location (Kalinic, 2018). Kernel density estimation (KDE) aggregates data points within a user-specified search radius and represents the density of points by creating a continuous surface area (Park et al., 2016). The PDE spatial model generates

new raster data, recreates each cell based on the characteristics of the closest neighbouring cells, and depicts density levels in more detail (Amiri et al., 2018). The LD calculates a magnitude-per-unit area from polyline features that fall within a radius around each cell.

2.5.2 Interpolation methods

Spatial interpolation is the procedure of estimating the values of the variable under study at un-sampled locations using point observations within the same region (Deligiorgi & Philippopoulos, 2011). Spatial interpolation is based on Tobler's first law of geography: the closer the point of space is to another, the more likely it is to have similar features, and the farther away the point is, the less likely it is to have similar features (Jia, Zheng, & Miao, 2018). Among interpolation methods are inverse distance weighting (IDW), kriging, spline, and natural neighbour. The IDW method substantially assumes that the rate of correlations and similarities between neighbours is proportional to the distance between them, which can be defined as a distance reverse function of every point from neighbouring points (Setianto & Triandini, 2015). The IDW is considered simple to use (Paramasivam & Venkatramanan, 2019). Kriging estimates an unobserved location of variable value based on the weighted average of adjacent observed sites within a given area (Setianto & Triandini, 2015). Kriging is a multistep process that starts with the exploratory statistical analysis of the data, variogram modelling, creation of the surface, and (optionally) exploration of a variance surface (Paramasivam & Venkatramanan, 2019). The spline estimates the values of unknown points using a mathematical function that minimises the overall surface curvature, resulting in a smooth surface that passes exactly through known input points, thus minimising the total curvature of the surface (Amiri et al., 2018). The natural neighbour interpolation scheme is based on Voronoi tessellation and is a local interpolant, where the estimated function is a linear, appropriately weighted average of the nearby data points (Deligiorgi & Philippopoulos, 2011).

2.5.3 Spatial autocorrelation methods

Spatial autocorrelation techniques test how the distributions of point occurrences are related to each other. Positive spatial autocorrelation is where occurrences are clustered or close occurrences have similar values to those farther apart (Dana & Cooper, 1964). The two hotspots (spatial autocorrelation) methods are Moran's I and Getis-Ord G. The Moran's I and Getis-Ord G are global measurements of the overall pattern of spatial

autocorrelation displayed by numerical data and test the hypotheses that similar values tend to cluster together, be randomly distributed, or be dispersed more evenly across an area than would be expected by chance. Similarly, the local versions of Moran's I and Getis-Ord G statistics: Ansellin local Morans I and Getis-Ord Gi* provide statistical evidence for the presence of clusters that differ from expected values at specific locations (Mueller-Warrant et al., 2008). For point data that are aggregate counts (representing the number of incidents within a certain geographic area, e.g., census blocks), the spatial autocorrelation technique is an appropriate method to test for clustering (Dana & Cooper, 1964). The difference between the spatial autocorrelation method and other methods of hotspot mapping is that the spatial autocorrelation method identifies statistically significant hotspots.

2.6 Remote sensing

Remote sensing (RS), also called Earth observation, refers to obtaining information about objects or areas on the Earth's surface without physical contact with the object or area (Dyring, 1973). The use of earth observation satellites for mapping and monitoring land cover occurred when the first Landsat satellite was launched in July 1972. The Landsat satellite provides data crucial to improving our knowledge of the Earth's land, ocean, atmosphere, ice and snow (Jong et al., 2006). Since the first launch of the earth observation satellite, remote sensing has been increasingly used to acquire information about environmental processes such as agricultural crops, land cover, vegetation dynamics, water quality, urban growth, seabed topography etc. (Jong et al., 2007). Remote sensing techniques effectively monitor, and measure land-cover change over large spatial and temporal extents. They may provide practitioners with insights into future land-use change processes (Bailey et al., 2016). Remote sensing uses different parts of the electromagnetic spectrum to record the characteristics of features (Mirkatouli et al., 2015).

2.6.1 Remote sensing platforms

Remote sensing platforms are broadly grouped into three: Ground (Terrestrial), aerial (manned and unmanned) and space-based (Satellite). Land cover and land-use data were mainly acquired from terrestrial remote sensing from ground-based platforms. However, new sensor developments have given rise to various platforms that can be used to capture remote sensing data. Although Earth-orbiting satellites and fixed-wing aircraft are the

most common, helicopters, balloons, masts, and booms are also used (Barnsley, 1999), including unmanned aerial vehicles (UAV).

Ground observation platforms include – handheld platforms, cherry pickers, towers, portable masts, vehicles etc. Portable handheld photographic cameras and spectroradiometers are mostly used in laboratory and field experiments as reference data and ground truth verification (Yanow, 2018). Ground-based platforms (hand-held or mounted on a tripod) are also used for sensor calibration, quality control and the development of new sensors (Ahmad et al., 2019). Ground-based platforms are good for more detailed studies of a specific object, such as species level. Many researchers have used ground-based remote sensing. For instance, Prudente et al. (2021) estimated the biophysical parameters of soybeans using NDVI GS (GreenSeeker 505 handheld active sensor) and NDVI FS (FieldSpec4 model Standard-Res passive sensor) different terrestrial remote sensing. Also, Kato et al. (2013) estimated leaf area index (LAI) of mixed forest stands in Christchurch, New Zealand using a portable terrestrial laser scanner (TLS).

Aerial photography has a long history of use in urban geography and has remained useful today (Longley, 2002). It provides a detailed picture of the Earth's surface over a relatively small area using an aeroplane and, recently, UAV fitted with cameras of different types (e.g. active and passive sensors, multi and hyperspectral etc.). Aerial photography provides the highest spatial resolution and textural of land cover objects than satellite remote sensing. Aerial photography is still used for large-scale mappings, such as in route surveys, town planning, construction project surveying, cadastral mapping etc. (Dyring, 1973). The flying height could be determined and adjusted, and the type of sensors chosen based on the project requirement, making them versatile. Different sensors could be fitted on the same aeroplane by changing them after use, unlike the satellite system that carries onboard a sensor which cannot be changed after a single mission. In theory, aerial photos can be readily acquired at any time. However, there are limitations, such as financial support and whether a licence from the national aviation authorities is required. Also, flight planning (especially using an aeroplane) could be laborious and can be affected by weather and the availability of an airstrip and does not cover a large area like the satellite image. Thus, their availability can also be limited, especially for land cover monitoring, since spatiotemporal information about a particular scene is required

(Varga et al., 2010). Arial photographs have been used in many applications: monitoring of vegetation health (Terzioğlu et al., 2009), survey and mapping (Everitt, Yang, & Davis, 2010); generation of topographic information (Ajayi et al., 2018; Ajayi et al., 2017), and much more.

Various satellites carrying remote sensing sensors were launched into space orbit in the early 1960s to observe and monitor the Earth and its environment. Images from sensors mounted on the satellites are generally called satellite images. Modern remote sensing systems provide satellite images suitable for medium-scale mapping used in natural resources surveys and monitoring such as forestry, geology, watershed management etc. (Dyring, 1973). Satellites provide a relatively low-cost larger view of the earth's surface, which makes them an efficient method for large-scale mappings such as desertification and land cover classification (Jafarbiglu & Pourreza, 2022). For a place like the Niger Delta, satellite images are better. Historical images are available at no cost for extracting land cover information and monitoring vegetation health. Remote sensing sensors are divided into two categories based on signal sources: active and passive. Passive sensors detect natural radiation emitted or reflected by the object or the surrounding area being observed (e.g. reflected sunlight, film photography, infrared, radiometers). Their major disadvantage is that they are affected by cloud cover and cannot capture images at night unless the amount of energy emitted or reflected from the object being recorded is large enough. Passive sensors (optical satellite systems) include Landsat, SPOT, EROS, GeoEye, and World View. From the two categories of sensors based on signal sources, currently, there are three systems of sensors on the satellite platform. The Lidar, multispectral and hyperspectral sensors. The lidar has already been discussed in section 2.6.1, while the multispectral and hyperspectral sensors will be discussed in the next sections.

2.6.2 Remote sensing systems on satellite platform

2.6.2.1 Lidar remote sensing

On the other hand, active sensors emit their own energy to scan objects and areas. A sensor then detects and measures the radiation reflected or backscattered from the target (Adamu, 2016). Active sensors include Radio Detection and Ranging (RADAR) and Light Detection and Ranging (LIDAR). The choice of the dataset is a function of many

factors, including the project's requirement, data availability, and the study area's size. Both active and passive sensors have been used for land cover mapping or detecting the impact of oil spills on vegetation. For example, Ahmad & Idris (2022) used Synthetic-Aperture Radar (SAR) images from dual-polarized Sentinel-1 and Multi-Spectral Instrument (MSI) from Sentinel-2 to study the impact of oil spills on mangrove forest in Pantai Cermin, Negeri Sembilan. Similarly, Unger et al. (2015) quantified land cover change caused by petroleum exploration and production in the Haynesville shale region using Landsat Thematic Mapper (TM) imagery. Generally, land-cover and land-use monitoring frequently use passive sensors (Turner et al., 2003) due to the availability of temporal data, especially from the Landsat archive.

2.6.2.2 Multispectral remote sensing

Remote sensing has evolved from traditional aerial photography to multispectral scanners in the past half-century (Mutanga et al., 2016). Even though aerial photographs remain significant today, multispectral scanners have gained popularity due to their wider coverage, higher frequency and low cost, leading to a recent interest in assessing the potential of satellite imagery in urban mapping (Longley, 2002)**,** especially for land cover/mapping at regional, continental and global scales. Satellite imagery has been widely used in various applications, including classifying land use, monitoring crop and forest harvests, tracking beach erosion, and determining regional geological structures (Ooi & Lim, 2006). The satellite is in constant orbit around the earth throughout its life circle, acquiring data for a particular scene, unlike the aerial photo, which is often limited to a particular scene at a specific point in time. Spaceborne sensors provide multispectral, spatial and temporal data used to analyse dynamic changes associated with the Earth's resources, such as land and water (Ramachandra & Kumar, 2004). They have been the most successful approaches for detecting land cover change. In the past two decades, there has been a growing trend for the development of change detection techniques using remote sensing data (Chen et al., 2003). Remote sensing has been used in monitoring the expansion and process of land cover change (El Hassan, 2004; Kundu & Dutta, 2011).

The major advantage of Earth observation is that it provides spatiotemporal information (sometimes free to the user) about the Earth's surface from a small to a large extent of land, making it the best tool for providing a dataset for land cover change detection/modelling and extracting land cover-related information. Available data from remote sensing missions have provided a wealth of complementary data, immensely

supporting efforts towards the precise determination of land use and quantifying subtle changes in land use management or intensity (Joshi et al., 2016). Since the advent of remote sensing, it has been used in many fields, such as mapping and land cover change detection. It has become a vital research and application area for remote sensing data analysts (Hester et al., 2010). It has proven to be a valuable data source for the efficient extraction of land-cover change information. Rimal et al. (2017) evaluated the LULC changes and urban expansion of Jhapa district of Nepal. They identified spatio–temporal dynamics of LULC using six time-series atmospherically-corrected surface reflectance Landsat images from 1989 to 2016.

2.6.2.3 Hyperspectral remote sensing

Hyperspectral remote sensing, also known as spectroscopy, spectrometry and spectroradiometer, means spectra with many narrow, contiguously spaced spectral bands (Shukla & Kot, 2016). Spectroradiometers can be both imaging and non-imaging, used on remote sensing platforms and provide images similar to conventional multispectral scanners with a much higher spectral resolution (Kumar et al. 2002). Hyperspectral data have been used to discriminate vegetation in many areas and environments (Jensen et al., 2007). Imaging spectroscopy lately emerged as a very efficient remote sensing technique to improve the understanding of Earth's functioning (Briottet et al., 2011). Hyperspectral data can be acquired from satellite, aerial and terrestrial-based platforms. However, due to growth of satellite remote sensing, hyperspectral Remote Sensing (HRS) platforms have developed from ground-based and airborne platforms into spaceborne satellite platforms (Zhong et al., 2021). This has greatly promoted their civil application in agriculture, forestry, and environmental monitoring. Hyperspectral satellites have emerged as a new generation of remote sensing (Mohamadi et al., 2016), with a dual advantage of the traditional spectroscopy technology and the modern imaging system (Qian, 2021).

The advantage of hyperspectral sensors over multispectral sensors is their higher spectral resolution, which is suitable for detecting, identifying and quantifying surface materials (Shukla & Kot, 2016). Satellite hyperspectral systems also allow for coverage of larger areas at a fraction of the cost of airborne surveys but at the expense of lower spatial detail, which makes the data quality poor (Liu et al., 2018), especially for vegetation studies at the leaf scale. Table 2.3 shows different space-based hyperspectral sensors. Hyperspectral sensors mounted on an aeroplane have been available for over two decades and can collect

landscape images with high spatial and spectral resolution (Olmanson et al., 2013). However, they do not allow regular and synoptic coverages over large areas as space-borne sensors. Also, they produce images with lower angular effects due to their much smaller field of view (Transon et al., 2018).

Similarly, terrestrial-based Field spectroscopy has emerged as a useful tool for assessing the degradation of biochemical and biophysical forest parameters such as chlorophyll and other pigment concentrations at leaf and canopy levels (Arellano et al., 2017). Its major disadvantage is that it does cover a large spatial extent. Also, there is a need for visitation to the field, which might be dangerous due to security concerns in places like the Niger Delta unless security is guaranteed, like during the fieldwork for this research. Despite the major disadvantage of Field spectroscopy, it is ideal for this research to characterise the impact of oil extraction activities on vegetation at the leaf scale. Unlike space and airborne platforms, the main advantage is that it allows plant species studies. Similarly, field spectroscopy is technically less challenging. The sensing instrument can remain fixed over the subject of interest for much longer, and the path length between the instrument and the object being measured is reduced (Milton et al., 2006).

Table 2.3: The satellite-based hyperspectral sensors

Sensor	Year of lunch	Country/Organisation	Spectral bands	GSD
EO-1 (Hyperion)	2000	US(NASA)	242	30
PROBA-1(CHRIS)	2001	EU/UK	63	34
HICO	2009	US(NASA)/Japan	128	90
Tiangong-1	2011	China(CASC)	64	20
HySIS	2018	India(ISRO)	30	256
PRISMA	2019	Italy	250	30
EnMap	2020	Germany	228	30
HISUI	2020	Japan	185	30
GaoFen-5(2)	2021	China(CASC)	330	

2.6.3 Extraction of land cover information and biophysical parameter from remote sensing data

In general, the remote sensing satellite data could be grouped into three categories of spatial resolution (pixel size): low, medium and high spectral resolution (wavelength ranges), temporal resolution (frequencies of the satellite to visit the same scene), and spatial extent (size of the area captured) (Turner et al., 2003) (Table 2). The information

that may be extracted from remotely sensed data is directly related to the sensor and the characteristics of the images it produces.

Remote sensing data can be used for numerous applications in three different ways: i) Mapping/Monitoring of earth resources, ii) Retrieval of bio-geo-physical parameters, which are used in models to predict the changes in geosphere and biosphere, iii) Management/Decision Support, where remote sensing derived information is used for decision making for sustainable management of earth resources (Steven et al., 2006). Extracting and quantifying the biophysical parameters of vegetation cover is extremely important when monitoring land cover and associated changes, identifying vegetation stress, and assessing crop production (Shelestov et al., 2017).

Table 2.4:Examples of some satellites based on various resolutions

Resolution	Spatial resolution (m)	Temporal resolution (days)	Spectral(band)	Swath width
Low	1000 (AVHRR) 250(MODIS) 500 (MODIS) 1000(MODIS)	2 times 1 to 2	5 36	2,500 2330 by10
Medium	30 (Landsat) 20(SPOT-4 multispectral) 10 (SPOT-4 panchromatic)	16 26	4	60
High	1(panchromatic) IKONOS 4 (multispectral) IKONOS 0.65-0.73(panchromatic)Quick Bird 2.62-2.90(Multispectra)Quick Bird)	Off nadir 3-5 Nadir 144	1 4 1 4	12

Note: AVHRR: Advanced Very High-Resolution Radiometer; MODIS, Moderate Resolution Imaging Spectroradiometer.

Both the hyper- and multispectral sensors are based on the same physical technology of recording radiance in the Visible to Near-InfraRed (VNIR) and Short-Wave InfraRed (SWIR) of the spectrum, VNIR spanning 400–1000 nm and SWIR 1000–2400 nm (Transon et al., 2018). Different land cover objects behave differently within different

regions of Electromagnetic wavelengths known as spectral signatures. The multiple spectral responses from land-cover features are organised into land-use classes (Myint, Wentz, & Purkis, 2007) and used to calculate various vegetation indices to monitor vegetation's health. For example, soil reflectance is generally lower in near-infrared (NIR) wavelengths and higher in red wavelengths than vegetation reflectance (Tote, Delalieux, Goossens, Williamson, & Swinnen, 2014), which is reflected more in NIR.

Also, high-resolution satellite sensors can provide credible geographical feature extraction of land cover information and change detection at a small or local scale (Kumar & Arya, 2021). But medium-resolution imagery like Landsat is usually used for a large-scale area like the Niger Delta. A high resolution like Ikonos imagery will provide a large quantity of data, high processing load, cost and time and, analysing these imagery data will create a substantial challenge. Landsat has more data covering many decades, making them suitable for long-term monitoring of land cover changes. Similarly, Landsat has more spectral bands, which are useful for extracting land cover information and biophysical parameter at the plot scale using vegetation indices such as NDVI. Many researchers have used Landsat-derived NDVI to monitor the health of vegetation. Ahmad et al. (2017) identified prospective hydrocarbon seepage areas within the vegetation cover in Kifl Oil Field and Adjacent Areas South of Iraq using NDVI from Landsat 8 (OLI). Similarly, Landsat has been used to extract land cover information by various researchers. Kuenzer et al. (2014) model land surface dynamics in the Niger Delta from 1986 to 2013 using Landsat data, and Coulter et al. (2016) classified and assessed land cover and land use change in southern Ghana using dense stacks of Landsat 7 ETM+ imagery using 2000 and 2010.

2.7 Assessing and monitoring changes in vegetation health using earth observation data

Natural environments and their biodiversity are increasingly endangered by many human-induced environmental perturbations (Wang & Sousa, 2009). Changes in land cover – especially that of vegetation in response to environmental factors or contamination – may not always be in the form of a complete conversion from one type to another but instead could be in the form of degradation (e.g., a reduction in the health or quality of the vegetation). The application of remote sensing in vegetation monitoring is a relevant topic that can detect vegetation stress due to hydrocarbon seepage (Asri et al., 2020). The

canopy reflectance of plants is determined by the optical properties of leaves, the amount of green biomass, canopy architecture and leaf angle distribution and alterations in these variables caused by oil pollution and other environmental stresses that induce changes in canopy reflectance can be detected by remote sensing and used as indicators for oil pollution of soils (Zhu et al., 2013). The health of the vegetation can be assessed and monitored using hyperspectral and multispectral vegetation indices. The scale at which remote sensing studies measure attributes of vegetation conditions varies with the sensor used. Sensors vary in their spatial, spectral, radiometric and temporal resolutions of data collection and, therefore, their ability to record and monitor vegetation attributes (Lawley et al., 2016)..

2.7.1 Hyperspectral remote sensing for monitoring vegetation health

Field spectroscopy and hyperspectral remote sensing have become effective tools for assessing the degradation of biophysical and biochemical forest parameters, such as chlorophyll and pigment concentrations at the leaf and canopy levels (Arellano et al., 2017). Hyperspectral data can measure vegetation's biochemical and biophysical properties and how these parameters vary across the ecosystem (Onyia et al., 2018). The narrow bandwidths of a hyperspectral sensor are sensitive to subtle variations in the reflectance of vegetation (George et al., 2018; Jensen et al., 2007). Narrow band hyperspectral remote sensors record reflected radiant energy from a plant at a high number of wavebands and provide timely and reliable information about the current plant physiology in a cost-effective and timely manner (Maimaitiyiming et al., 2017). The reflectance of vegetation is directly related to plant physiology (Omodanisi & Salami, 2014).

Many studies have used the reflectance of plants to study their physiology. Among the studies are: investigating the potential of field spectroscopy for characterizing the physiological status of grapevines exposed to different levels of water stress based on in situ measurements (Maimaitiyiming et al., 2017). Similarly, Cotrozzi et al. (2020) predicted variation in physiological and anatomical leaf traits related to water status under varying water availability in six maize (Zea mays). Hyperspectral sensors are typically in the form of airborne scanners or field-based instruments (Kumar et al., 2002). The main advantage of the field-based vegetation condition assessment approach, which comprises field spectroscopy, is its capability to assess underwood conditions (Tehrany et al., 2017) and provide plant-specific spectral information. Accordingly, field-based vegetation

condition assessment approaches have been used to assess the health of vegetation for various applications, including the impact of oil spills on vegetation. Hyperspectral remote sensing provides new data for developing vegetation indices (Zhu et al., 2013) for assessing the health of vegetation, such as the hyperspectral vegetation indices and red edge position.

2.7.1.1 Hyperspectral vegetation indices (HVI)

Hyperspectral vegetation indices (HVIs) have been widely used in environments to evaluate the impacts of hydrocarbon pollution on vegetation (Serrano-Calvo et al., 2021). The availability of data from field-based sensors makes it possible to develop different HVIs for assessing the health condition of vegetation. HVIs are proposed based on the absorption and reflectance properties in specific regions of the high-resolution spectrum, which can detect some plant characteristics that traditional multispectral remote sensing cannot (Zhu et al., 2013). Vegetation properties measured with HVIs can be divided into three main categories: 1) Structure; 2) Biochemistry, and; 3) Plant physiology/stress(Roberts et al., 2011). Many HVIs have been developed for various applications, such as estimating the plant N concentration of winter wheat in the North China Plain for different growth stages and years (Li et al., 2010), monitoring oil pollution in an area of eastern China (Zhu et al., 2013), and extracting a useful "physiological reflectance index" (PRI) from diurnally changing reflectance signatures of sunflower canopies (Gamon et al., 1992).

2.7.1.2 Red edge position (REP)

One of the best remote sensing descriptors of chlorophyll concentration is the red edge position (REP), the point of maximum slope in vegetation reflectance spectra (Filella & Peñuelas, 1994). The importance of the REP parameter is closely related to various physical and chemical parameters of vegetation, and it is commonly employed to infer the growing states of vegetation and monitor plant activity (Jiang et al., 2019). The REP is strongly correlated with foliar chlorophyll content. It provides a very sensitive indicator for various environmental factors affecting leaves, such as stress, drought and senescence (Baranoski & Rokne, 2005).

REP has been utilised in many studies of plant reflectance. Among them are the studies of reflectance spectra of samples of Cenchrus ciliaris, which is a grass grown in a greenhouse under three levels of nitrogen supply by Onisimo Mutanga & Skidmore

(2007), predicting high-yielding varieties of rice based on the spectral reflectance in REP (Abbasi, Darvishsefat, & Schaepman, 2010), plant chlorophyll content, biomass and Relative Water Content (RWC) evaluation of Capsicum annuum and Phaseolus vulgaris plants under different nitrogen and water availabilities, and plants of Gerbera jamesonii with different hydric status (Filella & Peñuelas, 1994). In addition, REP has been used to assess the spectral characteristics of polluted and unpolluted vegetation from oil spillage based on the ASD FieldSpec pro measurements at plot scale in Lagos and Ogun States in south-western Nigeria (Omodanisi & Salami, 2014).

2.7.2 Multispectral satellite-based remote sensing for monitoring vegetation health

Detecting the vegetation affected by oil spills in oil-polluted environs such as mangrove forests can be challenging using in situ measurements and laboratory-based analysis techniques due to security challenges and difficult terrain. As a more practical alternative, satellite remote sensing is an effective tool for detecting and monitoring vegetation health and status in polluted areas (Adamu, 2016)**,** especially over a large area. It provides spatiotemporal data, although it is not capable of assessing underwood. Remote sensing of vegetation is achieved by measuring electromagnetic wave reflectance information from canopies using passive sensors (Xue & Su, 2017). Monitoring changes in the health and pattern of vegetation using multispectral satellite-based spectral indices is important for natural resource management and monitoring. Multispectral vegetation indices are those formulated using multispectral data using the reflectance at specific wavelengths known as broadband multispectral vegetation indices (BMVIs) and narrow-band multispectral vegetation indices (NMVIs) (Zhu et al., 2013). Vegetation indices (VIs) represent a powerful and effective way of monitoring vegetation status, growth, and biophysical parameters, especially for aquatic ecosystems, whose characterisation is extremely time-consuming and expensive (Villa, Bresciani, Braga, & Bolpagni, 2014). However, selecting a VI for a particular application is difficult because there is currently no unified mathematical expression that defines all VIs due to the complexity of the different light spectra combinations, instrumentation, platforms and resolutions used (Xue & Su, 2017)**.**

Remote sensing of vegetation has advanced significantly over the past half-century due to its ability to retrieve useful plant biochemical, physiological and structural quantities across a range of spatial and temporal scales (Houborg et al., 2015). Progression in optical sensor technology has facilitated a great opportunity to understand vegetation

health/quality at various spatiotemporal scales previously regarded as complex using remote sensing data with varying footprints and resolutions, leading to remarkable progress in crop, forest and rangeland monitoring (Mutanga et al., 2016). Various earth observation data sets from different sensors are commonly used for monitoring vegetation health. Generally, Tehrany et al. (2017) grouped them into three satellite sensors: 'environmental monitoring' satellites (e.g., Landsat metre-scales), global weather satellites (e.g., MODIS at kilometre-scale) and civilian satellites (e.g., Quickbird, RADAR at sub-meter scale). Satellite-based vegetation monitoring has proven to be an important source of information on vegetation growth and vigour from regional to global scales (Swain et al., 2017) and in polluted areas, as revealed from previous research using VIs derived from remotely sensed satellite data to monitor vegetation health (Adamu et al. 2015).

Landsat data have become one of the most commonly used satellite data for monitoring the health of vegetation around the globe due to their free access and high temporal and spatial resolution. The launch of the Landsat (ERTS-1) mission in 1972 triggered investigations surrounding its capability for vegetation monitoring and categorisation (Houborg et al., 2015). Monitoring vegetation health is important in many ways and has many diverse applications. It can be used to forecast crop yield and assess natural forest expansion (Mancino et al., 2014), biodiversity and conservation (Ochege et al., 2017), drought monitoring (Amani et al., 2017; Kogan et al., 2017), and detecting oil pollution (Adamu et al., 2015), among others. Among various vegetation indices used for monitoring vegetation health is the normalized difference vegetation index (NDVI). The NDVI is calculated as the difference between near-infrared and visible reflectance values and has proven to be a robust indicator of terrestrial vegetation productivity (Wang et al., 2001). NDVI became popular in the last three decades for investigating the quality of vegetation cover, which has remained the most well-known and used index to detect live green plant canopies in multispectral remote sensing data (Fabiyi, 2011).

2.8 Land cover change detection using earth observation data

Many regions worldwide are experiencing rapid, widespread changes in land cover (Mas, 1999). Knowing the positions and the intensity of land cover changes will benefit the society for planning purposes and other applications (Kuta & Comber, 2015). Change is the transformation or modification of something over a period of a well-defined, enduring structure, not minding the complexity of the structure. The important thing is that the

structure exists continuously over its transformation (spatiotemporal). Change detection is the apprehension of change in the world around us through observing it at different periods (Carincotte et al., 2006; Unger et al., 2015). Change detection measures the distinct data framework and thematic change information that can guide more tangible insights into an underlying process involving land cover and land use changes than the information obtained from continuous change (Ramachandra & Kumar 2004). Some changes are visible (i.e., conversion from one land cover type to another), while others are not visible (e.g., subtle vegetation degradation). Many earth observation datasets exist for land cover change detection and modelling using classified land cover maps from various sensors, spatial, radiometric and spectral resolution. Monitoring land cover changes using remote sensing data has the advantage of synoptic view, repetitive coverage and cost-effectiveness (Omo-Irabor & Oduyemi, 2007)

2.9 Land cover classification

Classification is an automated computer-assisted grouping of pixels in remotely sensed images into land cover classes by converting data (images) into land cover information. It is usually performed to retrieve land use/cover information using statistical pattern recognition or classification techniques (Sharma et al., 2016). The landscape is usually composed of a multifaceted combination of both built-up and natural objects, including but not limited to paved roads, buildings, bridges, fences, railways, trees, and grass cover (Yan et al., 2015), which need to be grouped into various land use/cover types. Classification is a vital process in remote sensing that relates pixel values to land cover classes on the surface (Zhang & Roy, 2017). The classification approach chosen depends on many factors, such as the application, how familiar the analyst is with the study area, and the required accuracy. The multispectral mapping of landscapes consists of depicting boundaries around geographically located classes and their various attributes and relations (Robinove, 1981). Generally, digital image classification is performed to produce land cover maps from remote sensing data, mainly for large areas, and there are two types of classification techniques, supervised and unsupervised (Saha, Arora, Csaplovics, & Gupta, 2005). Many researchers have adopted different classification methods based on their requirements, with some even comparing the two methods. Digital image classification comprises of four steps: 1) image pre-processing to reduce haze, atmospheric correction, computing band ratios, geometric correction, etc.; 2) training sample selection to select a particular feature for describing the pattern; 3) decision:

selecting a suitable technique for comparing the image pattern according to the target; and 4) assessing the accuracy of the classification (Mahmon & Ya'acob, 2014; Seetha et al., 2008). Although a training sample may not be needed for unsupervised classification, it may be needed for accuracy assessment.

2.9.1 Land cover Classification techniques

Land cover classification is divided into two basic techniques: unsupervised and supervised (Karan & Samadder, 2018). Unsupervised classification is the classification of all pixels with unknown identities that are blindly grouped into a certain number of clusters according to the similarities in their digital numbers (Gao, 2009). The classification is more machine-dependent, with the analyst only indicating the number of proposed land cover clusters while the machine controls the assignment of the classes. Unsupervised classification techniques are of high interest where an image is classified based on its reflectance values only without taking field measurements into account because field knowledge is only needed to identify the classified groups (Ibrahim et al., 2009). However, supervised classification is the most commonly used technique for quantitatively analysing remote sensing image data. It is based on the concept of segmenting the spectral domain into regions that can be associated with the land cover classes of interest to a particular application (Richards, 2013). Supervised classification forms the basis of what we have recently come to call data mining, which originated in statistics in the early nineteenth century under the moniker discriminant analysis (Cook & Swayne, 2007). In supervised classification, the analyst assigns the pixels that belong to a cluster to the machine, i.e., the analyst "supervises" the pixel categorisation process by stating to the computer algorithm numerical descriptors of the various land cover types present in a scene (Lillesand et al., 2008). Knowledge of the study area is vital for supervised classification. It can produce more accurate results than unsupervised classification since it can handle mixed pixels better than unsupervised pixels to a certain level. Supervised classification is known to be superior to unsupervised approaches. Supervised classification is superior to unsupervised classification (Inglada et al., 2017). It is less affected by mixed pixels in the land, and it is the favourite of most authors for land cover classification, such as: Egorov et al. (2015), Thakkar et al. (2017) and Lv et al. (2016). As mentioned earlier, supervised classification is divided into two stages: training and classification stages involving four steps. In the training stage, spectral signatures for various predefined land cover classes in the scene are defined and used by

the machine as the basis for its classification. The training stage is both an art and a science that requires close interaction between the image analyst and the image data (Lillesand et al., 2008). The success of supervised classification hinges on the quality of the training data. Rawat et al. (2013) quantified the land use/cover changes in Ramnagar town, India, from 1990 to 2010 using the supervised classification maximum likelihood technique. Although many classifiers exist, there are two main groups of methods among various classification methods: *soft* and *hard* classification. However, no single optimum method performs best for all problems, with each classifier having its merits and demerits depending on the dataset and the land cover type on which they are used (Lee et al., 2011).

2.9.2 Hard classification

The hard traditional (crip) classification approach is used when the objects/features have well-defined boundaries. Hard classification bypasses the requisite of class probability estimation and directly estimates the classification boundary (Lee et al., 2011). Hard classifiers make a definitive decision that each pixel in land cover is allocated to a single class, which may produce large errors in area estimation, especially from coarse spatial resolution data due to the mixed pixel problem (Choodarathnakara, et al., 2012; Sharma et al., 2016). The common classifiers in this group are maximum likelihood, minimum distance, artificial neural networks, decision tree, and support vector machine. From various literature, many works have been done employing hard classification. It seems as if it is more popular among researchers in the field of remote sensing probably because hard classification is easier to implement and detect land cover changes since only two maps are needed between any two dates, unlike the soft classification, which will require each land cover class to be compared with other land cover classes. The soft classification produces maps per land cover class, i.e., if you have five land cover classes per map, that means five maps for each, unlike the hard classification, which produces a single map containing all the land cover classes, making hard classification easier to manage in terms of volume of maps. Additionally, the area or size of soft map is not straight forward to compute, and the total sizes of all the classes are not equal to the total area.

2.9.3 Soft classification

The geographic space we live in comprises various land cover classes (continuous and discrete objects), both natural and manmade. Many do not have well-defined boundaries that can be mapped and visually represented. While humans can distinguish the

vagueness/fuzziness in land cover classes, representing it in map form is challenging since computers do not distinguish and recognise vagueness as humans do. Conventional image processing techniques assume that pure pixels in land cover cannot be appropriately represented as mixed pixels (Foody, 2002). Recently, soft classification methods have gained wider use due to their ability to represent and estimate land cover at the subpixel level, especially when using coarse-resolution satellite data with mixed pixels (Gu et al., 2015). A soft classification reveals more land use/cover information and potentially a more accurate result, especially for coarse spatial resolution data (Choodarathnakara et al., 2012; Sharma et al., 2016). Additionally, the output is not a single classified image. Instead, several images are obtained as the classified output (Tiwari et al., 1999) of land cover information, which is very important for land resource management (Sharma et al., 2016). The soft classification techniques commonly used are fuzzy logic, genetic algorithms, artificial neural networks and decision trees, with the last two used as both hard and soft classifiers.

2.9.4 Object-based classification

The ability to spatially quantify changes in the landscape and create land-cover maps using remote sensing coupled with object-based image analysis (OBIA) has improved classification techniques for developing land cover maps (MacLean et al., 2013). Remote sensing-based object-based image classification for land cover mapping purposes has attracted significant attention in recent years (Ma et al., 2017). The object-based approach overcomes the limitations and disadvantages of the traditional pixel-based approaches by generating and analysing meaningful image objects (i.e., groups of contiguous pixels) instead of individual pixels, reducing the speckle noise effect (Tamta & Bhadauria, 2015). Image segmentation divides an image into parts that have a high correlation with geographic objects represented in the image (Lizarazo & Elsner, 2009) and incorporates both spectral information (feature vector of the pixels) and spatial information (e.g., size, shape and adjacency to other pixels) in categorising and delineating suitable segments within an image for image classification (Geneletti & Gorte, 2003; Pei et al., 2017). Unlike traditional pixel-based analysis, object representation with image segmentation algorithms is a vital prerequisite for classification/feature extraction and further integration in GIS analysis (Dragut et al., 2014), which often requires the use of dozens, and sometimes hundreds of variables (Duro et al., 2012). The two main approaches in image segmentation are edge-based and region-based (Geneletti & Gorte, 2003).

Robertson & King (2011) noted that the object-based method produces thematic maps with more uniform and meaningful LULC objects and depicts change more accurately despite similarities in map accuracies from both object-based classification and maximum likelihood (MLC) methods using Landsat TM. The method to adopt is always difficult because many factors come into play, including the nature of the study area and the spatial resolution of the satellite image. A recent study by Ma et al. (2017) noted that variation in study areas makes it difficult to generalise research results since certain methods may display good classification accuracy in a certain study area but produce inconsistent results in other study areas. Their study involved constructing a database with 28 fields of data using qualitative and quantitative information extracted from 254 experimental cases described in 173 scientific papers and discovered the following:

1 Supervised object-based classification is currently experiencing rapid advances, while the development of the fuzzy technique is limited in the object-based framework;

2 Spatial resolution correlates with the optimal segmentation scale and study area, and Random Forest (RF) shows the best performance in object-based classification;

3 The overall accuracy benefits from higher spatial resolution images (e.g., unmanned aerial vehicles) or agricultural sites, where it also correlates with the number of targeted classes;

4 More than 95.6% of studies involve an area less than 300 ha, and the spatial resolution of images is predominantly between 0 and 2 m;

5 Some methods that may advance supervised object-based image classification were identified. For example, deep learning and type-2 fuzzy techniques may improve classification accuracy.

Some of their findings agreed with the study by Li et al. (2016), which stated that random forest (RF) and support vector machines (SVM) are highly suitable for classifications in agricultural areas and confirmed the expected general tendency of the overall accuracies to decline with increasing segmentation scale.

Although object-based classification involves an area of less than 300 hectares (ha) and with a predominantly spatial resolution of images between 0 and 2 m, some researchers have used datasets from Landsat sensors for object-based classification. Achieving the best classification results with Landsat images requires particular attention to the specifications of each classification method, such as selecting the right training samples,

choosing the appropriate segmentation, pre-processing calibration, and choosing the right classifier: each classification method applied on Landsat images has its strengths and limitations (Phiri & Morgenroth, 2017).

Robertson & King (2011) used the Landsat Thematic Mapper 5 (TM) dataset and discovered that the object-based maps represented change more accurately than maximum likelihood classification (MLC)-derived change maps in the region of eastern Ontario for the period 1995–2005. Additionally, Reyes et al. (2017) used object-based analysis on medium-resolution images (Landsat TM) in the Province of Pontevedra in Spain, which has a complex landscape with different coexisting elements, such as mixed hardwood and coniferous forests, scrublands, natural grassland, agricultural areas, water surfaces, bare soils and urban and industrial areas. Frohn et al. (2011) also used segmentation and object-oriented processing of single-season and multi-season Landsat-7 Enhanced Thematic Mapper Plus (ETM+) to classify wetlands in a 1560 km^2 study area in north-central Florida. They discovered that the result outperformed the traditional MLC in accurately mapping the wetlands, with an overall accuracy of 90.2%.

Authors such as Frohn et al. (2011), Naboureh et al. (2017), and Yu et al. (2016) have used the Landsat dataset for object-based image classification for land cover mapping. Despite the supposed accuracy of object-based image classification over the traditional pixel-based classification, it is not free from the uncertainty associated with pixel-based classification. Uncertainty occurs in any segmented image and can affect further image processing, particularly in areas where objects with uncertain boundaries (so-called fuzzy objects) dominate, and the indication of segmentation uncertainty is important (Lucieer et al., 2003).

2.9.5 Soft object-based image classification (SOBIC)

Although many authors have reported that object-based image classification method are often more accurate than traditional spectral pixel-based classification (Dornik et al., 2017), the parametersization of crisp segmentation models commonly requires significant user interaction, making it difficult to employ such methods for the automated processing of large datasets as well as producing image objects that are delimited by clearly defined boundaries (Lizarazo & Elsner, 2009). Additionally, some important issues and classification assumptions are often overlooked or partly addressed in object-based image analyses (Costa et al., 2017). This is because the mixed pixel is usually associated with

remote sensing data no matter the resolution of the data, and the segmented image also contains mixed pixels due to the nature of land cover classes as well as under or overestimation segmentation of the classes used for training, which are inherently assumed to be pure.

Combined pixel-based, pixel groupings and object segmentation offer more novel techniques for image classification (Al Fugara et al., 2009) and is a less explored territory (Costa et al., 2017; Lizarazo & Elsner, 2009), despite the inherent novelties it brings into image classification and land cover change mapping/modelling. Object-oriented image classification based on fuzzy logic allows the integration of a broad variety of different object features, such as spectral values, shape, and texture (Yoon et al., 2003). In predominantly mangrove vegetation, such as the Niger Delta, there is a need for techniques that will delineate the different vegetation types. Innovative remote sensing techniques, such as spectral unmixing and object-based image analysis, offer unique forest mapping approaches by quantifying proportional species composition at the pixel level and utilising ancillary environmental data for forest classifications (Gudex-Cross et al., 2017). Heumann (2011) stated that accurate mapping of fringe mangroves using remote sensing data remains a challenge due to the spectral similarity of mangroves and associated species, a lack of clear zonation between species, and mixed pixel effects, especially when vegetation is sparse or degraded. Due to relatively coarse spatial resolution and spectral confusion with landward vegetation, traditional remote sensing methods have failed to accurately map fringe mangroves and true mangrove species (Heumann, 2011). Some researchers who have applied object and fuzzy classification to remote sensing datasets are Al Fugara et al. (2009); Feizizadeh, Blaschke, Tiede, & Moghaddam (2017); Gudex-Cross et al. (2017); Lizarazo & Elsner (2009); Wang et al., (2004).

2.9.6 Assessing classification accuracy

Accuracy assessment should be a vital part of a program that maps land cover from remotely sensed imagery (Foody & Boyd, 2013) because the value of the classified map depends on the accuracy of the classification (Foody, 2002; Hashemian et al., 2004; Mahmon and Ya'acob, 2014). The classification accuracy is the degree to which the classified image agrees with reality (Janssen & van der Wel, 1994) and has received widespread attention in the remote sensing community (Congalton, 1988). Assessing the accuracy of land cover maps generated from remotely sensed data is expensive, time and

money-demanding (Congalton, 1988; Hashemian et al., 2004) and is inhibited by the absence of high-quality ground reference data (Foody & Boyd, 2013). Traditionally, accuracy assessment involves identifying a set of reference (samples) points on the classified image, which are visited on the ground (ground truth) to verify if the map is the true representation of ground features. Sampling becomes the means by which the accuracy of the land cover map can be derived because total visitation (where it is possible to do so) of all mapped areas for verification is impossible, and using the wrong sampling approach can be costly and yield poor results, which may introduce significant biases into the error matrix and over or underestimate the true accuracy (Hashemian et al., 2004). But a ground sample may not be possible, especially when the classified map is several years behind the time of visitation. Some land cover types might have changed, especially in urban areas where the analysis may not know what existed in the past. For example, validating an image of the year 2000 in 2022 may not be accurate because the land cover in some places might have changed. Secondly, site validation might not be feasible due to the size of the study area, inaccessibility and security concerns, especially for places like the Niger Delta. An alternative is to use a high-resolution google earth image. Google Earth's high-resolution imagery is important for accuracy assessment (Tilahun, 2015). It enables historic temporal images of the same or close time image with the classified image to be used for sampling and "ground" truthing for accuracy assessment. Google earth image has been used by Olofsson et al. (2014) as a source of reference data for ground truth and validation for land cover accuracy assessment. For this research, the google earth image was used as "ground truth" for the reasons mentioned earlier.

There are various sampling schemes, including simple random sampling, stratified sampling, systematic sampling, systematic nonaligned sampling and cluster sampling. Spatial complexity (size of the study region and object characteristics) of a given environment dictates the appropriate sampling scheme(s) to be used for creating error matrices necessary to assess the accuracy of maps generated from remotely sensed data (Congalton, 1988; Hashemian et al., 2004). The results of a study of sampling methods for accuracy assessment of classified remotely sensed data by Hashemian et al. (2004) show that for a large area, simple random sampling and stratified random sampling methods overestimate the overall accuracy, while systematic sampling and stratified systematic unaligned sampling methods performed better with Simple Random Sampling being the most efficient methods. However, simple and stratified random sampling

produces good results for a smaller area. Congalton (1988) and Hashemian et al. (2004) show that both the stratified systematic unaligned and systematic sampling schemes are not good for a large area.

2.10 Change detection mapping techniques

Many techniques have been developed for change detection (Devi & Jiji, 2015; Lu et al., 2003; Pathak, 2014**).** The change detection techniques can be organised into algebraic/statistical, vector/transformation, classification or mixture categories. Additionally, there is no universally optimum technique; the choice depends upon the application (Madanian et al., 2012; Ross & Bhadauria, 2015) because different change detection algorithms have their own merits, and no single approach is optimal and applicable to all cases. Usually different algorithms are often compared to find the best change detection results for a specific application. Ultimately, change maps using the post-classification technique of two images will only be generally as accurate as the product of each classification's accuracy (Pathak, 2014). Previous studies have shown that image differencing, principal component analysis, and post-classification comparison are the most commonly used methods for change detection. However, spectral mixture analysis and artificial neural networks combined with GIS and remote sensing data have become important techniques for change detection applications in recent years (Lu et al., 2003).

Mas (1999) tested six change detection procedures; image differencing, vegetative index differencing, selective principal components analysis (SPCA), direct multi-date unsupervised classification, post-classification change differencing, and a combination of image enhancement and post-classification comparison; on Landsat Multispectral Scanner (MSS) images. They discovered that post-classification comparison was the most accurate procedure and offered the advantage of indicating the nature of the changes. Additionally, four change detection techniques, namely, post-classification, image differencing, image rationing and principal component analysis, were applied by Afify (2011) to assess, evaluate and monitor the nature and extent of land cover changes and classify the changed areas according to ‘‘from-to’’ in New Burg El-Arab city from 1990 to 2000. The results indicated that the post-classification change detection technique provided the highest accuracy. There are different change detection categories with various techniques under them. Lu et al. (2003) and Ross & Bhadauria (2015) categorise change detection into seven categories comprising thirty techniques (Table 2.5), while

Rama et al. (2016) summarise ten various change detection techniques in Table 2.6 and their strengths and limitations (Table 2.4). Some researchers also compared different techniques within the same categories. Madanian et al. (2012) used image differencing, image rationing, and image regression under the Algebra-based approach to study land use/cover changes in Falavarjan, Iran.

Table 2.5:Change detection technique categories(Ross & Bhadauria, 2015).

	Techniques categories	**Example of technique**
1	Algebra-based approach.	• Image differencing. • Image regression. • Image rationing. • Vegetation index differencing. • Change vector analysis.
2	Transformation.	• PCA. • Tasseled Cap (KT). • Gramm-Schmidt (GS). • Chi-Squa.
3	Classification-based post-classification.	• Spectral-Temporal Combined Analysis. • Comparison. • EM Transformation. • Unsupervised Change Detection. • Hybrid Change Detection. • Artificial Neural Networks.
4	Advanced models.	• Li-Strahler Reflectance Model. • Spectral Mixture Model. • Biophysical Parameter Method.
5	GIS.	• Integrated GIS and RS Method. • GIS Approach.
6	Visual analysis.	• Visual Interpretation.
7	Other change detection techniques.	• Measures of spatial dependence. • Knowledge-based vision system. • Area production method. • Combination of three indicators: vegetation indices, land surface temperature, and spatial structure. • Change curves. • Generalised linear models. • Curve-theorem-based approach. • Structure-based approach. • Spatial statistics-based method.

Table 2.6:Strengths and limitations of different change detection techniques (Rama et al., 2016).

Technique.	**Strong point.**	**Limitation Simple.**
Image differencing.	Simple to implement and interpret.	Nature of change not found. Accuracy depends on threshold selection.
Rationing vegetation.	The effect of different Sun angles, shadows and topography is reduced.	Non-Gaussian distribution of image makes threshold selection difficult.
Vegetation index differencing change.	Widely applied for both human-induced and natural forest cover change detection.	Threshold identification for detection of vegetation changes represents a key issue.
Change vector analysis.	It offers qualitative information of the direction and intensity of change. CVA is applicable to any number of spectral bands.	Not providing concisefrom–to information. Accuracy depends on the image quality, geometric correction and threshold.
Tasseled Cap transformation.	Data redundancy reduced. Scene independent.	Difficult to interpret and label change information.
Principal Component Analysis.	Useful to identify where changes occurred.	Difficult to interpret the result. Knowledge of the study area is essential.
Post-classification comparison.	Provides from-to change results. Normalise the atmospheric, sensor differences.	Accuracy depends on the classification accuracy of individual images.
Cluster approach.	Simple & need not require any explicit assumption about the underlying classes.	Labelling change among a matrix of many overlapping classes may be difficult or non-informative.
Artificial Neural Network.	Provide complete from-to change information and the nature of change.	Requires accurate training and testing classifications.
Decision Tree approach.	This technique can be applied to any spectral data or GIS data.	Error in training data will produce poor result.

2.11 Overview of land cover change detection applications related to the oil industry

Oil and gas development results in a complex system of oil well pads, roads, pipelines, and other infrastructure (Unger et al., 2015). Consequently, land cover change detection

studies to determine the impact of oil/hydrocarbon have been carried out in many parts of the world. Arellano et al. (2015) used three vegetation indices (SR, NDVI and $NDVI_{7057}$) for the detection of oil contamination in forests in the Ecuadorian Amazon using satellite imagery from EO-1 (Earth-Observation 1) Hyperion with supporting field data on soils and foliar properties to produce a map of the spatial pattern of forest oil contamination. Additionally, Ungeret al (2015) detected changes and quantified the amount of land within the Haynesville Shale area that had been converted from forestland and agricultural land to oil and gas well pads using Landsat Thematic Mapper (TM) imagery from 1984 to 2011, using unsupervised classifications for a time series analysis. Yu et al. (2015) detected land cover change due to climate change and oil/gas development in north-western Siberia using multiple sources of remotely sensed imagery. They discovered that 10.8% of the area experienced a decrease in vegetation cover due to oil and gas development and logging activities, especially within 100 m from disturbed sites. Prins (2009) mapped human activity in the oil concession area in southern Sudan using Landsat images between 1999 and 2003 during the preliminary phase of oil exploration and development and discovered an increase in oil infrastructure and road construction.

2.11.1 Other relevant applications of land cover change detection

Accurate and timely land cover change detection at both global and regional scales is essential for studies related to natural resource management and global environmental change using satellite remote sensing, which has been widely used in land cover change detection over the past three decades (Qin et al., 2013). Change detection has found many applications, including land-use changes, habitat fragmentation, the rate of deforestation, coastal change, and urban growth, through the use of spatial and temporal analysis techniques, such as GIS and remote sensing, along with digital image processing techniques (Ramachandra & Kumar, 2004). Change detection has become a valuable tool for studying biophysical and anthropogenic alterations to the Earth's surface (Unger et al., 2015). It continues to affect resilient human communities and ecosystems due to climate change (Mwalusepo et al., 2017). It has also been used to assess nutrient fluxes at the watershed scale in oligotrophic lakes through spatially explicit modelling techniques (Fuentes et al., 2017).

2.12 Geographical information science in land cover change mapping

The combination of remote sensing and geographical information systems (GIS) with expert systems has emerged as a new research frontier (Sharma et al., 2016), widely used and recognised as a powerful and effective tool in detecting land use/land cover change (Kumar et al., 2015), observing, mapping and managing natural assets (Tamta & Bhadauria, 2015) and modelling land cover change. Traditional methods and techniques for monitoring and mapping land use/cover changes, especially in developing countries, are time-consuming and costly, making researchers focus on GIS and remote sensing techniques (Amini Parsa & Salehi, 2016). Remote sensing data not coupled with GIS-based modelling concepts may not develop their full potential in modifying and adapting environmental management principles and mitigation strategies (Hill et al., 2006). GIS and RS will complement many existing cases of wetlands (including mangrove restoration developments) and provide the government and all stakeholders involved in the development of the Niger Delta region with a strategic framework for identifying and calculating projects and programs for the restoration of degraded mangroves and the development of conservation action plans for the sustainable management of Niger Delta mangroves (Adedeji, Ibeh, & Oyebanji, 2011). Some researchers who have used remote sensing and GIS are Eyoh & Okwuashi (2016), to examine the spatial and temporal dynamics of land use/land cover in the Niger Delta region from historical multispectral remote sensing datasets from 1986-2016. Additionally, Kuppusamy & Ganesan (2016) analyse the spatial and temporal environmental changes in Ogoni land due to the intensity of oil spills from 1984 to 2015.

2.12.1 Spatial analysis of land cover change dynamics.

Detecting land cover changes is an important tool for understanding the forces shaping the landscapes (Urban & Wallin, 2002). Spatial analyses of land use/land cover change, such as where and the type of land use/land cover has changed and to what extent this change relates to social and biophysical factors, including why, is important for spatial planning purposes (Karsidi, 2004). The spatial statistics itself is based on the assumption that nearby georeferenced units are associated, including spatial association, pattern analysis, scale and zoning, geostatistics, classification, spatial sampling, and spatial econometrics (Getis, 2005). Remotely sensed data are often highly spatially autocorrelated, and various techniques have been developed to assess the spatial dependence characteristics of remotely sensed imagery (Ganguly et al., 2016). One of the

most popular spatial statistical methods for detecting land use/land cover change (LULCC) hotspots is cluster analysis, which is an effective method for determining areas showing a maximum number of concentrations of land transformations. However, it remains a particularly challenging task to detect hotspots using clustering techniques (Rowland, 2010).

To effectively characterise the impact of oil extraction activities on the land cover in the Niger Delta, there is a need for a multiscale analysis of the land cover changes, especially the vegetation. Integrating oil extraction activities data (oil spills, pipelines, and oil well) with land cover information generated from hyperspectral and multispectral remote will reveal how oil extraction activities have affected the land cover in the Niger Delta. Geographical information systems (GIS) have emerged as a technology that could integrate data from different sources, such as oil extraction activities data and land cover change information. In this study, geospatial technology will be used to understand and visualise the spatial distribution of oil extraction activist data and how they impact the land cover changes in the Niger Delta.

Chapter 3 Methodology

3.1 Introduction

This chapter briefly describes the methodologies for each main research chapter (with the detailed methodologies described in each main research chapter 4-7). This chapter also describes the study area, the traditional Niger Delta. Multi-scale land cover change detection is adopted for these studies to examine the impact of oil extraction activities on the land cover in the Niger Delta, especially the vegetation up to plant-specific. The advantage of this approach is that it allows the impact of oil extraction activities on plant-specific levels to be assessed by utilising both hyperspectral and optical remote sensing. In some cases, the vegetation impacted by oil spills experiences degradation instead conversion to other land cover types. Therefore, a multi-scale land cover change detection, as shown in Figure 3.1, will give more information about the general land cover changes at the landscape scale as well as the information on the state of the health of various vegetation types and some plant species at leaf and plot scales in the Niger Delta.

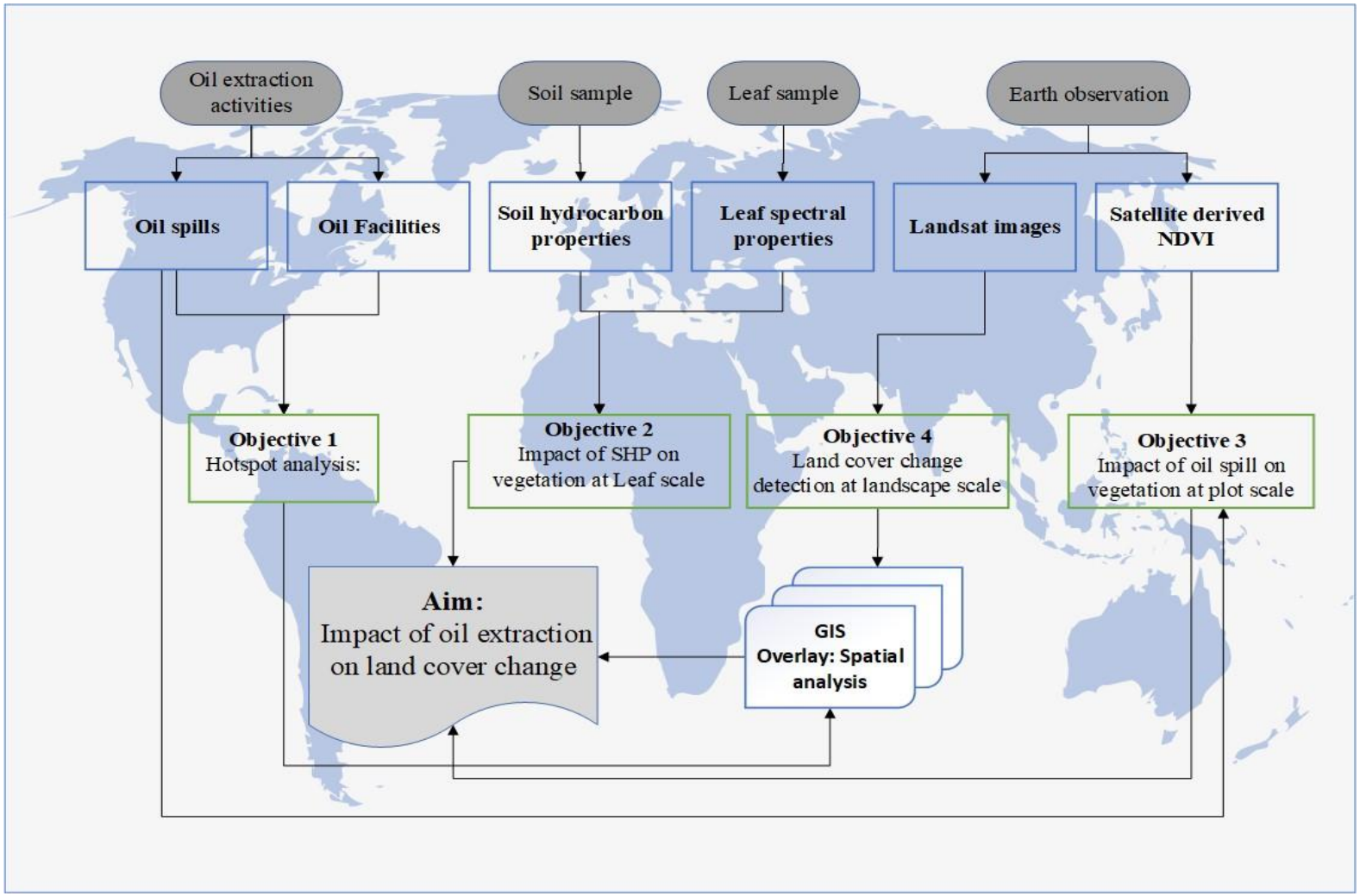

Figure 3.1: General methodology flow chart.

3.2 Study Area.

The Niger Delta region is made up of nine oil-producing states, sometimes referred to as the political Niger Delta, hosting approximately 1500 communities and different oil and gas companies where significant oil and gas productions are currently taking place (Umar et al., 2021). The climate in the Niger Delta region has been categorised as a wet equatorial climate characterised by persistent cloud cover and few sunshine hours, which produces damp weather conditions for most parts of the year (Umar et al., 2019). The vegetation in the Niger Delta comprises mangroves, which cover the coastal region of the delta, along with brackish lagoon and river systems, freshwater swamp forest, rainforest and derived savannah (Ayanlade & Howard, 2017). The dominant mangroves are Red Mangroves (Rhizophoraceae) and White Mangroves (Avicenneaceae), which form more than 90% of the vegetation in the mangrove zone.

Traditionally, the Niger Delta comprises three states of Rivers, Bayelsa and Delta States in Nigeria. These three states account for approximately 70% of Nigeria's oil spillage incidences, while the remainders are in other oil-producing states. The study area is located within longitude 4° 55' E and 7° 39' E and latitudes 4° 7' N and 6° 33' N. Figures 3.1a and b show the traditional Niger Delta in Nigeria and the three states overlaid on a satellite image. Rivers State was formed in 1967 when it was split from the former Eastern Region, and it borders Imo and the Abia States to the north, Akwa Ibom State to the east, and Bayelsa and Delta State to the west. Delta State was created in 1991, while Bayelsa State was created in 1996 from Rivers State, making it one of the newest states in Nigeria. The dominant ethnic groups are Ikwerre, Ijaw and Ogoni, River state, Igbo (Anioma people), Urhobo, Isoko, and Itsekiri in Delta State, with Bayelsa also being the ancestral home of the Isoko people and the Urhobo people in the Sagbama Local Government Area. Ijaw, the dominant ethnic group in Bayelsa State, is also found in the Rivers and Delta states. All the states are oil and agricultural producing states. Figure 3.1a shows the study area, the traditional Niger Delta in red and the political Niger Delta in green in relationship to Nigeria, while Figure 3.2b shows the study area overlaid on Google Earth imagery.

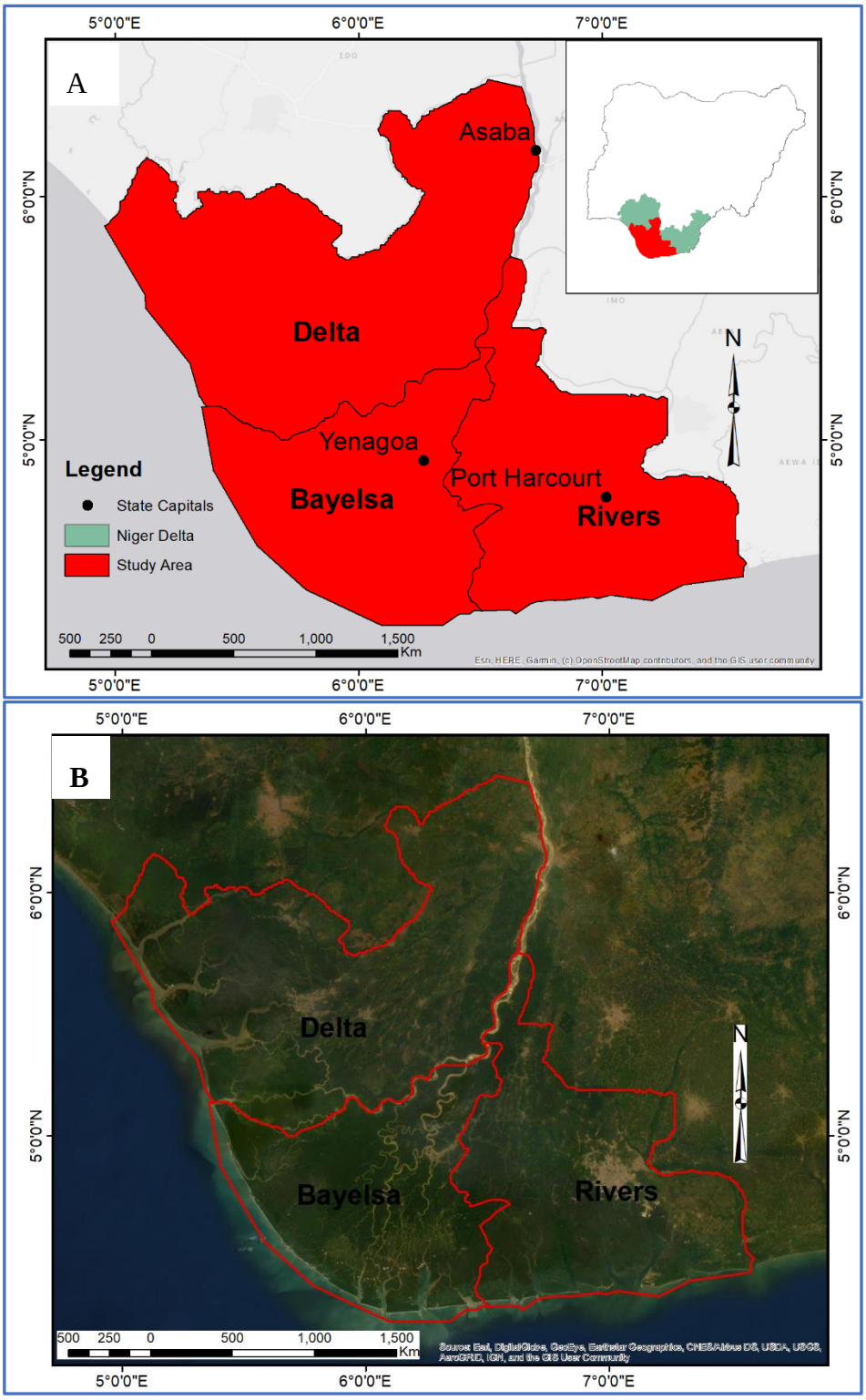

Figure 3.2: Study Area (a) in relation to Niger delta and Nigeria and (b) study area overlaid on Google image.

3.3 Data

3.3.1 Oil spills and oil facilities

Oil spill data were downloaded in Microsoft Excel format from the Nigerian Oil Spill Monitor website (https://oilspillmonitor.ng/) collected by the National Oil Spill Detection and Response Agency (NOSDRA), which was established in 2006 by the National Assembly of the Federal Republic of Nigeria Act of 2006. The data contain both spatial and attribute data for most of the spill points, including the name of the Local Government Areas, incident date, and oil spill volume. NOSDRA depends on the voluntary engagement and support of oil companies to provide data, logistics, quantity estimates, soil/water samples, and clean-up operations. The data gathered and displayed by NOSDRA provided by oil companies are often incomplete because of the operating environment, which is tensed up with insecurity and logistical difficulties. The data represents NOSDRA's knowledge of incidents at a particular moment and are subject to change as new information arises and new records are added daily. This means that there could be more spills that are unrecorded. A total of 12,117 oil spill incidents were recorded in Nigeria from 2007 to 2019, with only approximately 8612 points having geographic coordinates that could be used for spatiotemporal analysis.

Oil facilities, such as oil/gas wells and oil/gas pipelines, were digitised from an oil facility map of 2007 produced by the Global Exploration & Production Service, covering the entire Niger Delta on a scale of 1:750,000. The map was georeferenced using geographic coordinates from four map edges, while linear transformation and resampling were applied. The map was projected to the WGS 84 Universal Transverse Mercator grid system to integrate other data, such as satellite imagery and oil spill data, into the WGS 84 coordinate system. Shapefiles were created for each component: points for oil/gas wells and lines for oil/gas, and the features were manually digitised. It was discovered that the oil pipelines were not accurately located on the map. Hence, high-resolution satellite imagery was used for digitising the pipelines. The locations of oil spill clusters also served as a guide during digitising the oil pipelines since most oil spills occur along the oil pipelines. A total of 1046 oil wells were digitised in ArcGIS 10.4, out of which 498 fell within the study area and were thus selected and used to produce oil well density maps covering the period up to 2007.

The oil spills and the oil facilities data were used for spatiotemporal hotspot analysis of oil spills and oil facilities; oil pipelines and wells (chapter 4) and the assessing the impact of oil extraction on land cover changes (chapter 7), while the oil spill data only was used for monitoring the impact on vegetation (chapter 6). Table 3.1 is the annual oil spills statistics of recorded oil spills in Nigeria. At the same time, Figures 3.3 a and b show the spatial distributions of oil and gas wells and oil pipeline networks.

Table 3.1: Recorded oil Spill incidences in Nigeria from 2007 to 2019. (NOSDRA)

Year	Total Number of oil Spill	Oil spill with coordinates	Spills points for analysis
2007	989	101	99
2008	948	146	95
2009	810	321	278
2010	860	599	492
2011	1032	799	709
2012	1095	942	801
2013	1678	1478	1277
2014	1545	1490	1335
2015	881	844	775
2016	582	567	514
2017	419	401	363
2018	385	370	347
2019	616	594	537
Total	11840	8650	7622

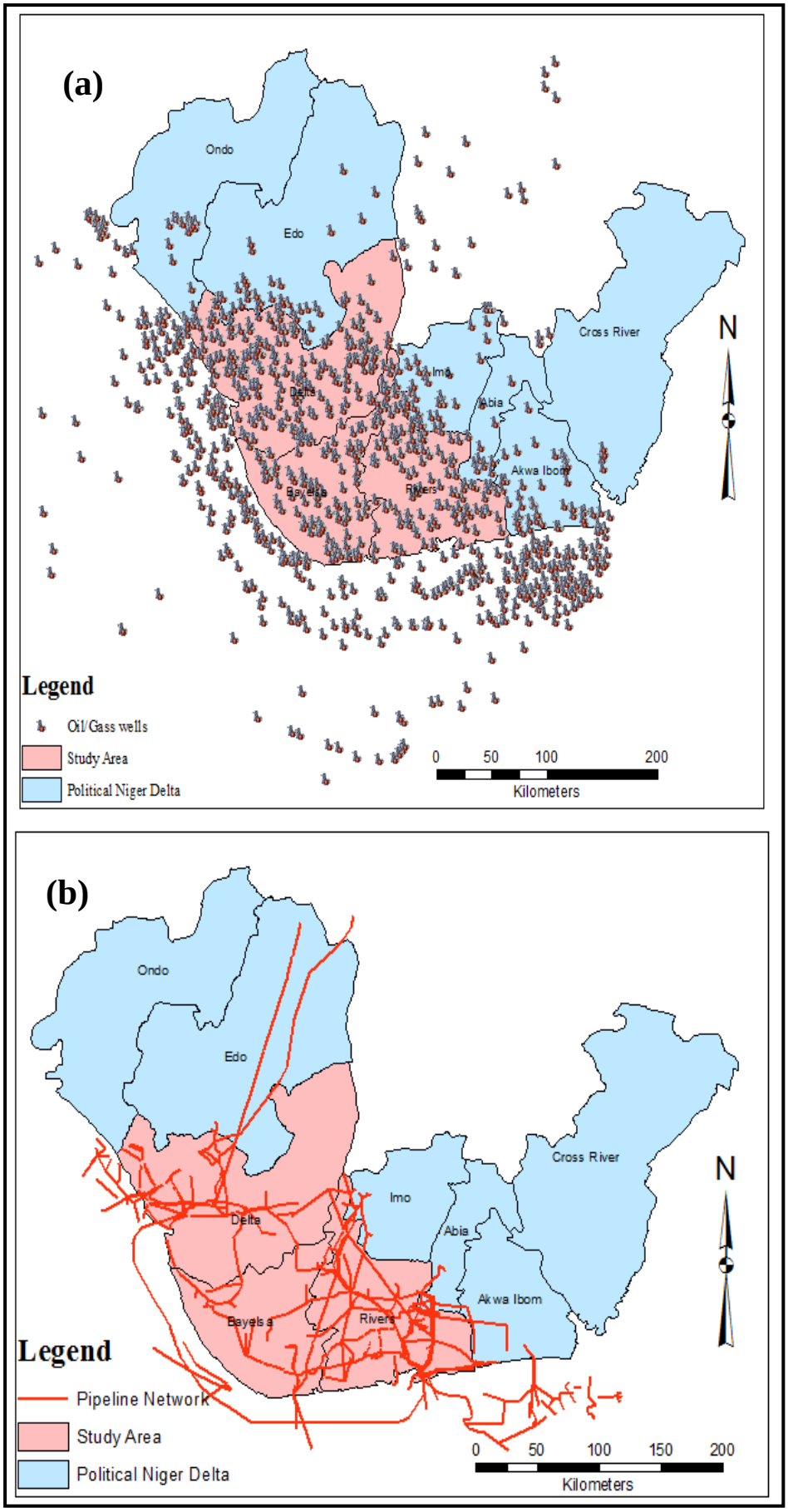

Figure 3.3: Oil facilities map in Nigeria: (a) oil wells and (b) oil/gas pipelines.

3.3.2 Leaf spectra and soil samples

Spectral samples of leaves and soil samples at oil spill sites were collected during a field visit in December 2018 to the Niger Delta region. The timing of the trip was chosen because the weather conditions were more favourable, with almost zero rainfall. Before the fieldwork, a reconnaissance trip was carried out in June 2018, accompanied by staff from the University of Port Harcourt, Nigeria, and some community members. The sample collection sites were chosen based on accessibility to the site since it was not viable to perform random sampling due to insecurity in the region. It is noted that this could introduce some degree of unavoidable bias in the results obtained. Leaf samples from five different plant species from different families at oil spill locations with different levels of hydrocarbon pollution were sampled. They include samples from trees, grasses, and mangroves. The sample collection areas were divided into 30 m-by-30 m plots to match the spatial resolution of Landsat imagery, which was used for both temporal monitoring of the impact of oil spills on the land cover using NDVI and land cover change detection.

3.3.3 Satellite data

3.3.3.1 Satellite Images

The main datasets used in this thesis were acquired from Landsat 4/5 (1987), Thematic Mapper (TM), Landsat 7 (2003), Enhanced Thematic Mapper Plus (ETM+), and Landsat 8 (2016) Operational Land Imager (OLI)/Thermal Infrared Sensor (TIRS) instruments. The Landsat images were limited to three dates due to cloud cover and Landsat 7 Scan Line Corrector (SLC)-off, which affects all Landsat 7 images collected after May 31, 2003, when the Scan Line Corrector (SLC) failed. There have been limited studies on land cover mapping in the Niger Delta as the area is one of the most affected worldwide by the gaps in the Landsat archive and a consistent cloud cover (Nababa et al., 2020). Though the Scan Line Corrector would have been corrected using various interpolation methods, however, the image is mostly good for visualization, but the problem of cloud cover will still persist. The interpolation is based on the assumption that the same-class neighbouring pixels around the un-scanned pixels have similar spectral characteristics and that these neighbouring and un-scanned pixels exhibit similar patterns of spectral differences between dates (Chen et al., 2011), which may not be true for a heterogeneous study area like the Niger Delta.

These data comprised Calibrated Level 1 data products downloaded from the USGS website (https://glovis.usgs.gov/app?fullscreen=1). Landsat sensor data were used because they provide the highest temporal resolution at medium spatial resolution for the period required for this study. All the images were calibrated for time-series analysis, geometrically corrected, and projected to WGS84 Universal Traverse Mercator Projection Zones 31 and 32. The essential goal of the new Landsat product is to provide a consistent Landsat archive with improved geometric and radiometric quality across different sensors (Li et al., 2018; Zanter, 2019). The calibration employs algorithms and processes that improve Landsat data by converting the DN values of the data to spectral radiance and reflectance at the sensors level, followed by the removal of atmospheric effects (Landsat-Missions, n.d.). Table 3.2 presents the list of sensors, path/row, date of acquisition, the UTM zone, and pixel sizes, while Figures 3.4a, b and c provide illustrations of 1987, 2002/2003 and 2015/2016 false-colour composites. These false-colour composites were used for land cover change modelling in Chapter 7.

Table 3.2: Landsat sensor platforms, paths/rows and pixel sizes.

Satellite	Sensor	Path/Row	Date of Acquisition	UTM Zone	Pixel sizes(m)
L5	TM	188/57	21/02/1987	32	30
L4	TM	189/56	21/12/1987	32	30
L4	TM	189/57	21/12/1987	31	30
L5	TM	190/56	03/02/1987	31	30
L7	ETM	188/57	08/01/2003	32	30
L7	ETM	189/56	30/12/2002	32	30
L7	ETM	189/57	30/12/2002	31	30
L7	ETM	190/56	21/12/2002	31	30
L8	OLI_TIRS	188/57	04/01/2016	32	30
L8	OLI_TIRS	189/56	26/12/2015	32	30
L8	OLI_TIRS	189/57	26/12/2015	31	30
L8	OLI_TIRS	190/56	02/01/2016	31	30

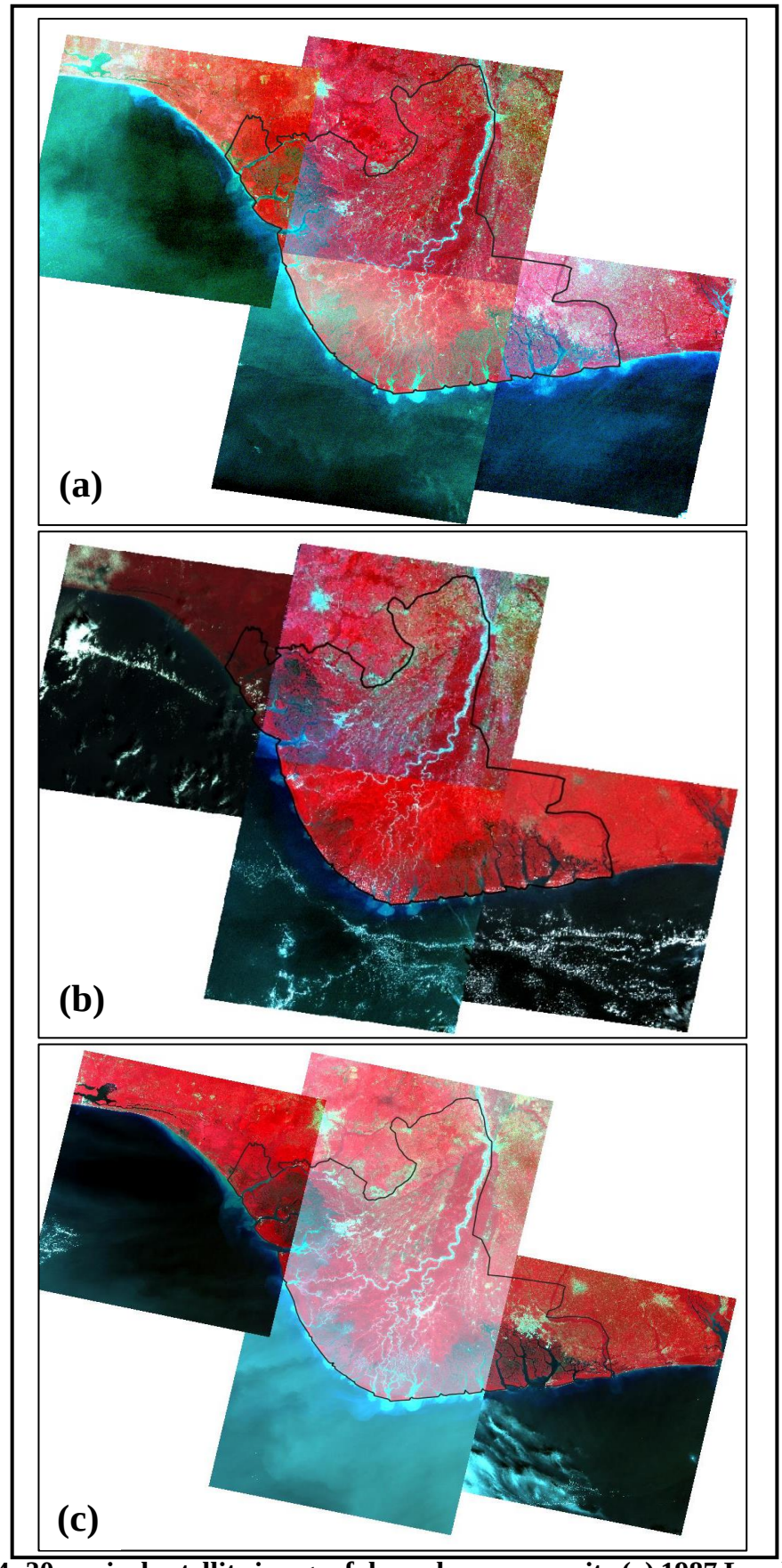

Figure 3.4: 30 m pixel satellite images false-colour composite (a) 1987 Landsat 5 TM 234 Band composite, (b) 2003/2003 Landsat 4 TM 234 band composite, and (c) 2015/2016 Landsat 8 OLI 345 234 band composite.

3.3.3.2 Satellite-derived NDVI

Landsat Surface Reflectance-derived NDVI products were used to monitor the effect of oil spills on vegetation. They are a product from section 3.3.3.1 processed to Landsat Level-2 Surface Reflectance products (https://www.usgs.gov/landsat-missions/landsat-normalised-difference-vegetation-index). The NDVI is an index of plant greenness, which is also an indicator of the density of plants (Okoro, Schickhoff, Böhner, & Schneider, 2016) based on the reflectance properties of the areas covered by the vegetation (Rujoiu-Mare & Mihai, 2016). The NDVI is calculated using $\mathrm{NDVI} = (\mathrm{NIR} - \mathrm{RED})/(\mathrm{NIR} + \mathrm{RED})$. The RED and NIR represent the spectral reflectance measurements acquired in the red (visible) and near-infrared regions. Tables 6.1 and 6.2 in Chapter 6 shows the Landsat sensor platforms, paths/rows, pixel sizes, and NDVI acquisition dates for satellite-derived NDVI. NDVI was used instead of other vegetation indices because it has been proven effective in detecting the oil spill's impact on vegetation. The NDVI is the most suitable index to detect the effects of petroleum pollution on vegetation (Arellano et al., 2015). Adamu (2016) discovered that the NDVI is the most sensitive to the effects of oil pollution on vegetation in the mangrove forest South-West of Port Harcourt City in the Niger Delta out of 20 broadband multispectral vegetation indices (BMVIs) derived from Landsat satellite. Using NDVI will also enable the results from this research to be compared with other authors that have used it in some parts of the Niger Delta to investigate the impact of oil spills on the vegetation.

3.4 Methodological approach

3.4.1 Hotspot analysis.

Before undertaking the hotspot analysis, the oil spill data was prepared in ArcMap 10.4. The oil spill points were first plotted, and the spills that fell within the study area were selected for the hotspot analysis. A total of 8650 oil spill incident points were recorded with coordinate values between 2007 and 2019. However, only 7622 oil spill incidents within the study area were selected and analysed since some were outside the study area.

For oil spill locations, the hotspot analysis was based on two spatial distribution techniques: Moran's I and the Getis-Ord General statistic, which are global measurements of the overall pattern and trend of spatial autocorrelation displayed by numerical data. At the same time, cluster analysis was performed using the Getis-Ord Gi* local statistic.

Kernel density estimate (KED) was used for the oil wells and pipeline hotspot mapping. The detailed method is discussed in Chapter 4.

3.4.2 The effect of soil hydrocarbon properties on vegetation at the leaf-scale

3.4.2.1 Spectral measurements

Spectral measurements of leaf samples were performed using an Analytical Spectral Devices (ASD) FieldSpec Pro. The ASD FieldSpec Pro instrument is the industry standard for a broad range of challenging remote sensing applications and offers superior signal-enhancing features and high resolution within the 350-2500 mm spectral range. The instrument is backpack-mounted, it can collect spectral measurements on the go (fsf.nerc.ac.uk/instruments/asd_FieldSpec.shtml) and can also be used in a laboratory setting with appropriate illumination. The spectroscopy is discussed in detail in chapter 5.

3.4.2.2 Soil sample analysis

The interaction between hydrocarbons and the soil reduces the amount of oxygen and increases the CO_2 concentration, soils turn acidic and mobilise minerals, affecting vegetation health (Arellano et al., 2015). The soil samples collected during the field were analysed at the British Geological Survey Lab, Keyworth, to determine the amount of hydrocarbons and other properties of the soil, which were then used for correlation analysis with the leaf spectral properties to determine the effect of soil hydrocarbon characteristics on the health of vegetation. Solid-phase microbial toxicity (EC50), total organic carbon (TOC %), total petroleum hydrocarbons (TPH) and Rock-Eval analyses were conducted on the soil samples. The detailed method is discussed in Chapter 5.

3.4.2.3 Spectral analysis

The ASD FieldSpec Pro measured leaf reflectance spectra were converted to the first derivative, and then the red edge position (REP) was extracted for each leaf sample. Also, Spectral resampling was performed using the Spectral Library Resampling tool in ENVI. This tool performs multiplication-based convolution of all laboratory spectra to wavebands of three satellite sensors: Heperion, Sentinel 2 and Landsat 7). Similarly, the spectra were also used to compute several HVIs: Modified Normalised Difference Index (mND_{705}), Modified Datt index (MDATT index), Normalised Difference Vegetation Vigour Index (NDVVI) and Photochemical Reflectance Index (PRI). The REP and HVIs were used to analyse the spectral properties of different leaf species with soil hydrocarbon parameters.

3.4.3 Monitoring the impact of oil spills on vegetation at the plot scale

Regression and Student's paired t-tests were used to analyse the impact of oil spills on vegetation in the Niger Delta. This analysis is broadly divided into two parts. The first part investigated the factors that influenced the detectability of the impact of oil spills on vegetation health using spectral indices derived from satellite images. The second part conducted temporal monitoring of vegetation health/recovery after an oil spill for some period by comparing changes in NDVI between spill sites and no-spill sites. First, the oil spill sites in the database were plotted in ArcGIS and converted to shapefiles. Not all spill occurrences had a recorded spill volume, so only those with a recorded volume were retained for analysis. The regression and t-test analyses were performed to examine the relationship between oil spill characteristics, volume and time after the oil spill, and vegetation health and to test for statistical differences between the response of vegetation in the spill and non-spill sites. NDVI from Landsat images was used because it has been used and found to be able to detect the impact of oil spills on the mangrove vegetation in the Niger Delta by Adamu (2016); Adamu et al. (2018); Obida et al. (2021). The detailed method is discussed in Chapter 6.

3.4.4 Land cover change dynamics in response to oil extraction

3.4.4.1 Pre-classification analysis

Three spectral bands (234 for 1987, 2002 and 345 for L8 OLI_TIRS false colour, which are spectrally equivalent) of Landsat imagery were used for land cover classification since vegetation is the predominant land cover, and the band combination is good in depicting vegetation. A layer stacking operation collated the three Landsat bands into a single colour composite image. Then, the layer-stacked images from four Landsat scenes covering the study area were mosaicked into a single image. Mosaicking is the merger of several arbitrarily shaped images to form one large radiometrically balanced image so that the boundaries between the original images are not seen (Inampudi, 1998). The mosaicked images were clipped (subset) to the extent of the study area.

3.4.4.2 Supervised land cover classification

The land cover supervised classification was performed in three stages: image segmentation, training site development and classification. In object-based classification, the main goal of image segmentation is to partition an image into uniform and homogeneous attribute regions based on some likeness measure (Chen & Ludwing,

2017). The segmented image was used to develop a set of training sites and input. The supervised classification was performed using six different soft and hybrid classifiers in TerrSet 2020 Geospatial Monitoring and Modelling Software on 2016 Landsat image. These were the Bayesian (BAYCLASS), Mahalanobis typicalities (MAHALCLASS), linear spectral unmixing (UNMIX), and self-organising map (SOM) neural network classifiers. The hybrid hard and soft classifiers are the decision forest and support vector machine (SVM). These classifiers were all used for land cover classification, and the best performing classifier was chosen for land cover change detection.

3.4.5 Soft classifiers algorithms

The classifiers used were chosen to represent a variety of algorithms, including those used in the study area and those that have not been used in the study area but have performed well in other study areas. The classifiers used in this research are Artificial Neural Network algorithm (ANN), Machine Learning algorithms, probabilistic and Mahalanobis Typicality Image classification using neural networks is done by texture feature extraction and then applying the back propagation algorithm .

3.4.5.1 BAYCLASS and Bayesian Probability Theory (Bay)

BAYCLASS is the direct extension of the maximum likelihood module. It outputs a separate image to express the posterior probability of belonging to each considered class according to Bayes 'Theorum. $p(h|e)$ = the probability of the hypothesis being true given the evidence (posterior probability) $p(e|h)$ = the probability of finding that evidence given the hypothesis being true $p(h)$ = the probability of the hypothesis being true regardless of the evidence (prior probability).

3.4.5.2 Mahalanobis Typicality (MAHALCLASS)

The Mahalanobis distance image classification algorithm was developed by an Indian applied statistician Mahalanobis in the 1930s (Talukdar et al., 2020). The Mahalanobis is a class statistic-based classifier that is direction-sensitive in operation and has an advantage over the maximum likelihood procedure because it is faster and retains a degree of direction sensitivity (Richards & Jia, 2006). To classify a test pixel that belongs to one of the N numbers of classes, the estimation of the covariance matrix of each class is done first, which is typically established on the training data known for belonging to such class(Karan & Samadder, 2018). After that, the algorithm computes the Mahalanobis

distance to every class and classifies the test pixel as belonging to that class for which the MLD is minimum.

3.4.5.3 Support vector machine (SVM)

The Support vector machine(SVM) was originally designed for binary classification (Hu et al., 2014). SVM is a group of relatively new machine-learning algorithms designed to find optimal classification solutions (Townshend et al., 2012). SVM are non-parametric learning algorithms that can compete with the best available machine learning algorithms and work well with a small training data set with high classification accuracy (Sharma et al., 2016). SVM classification methods offer more flexibility in the relationship between the inputs and the probability of the classes (Berrett & Calder, 2016)

3.4.5.4 Decision Forest (DF)

Decision forest is currently one of the most popular classification procedures in use. It implements the random decision forest (RDF) algorithm, a modification of the random forest algorithm (Eastman, 2020). Its classification is based on many trees derived from different random draws of training data and different random selections of input variables. It is a popular classifier because it can perform well with classes that are not normally distributed. Both the SVM and DF are nonparametric statistical and hybrid (hard and soft) classifiers.

3.4.5.5 Self-Organising Feature Map (SOM)

SOM is one of the neural network classifiers that can produce both hard and soft outputs. The SOM has both vector quantisation and vector projection properties and can be used for unsupervised and supervised classification (Li and Eastman 2010). A SOM network is made up of two layers; an input layer containing one neuron for each of the input variables, and an output layer made up of a two-dimensional array of neurons (Grebby et al., 2011). The self-organizing map (SOM) neural network was developed by Kohonen (1982). The SOM can undertake both unsupervised and supervised image classification and, can output both soft and hard map

3.4.5.6 UNMIX and the Linear Mixture Model

The UNMIX module is used to classify remotely sensed images using Linear Spectral Unmixing (LSU -- also called Linear Mixture Modelling). The approach assumes that a pixel value is a combination of the means of the signatures of all the classes present in

the pixel which lead to an aggregate signature that is an area-weighted average of the signatures of the constituent classes (Eastman, 2016).

3.4.6 Post-Classification analysis.

The land cover post-classification analysis includes accuracy assessment, classified map clean-up, and land cover change detection. The initial accuracy of the land cover maps from the six classifiers was assessed using a confusion matrix with high-resolution images from google earth used for ground truthing. Due to the size of the study area, inaccessibility, and security concerns in the Niger Delta, instead of a site visit approach for ground truth to collect or validate the classified map, an alternative approach of using a high-resolution google earth image was explored. Google Earth's high-resolution imagery is important for ground-truthing because it provides temporal images of the same or close time image and has some advantages over the traditional approach, as stated in section 2.9.6. The method used to generate the ground truth sample point is explained in section 7.2.3.3

After the accuracy assessment (detailed in section 7.2.3.3), the classifiers were narrowed down to two best-performing classifiers based on the overall accuracy of the confusion matrix. They were further subjected to visual analysis to determine the best classifier choice to meet the research objective. Olofsson et al. (2014) suggested that land cover maps should be visually inspected, and obvious errors should be identified and corrected before conducting the accuracy assessment. Of the two best-performing classifiers, Mahalanobis typicalities and Bayesian, the Bayesian classifier was the best, with fewer spectral similarities among the land cover class and was chosen for the land cover mapping. Post-classification clean-up was carried out on the maps produced by the Bayesian classifier to overcome the problem of spectral similarities associated with two or more land covers, which were still evident. After the map clean-up, the final accuracy assessment was performed on the cleaned map, which was used as input for land cover change detection. The land cover change was detected in terms of conversion and degradation using land cover maps and NDVI maps, respectively. Lastly, spatial analysis of the land cover changes was performed in the GIS environment to determine the relationship between land cover changes and oil extraction activities in the Niger Delta.

.

Chapter 4 The spatiotemporal distribution of oil spills and oil facilities in the Niger Delta region

4.1 Introduction

Hazardous materials are indispensable for a production-driven economy (Park et al., 2016). Environmental pollution has become one of the most severe threats to human survival (Wang, Li, & Xi, 2016). Oil spills and other environmental pollution have led to a persistent and growing interest in better understanding the potential ecological, environmental, social, economic, cultural, and epidemiological implications of catastrophic spills, regardless of their form (Nelson & Grubesic, 2017). The prevalence of oil spills in the Niger Delta has led to severe environmental degradation and a range of impacts on the human population (Obida et al., 2017). Oil spills, which are considered a serious environmental problem (Ivanov & Zatyagalova, 2008), are reasonably well documented in Nigeria. However, information on potential impacts on the population and environment is limited (Obida, Blackburn, Whyatt, & Semple, 2018). The impact of oil spills due to oil extraction activities, usually on the land cover in the Niger Delta, is visible and has brought untold hardship to humans, fauna, the region's environment and land cover. A visit to the Niger Delta shows a beautiful landscape destroyed by the oil spill incidence over the years. Cleanup and remediation of the environment are urgently needed to save the lives of humans, animals and the environment. However, understanding the nature of oil spill incidences in the Niger Delta will provide the required information needed to handle the effect of oil spills in the area. Oil spill modelling is essential for planning and preparing for and responding to and mitigating actual spill events (Nelson & Grubesic, 2017). It could be used to understand the land cover changes in temporal and spatial domains in the Niger Delta. It is critical, therefore, to track the incidents using appropriate and timely data collection and analytical techniques even if the harmful effects are not currently visible.

Geographical information systems (GIS) have proven to be an efficient tool for collecting, visualising, and analysing oil spills by incorporating spatial and temporal information (Giziakis et al., 2013). Spatial-temporal hotspot pattern analysis of environmental pollution incidents provides an indispensable source of information for further developing incident prevention measures (Ding et al., 2015). Hotspots, which are concentrations of occurrences within a limited geographical area that appear over time (Levine, 2007), can reveal statistically

.

significant clustering in the spatial pattern (Harris et al., 2017; Stopka et al., 2014) of oil spill incidences in the Niger Delta.

Hence, to fill the research gap identified in 1.3, this chapter focuses on mapping and examining the spatiotemporal evolution and changes detection of oil spill hotspots, oil facilities hotspots and the spatial distributions of oil facilities in the Niger Delta using spatial statistics. The oil spill hotspots trend over a period of 13 years will be used to identify locations that are constantly exposed to oil spills. To the best of my knowledge, this is the first study conducted in the study area that looks at annual oil spill hot spots and detects changes that have occurred between any two hotspot dates. Prioritising relevant locations of constant exposure to oil spills will help better understand the existing problems in the Niger Delta. Therefore, the identification of hotspot locations could help the government, oil companies, and decision-makers formulate policies that could combat future spills. Furthermore, identifying the most vulnerable oil pipelines, understanding the impact of the oil spills on land cover, and identifying possible factors encouraging oil pipeline sabotage could help pipeline surveillance and land cover restoration, especially for vegetation and water.

Spatial statistics can be used to establish the statistical relationship among data based on their locations and identify spatial dependence through correlation and self-correlation within data related to their geographical positions over a period of time (Wang et al., 2016). With this in mind, the main aim of this chapter is to evaluate the spatiotemporal distributions of oils spills and production facilities in the Niger Delta. The main objectives are to conduct (1) temporal analyses of oil spill data; (2) hotspot analyses of oil spills and oil facilities; and (3) spatial analyses between oil spill hotspots and oil facilities.

4.2 Methodology

Figure 4.1 is the graphical summary of the methodological approach used for this chapter.

.

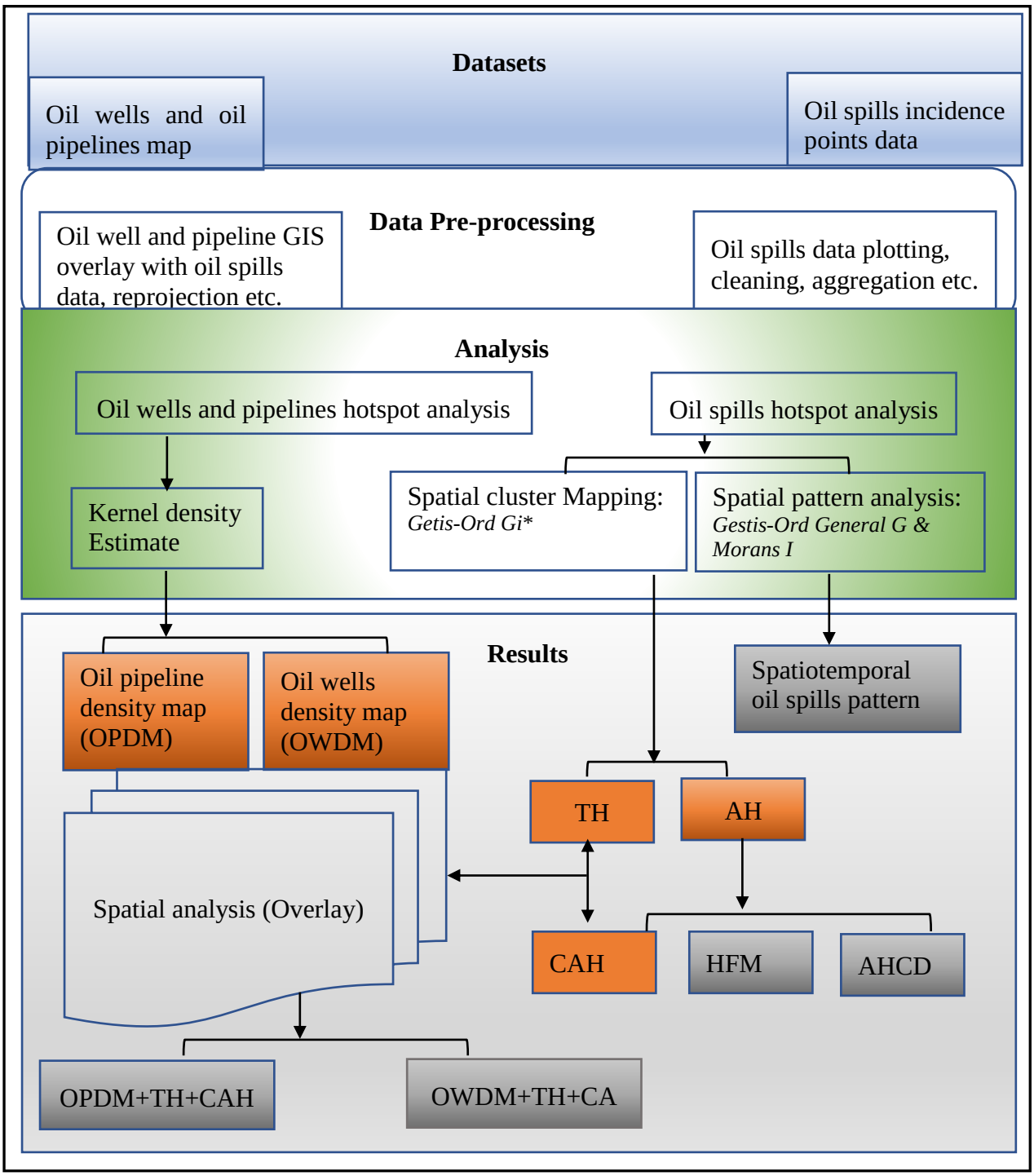

Figure 4.1: Methodology flow chart.

AHS=Annual hot spot, CAH=Combined annual hotspot, TH=Total hotspot, HFM Hotspot frequency map, AHCD=Annual hotspot change detection

.

4.2.1 Data

4.2.1.1 Oil spill and oil well data

The oil spill data were obtained from the official website of the Nigerian Oil Spill Monitor (https://oilspillmonitor.ng/) as described in Section 3.3.1. These data were compiled by the National Oil Spill Detection and Response Agency (NOSDRA), established by the National Assembly of the Federal Republic of Nigeria Act of 2006. This oil spill incident record is dated from 2007 to 2019 and presented alongside their geographic coordinates. Figure 4.2 shows the distribution of oil spill occurrences used for the hotspot analysis, and a total of 7622 oil spill incidences were used. Additionally, the oil well and pipeline map from 2007 was generated based on the digitisation of the Global Exploration & Production Service map, as also described in Section 3.3.1. The map of the spatial locations of oil spill incidence, oil wells and the pipeline are shown in Figures 3.2 a and b in section 3.3.1.

4.2.2 Methods

4.2.2.1 Data preparation

Since the focus of oil spill incident data hotspot analysis was to assess incident intensity more than in analysing the spatial clustering of any particular value associated with the incidents, the data were aggregated prior to analysis. The oil spill points were aggregated to collect and summarise oil spills incidence point features within a set of boundaries. Aggregating point data into territorial units fosters a more comprehensible presentation of results (Burian et al., 2022). Before the oil spill data aggregation, a fishnet was created using Create Fishnet tool in ArcGIS to construct a polygon network of regular grids over the point features. To choose the fishnet size, the Optimised Hot spot Analysis was performed on combined oil spills data from 2007 to 2019 in ArcGIS, which returned a hotspot with a grid size of approximately 3000 m. The aggregation strategy using fishnet serving as administrative units that remain fixed across multiple analyses enhanced making comparisons between annual hotspots and detect changes in annual hotspots at the same scale. The number of spill events falling within each grid polygon was then computed using spatial Join Tool in ArcGIS. Any grid polygons outside the study area and those containing zeros were disregarded from the analysis.

4.2.2.2 Spatiotemporal pattern analysis

There are three types of outcomes of hotspot analysis each for Moran's I and Gestis-Ord General G. Dispersed, random, and clustered (Moran's I), and low-clusters, random and high clusters (Gestis-Ord General G). The global Moran's I is based on the covariance relationship

.

of the statistical correlation coefficient (Cheng et al., 2018), which measures spatial autocorrelation based on feature locations and attribute values. At the same time, Getis-Ord General G identifies statistically significant hot and cold spots by measuring the degree of clustering for either high or low values. Large positive values indicate that higher than average values are clustered, whereas large negative values indicate lower than average values (Mueller-Warrant et al., 2008). The Getis-Ord statistic gives more intuitive results and a better visual representation than Moran's I index. It has the advantage of distinguishing high-value clusters or low-value clusters (Ding et al., 2015). The z-score and *p*-value_measure the statistical significance, which informs whether to reject the null hypothesis, stating there is no spatial cluster of feature values.

The spatial join tool in ArcGIS was used to aggregate the oil spill incidence points for each year within each polygon of the fishnet. The aggregated annual oil spill incidence data were used as an input for the pattern analysis of oil spills for 2007-2018 and the combined total oil spills from 2007 to 2019.

Moran's *I* statistics for spatial autocorrelation are given as follows:

$$I = \frac{n}{So}\frac{\sum_{i=1}^{n}\sum_{j=1}^{n} z_i z_j}{\sum_{i=1}^{n} z_i^2 y} \qquad \text{Eq 4.1}$$

wherez_i is the deviation of an attribute for i from its mean $(x_i - \bar{X})$, $\omega_{i,j}$ is the spatial weight between featurei,j,n is equal to the total number of features, and So is the aggregate of all the spatial weights:

$$S_o = \sum_{i=1}^{n}\sum_{j=1}^{n} \omega_{i,j} \qquad \text{Eq 4.2}$$

The z_I-score for the statistic is computed as:

$$z_I = \frac{I - E[I]}{\sqrt{V[I]}} \qquad \text{Eq 4.3}$$

where:

$$E[I] = -1/(n-1) \qquad \text{Eq 4.4}$$

$$V[I] = E[I^2] - E[I]^2 \qquad \text{Eq 4.5}$$

While

The general G statistic of the overall spatial association is given as:

$$\boldsymbol{G = \frac{\sum_{i=1}^{n}\sum_{j=1}^{n} \omega_{i,j} x_i x_j}{\sum_{i=1}^{n}\sum_{j=1}^{n} x_i x_j}, \forall j \neq i} \qquad \text{Eq 4.6}$$

.

Where $x_i$and x_j are attribute values for features$i$ and $j\omega_{i,j}$ is the spatial weight between features$i$ and$j$. n is the number of features in the dataset, and $\forall j \neq i$ indicates that features$i$ and$j$ cannot be the same feature.

The zG for the statistic is computed as:

$$\boldsymbol{zG} = \frac{\boldsymbol{G}-\boldsymbol{E}[\boldsymbol{G}]}{\sqrt{\boldsymbol{V}[\boldsymbol{G}]}} \quad \text{Eq. 4.7}$$

where:

$$\boldsymbol{E}[\boldsymbol{G}] = \frac{\sum_{i=1}^{n}\sum_{j=1}^{n}\boldsymbol{\omega_{i,j}}}{\boldsymbol{n(n-1)}}, \forall \boldsymbol{j \neq i} \quad \text{Eq. 4.8}$$

$$\boldsymbol{V}[\boldsymbol{G}] = \boldsymbol{E}[\boldsymbol{G^2}] - \boldsymbol{E}[\boldsymbol{G}]^{\boldsymbol{2}} \quad \text{Eq. 4.9}$$

4.2.2.3 Hotspot mapping

The Getis-Ord Gi* local statistic was computed for the annual oil spill data for 2007-2019. The annual oil spills and combined total oil spill incidences between 2007 and 2019 were used to determine the annual hotspots (AHS) and total hotspots (TH) from 2007 to 2019. The combined annual hotspot CAH was obtained by merging all the AHS from 2007 -2019. AHS are hotspots for each year, while the TH is the hotspot when all the annual oil spill data from 2007 – 2019 were combined as one set of data. The hotspot analysis was performed using the aggregated annual and combined total oil spill incidence data (described in 4.2.1.2). The Fixed Distance Band method, which is the default recommended for the conceptualisation of the Spatial Relationships for Hot Spot Analysis (Getis-Ord Gi*) tool in ArcGIS 10.4.1 software performs well for point data and was used as a threshold distance to ensure that each oil spill incidence point had a neighbour. The Getis-Ord Gi* statistic considers each different features within the context of the neighbouring feature to determine statistically significant hot spots (Park et al., 2016). The resultant z-scores and p-values indicate where features with either high or low values cluster spatially. The Getis-Ord Gi* local statistic is given as:

$$G_i^* = \frac{\sum_{j=1}^{n}\omega_{i,j}x_j - X\sum_{j=1}^{n}\omega_{i,j}}{S\sqrt{\frac{[n\sum_{j=1}^{n}\omega^2{}_{i,j} - (\sum_{j=1}^{n}\omega_{i,j})^2]}{n-1}}} \quad \text{Eq. 4.10}$$

where$x_j$is the attribute value for j, $\omega_{i,j}$ is the spatial weight between feature i and$j$, n is equal to the total number of features and:

$$\bar{X} = \frac{\sum_{j=1}^{n}x_j}{n} \quad \text{Eq. 4.11}$$

$$S = \sqrt{\frac{\sum_{j=1}^{n}x_j{}^2}{n} - (\bar{X})^2} \quad \text{Eq. 4.12}$$

The G_i^*statistic is a z-score, so no further calculations are needed.

.

4.2.2.4 Spatiotemporal annual hotspot change detection

This analysis was conducted to determine how the hotspots evolve annually across the study area. The first step in mapping the spatiotemporal hotspot changes was to convert the vector hotspot maps into rasters containing integers with the same cell sizes as the input vector polygon. The next stage was reclassifying the converted raster into Boolean images with values of 1 and 0. Reclassifying data means replacing input cell values with new output cell values with input data from any supported raster format (ESRI, 2002). A value of 1 was given to the locations with hotspots, while 0 was allocated to "No data" locations where hotspots did not occur. The raster calculator tool in ArcGIS was used to compute the various changes in the annual hotspots using the reclassified hotspot raster maps. For consistent hotspot (CH) in any locations between 2 dates, multiplication of the reclassified raster maps with 1 and 0 values was performed. In contrast, subtraction was used for the disappeared hotspots (DH) and appeared hotspots (AH) using eq 4.13 and eq 4.14. Similarly, just like the CH, for hotspot frequency map (HFM) for all dates from 2007 -2019 was performed by adding all the reclassified annual hotspot raster maps using eq 4.15, which returned values based on the number of years the hotspot had occurred

$CH = hs^1 \times hs^2$ Eq. 4.13

$DH \text{ and } AH = hs^2 - hs^1$ Eq. 4.14

which will return either -1(DH) or 1(AH)

$HFM = hs^1 + \ldots\ldots hs^n$ Eq. 4.15

where hs^1 = first date hotspot (previous year)

hs^2 = second date hotspot (later year)

hs^n = hotspot at a particular number of years.

Using eq 4.13, a location with values of 1 in any of the output maps means that such a hotspot did not change between two consecutive years (i.e., no change). For equation 4.14, the DH and AH, a value of -1 are areas with a hotspot in $hs^{1,}$ which could not be found at those same locations in hs^2, while a value of 1 is an area without hotspot $hs^{1,}$ which suddenly appeared in hs^2. For eq 4.15, the number correspond with the frequency (number of years) a hotspot has occurred at a particular location.

.

4.2.2.5 Kernel density estimate of oil wells and pipelines

For spatial analysis and visualisation of oil wells and oil pipelines, the kernel density estimate (KDE) was used. The objective of KDE is to produce a smooth density surface of point events over space by computing event intensity as density estimation (Lin et al., 2011). KDE is specifically suitable for detecting hotspots (Kalinic, 2018), and it is considered the most accurate of these common hotspot mapping techniques (Chainey, 2013). It is particularly useful in detecting hotspots due to the series of estimations (Kalinic, 2018). The KDE was chosen to map the hotspots of oil facilities because it can also calculate a magnitude-per-unit area from polyline features, such as oil pipeline (network-based kernel) and the oil wells' location (points).

4.3 Results

4.3.1 Temporal oil spill pattern

Table 4.1 shows the monthly and annual distribution of oil spill incidences from 2007 to 2019, revealing the months with the lowest and highest number of spill incidences in each year and the years with and without recording the highest number of oil spill incidences in any month. Monthly spills (MS) are the number of spills in a month within each year (in columns), whereas the Annual Monthly Total (AMT) is the total spills per month for all the years (i.e., all the spills in January for all the years; the rows). The Annual-Monthly Highest Number of Spills (AHNS) and Annual-Monthly Lowest Number of Spills (ALNS) are the highest or lowest number of spill incidences per annum that fall in a particular year (number of the highest or lowest number of spills that occurred in January). The rows in orange show the months with at least one highest oil spill incidence in a particular year, while the green rows are months that never experienced the highest oil spill in any given year. The text in red and green are the highest and the lowest oil spill incidences in a month in a particular year. For example, in 2007, the highest and lowest oil spill incidences occurred in July (15 spills) and March-April (4 spills). From Table 4.1, the most oil spills occurred in January 2014, with 165 spills (which incidentally has the highest annual total oil spill incidence), while the fewest spills were recorded in April and May 2007, with 4 spills each (which incidentally has the lowest annual total oil spill incidence). Additionally, based on the monthly summary, the month of May has both the highest AMT (695), which accounts for 9.81% and AHNS (4), while April has the lowest AMT (504), which accounts for 7.11%.

.

Table 4.1: Monthly and annual oil spills within the study area.

	Years													Total oil spills (TOS)			
Month	2007	2008	2009	2010	2011	2012	2013	2014	2015	2016	2017	2018	2019	AMT	AMT (%)	AHNS	ALNS
Jan	5	3	21	32	42	75	62	165	61	56	35	31	73	588	8.30	2	3
Feb	6	5	20	32	35	59	65	127	74	34	28	28	36	513	7.24	0	2
March	4	5	24	33	61	58	106	124	73	43	40	30	40	601	8.48	0	1
April	4	4	22	36	31	50	90	132	59	25	19	32	58	504	7.11	0	1
May	9	7	25	58	44	88	147	136	81	41	22	37	43	695	9.81	4	0
June	12	6	20	29	71	81	90	98	65	45	48	33	51	598	8.44	0	0
July	15	9	28	35	62	74	106	99	53	48	52	32	42	613	8.65	2	0
Aug	9	9	27	51	75	63	101	114	59	51	32	22	55	613	8.65	0	0
Sept	7	9	23	47	63	57	101	93	69	48	19	25	47	561	7.92	0	0
Oct	13	11	23	45	84	49	126	75	48	55	18	21	39	568	8.02	1	5
Nov	6	14	13	42	84	76	140	91	87	41	29	37	30	660	9.32	4	1
Dec	9	13	32	52	57	71	143	81	46	27	21	19	23	571	8.06	1	1
Total (AS)	99	95	278	492	709	801	1277	1335	775	514	363	347	537	7622	100	14	14

MS= Monthly spills, AMT=Annual Monthly Total, AHNS=Annual Highest number of spills, ALNS= Annual Lowest number of a spill. Green rows=months without recording the highest number of oil spills in any year, orange rows=months with at least one highest oil spill, red cell= the highest annual oil spills in 2014. The red and blue text represents the highest and lowest oil spill incidences for a particular year.

.

.

Figure 4.2 presents a graphical representation of the monthly and annual oil spills from 2007 to 2019. It can be observed that the oil spill incidence pattern changes per month for each year, with 2014 having the highest annual and monthly (January) oil spill incidences, and the number of annual spills increased linearly up to 2014 before decreasing exponentially from 2015 to 2018m when it went up again slightly in 2019 (January). This indicates that the pattern of oil spills per year could be difficult to predict. Figure 4.3a presents the annual number of oil spills by cause. It shows that 'sabotage' (ST) was responsible for the most oil spill incidence, while corrosion of an oil pipeline (CS) accounted for the fewest oil spill incidences in the study area for all years. For instance, in 2014, ST totalled 1147, which is far higher than the remaining three causes combined, and the trend is the same for all years. For equipment failures (EF) and other causes, spill incidences vary from one year to another. For example, while EF was higher than others in 2012 (69 against 60), it was lower than others in 2013 (71 against 169). The Total annual spill shows that (17.5%) and (16.8%) of spills occurred in 2014 and 2013, accounting for 34.3% of all the oil spills in the study area between 2007 and 2019. The pie chart in Figure 4.3b shows that ST accounts for 80% of all oil spills in the study area, while CS, EF and others accounted for 5%, 8% and 7%, respectively.

.

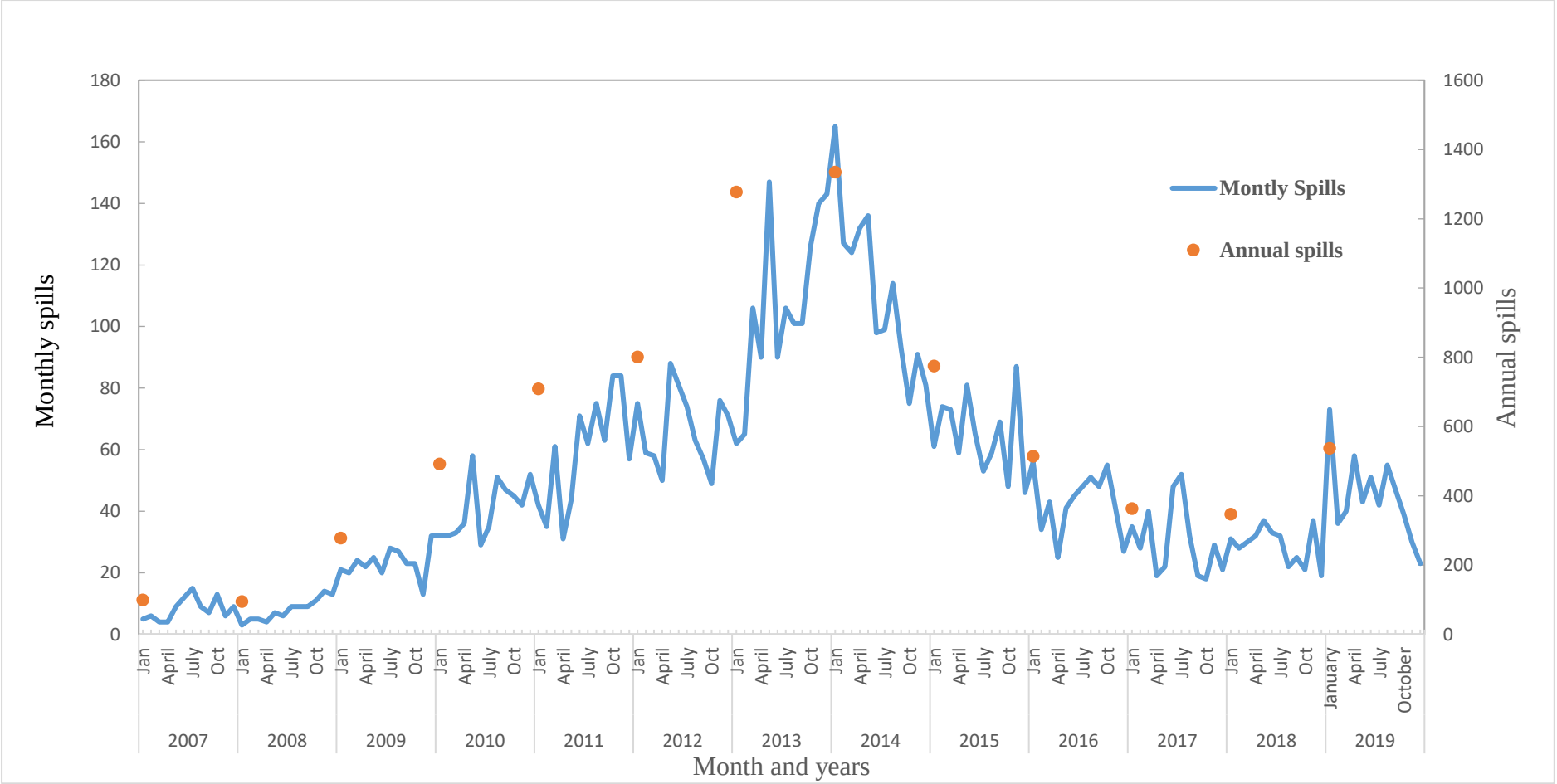

Figure 4.2 Monthly and annual oil spills from 2007 to 2019.

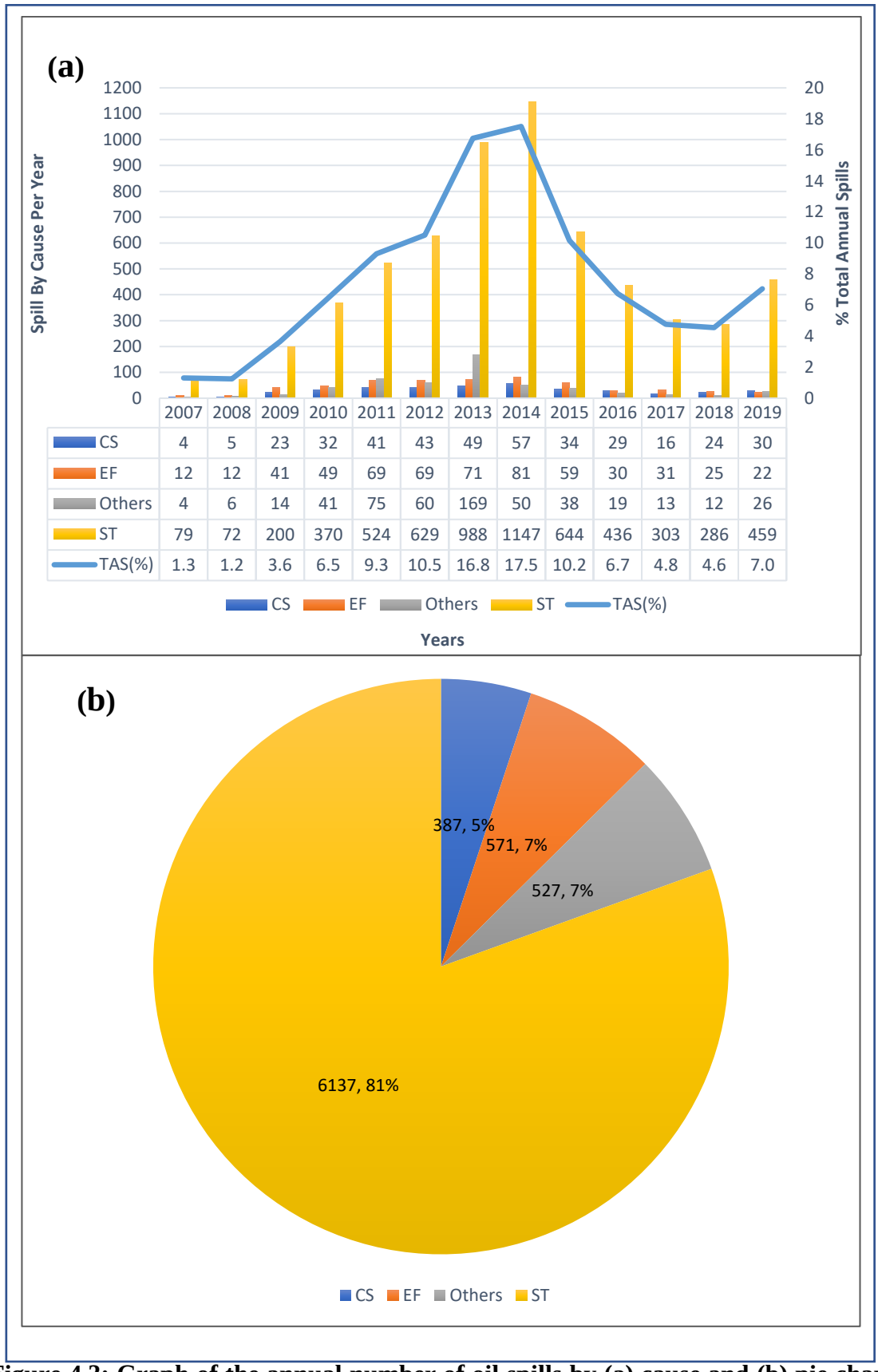

Figure 4.3: Graph of the annual number of oil spills by (a) cause and (b) pie chart of the total oil spill by cause.

Note: CS=Corrosion of an oil pipeline, EF=Equipment failures, ST=Sabotage.

4.3.2 Spatial distribution of oil spill incidences and oil facilities

Figure 4.4 shows the spatial distribution of oil spill incidences during 2007-2019, along with the locations of oil pipelines. The map shows that most oil spills occur along oil pipelines, with only a few occurring in places away from pipelines, which could be associated with other oil facilities, such as oil wells and flow stations. (Figure 4.4a). The oil spills tend to be more clustered around the north/eastern part of the study area (Amoku-Ahoada) as well as along the oil pipeline located in the south-eastern (close to Port Harcourt) and southern (around Ijaw South) parts of the area. In Figure 4.4 b, which shows the spatial distributions of oil wells, it can be observed that oil wells are fairly evenly distributed across the study area. However, fewer numbers are located in the northern part of the study area around Agbor and Asaba. Additionally, oil wells are not necessarily clustered along the oil pipeline alone, unlike oil spills.

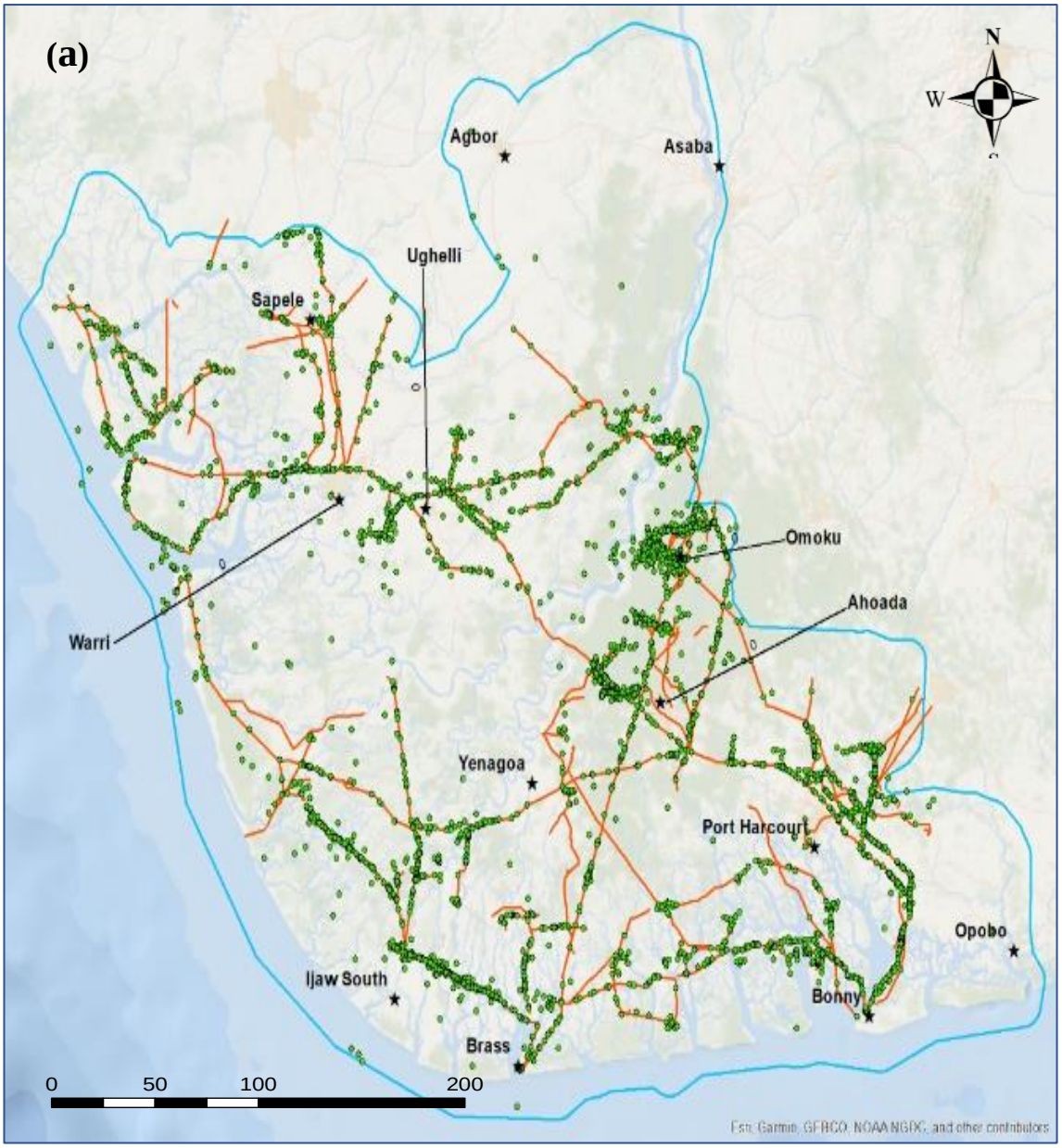

Figure 4.4: Spatial distribution of oil spills from 2007 to 2019 and oil wells cont.

Green=oil spill locations

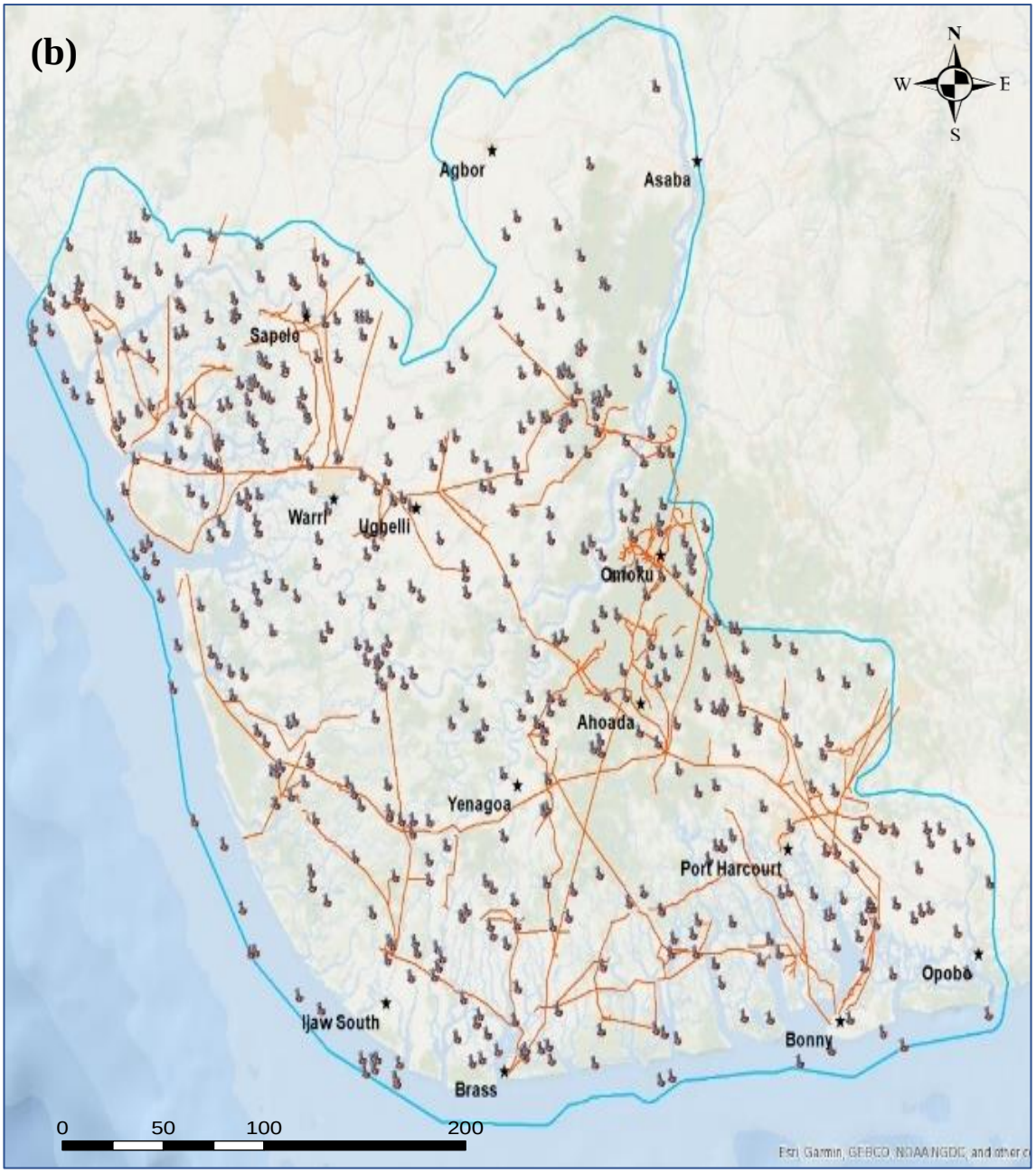

Figure 4.4: Spatial distribution of (a) oil spills from 2007 to 2019 and (b) oil wells within the study area overlaid on the oil pipelines.

Figure 4.5 shows the spatial distributions of oil spill incidences by causes. Among the four causes of oil spills, it can be observed that sabotage has more oil spill incidence clusters (Figures 4.5 d), while corrosion of the oil pipelines has the least clusters (Figures 4.5a). Additionally, the oil spills caused by others and equipment failure have almost the same clusters (Figure 4.5b and c).

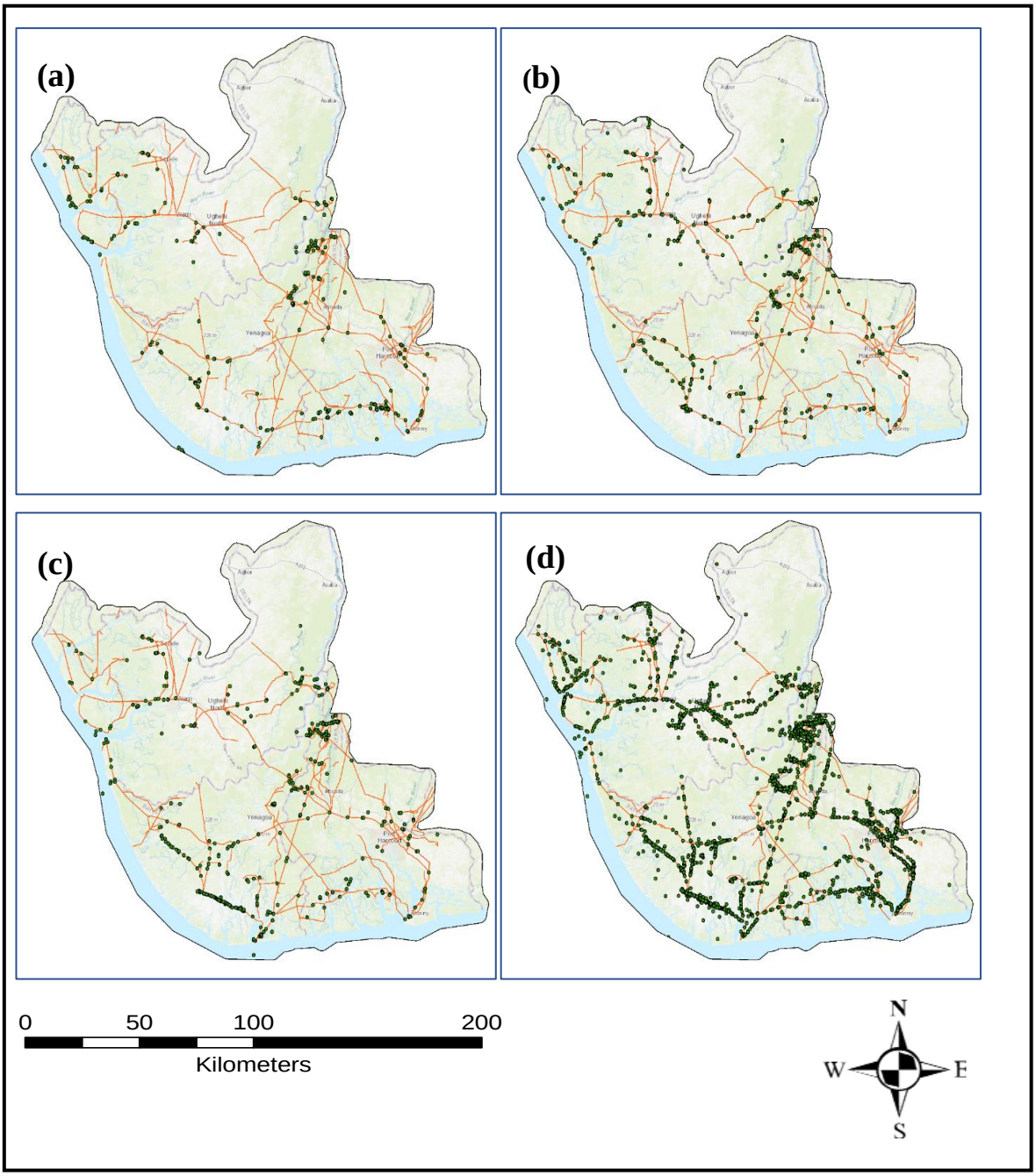

Figure 4.5: Distributions of oil spills by causes (a) Corrosion, (b) Equipment Failure, (c) others and (d) Sabotage.

4.3.3 Spatiotemporal oil spill pattern

Tables 4.2 and 4.3 show the global statistics that describe the spatial patterns of oil spill incidence from 2007 to 2019 using global indicators of Moran's I and Gestis-Ord General G. The results from the global statistics do not provide information about spatial clustering in a location, but rather looks at the spatial pattern across the whole study area. For Moran's I statistic (Table 4.2), six clusters were found in 2007, 2009, 2013,2014, 2015, 2016 and for the overall period 2007–2019, while random patterns were found in

2008, 2010, 2011, 2012, 2017 and 2018; no years were characterised by a dispersed pattern. The year 2013 has the highest Moran's I z-score of 8.0430 and a p-value <0.001, while the year 2012 has the lowest z-score of -0.7707 with a p-value of 0.441(Table 4.2). The more intense the clustering of high values (i.e., a hotspot), the smaller the negative z-scores, and the more intense the clustering of low values (i.e., a cold spot), while a z-score near zero indicates no apparent spatial clustering (Ibrahim et al., 2015; Jana & Sar, 2016)**.** For Gi*, the larger the positive z-score, the more intense the clustering of high values (hot spot), and the smaller the negative z-scores are, the more intense the clustering of low values (cold spot), while a z-score near zero indicates no apparent spatial clustering (Ibrahim et al., 2015; Jana & Sar, 2016)**.**

Table 4.2: Spatial autocorrelation (Moran's I) of oil spill incidents from 2007 to 2018.

Years	Moran's I	EI	Variance	z-score	*p*-value	Pattern
2007	0.1245	-0.0135	0.0015	3.5435	0.0004	**clustered**
2008	-0.0011	-0.0112	0.0005	0.4369	0.6622	random
2009	0.0640	-0.0038	0.0002	4.5537	0.0000	**clustered**
2010	0.0041	-0.0021	0.0001	0.8469	0.3970	random
2011	-0.0010	-0.0015	0.0000	0.1475	0.8827	random
2012	-0.0042	-0.0013	0.0000	-0.7707	0.4409	random
2013	0.1019	-0.0014	0.0000	23.4444	0.0000	**clustered**
2014	0.0108	-0.0008	0.0000	4.0432	0.0001	**clustered**
2015	0.0319	-0.0014	0.0000	7.7092	0.0000	**clustered**
2016	0.0382	-0.0021	0.0001	4.4929	0.0000	**clustered**
2017	0.0038	-0.0028	0.0001	0.9575	0.3429	random
2018	-0.0074	-0.0030	0.0001	-0.4299	0.6672	random
2019	-0.0017	-0.0017	0.0000	-0.0930	0.9259	random
2007-2019	0.1036	0.0003	0.0000	78.8286	0.0000	**clustered**

Table 4.3: Gestis-Ord General G of oil spill incidents from 2007 to 2019.

Year	O G	EG	Variance	Z Score	*p* Value	Pattern
2007	0.1925	0.1632	0.0001	2.6442	0.0082	**high-clustered**
2008	0.2430	0.2517	0.0000	-1.5087	0.1314	random
2009	0.0977	0.0953	0.0000	1.4835	0.1379	random
2010	0.1317	0.1301	0.0000	1.1740	0.2404	random
2011	0.2386	0.2407	0.0000	-1.4456	0.1483	random
2012	0.1802	0.1797	0.0000	0.3475	0.7282	random
2013	0.1736	0.11188	0.0000	8.1384	0.0000	**high-clustered**
2014	0.1151	0.1106	0.0000	3.0111	0.0026	**high-clustered**
2015	0.1604	0.1478	0.0000	4.8358	0.0000	**high-clustered**
2016	0.0862	0.0809	0.0000	3.4620	0.0005	**high-clustered**
2017	0.2096	0.2070	0.0000	1.3234	0.1857	random
2018	0.1155	0.1129	0.0000	2.3951	0.0166	**high-clustered**
2019	0.9966	0.9965	0.0000	0.1370	0.8910	random
2007 - 2019	0.1222	0.1152	0.0000	13.9795	0.0000	**high-clustered**

Note: O G= Observed General; E G= Expected General G

For the Gestis-Ord General statistics in Table 4.3, seven cases of high-clustering were found in 2007, 2013, 2014, 2015, 2016 and 2018, as well as for the full period of 2007–2019. Random patterns were found in 2008, 2009, 2010, 2011, 2012 and 2017, while low degrees of clustering were not found in any year. 2015 has the most intense high-clustering with a z-score of 4.8367 and a p-value <0.001, unlike Moran's I, where the strongest clustering was observed in 2013. Generally, Moran's I produce higher z-scores and lower *p*-values for the various years. For instance, the highest Moran's I z-score is 23.44 (for the year 2013), while the corresponding Gestis-Ord General G z-score is 8.14.

4.3.4 Spatiotemporal hotspot mapping

Figure 4.6 shows the spatiotemporal distribution of oil spill hotspots and the oil pipelines in the Niger Delta study area from 2007 to 2019. From Figure 4.6, it can be observed that the oil spill hotspots are located across the study area, with some consistently found at a location for more than a year. Some are found in the south, the north-eastern part and the centre of the study area for only a particular year. For example, the hotspot was only located in the north/western part in 2007 (Figure 4.6a) and the north/eastern part only in 2008 (Figure 4.6b). However, hotspots were found in the north-eastern, central and southern parts in 2009, 2010, 2011, and 2012 (Figure 4.6c, d, e and f), in the north-eastern and southern parts in 2013 and 2014 (Figure 4.6g and h), in the southern part only in 2015 (Figure 4.6i), around the central and southern parts in 2016 (Figure 4.6j) and in the central

and north-eastern parts of the study area in 2017, 2018 and 2019 (Figure 4.6k, l and m). Figure 4.7 shows the map of hotspot frequencies, which shows the number of years that a location has had a hotspot, from a minimum of 1 (green) to a maximum of seven (red) years. The map shows that the southern part of the map labelled A has the most recurrent oil spills in the Niger Delta. Figures 4.8a and b show the hotspots from 2007 to 2019. However, Figure 4.8a depicts the total hotspots (TH) obtained from Getis-Ord Gi* analysis of the combined oil spill data for 2007-2019. Figure 4.8b, on the other hand, shows the combined annual hotspots (CAH) map based on combining all of the individual hotspot maps shown in Figure 4.6. The maps look similar, revealing hotspots located around the north/eastern and southern parts of the map. However, the CAH shows more hotspots distributed across the study area, especially the north-western part. As seen in Figure 4.6, in only 2007, hotspots occurred in the north-western part of the study area.

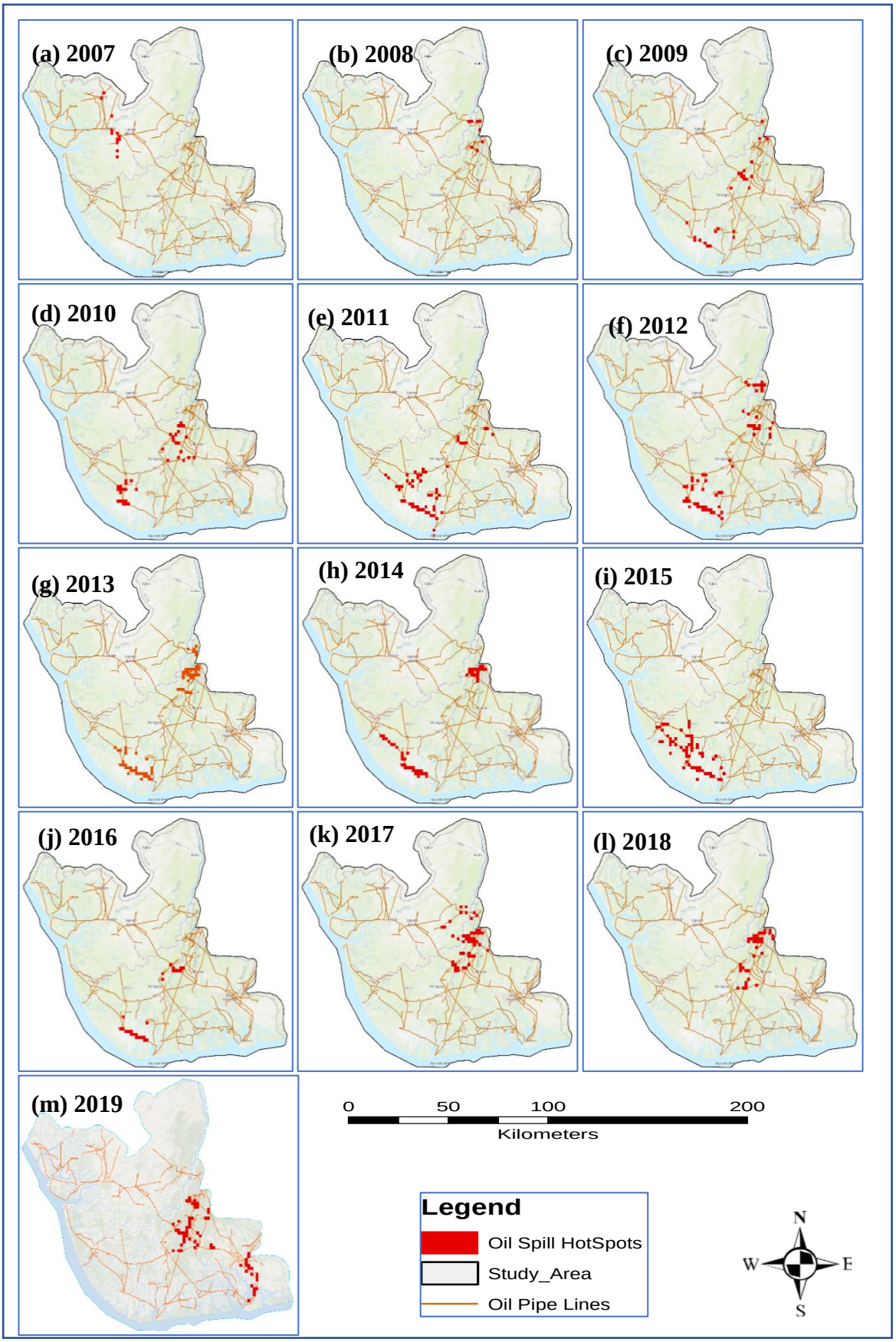

Figure 4.6: Oil spill hotspots for the years: (a)2007, (b)2008, (c)2009, (d)2010, (e)2011, (f)2012, (g)2013, (h)2014 (i) 2015, (j)2016, (k)2017, (l)2018 and (j) 2019.

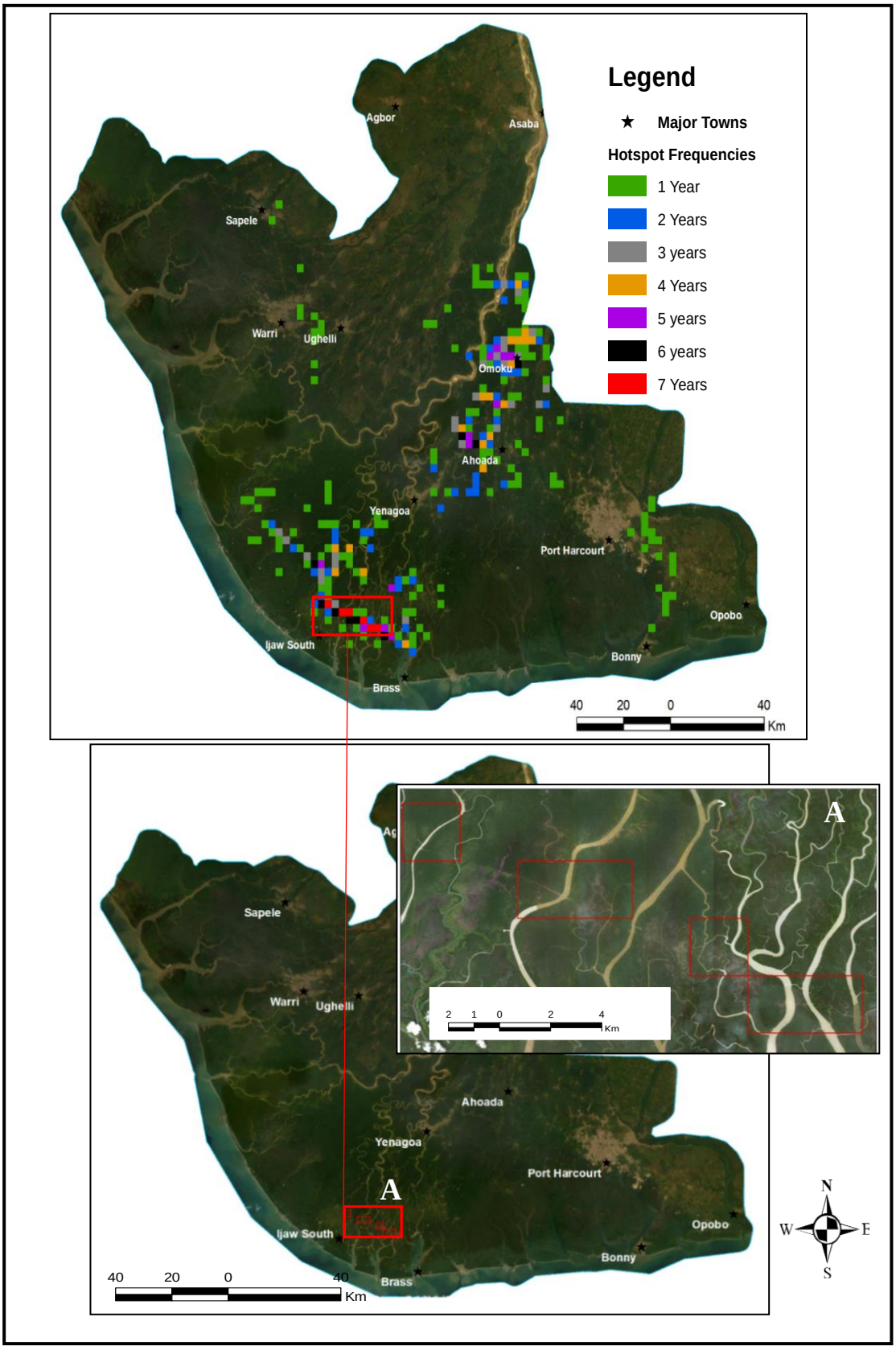

Figure 4.7: Map showing the frequencies of oil spill hotspo ıtions. Insert A highlights the most frequent hotspot location.

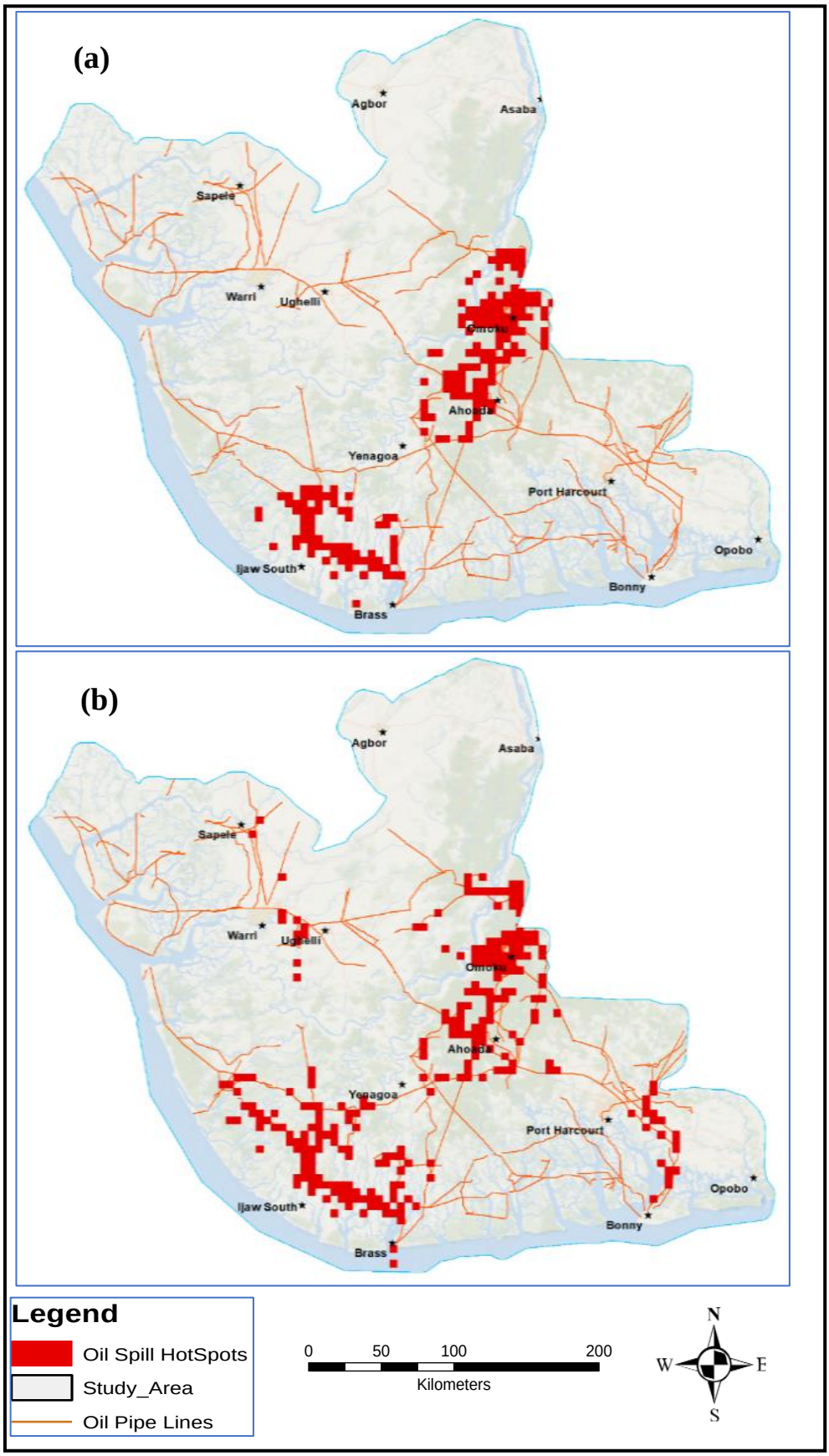

Figure 4.8: Hotspots based on (a) the combined total oil spill data for all the years (total hotspot; TH) and (b) combined annual hotspot (CAH) from 2007 to 2019.

4.3.5 Hotspots by causes

Figure 4.9 shows the oil spill hotspots based on causal factors as corrosion of the oil pipeline, equipment failure, others, and sabotage (Figure 4.9a, b, c and d). For oil pipeline corrosion, the hotspots are more clustered around high-density oil pipelines in the north-eastern near Omuko (Figure 4.9a). Hotspots due to equipment failures are relatively dispersed around Omuko and Ijaw south, with a few found around the central part of the study area (Figure 4.9b). For other causes, the hotspots are distinctively found around Omuko and Ijaw southern parts of the study area (Figure 4.9c.) For the sabotage, the pattern of hotspots is more intense and has a similar pattern to equipment failure, with hotspots located around Omuko and Ijaw South and a few found around the central part of the study area (Figure 4.9d).

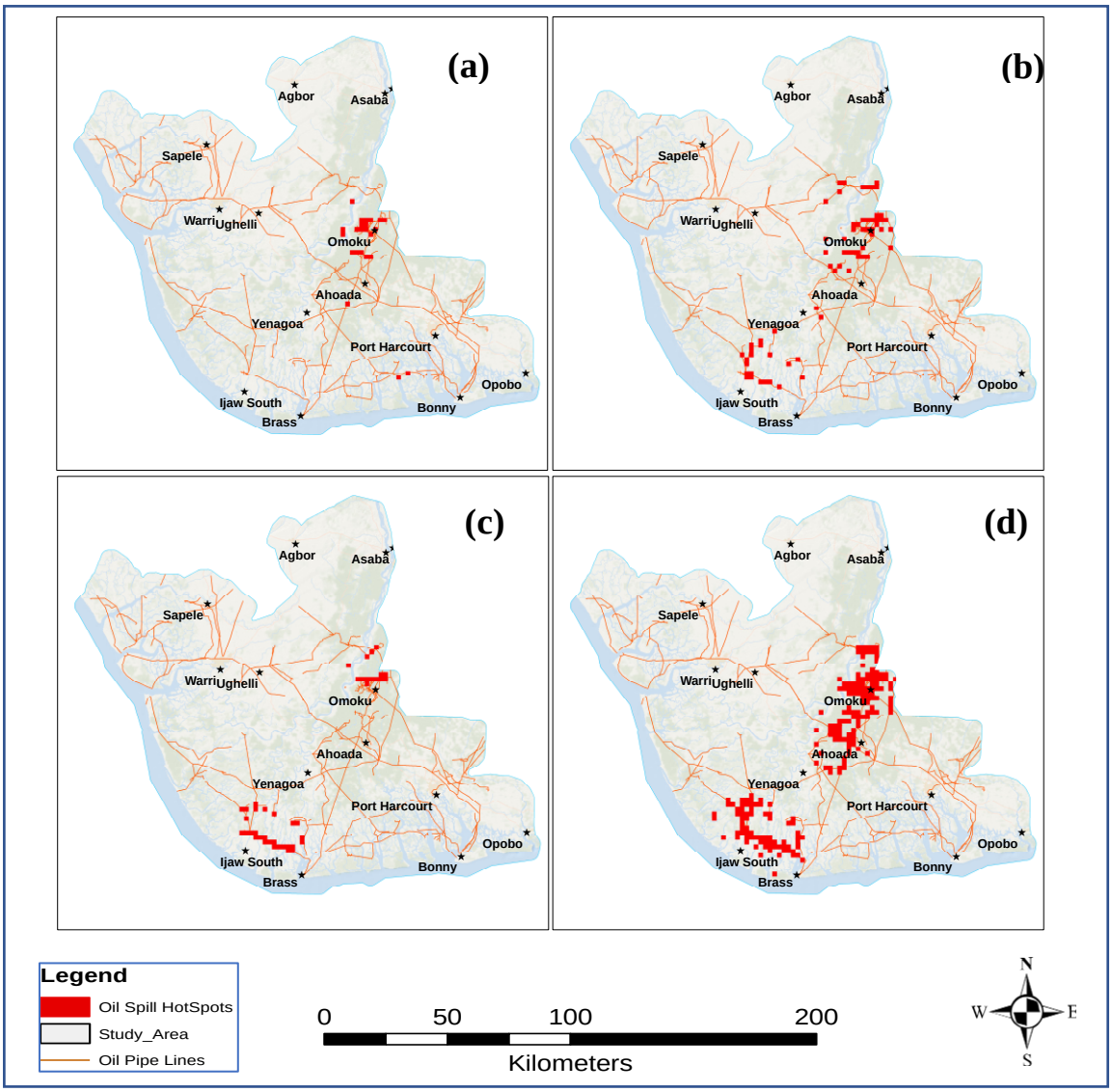

Figure 4.9: Hotspots by cause: (a) Corrosion, (b) equipment failure, (c) others, (d) sabotage.

4.3.6 Annual hotspot change detection

Figure 4.10 shows the spatiotemporal changes in hotspots between any two given dates. The green colour relates to a consistent hotspot (CH) found in two consecutive years; blue represents a disappeared hotspot (DH) that was found in the earlier year but then disappeared in the following year; red indicates an appeared hotspot (AH) that was not present in an earlier year but then appeared in the following year. Figure 4.10 clearly shows that the locations of hotspots varied quite significantly between consecutive years. The changes are mostly around Omuko, Ahoada, and Ijaw south, with few hotspot changes located around Yenagoa and just a one-time change located around Warri. The changes between 2007 and 2008 are unique compared to others because it has no CH, while 2008-2009 has just one recurrent hotspot located in the north-eastern part of the study area (around Omuko), as shown in Figures 4.10a and b. Similarly, the changes for 2017-2018 and 2018-2019 were all located in the north-eastern part of the study area (Figure 4.10k and l), while a new hotspot appeared around Port Harcourt in 2019. The reason for no change in the hotspots around Ijaw South in 2017-2018 and 2018-2019 is that there were no hotspots in those locations in previous years (Figure 4.6k and i).

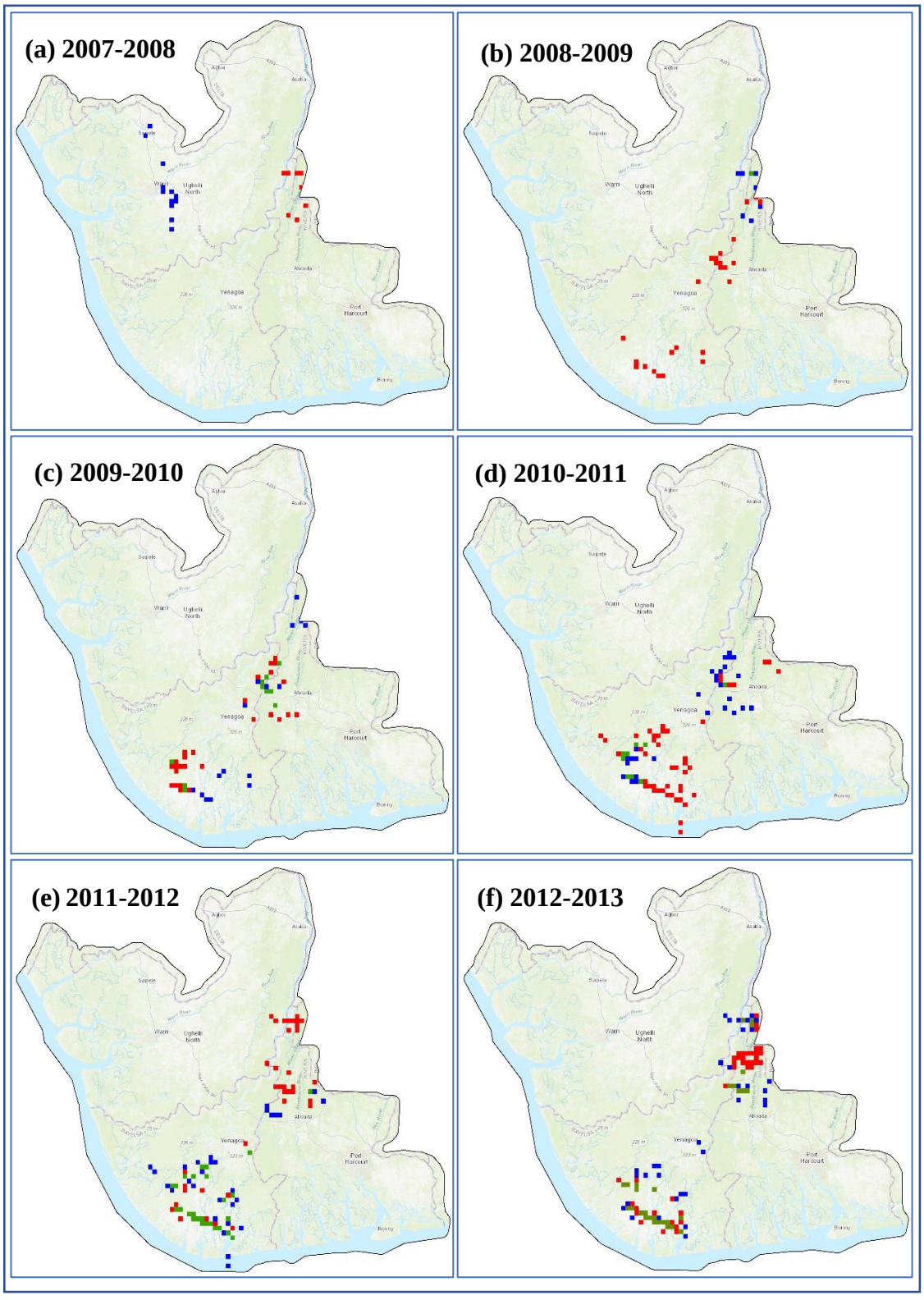

Figure 4.10: Spatiotemporal annual changes in hotspot locations cont..

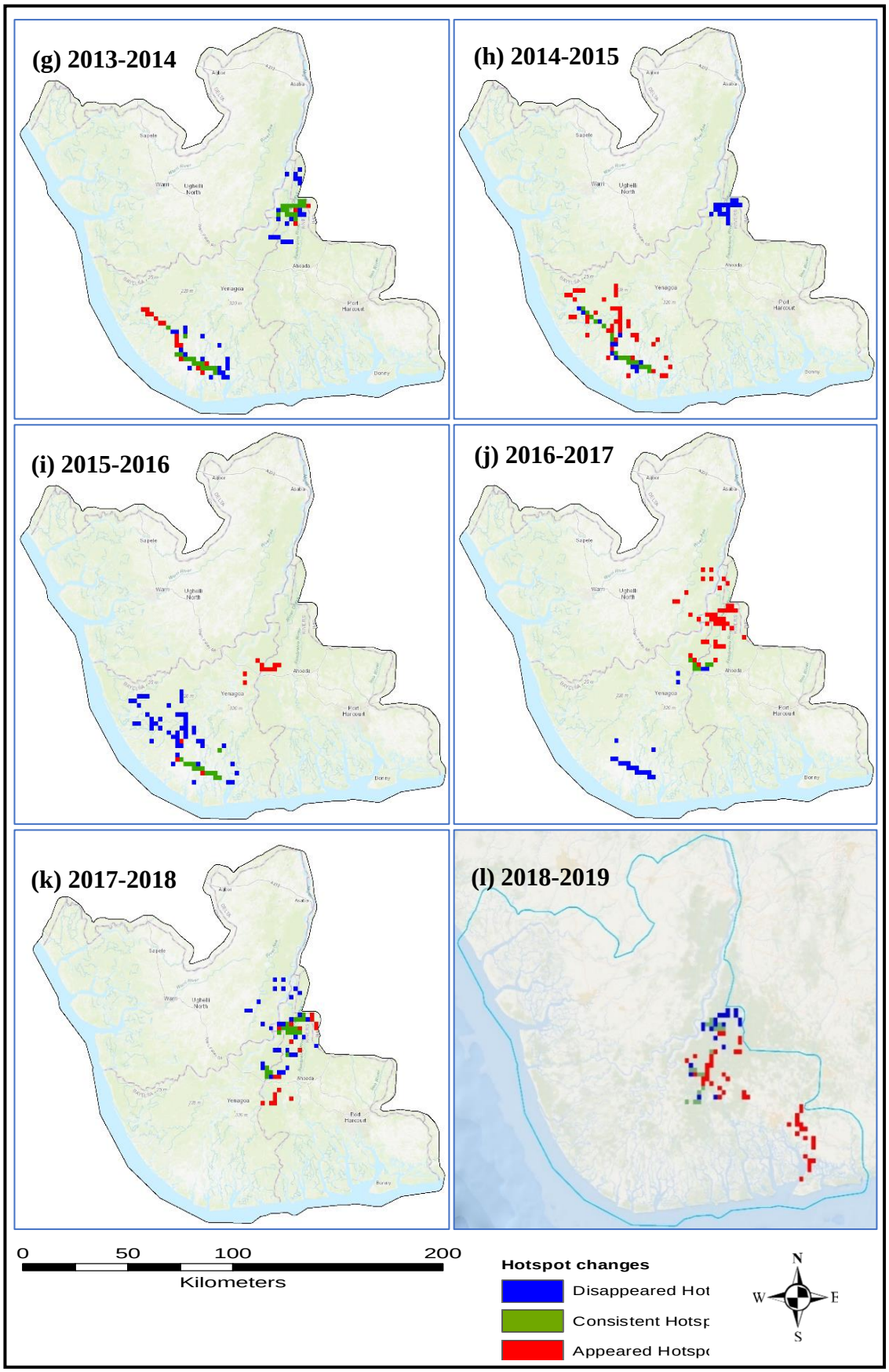

Figure 4.10: Spatiotemporal annual changes in hotspot locations (a) 2007-2008, (b)2008-2009, (c)2009-2010, (d) 2010-2001, (e)2011-2012, (f)2012-2013, (g)2013-2014, (h)2014-2015 (i) 2015-2016, (j)2016-2017, (k)2017-2018 and (l)2018-2019.

4.3.7 The spatial relationship between oil facilities and oil spill hotspots

Figure 4.11 shows maps of oil well density and oil pipeline density in relation to the oil spill hotspots (CAH). The density maps show different levels of oil well and oil pipeline densities from very low density (VLD), low density (LD), medium density (MD) and high density (HD). Regarding the oil wells, the high-density areas are located around Sapele and Amoku, with the VLD found at the extreme northern part of the study area around Agbor and Asaba (Figure 4.11a). At the same time, the pipeline has more VLD spread across the study area, especially around Amoku, Ahoada, and Sapele, with an LD located around Agbor and Asaba and the central part of the study area and Ijaw South (Figure 4.11b). Figures 4.11c and d show an overlay of the CAH on the oil wells and pipeline density maps. The oil well density map shows that CAH is mostly located within the high-density area of the oil wells. In contrast, more than half of the CAH is located within the high-density area of the pipeline, with some also located within the LD area on the southern part of the study area around Ijaw South. The pipeline around Ijaw south needs closer monitoring because it has become a highly vulnerable pipeline for oil spills.

Figures 4.12 and 4.13 show the oil spill hotspots by causes overlaid on top of the oil wells and pipeline density maps. This helps illustrate the link between the density of oil wells and pipelines to the causes of oil spills. Figure 4.12 shows that almost all the oil spills hotspots are within the MD and HD areas of the oil well. Figure 4.13 shows that the hotspots for corrosion (Figure 4.13a) and EF (Figure 4.13b) are almost located within the HD and MD areas of the oil pipeline density map, especially around Omoku. Oil spills hotspots associated with other causes (Figure 4.12c) and sabotage (Figure 4.13) occur within areas of HD and MD around Omoku and Ahoada, and some hotspots occur within MD in the southern part of the study area around Ijaw South. The pipeline around Ijaw South is particularly under threat from sabotage due to its location in the mangrove, which helps conceal acts of vandalism and theft. The hotspot caused by sabotage has a higher concentration within that pipeline location than other types of oil spill cause hotspots.

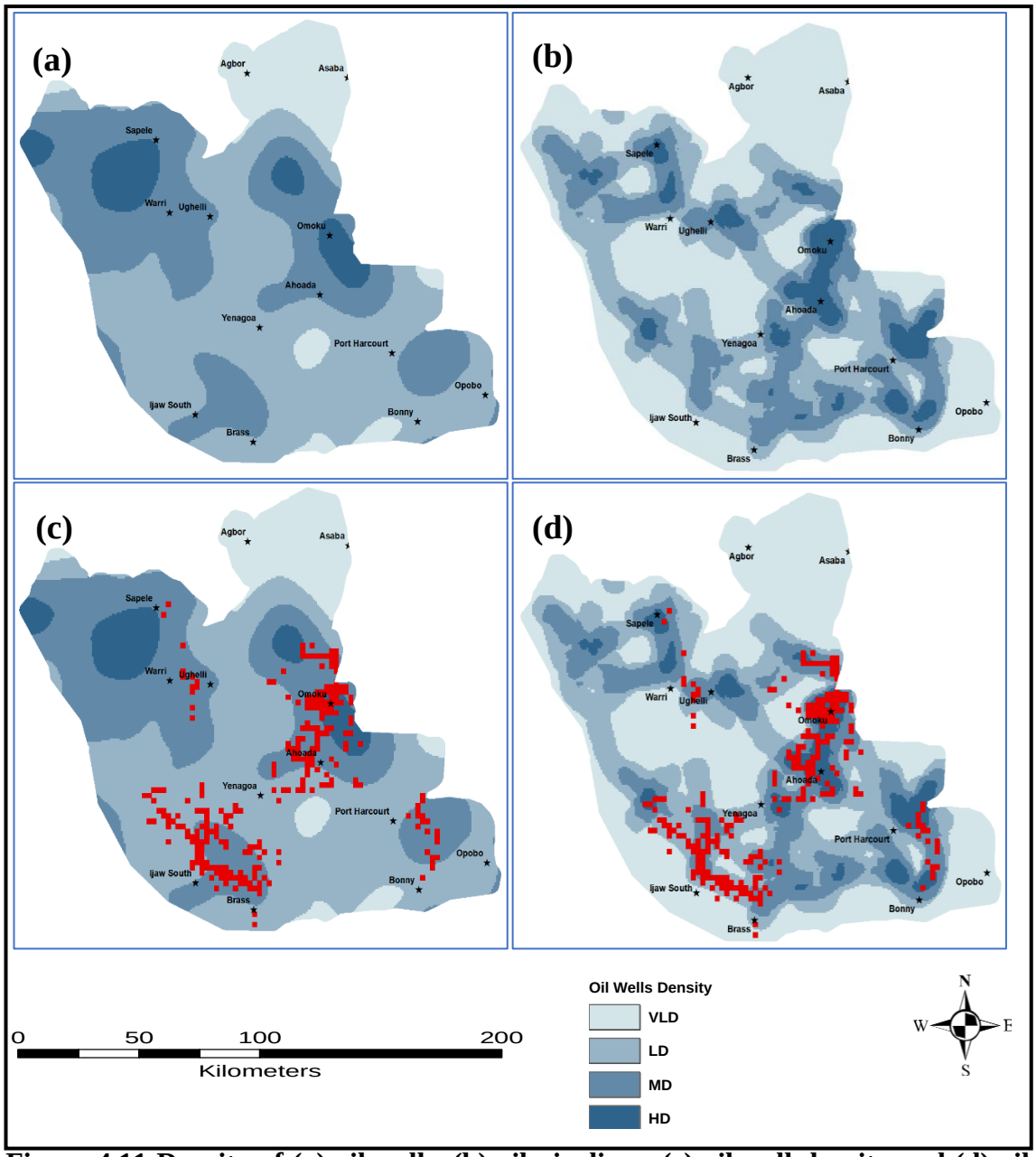

Figure 4.11:Density of (a) oil wells, (b) oil pipelines, (c) oil well density and (d) oil pipeline overlaid with combined annual hotspots (CAHs) from 2017 to 2019.

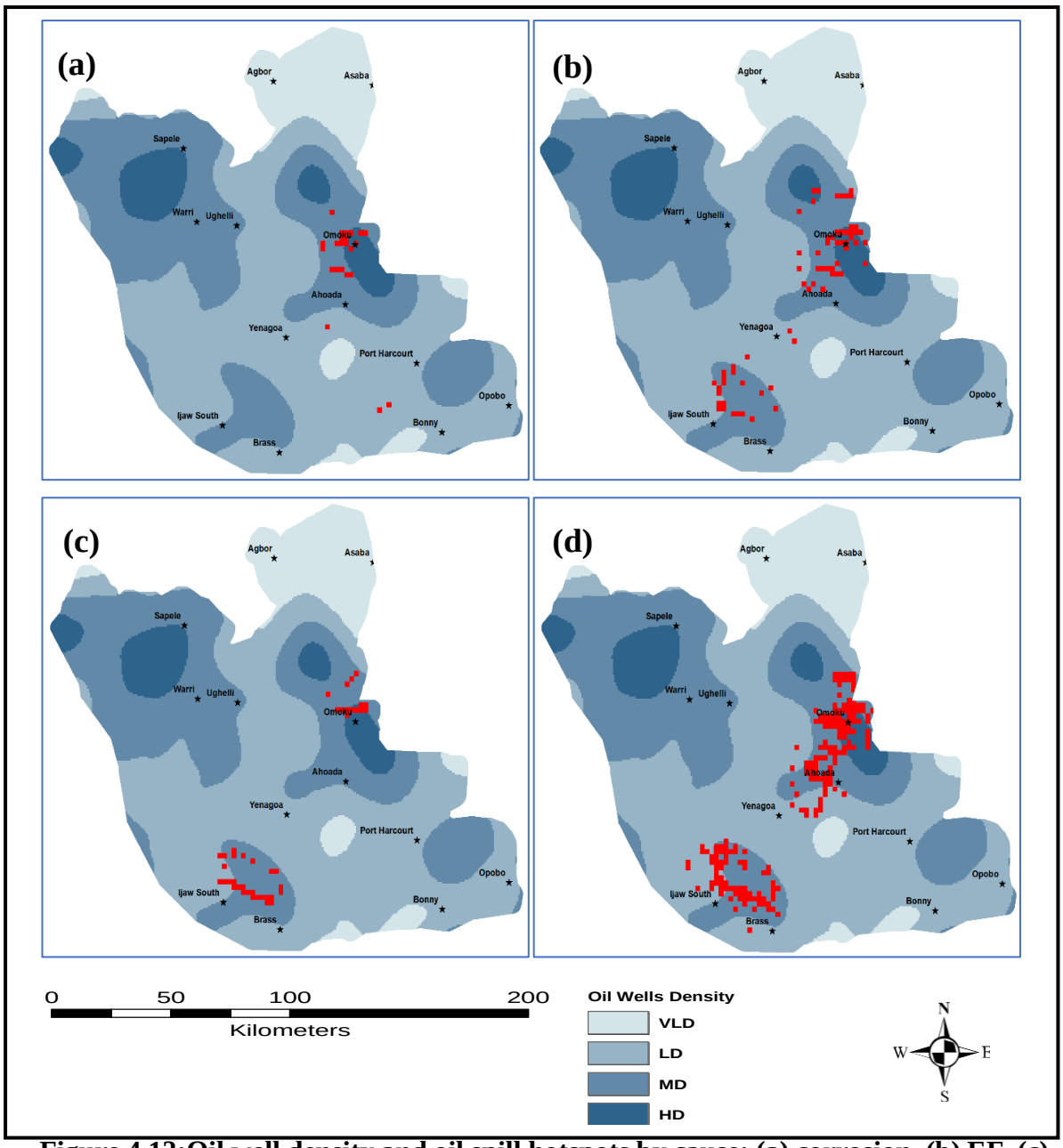

Figure 4.12:Oil well density and oil spill hotspots by cause: (a) corrosion, (b) EF, (c) others and (d) sabotage.

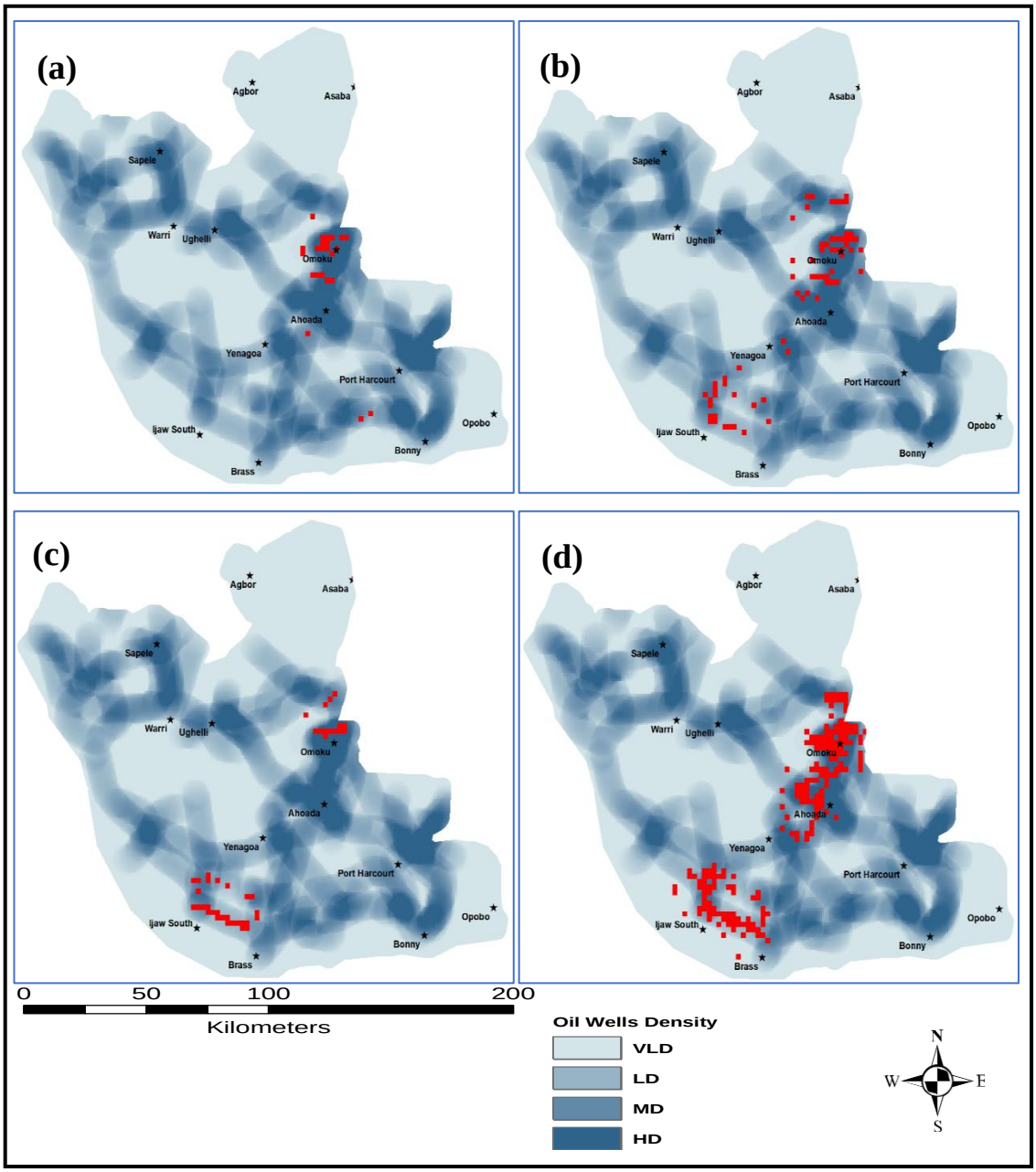

Figure 4.13: Oil pipeline density and oil spill hotspots by cause:(a) corrosion, (b)EF, (c) others and (d) sabotage.

4.4 Discussion

4.4.1 Temporal oil spill incidence pattern and trend

The temporal distribution of oil spills in the Niger Delta varies from month to month and years, with some years and months recording more than ten times more oil spills than other months and years (Table 4.1). The temporal analysis of oil spill incidence in the three states of the Niger Delta (Bayelsa, Delta, and River states) from 2007 to 2019 showed different levels of variability in the monthly and annual oil spill incidences. The

annual-monthly oil spills show no particular trend, and the same number of spills can be observed in a different month in the same year, with some having the same number of consecutive monthly spills – for example, March-April 2007(4 spills each) and January-February 2010 (32 spills each). The implication is that there appears to be no particular month within a year when oil spills are likely to occur or a more favourable month for the activities of vandals since 81% of the recorded oil spill incidences is caused by sabotage. Unlike the monthly, annual-monthly total, the months of January, May, July, October, November, and December (2007-2019) have the highest recorded number of oil spill incidences, with May being exceptionally higher, having recorded the highest number of spill incidences per month for four different years (2010, 2012, 2013 and 2018) out of the twelve years. The month of May also has the highest annual-monthly total of 695 spills, representing 9.81% of the total monthly spills.

On the other hand, February-April, June and August-September have the lowest number of monthly spills, with April recording the lowest number of oil spill incidences of 504. Although it is difficult to determine why May seems more favourable for oil spills in the Niger Delta, it could serve as useful information to develop a preventive measure to combat sabotage activities. Oil pipeline sabotage is the major cause of oil spills (Okoye & Okunrobo, 2014), usually caused by militants and other thieves that puncture oil pipelines (known as bunkering) and other facilities to steal crude oil. In terms of the annual total oil spill, while 2007 recorded the lowest number of 99 spills, 2014 recorded the highest number of 1335 spills, which is more than 10 times the lowest. The annual trend shows that the incidence of oil spills in the Niger Delta is difficult to predict due to high inter-annual variability. For example, while 1335 oil spills were recorded in 2014, 775 were recorded a year after in 2015, an approximately 42% reduction.

Social-economic and political drivers in the Niger Delta region have caused oil spills in the Niger Delter affecting the environmental. While the MS trend fluctuates without rising or falling, the continual rise in AS from 2007 until 2014, when it peaked and started falling continually from 2014 to 2018, and rose again in 2019 (Figure 4.2a) indicates that if appropriate policies are put in place, the oil spill could be reduced to the barest minimum. The significant drop in spill incidences in 2015 was partly due to uncertainties associated with the 2015 general elections in Nigeria (Obida et al., 2018). The high rate of sabotage in 2014 was because the militants resorted to threats and the destruction of the oil pipeline, hoping “force” Nigerians to vote for President Goodluck Jonathan held

from Niger Delta and was seeking re-election in 2015. The militants feared the presidential amnesty program, which gives a monthly stipend to the repentant militants, could be stopped if the presidential candidate from the opposition party who is from another region wins the election. But at the beginning of 2015, before the election held in March 2015, the militants were persuaded to stop the destruction of the oil pipeline, including President Jonathan, the current present then, who eventually lost the election. After the new president took over and continued with the amnesty program, there was a significant drop in sabotaging of oil pipelines in 2015 which was associated with the federal government of Nigeria negotiating with the militants and stakeholders in the Niger Delta and the increased effort of the security personnel in limiting the activities of oil thieves. The continued dialogue with the community and a sense of serious commitment by the federal government of Nigeria and the multinational oil company in addressing some communities' concerns (cleaning the polluted land, more infrastructures etc.) and actively engaging the youth in productive ventures could continue to lead to the decree in the AS in the Niger Delta.

The high rate of oil spills caused by Sabotage (Figure 4.3b) should concern the Federal government of Nigeria that its citizens could wilfully destroy national assets such as oil facilities. Although oil pipeline sabotage occurs in other regions, including South America, Asia, the Middle East, and other countries, it is more common in Nigeria due to the cultural, socioeconomic, geopolitical and environmental perceptions of the people and government (Umar et al., 2021). The lack of patriotism by those who destroy oil facilities is caused by many administrations' neglects of the region. The Niger Delta youth feel that the money from the oil sales from their region has been used to develop other regions, leaving the youth sad. Hence, some of them sabotage oil pipelines to steal oil for sale either locally or at international markets. Despite the efforts to promote development in the Niger Delta through the establishment of the Niger Delta Development Commission (NDDC), the Amnesty program for the militants and improvements of revenue derivation for the oil-producing states in the region from 1 to 13% over the years etc, however, no significant development is achieved partly due to inconsistency in programs implementations and corruption (Umar & Hajj Othman, 2017). Sabotage as the main cause of the oil spill in the Niger Delta was reported by Agbonifo (2016), Mba et al. (2019), Obida et al. (2018) and Umar & Othman (2017)

The remaining causes are others (whose causes are typically unknown) corrosion of the oil pipeline and equipment failures are the consequencie of any oil producing society which could be minimised using global best paraction. For instance equipment failure are mostly attributed to the failure of oil production companies to meet acceptable standards of maintenance and their slow responses to tackle oil spills (Obida et al., 2018)

4.4.2 Spatial distribution of oil spill incidences and oil facilities in the Niger Delta

The location of the oil pipeline greatly influences the spatial distribution of oil spill incidences. Oil spill incidences and the pipeline are spread unequally, whereas the oil wells are more evenly distributed across the study area (Figures 4.4a and b). The oil pipeline network in the Niger Delta cuts across the study area with oil spills clustered along the oil pipeline routes, as expected (Obida et al., 2018), since sabotage of the pipeline is the main cause of spills. What makes the spill in the Niger Delta different from other parts of the world is the people who intentionally break the pipeline to steal oil without minding the damage such action will have on the public health, animal and the environment. For instance, in the US and Canada, most oil spills happen at petroleum production facilities, wells, production collection facilities, and battery sites (Fingas, 2017). Similarly, the oil well has little spatial relation with the oil pipeline because not all oil wells are linked to oil pipelines, although some are close to the pipeline (Figure 4.4b).

From the maps showing the spatial distribution of spills by causes in Figure 4.5, sabotage has the highest distribution of oil spill clusters compared to the other three causes combined. The spatial distribution of oil spills is almost the same for all causes, except that the oil spills caused by corrosion and equipment failure are less clustered in the southern part of the study area (Figures 4.5a and b). The reason is that the pipeline network in the southern part around Ijaw South is less extensive, and so less equipment is likely to be present and possible to sabotage. The pipeline may not be as old as the pipeline from other parts of the study and may not be exposed to factors that cause pipeline corrosion. The spatial distribution of oil spills by causes is key in addressing the cause of oil spill incidences in the Niger Delta. Understanding the causes and knowing the locations might help formulate policies/interventions strategies that could mitigate the causes of some of the oil spills since each cause may require a different type of approach and be carried out by different organisations. For instance, the oil spills caused by sabotage may require more surveillance by security personnel, while indications of ageing or damaged pipelines will help the company repair them. Additionally, information on

the spill caused by equipment failure could help the regulating bodies and oil companies locate other facilities that need inspection or replacement.

4.4.3 Spatiotemporal evolution of oil spill hotspots

The evolution of oil spill hotspot clusters and frequencies provides information on the impacted locations with statistically significant concentrations of oil spills, which could form the basis for further research into the effect of oil spills on land cover in the Niger Delta (especially water and vegetation). It could also provide indispensable information for further developing incident prevention measures (Ding et al., 2015). Additionally, to effectively manage the present oil spill-related environmental problems and quantify the damage, knowledge of past occurrences could help provide a solution to impacted areas and predict future damage. Based on the maps showing the evolution of the oil spill hotspot in the Niger Delta, some locations have sporadic hotspots appearing only once a year – e.g., in 2007 and 2019 around Warri and Port Harcourt, respectively (Figure 4.6a and j). Generally, while some years have hotspots located in both the northeast and the southern part of the study area around Omoku and Ijaw south, others have hotspots located in either the northeast or the south. Some years also have hotspots located in the central part of the study area around Yenegoa and Ahoda and the northeast and south. The most frequently affected area is the southern part of the study area around Ijaw south, which has had various levels of hotspot clusters for eight consecutive years from 2009-2017. The areas around Omoku and Ahoda are the next most affected by the occurrence of oil spills. The implication is that this location needs to be given more priority to implementing programs and policies such as oil spill remediation.

Locations around Ijaw south had the highest frequency of hotspots for seven years out of the 12 years considered. The isolated location of the pipeline in the mangrove makes it difficult for law enforcement agencies to monitor to prevent acts of sabotage. Also, its proximity to the coast for easy transportation of the crude into a waiting vessel on the sea could be another reason. Oil thieves usually break into wellheads and pipelines, install pumps, and use hoses that sometimes measure up to 2 km to load crude oil onto barges that travel through the delta, which is then transferred onto small tankers at the coast (Brock, 2013). The same location was identified by Obida et al. (2018) as being of the pipeline most affected by the oil spill. The less frequent (sporadic) oil spill hotspot locations of 1 year are mostly found around the Ughelly and Port Harcourt axes, although some are found around Ijaw South, Omoku and Ahoada.

Additionally, the data for total hotspot and combined annual hotspot in Figure 4.8 show that the areas most prone to oil spill incidences are predominantly found around the north-eastern and southern parts of the study area around Omoku-Ahodia and Ijaw south, respectively. However, some least affected areas are located around the north-western and south-eastern parts of the study area around Ughelly and Port Harcourt, respectively. Similarly, in terms of the hotspots by causes, the same locations are the areas most impacted by oil spill incidences. However, the spill hotspot due to pipeline corrosion is found in the north-eastern part of the study area only around Omoku (Figure 4.9), with hotspots due to sabotage being the most intense. Spatial pattern analysis can help combat environmental pollution by identifying potential exposure pathways and possible sources of pollution concerning sensitive areas around oil production sites (Whanda et al., 2016). Spatial pattern analysis provides a holistic understanding of the root causes, which could help decision-makers reduce oil spill incidents and increase public awareness of accident prevention by sharing historical incident data and providing dashboards using multidimensional visual analytics (Park et al., 2016).

4.4.4 Spatiotemporal oil spill hotspot changes detection

Although the spatial analysis (hotspots) can provide insight into the temporal and spatial patterns of environmental incidents, it fails to provide information on the interaction between space and time to determine if the level of incident risk in an area is subject to temporal fluctuations (Park et al., 2016). Detecting temporal changes in the hotspots is crucial in mitigating the impact of oil spills on the environment. In the Niger Delta, the hotspots fluctuate from year to year between 2007 and 2019. For example, in 2008, there were no consistent hotspots, only disappeared hotspots and appeared hotspots around the Warri and Omoku axis. This means that the persistence of oil spills varies across the study area. Generally, the area around Ijaw South has the highest concentrations of appeared hotspots (from 2008-2016) and consistent hotspots (from 20011-2016), except for 2008, 2018 and 2019. The level of DH around the south of Ijaw is minimal (the most prominent disappeared hotspots in 2016) compared to the locations around Omoku and Ahoada, which have high concentrations of appeared hotspots in 2012, 2013 and 2017 and only disappeared hotspots in 2015. The Ijaw south is the most vulnerable location to oil spills in the study area, followed by the locations around the Amoku-Ahoada axis, as seen in Figures 4.7 and 4.8. These results agree with Obida et al. (2018), where the oil pipeline experiences a higher oil spill intensity in these two locations. The temporal fluctuations

in the oil spill hotspot pattern could result from some factors that favour or deter oil pipeline vandals at a particular location in a given year. They likely move to more favourable locations with fewer security threats, leading to the emergence of a new hotspot. For example, AH around Port Harcourt in 2019 (Figure 4.10) is a first-time hotspot location (Figure 4.7m). This indicates that other places that are not currently oil spill hotspot locations could be potential hotspots in the future, while some current oil spill hotspots could disappear in future. Therefore, those vested to protect the oil pipeline should ensure extensive security coverage of the most vulnerable oil pipelines.

4.4.5 Factors influencing oil spill hotspot clusters

Understanding how oil wells and oil pipeline density and proximity to towns/cities and coastlines influence oil spill incidents could provide the required information for oil spill prevention/reduction programs. The temporal and spatial patterns of oil spill hotspots fluctuate, likely controlled by other spatial factors within the study area. For the oil wells and the oil pipelines, the densest distribution (having both HD oil wells and pipeline) is around Omoku. It also happens to be one of the areas with a high level of oil spill hotspot clustering after Ijaw south. This indicates a spatial relationship between oil spills locations and the density of oil wells and oil pipelines, which is expected because the spills are typically from the oil pipelines (Figure 4.11a-b). But for, the north-western part around Sapele-Warri has limited hotspot clusters of oil spills despite having MD and HD of oil well because the corrosion and sabotage of oil pipelines are less intense in those areas, unlike the north-eastern part around Omoku-Ahoada.

Similarly, almost all the oil hotspots due to corrosion are located within areas of MD and HD, with only a few found in LD around the Omoku-Ahoada axis (Figure 4.12a-d). The hotspots due to corrosion are highly spatially correlated with oil wells around the Omoku-Ahoada axis. Additionally, the South Ijaw has an MD of oil wells but a high cluster of hotspots, especially for EF, others and sabotage. The relationship between corrosion and the oil well density is because the oil pipelines transport the oil from wells to various facilities, such as refineries. These pipelines are mostly located around Omoko. The clustering of several pipelines, coupled with the incident of the corroded pipeline probably due to ageing, led to a hotspot of corrosion found around Omuko. Only Ijaw south has an LD of oil pipeline but with a high cluster of hotspots, especially those caused by others and sabotage (Figure 4.13 a-d). The Ijaw south happens to have the highest and the most frequent oil spill hotspot cluster even though it only falls in MD and LD of oil

wells and pipelines. Ijaw south has only a single oil pipeline, but it is the most targeted/sabotaged pipeline.

Based on the findings above, factors other than the density of the pipeline and oil well are also responsible for oil spills. For instance, unlike the locations Omoku-Ahoada with high HD pipelines and oil wells, Ijaw south has only LD and MD oil pipelines and wells. The proximity to towns and the pipeline's location could also be a factor that encourages or discourages the activities of oil bunkers. Oil theft and sabotage in the Niger Delta, either used in local refineries or sold on the international market, involves the local communities and some security agents, such as the high-ranking military officers who oversee the deployment of units to protect illegal refineries who pass key information to pipeline vandals who they work hand-in-hand with the informants from oil industries (Transparency International Defence and Security, 2019). The cluster around the Omoku-Ahoada axis could be due to the pipeline's proximity to town and communities involved in the oil theft since some are involved. Their proximity could also provide easy access to escape route with stolen oil to either local refinery (if crude) or sell it even within the community (if already refined). For the Ijaw south pipeline, its proximity to the coast and its isolated location in the swampy area, making it difficult to access, has been the most frequent spill site. The Niger Delta's swamps and shallow waters – where oil pipelines crisscross the region in a grid-like pattern–are most frequently targeted in these tapping operations (Shadow Governance Intel, 2017). Stolen Nigerian oil worth billions of dollars is sold every year on international markets via a complex criminal web that includes foreign oil traders, shippers, bankers, refiners, high-level politicians and military officials (Brock, 2013).

4.5 Conclusion

The spatiotemporal hotspot analysis of oil spills and oil facilities in the Niger Delta was conducted to provide spatial information that will be used with land cover information to assess the impact of oil extraction activities on the land cover changes. Similarly, the information can be used for pipeline monitoring and understanding the impact of oil extraction activities on land cover change. The major findings are as follows: The monthly and annual temporal trends of oil spill incidence in the Niger Delta vary. While the monthly oil spill incidence pattern is random, the annual oil spill incidence pattern increased until it peaked in 2014, with the highest number of spills and started a

downwards movement in 2015. It was also discovered that over 80% of oil spill incidences in the Niger Delta are caused by sabotage by third parties who damage the oil facilities to steal oil.

The distribution of oil spills is located along oil facilities, especially oil pipelines. On the other hand, the annual hotspot evolution, total hotspot and combined annual hotspots are mostly clustered around Omuko-Ahoada in the north-eastern part of the study area with a high and medium density of oil pipelines and wells, respectively, and around Ijaw-South in the southern part of the study area with a low and medium density of oil pipelines and oil wells, respectively. The hotspot change detection shows that hotspots are not consistent in one location but fluctuate from year to year between 2007 and 2019 with some occurring only once. However, the major locations where various changes were more prominent were around Omuko-Ahoada in the north-eastern and southern Ijaw part of the study area, with the south Ijaw being the most consistent hotspot location.

The most vulnerable oil pipeline is found in the southern part of the study area around southern Ijaw. The major factor responsible for the high rate of spills on this pipeline is its isolated location, which is far away from the built-up area and located in the mangrove with proximity to the seacoast, making it a favourable target for pipeline vandals.

Lastly, this study has provided information that other environmentalists and professionals can use to prioritise further research into the area with the most intense and frequent hotspots. The biodiversity of such locations needs to be studied to determine how these oil spills have affected plants and animals at these locations. The oil spill hotspot analysis could be integrated with the National Oil Spill Detection & Response Agency (NOSDRA) website, where the hotspot analysis could be updated weekly or monthly to help monitor oil spills. This could be achieved by building an artificial intelligence technology application to perform web-based spatiotemporal hotspot visualisation. Overall, the results of this study show that the spatio-temporal distribution of oil spills in the Niger Delta is consistent with many locations being persistently exposed to oil spills for several years. Thus, Chapter five will investigate the leaf-scale responses of some plant species in the Niger Delta to being exposed to hydrocarbons in the soil. Additionally, the oil spill data presented here will be used to study the impact of oil spills on vegetation at the leaf and plot scale based on hyperspectral and satellite imagery (chapters 5 and 6) and to

investigate landscape changes in land cover across the study area due to oil spills and extraction activities (chapter 7).

The next chapter will discuss the impact of soil hydrocarbon properties on some plant types in the Niger Delta exposed to oil spills

Chapter 5 Determining the effect of soil hydrocarbon properties on vegetation at leaf-scale

5.1 Introduction

The presence of hydrocarbons in the soil caused by oil spills can affect vegetation in several ways. The effects can be related to the growth of plants (stress), crop yield, and reduction in chlorophyll content (Anejionu et al., 2015; Osuagwu et al., 2013). Others are changes in the colour of leaves, stems and trunks (Adamu et al., 2016), and biophysical and biochemical alterations of the vegetation, leading to changes in the reflectance signature of vegetation (Adamu et al., 2015). In recent years, vegetation, the major land cover in the Niger Delta region, has been significantly affected by oil extraction activities. Pollution from oil spills is of great concern due to its capacity to degrade the ecosystem (Omodanisi & Salami, 2014). The impacts on vegetation, in particular, are devastating because it is the primary source of food, energy, timber and restorative materials (Yang et al., 2017) and is, therefore, an essential element in our world that must undergo remote monitoring (Kochubey & Kazantsev, 2012).

Monitoring the impacts of soil hydrocarbons on vegetation using remote sensing requires understanding the vegetation's spectral reflectance characteristics (Adamu et al., 2016). This then enables the detection of physiological abnormalities in the vegetation even before the appearance of visual symptoms (Piro et al., 2017). Both satellite and field-based remote sensing have been extensively used to monitor/investigate the health of vegetation around the world. Among these examples are monitoring the green roof vegetation health state in the sub-Mediterranean climate (Piro et al., 2017), monitoring mangrove spectral changes induced by oil spills (Pavanelli & Loch, 2018), monitoring forest health during a simulated disease outbreak (Dash et al., 2017), and assessing the vegetation status in the Sagbama oilfield environment in the Niger Delta region (Ochege, 2017).

One of the remote sensing-based vegetation health monitoring techniques is field spectroscopy, which provides hyperspectral measurements of the reflectance characteristics of the vegetation. Spectroscopy is the most flexible, efficient and established technology to fully characterise the vegetation health state compared to the other sensing techniques (Piro et al., 2017). When employed on vegetated surfaces, the spectral characteristics are a function of the status, composition and structure of the

elements measured (Lola et al., 2015). The main advantages of field-based vegetation condition assessment approaches are their capability to assess tree canopies (Tehrany et al., 2017) and provide plant/species data at the leaf-scale, which are particularly useful in assessing a plant or species' responses to the presence of soil hydrocarbons.

One way to extract useful information on vegetation status from hyperspectral reflectance data is the 'red edge' position (REP). The REP results from the contrast of red light absorption by plant chlorophyll and NIR scattering by plant biomass (Thorp et al., 2017). The 'red edge' is the point of maximum slope in vegetation reflectance spectra, which occurs between wavelengths of 680-750 nm. This is where the reflectance changes from very low in the chlorophyll red absorption region to very high in the near-infrared region because of leaf and canopy scattering (Filella & Peñuelas, 1994). Additionally, other chlorophyll-related spectral indices are widely used to assess various characteristics of vegetation and yield prognosis (Kochubey & Kazantsev, 2012). Importantly, hyperspectral data acquired via field spectroscopy are ideal for developing vegetation indices for detecting some characteristics that traditional multispectral remote sensing cannot (Zhu et al., 2013); these are commonly referred to as hyperspectral vegetation indices (HVIs). Various HVIs have been developed and applied to different vegetation types to examine their physiological properties. Some HVIs were developed and tested on a particular plant species, while others were developed for use across many plant species with varying structures, leaf types, etc. Among them are HVIs proposed by Lu et al. (2015), Nkeiruka et al. (2018), and Sims & Gamon (2002).

Over the years, many researchers have investigated the physiological responses of vegetation to environmental changes under controlled experimental conditions; however, only a few studies have been conducted in field conditions integrating remote sensing with field data (Onyia et al., 2018). Most of the research on the impact of oil spills on vegetation is satellite-based remote sensing, such as those conducted by Adamu (2016); Adamu et al. (2016, 2018); Adoki (2013); Mohamadi et al. & Xie (2016); Ochege et al. (2017); Onyia et al. (2018). These studies only investigated the relationship between oil spill volume and soil hydrocarbon content on vegetation indices without considering other soil geochemical characteristics that could affect the health of the vegetation. Moreover, these studies focus only on one vegetation type at the plot-scale instead of different plant/species types. However, it is important to assess individual plant types because the ability of plant species to tolerate hydrocarbon contamination differs

significantly (Gunderson, 2006). Hence, to fill the research gap identified in 1.3, the objective of this chapter focuses was to determine the impact of soil hydrocarbon parameters (SHP) on the health of plant types at the leaf scale using hyperspectral vegetation indices (HVIs) in the Niger Delta.

The research presented in this chapter is the first known study that seeks to correlate the spectral response (at fine spectral resolution via a field spectrometer) of vegetation (at leaf-scale) to a comprehensive range of soil hydrocarbon characteristics to investigate the effect of oil pollution on the health of vegetation. The only existing study that uses spectroscopy to assess the status of oil spill-induced stress in the vegetation in Lagos and Ogun States in south-west Nigeria, which is not part of the Niger Delta, was conducted by Omodanisi and Salami (2014), which only considered TPH and was not species specific. Accordingly, there is a need for a comprehensive investigation to determine the responses of different plant/species types to SHPs in the Niger Delta.

5.2 Study area

The location of the study was in the River state, Niger Delta, Nigeria. The sites of interest were located in Igwuruta, the upland in Figure 5.1 B1 and Bodo, the shoreline in Figure 5.1 B2. The two sites are approximately 53km apart and were chosen to represent two types of geography. The upland study area Igwuruta is a town in the Ikwerre Local Government Area of Rivers State, near the Omagwa community, which hosts the Port Harcourt International Airport and is just a few kilometres away from Port Harcourt city. As a semiurban town within a short distance of Port Harcourt, the primary occupations of the inhabitants are trading, public and private workers in various government and private companies, farming, etc. Igwuruta town is located between longitude 6º 59" 05' E & 7º 02" 55' E and latitude 4º 55" 23'N & 5º 00" 55'N. The shoreline study area Bodo means 'on the sea'. It is a traditional rural and coastal Ogoni community with 69,000 inhabitants, which is administratively part of the Gokana local government area of Rivers State, Nigeria (Pegg & Zabbey, 2013). The mangrove forests and waterways that line Bodo Creek are an integral component of the community's traditional livelihood structures. The primary occupation in Bodo was fishing and farming, but the oil spill rendered fishers jobless. Igwuruta town is located between longitudes 7º 13" 45'N & 7º 17" 38'N and latitudes 4º 33" 56'N & 4º 38" 52'N. Figure 5.1 shows the locations of the study areas of interest.

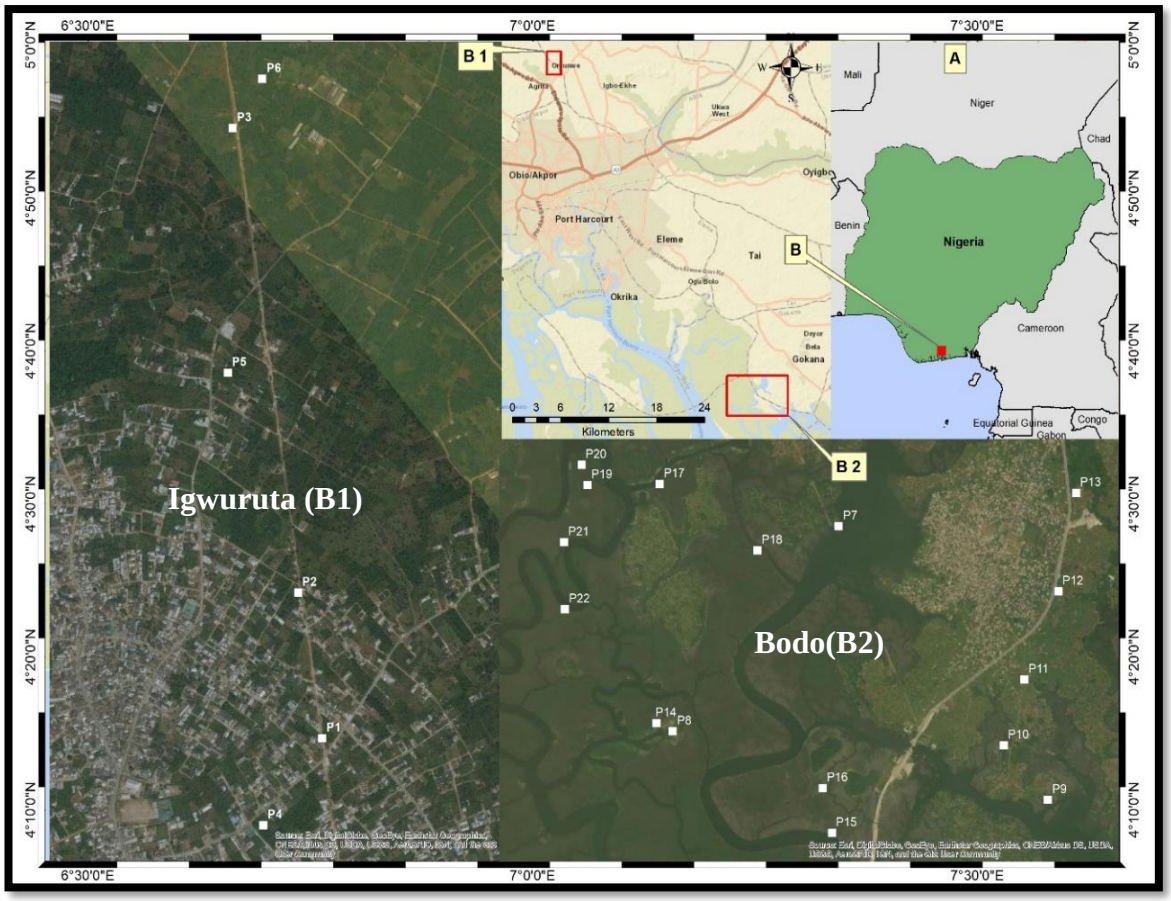

Figure 5.1: (A) Map of Nigeria (green) showing the (B) study area (in red), (B1) upland sample location (soil sample points P1-P6), and (B2) shoreline sample location for dryland (P7-P13) and mangrove (P13-P22).

5.2.1 Plant types

5.2.1.1 Awolowo grass

Chromolaena odorata (L), King & Robinson (Asteraceae, Eupatorieae*)* is a perennial shrub forming dense, tangled bush 1.5-2.0 m in height, occasionally reaching 6 m as a scrambler up trees (Koutika & Rainey, 2010). In Nigeria, this is known as Awolowo, Akintola or Queen Elizabeth weed, native to the Americas from southern Florida to northern Argentina, including the Caribbean islands (Uyi et al., 2014). Elephant grass has spread to the tropics, including Nigeria, and has been used in traditional medicine as an antispasmodic, antiprotozoal, antitrypanosomal, antibacterial, etc. (Igboh, Ikewchi, & Ikewuchi, 2009). It is a common weed found on wasteland, roadsides and farmlands, and it grows in most bushes in Nigeria (Taiwo et al., 2000). Awolowo grass is regarded as fallow because of its ability to be a nutrient sink, its potential benefit to the crop as a regular source of organic matter and nutrients after slashing, and its adaptability as a

fallow plant on acidic soils compared to some leguminous plants (Koutika & Rainey, 2010).

5.2.1.2 Elephant grass

Synonym Pennisetum, also called elephant grass, Napier grass and Uganda grass, is a tropical grass with its origin in humid tropical Africa, belonging to the family Poaceae (Danquah, Roberts, & Appiah, 2018). Elephant grass is the fastest growing plant globally and has long been an important forage crop in the tropics because of its high yields and nutrient value (Singh et al., 2015). There are two plant types of elephant grass, giant (tall) and dwarf (short), with varying heights from 2 to 6 m.

5.2.1.3 Mango tree

Mango (Mangifera indica L.) is an evergreen fruit crop indigenous to Southern Asia, especially eastern India, Burma and the Andaman Islands. Nevertheless, it is one of the most widely cultivated and traded tropical and subtropical fruit crops in the world (Dessalegn, Assefa, Derso, & Tefera, 2014). The largest Mango producing countries are India, China, Thailand, Indonesia, Pakistan, Mexico, Brazil, Bangladesh, Nigeria, and the Philippines (Kumar et al., 2021). Mango trees can reach a height of 15–30 m (50–100 ft). Most cultivated mango trees are between 3 and 10 m (10–33 ft) when fully mature. In contrast, wild, non-cultivated seedling trees often reach 15 m (50 ft) when found in favourable climates, and they can reach 30 m (100 ft) in forest situations (Bally, 2006). Generally, most of the mangoes in Nigeria are wild mangoes, which were also considered for this study.

5.2.1.4 Oil palm tree

Oil palm (Elaeis guineensis, Jacq.) is by far the most productive oil crop. This crop alone can fulfil the large and growing world demand for vegetable oils naturally abundant in all African rainforests (Barcelos et al., 2015). African oil palm has the highest productivity among cultivated oleaginous crops (Barcelos et al., 2015; Punnuri & Singh, 2013). The oil palm is an indigenous plant not only to the people of the Niger Delta region of Nigeria but also to all the people of tropical Africa; until 1900, the Niger Delta was at the forefront in the production of palm oil and palm kernel for export (Aghalino, 2000). Oil palm can reach 60-80 ft in height in nature but is rarely more than 20 or 30 ft in cultivation (Punnuri & Singh, 2013).

5.2.1.5 Mangrove vegetation

Mangroves are shrubs (small trees). The Niger Delta is home to the third-largest mangrove forest in the world (Anejionu et al., 2015; Kuenzer et al., 2014) and the largest in Africa (Ite et al., 2013; Kuenzer et al., 2014; Ohimain, 2003), stretching up to 50 km inland in some places (Musa et al., 2016a). The dominant mangroves in the Niger Delta are red mangroves (Rhizophoraceae) and white mangroves (Avicenneaceae), which comprise more than 90% of the vegetation in the mangrove zone, with Red Mangrove Rhizophora racemosa being the pioneer species (Ayanlade, 2014). Rhizophora racemosa is an essential tree for rural inhabitants living along the coastal region of the Niger Delta in general and Rivers State in particular, both socially and economically (Harcourt, 2012).

Figure 5.1 outlines the methodological approach taken in this chapter.

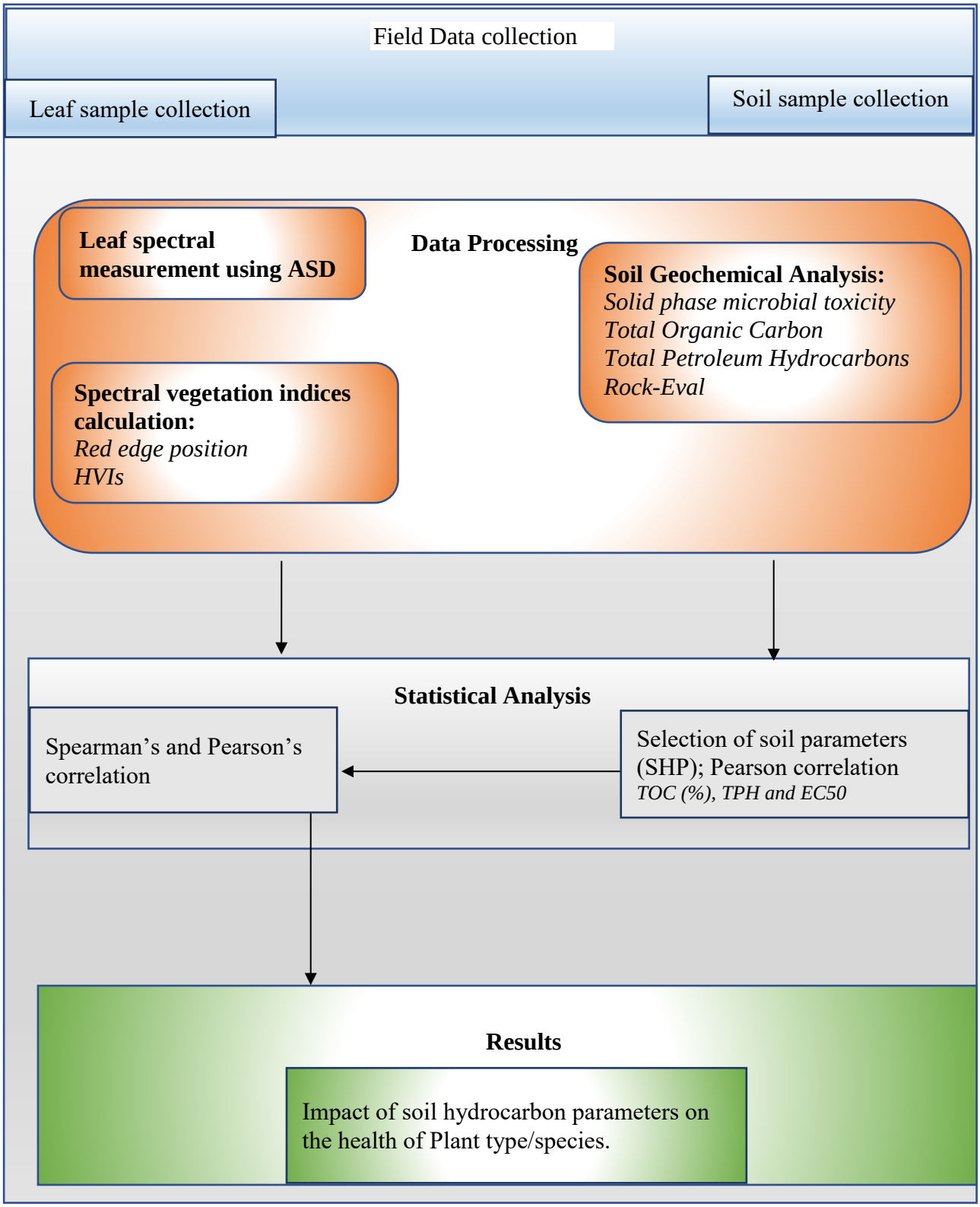

Figure 5.2. Methodology flow chart.

5.3 Data

Concurrent leaf and soil samples were collected at oil spill sites, and their geographic coordinates were recorded during a fieldwork campaign in the Niger Delta region of Nigeria in December 2018. The month was chosen because the weather conditions are more favourable during this season, with almost zero rainfall. Before the fieldwork, a reconnaissance trip was carried out in June 2018 to become familiar with the study area, accompanied by some academics from the University of Port Harcourt, alongside some local community members. The reconnaissance fieldwork also enabled potential sample collection sites to be identified based on accessibility to the sites in terms of logistics and security.

5.3.1 Leaf sample

Leaf samples from the five plant species were collected at locations with different levels of exposure to oil spills. Each sample plot was approximately 30 m-by-30 m square to fit the pixel size of the Landsat images. Leaf samples for each plant species were collected across each plot to capture a reliable representation of each plant type and kept in a cooling box, as shown in Figure 5.3. The sampled plants were Awolowo grass, elephant grass, mango tree, oil palm tree and mangrove vegetation (Figure 5.4). The leaf samples were located from plots corresponding to two types of land cover: dry land and mangrove. At least two to four types of plant samples were collected, while only mangrove plants were collected from the plots located in mangrove areas. A total of 21 plots were sampled, which consisted of five different types of plants.

Figure 5.3: Soil and leaf samples in a cooling box.

Figure 5.4: Sampled plot showing Mango, oil palm, Awolowo and Elephant. Field observation.

5.3.2 Soil sample

Soil samples were also collected alongside the leaf samples from within a plot. The soil samples were collected to determine the concentration of total petroleum hydrocarbons (TPHs) and other SHPs and then investigate how their presence affects the health of the vegetation (Arellano et al., 2015; Omodanisi & Salami, 2014). For each sample plot, five soil samples were collected from the four edges of the 30 m-by-30 m plot and one in the middle of the plot at a depth of 30 cm (Onyia et al., 2018). Oil residues highly contaminate the Niger Delta soil in the upper 20 cm (Little et al., 2018). The soil samples were collected using a portable soil auger from each plot (Figure 5.5), which was washed with water after each sample was collected to prevent cross-site contamination. Five soil samples were subsequently mixed into one composite sample representing the plot.

The collected soil and leaf samples were put in a plastic zip-locked bag, labelled and stored in a portable cooling box filled with ice packs to keep the sample cool (Abdullah et al., 2018) (Figure 5.3). The soil samples were frozen upon returning from the field to prevent exposure to a temperature above 30 °C. This was done to control further chemical reactions in the soil (Onyia et al., 2018). Figure 5.6 is the Mangrove plant exposed to oil spills.

Figure 5.5: Soil samples were taken with a portable auger.

Figure 5.6: Mangrove vegetation on hydrocarbon-polluted sites, with dead mangrove sites (top) due to oil spills in Bodo, Ogoni land in the River state. Observed during fieldwork.

5.4 Methods

5.4.1 Leaf spectral measurements and pre-processing

The spectral reflectance measurements of leaf samples were obtained using an Analytical Spectral Devices (ASD) FieldSpec Pro instrument loaned from the School of Geography (University of Nottingham) based on the guidelines provided by the Field Spectroscopy Facility (https://fsf.nerc.ac.uk/instruments/asd_fieldspec.shtml, n.d.). The ASD FieldSpec Pro is the industry standard for a broad range of challenging remote sensing applications. It offers superior signal-enhancing features and high resolution with a 350-2500 mm spectral range. The ASD Fieldspec Pro was used indoors in a laboratory setting instead of outdoor due to the security risk of taking such an instrument to the field in a place like the Niger Delta. All leaf spectra were measured within four hours of field collection to ensure they were still fresh during the analysis with negligible degradation in their biophysical condition.

A black box with a black, low-reflectivity material was constructed to prevent scattered light from objects other than the leaf samples from interfering with the measurement of the spectra. A blackboard equal to the size and thickness of the white panel used to calibrate the ASD Fieldspec Pro was employed to place the leaf samples (Figure 5.7a). Two 100 W Lowel-Pro lamps were fixed into the box to illuminate the leaf samples, as shown in Figure 5.6. When collecting spectral scans with the ASD Fieldspec Pro, the averaging for each scan was set to 100 to improve the signal: ratio. The ASD Fieldspec Pro was optimised to adjust it to the sensitivity of the instrument detectors according to the illumination condition at the time of measurement by taking a measurement of the whiteboard (Figure 5.7 b). After the instrument calibration, the whiteboard was replaced with the blackboard with the plant sample, and the plant sample was placed on it, covering at least 90% of the blackboard to ensure that field of view (FOV) was completely field. Typically, 4-6 spectral measurements were taken for each sample from different angles and positions to ensure that every aspect of the leaf sample was measured to obtain a representative spectrum.

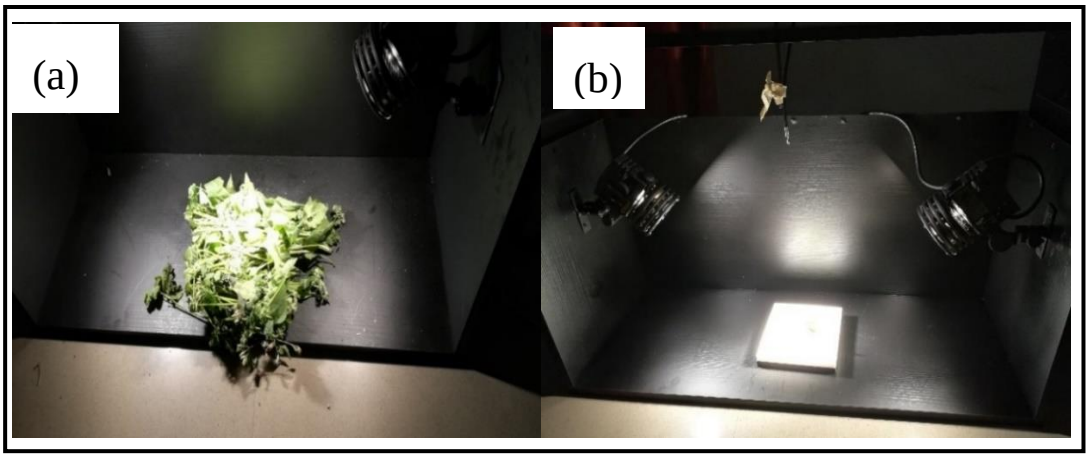

Figure 5.7: A black box containing (a) a plant sample and (b) two 100 W Lowel-Pro lamps and a whiteboard during instrument calibration. Field observation.

Post-processing of spectral measurements.

The spectral measurements of the leaves were post-processed using the ASD FieldSpec Pro software, ViewSpec Pro. The ViewSpec application is used for post-processing spectra files from ASD FieldSpec Pro (ASD, 2008) and includes many useful features, such as graphing, scaling, 1st derivative and conversion of the spectrometer's binary files into ASCII text files (Walker, 2009). The measured spectra of leaf samples were converted into spectral reflectance and 1st derivatives and exported as ASCII files. For the spectral shape analysis, the reflectance signatures were averaged for a particular plant type in a plot (Serrano-Calvo et al., 2021). Also, the spectral resampling to Hyperion , sentinel 2 and Landsat 7 was performed using the filter functions (User Defined Filter Function in ENVI) for each waveband of the sensors to assess how the plant species will appear on satellite imagery. A filter function is the sensitivity/spectral response of the satellite's sensor to specific wavelengths within the bandwidth for a given waveband. The spectral response performed a weighted average of the reflectance from the hyperspectral signature at the corresponding wavelengths, which then gives a single value of reflectance for each waveband for the sensor with the lower spectral resolution by multiply the spectral response values (0-1) from a filter function with the reflectance values for the corresponding wavelengths in the hyperspectral signature and then calculate the weighted average.

5.4.2 Soil geochemistry analysis

5.4.2.1 Solid-phase microbial toxicity (EC50 mg L^{-1})

The Microtox® Solid Phase Test (SPT) was used to assess the bioavailability of toxins within the sampled soils using the test organism *Vibrio fischeri* (strain NRRL B-1117),

which is a luminescent bacterium. The methodology followed that recently applied to evaluate soils and sediments from London and New York (Vane et al., 2020a, Vane et al., 2020b). This strain of the organism can be used to assess both acute and chronic toxicity in samples, as it is highly sensitive to a broad range of chemicals. The test was designed by the manufacturer to be used specifically on soils and sediments. Seven grams of dry weight of a soil sample was transferred to a beaker and 35 ml of SPT diluent (3.5% NaCl) was added. To analyse a representative sample, the suspension was then stirred for 10 minutes on a magnetic stirrer with a speed set to achieve a vortex depth in the liquid of approximately 50% of the liquid level at the beaker wall. Then, 1.5 ml of the suspension was transferred by pipette to cooled SPT tubes from a region adjacent to the beaker wall, approximately 2 cm above the bottom of the beaker, using a modified pipette tip with an enlarged opening (to accommodate any large particles present). The SPT tubes were cooled in an incubation block and placed in a water bath at 15°C. 1:2 serial dilutions of the sample were made in SPT tubes to give 2 controls and 13 dilutions in duplicate. These were then left for 10 minutes to equilibrate to temperature.

Meanwhile, freeze-dried bacteria were reconstituted in ultra-pure water (test reagent) and left in the reagent well of a Microtox® M500 Toxicity Analyser. A timer was then started, and 20 µl of test reagent was immediately transferred by pipette to each SPT tube. Each sample was mixed well and a tube filter was placed in the SPT tube to just above the liquid level. After 20 minutes, the samples were filtered to remove the sediment, and 0.5 ml of the filtrate was pipetted into glass cuvettes placed in the wells of the analyser, and a timer started for 5 minutes. After this time, the sample light output from each cuvette was measured in the analyser. The measurements were used to create a dose–response curve, and an EC50 value was calculated which indicate the level of toxicity in the soil.

5.4.2.2 Total organic carbon (TOC)

The total organic carbon content (TOC % wt/wt) was determined using an Elementar VarioMax C, N analyser operated in C mode. All soils were first prepared by acidification with HCl (50% v/v) to remove inorganic carbon (e.g., carbonate). The limits of quantification reported for a typical 300 mg sample were 0.18 % (wt/wt) (Vane et al., 2007).

5.4.2.3 Total petroleum hydrocarbons (TPH)

To measure the total petroleum hydrocarbon content (TPH), 1 g of ground sediment was extracted with a dichloromethane (DCM)/acetone (1:1 v/v) mixture using an accelerated solvent extraction system (ASE 200, Dionex). Extracts were reduced to dryness and reconstituted in 1 mL toluene, and 5 µL aliquots were spotted onto silica-rods (Chromarods-S III). The rods were developed for 21 minutes using *n*-hexane, for 8 minutes with toluene and 1.5 minutes with dichloromethane/methanol (9:1 v/v). The concentrations of saturated and aromatic hydrocarbons were determined using an Iatroscan Mk6 s instrument (Vane et al., 2020a; Vane et al., 2020b). The calibration was performed for saturated hydrocarbons using pristane, aromatic hydrocarbons using triphenylene, and resins using an in-house purified standard extracted from combined urban road-run-off sediments. TPH was calculated as the sum of saturated and aromatic hydrocarbons. The limit of quantification (LoQ) for total non-volatile petroleum hydrocarbons was 3 mg/kg.

5.4.2.4 Rock-Eval (PI & HI)

Rock-Eval is used as industrial standard hydrocarbon exploration method (bulk rock) for measuring product index (PI) and hydrogen index (HI), Hydrocarbon pollution was assessed using a Rock-Eval (6) pyrolyzer. Powdered samples (20 mg dry wt.) were heated from 300°C to 650°C at 25°C min-1 in an inert atmosphere of N2, and the residual carbon was then oxidised by the addition of a constant flow of clean compressed oxygen-containing air at 300°C to 850°C (Thomas et al., 2019; Waters et al., 2019; Whitelaw et al., 2019). Free and bound hydrocarbon contents (S1, S2) were measured using a flame ionisation detector (FID). All the soil analysis were carried out at the British Geological Survey (BGS) in Keyworth.

5.4.3 Spectral characterisation using vegetation indices

5.4.3.1 First derivative and red edge position (REP)

Derivative analysis was used to detect spectral absorption features, reduce spectral variations due to illumination and baseline shifts to reveal absorption features masked by broader interference from other leaf components and biochemical properties (Serrano-Calvo et al., 2021). A common means of using spectral derivatives in the remote sensing of plant physiology has been to characterise the red edge (Blackburn, 1998). The red edge, which is the point of maximum slope in vegetation reflectance spectra of 1st derivatives,

occurs between wavelengths of 680-750 nm, where the reflectance changes from very low in the chlorophyll red absorption region to very high in the near-infrared region due to leaf and canopy scattering (Filella & Peñuelas, 1994). For this research, the red edge position (REP) was derived from the wavelength of the peak values of the 1st derivative graphs.

The next analysis was the calculation of hyperspectral vegetation indices (HVIs). Many HVIs have been developed to estimate leaf pigment content (Sims & Gamon, 2002). Most of the published HVIs have a strong relationship with leaf chlorophyll content (Lu et al., 2015) and have been tested for only one or at most a few related species. Therefore, it is currently unclear which HVIs can be applied across different species with variable leaf structure characteristics (Sims & Gamon, 2002). To overcome such challenges, the HVIs previously applied either across species or previously utilised in the study area were carefully selected owing to the difference in leaf surface structures between the different plant species sampled in this study.

5.4.3.2 Modified Normalised Difference Index (mND_{705})

The mND_{705} spectral is an index for predicting leaf pigment content that is relatively insensitive to species and leaf structure variation, which could be applied in larger-scale remote-sensing studies without extensive calibration developed by Sims & Gamon (2002). They found that previously published spectral indices provided relatively poor correlations with leaf chlorophyll content when applied across various species and plant types. By developing a new spectral index that reduces the effect of differences in leaf surface reflectance, they significantly improved the correlations with chlorophyll content. The mND_{705} index developed by Gitelson & Merzlyak (1994) was modified using wavelengths at 705 and 750 nm, which are based on the chlorophyll index to compensate for high leaf surface reflectance by eliminating the effect of surface reflectance by incorporating the reflectance at 445 nm (Sims & Gamon, 2002).

$$mND_{705} = (R750 - R705)/(R750 + R705 - 2R445) \quad \text{Eq. 5.1}$$

where R= the reflectance at a particular wavelength (in nm).

5.4.3.3 Modified Datt index (MDATT index)

The MDATT index was developed by Lu et al. (2015) for remote estimation of chlorophyll content in plants with varying leaf surface structures based on the Datt

(1999b) principle by introducing a third band into the index. The MDATT index was modified to compensate for high leaf surface (specular) reflectance and scattering from the mesophyll, which tends to alter reflectance across the whole visible and near-infrared spectrum. Among the reflectance indices tested by Lu et al. (2015), the MDATT index performed best among all the indices. It could be the best vegetation index for estimating leaf Chl content, regardless of the leaf side or species (Lu et al., 2015):

MDATT index =(R719−R726)/(R719−R743) Eq. 5.2

5.4.3.4 Normalised Difference Vegetation Vigour Index (NDVVI)

Onyia, Balzter, & Berrio (2018) developed the normalised difference vegetation vigour index (NDVVI) as a new method for monitoring the impact of oil pollution on biodiversity at a regional scale in the Niger Delta region using integrated satellite remote sensing and field data for biodiversity monitoring. NDVVI was used on vascular plants of various species observed in polluted and unpolluted (control) locations. The NDVVI variants were estimated from Hyperion wavelengths sensitive to petroleum hydrocarbons, and the NDVVI variants accurately predicted species diversity compared to traditional narrowband vegetation indices.

NDVVI = (Ri − Rj)/(Ri + Rj) Eq. 5.3

where:

Ri = reflectance at least sensitive wavelength =R

Rj = reflectance at most sensitive wavelength=R

Therefore:

NDVVI844,447= (R844 – R447)/(R844 + R447) Eq. 5.4

5.4.3.5 Photochemical reflectance index (PRI)

The photochemical reflectance index (PRI), derived from narrowband reflectance at 531 and 570 nm wavelengths, was used to explore photosynthetic radiation use efficiency for 20 species representing three functional types: annual, deciduous perennial, and evergreen perennial by Gamon, Serrano, & Surfus (1997). Although initially developed

to estimate xanthophyll cycle pigment changes, it was related to carotenoid/chlorophyll ratios in green leaves (Sims & Gamon, 2002).

$$PRI = (R531 - R570)/(R531 + R570) \quad \text{Eq. 5.5}$$

5.4.4 Statistical analysis

Pearson's correlation analysis was used to assess the correlation between the leaf spectral characteristics and the soil geochemistry analyses to determine the effect of the presence of hydrocarbons in the soil on the health of vegetation. However, many of the soil characteristics analysed are inherently correlated with each other and therefore considered redundant. Therefore, the SHPs that were positively strongly correlated with TPH were first identified and removed from subsequent analysis. Parameters with with *R*-values <0.5 were considered to be weakly correlated and retained. Parameters that had a strong correlation (p>0.5) with TPH were deemed to be essentially providing redundant information and therefore discarded. Spearman's and Pearson's correlation analyses were then used to test the hypothesis that various plant types are affected by the remaining SHPs, leading to reduced leaf chlorophyll content in plant families. The relationship between the SHP (TPH and soil parameters), i.e., and the spectral properties of leaves samples, may not be linear; hence, both Spearman's and Pearson's correlations were used. The Pearson's correlation coefficient is typically used for jointly normally distributed data (data that follow a bivariate normal distribution). In contrast, Spearman's rank correlation measures a monotonic association of continuous data, ordinal data, or data with relevant outliers (Schober & Schwarte, 2018).

5.5 Results

5.5.1 Soil geochemical analysis

5.5.1.1 Selection of hydrocarbon parameters

Table 5.1 shows the correlation between soil hydrocarbon parameters (SHPs) – resin, aromatic and aliphatic content, TPH, PI and HI. The results show that the hydrocarbon parameters are strongly correlated with TPH, with resin having R=0.99, aromatic and aliphatic both having *R*=1, PI (0.57) and HI (0.61), respectively. The results show a strong correlation between TPH and other hydrocarbon parameters. When the TPH is high, the other hydrocarbon parameters are likely going to be high and likely have a similar impact on the vegetation. Hence, the THP was subsequently correlated with the general soil

parameters, Microtox (EC50 mg L^{-1}) and Total Organic Carbon (TOC (%)), to determine their impact on the vegetation. The result helped in narrowing down the hydrocarbon parameter to just the TPH.

Table 5.1: Pearson's correlation analysis of hydrocarbon and soil parameters.

Soil parameters	Resin	Aromatic	Aliphatic	TPH mg kg^{-1}	PI	HI
Resin	1	0.99	0.99	0.99	0.59	0.66
Aromatic	0.99	1	1	1	0.57	0.61
Aliphatic	0.99	1	1	1	0.59	0.63
TPH mg kg^{-1}	0.99	1	1	1	0.58	0.62
PI	0.59	0.57	0.59	0.58	1	0.84
HI	0.66	0.61	0.63	0.62	0.84	1

5.5.1.2 Soil hydrocarbon parameter

Table 5.2 details the soil sample plot number, plant type sampled from each plot and the selected SHPs with the red text indicating the average values of SHP for upland and shoreline sample sites and the combined upland and shoreline sites. The plant types are Awolowo grass (AG), Elephant grass (EG), oil palm tree (OP), mango tree (MT) and mangrove (MG). A total of 22 plots and five types of plant types/species were sampled, thirteen from both upland and shoreline sites (P1-P13) and mangrove land (P14-P22). For dryland, six upland plots were sampled in Igwuruta-Porthacourt (P1-P6), and seven were sampled in Bodo close to the shoreline (P7-P13). For the plots at Igwurata-Porthacourt, three plant types (Awolowo grass, Elephant grass and Oil palm tree) were sampled, except at P2, which had only Awolowo grass and Elephant grass. Table 5.2 shows different levels of concentration of SHP in the soil of sampled plots. In terms of THP, the content is relatively similar for both dryland and mangrove sample plots, with values ranging from 89 mg kg^{-1} to 2606 mg kg^{-1}, except for P20 (mangrove), which had a TPH of 42996 mg kg^{-1}. TOC (%) has variable concentration levels, with mangroves having a higher concentration of TOC (%) between 0.61% and 26.17% and dryland between 0.50% and 2.21%. The level of toxicity in the soil is grouped into nontoxic (EC50 > 10,000 mg L^{-1}), moderate toxicity (EC50 10,000-5000 mg L^{-1}), and highly toxic <5000. On this basis, mangrove soils have a high level of toxicity, as shown by the EC50 with P14-P18 having EC50 $\leq$ 5000 mg L^{-1}, along with one moderate toxicity (P22) with EC50 10,000-5000 mg L^{-1} and three nontoxic plots P19-P21 with EC50 >10,000 mg L^{-1} (Table 5.2). For the

sample plots on the land, the level of toxicity was low, with EC50 >10,000 mg L^{-1} except for P10, which had EC50 >5000 to <10,000 mg L^{-1}.

Figure 5.8 shows a boxplot for TPH, EC50 and TOC (%), with the TPH measurement at P20 (24996 mg kg^{-1}) removed from the mangrove boxplot because it is an outlier that could affect the boxplot. For example, the TPH concentrations for mangroves and drylands are low. Additionally, Figure 5.9 shows maps of the SHP content for both dryland (shoreline) and mangrove combined in Figure 5.9a and dryland (upland) in Figure 9.5b. The results show that all the SHPs are more concentrated in the mangrove (P14-P21) in the north-west and south-west location of the study area except the toxicity in the north-east and south-east (P18. P9-P10), which are located on dry land (shoreline). For the upland, EC50 concentration is none toxic but more concentrated in the southern part of the map (P2 and P4), while the TOC (%) are highly concentrated toward the northern part of the study area (P5). Also, the TPH has a high concentration in the southern part of the study area

Table 5.2. Soil sample plot number, plant types sampled from each plot and soil parameters.

Plot No	Plants Types	Microtox: EC50 mg L^{-1}	Total Organic Carbon:TOC (%)	Total TPH mg kg^{-1} (dry weight sediment)
P1	AG,EG, OP	27899	1.58	642
P2	AG,EG	19561	1.66	2247
P3	AG,EG, OP	27309	1.86	1508
P4	AG,EG, OP	18922	1.24	89
P5	AG,EG, OP	23128	2.15	136
P6	AG,EG, OP	36496	1.38	151
P7	AG,EG, MT, OP	40423	0.8	212
P8	AG,EG, MT, OP	33671	0.5	163
P9	AG,EG, OP	13278	1.29	2606
P10	AG,EG, MT, OP	7986	1.27	770
P11	AG,EG, MT, OP	20364	1.37	89
P12	AG,EG, MT, OP	37792	0.96	89
P13	AG,EG, MT, OP	10975	2.21	1174
P14	MG	4848	13.98	396
P15	MG	2525	26.17	89
P16	MG	3990	13.63	1887
P17	MG	2992	17.06	399
P18	MG	2672	15.74	393
P19	MG	19168	1.97	996
P20	MG	14248	13.85	42996
P21	MG	29720	0.61	329
P22	MG	6455	12.83	826
ADL		22446	1.40	760
AM		9623	12.90	5368
TA		18383	6.10	2645

Note: AG=Awolowo grass, EG=Elephant grass, OP=Oil palm, MT=Mango Tree, MG=Mangrove, ADL=average values for dryland, AM=average values for mangrove, TA=Total average values for each soil property. The red text indicates the average values of SHP for upland and shoreline sample sites and the combined upland and shoreline sites.

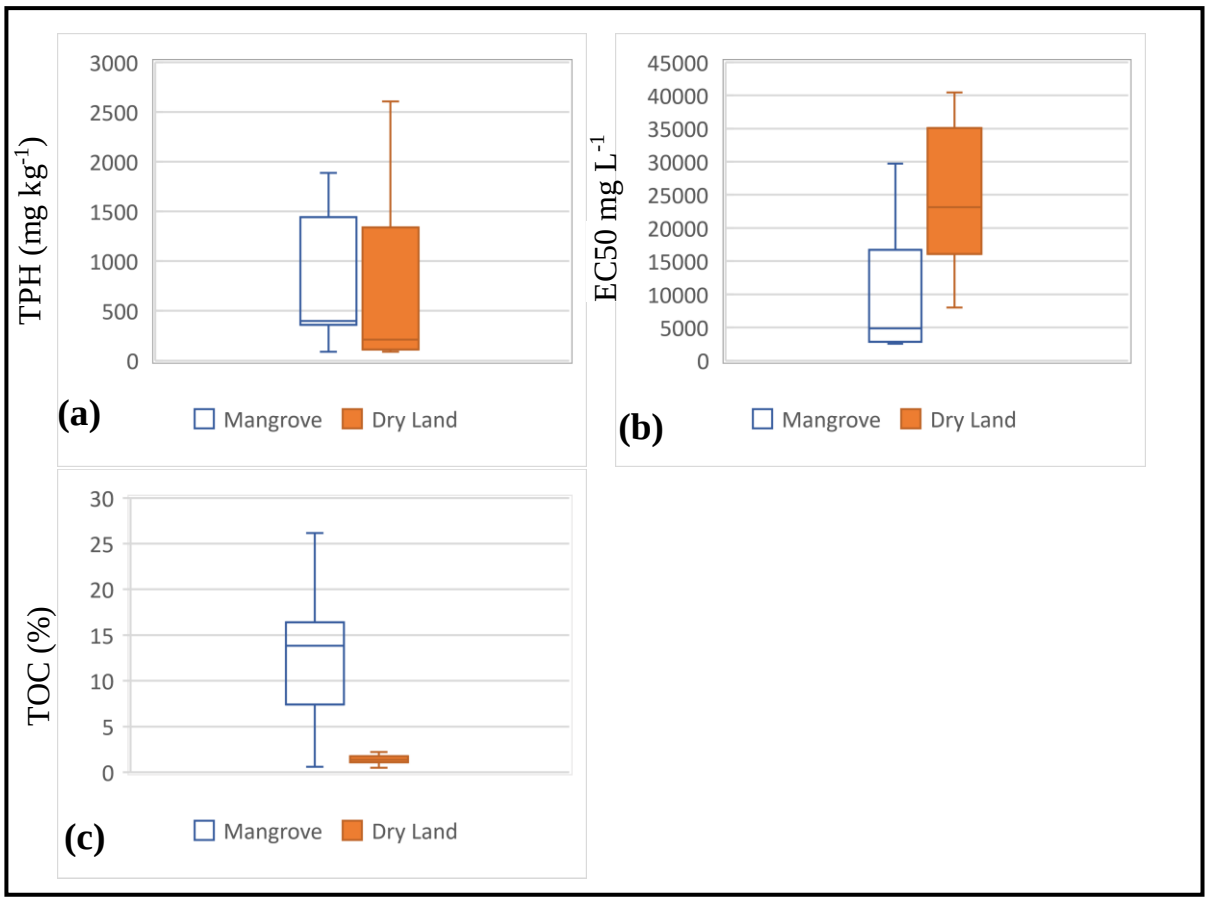

Figure 5.8: shows a boxplot for (a) TPH (mg kg^{-1}), (b) EC50 and (c) TOC (%).

The TPH measurement at P20 (24996 mg kg^{-1}) was removed from the mangrove boxplot because it is an outlier that could affect the boxplot

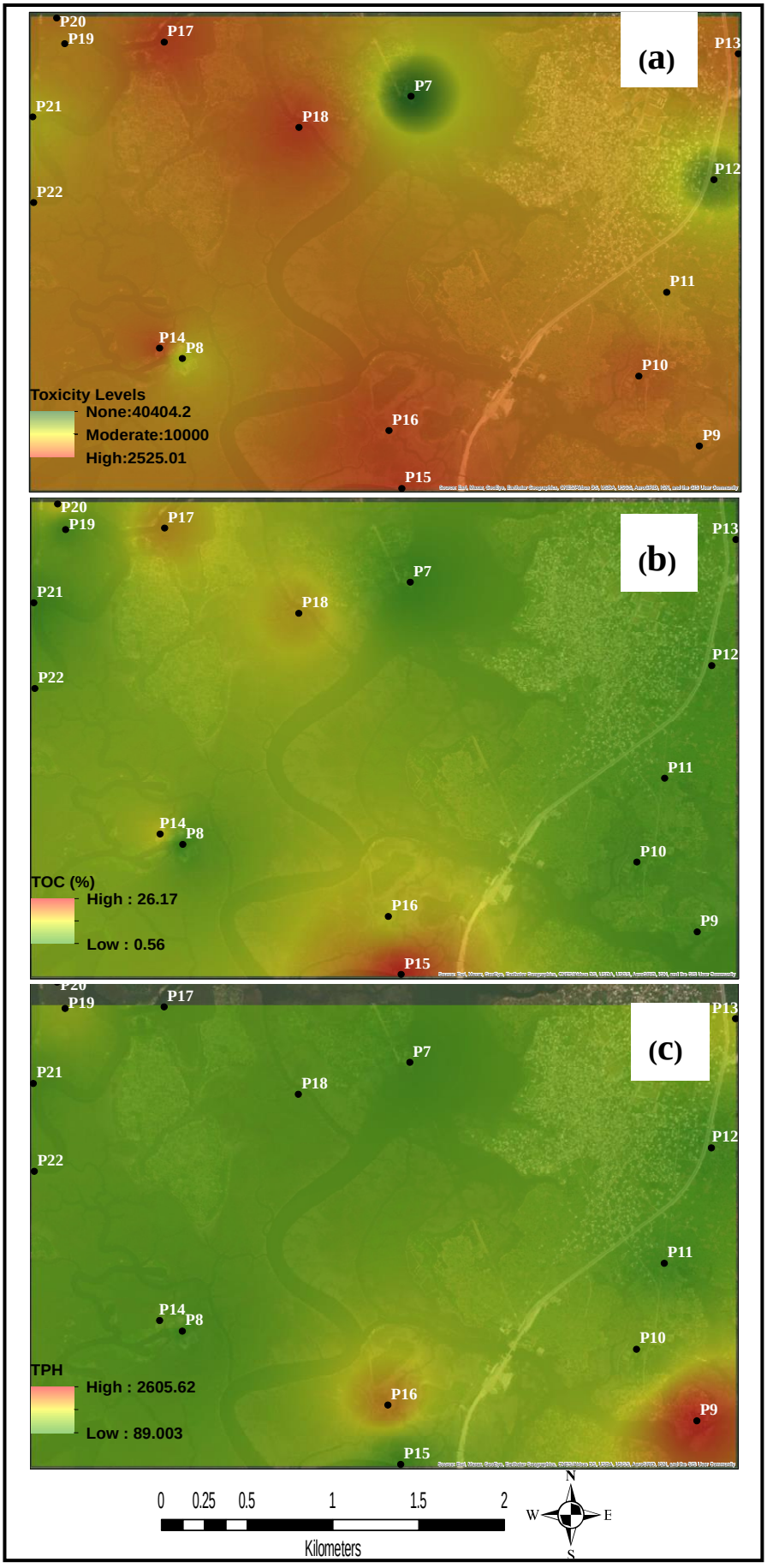

Figure: Soil hydrocarbon parameter content Cont.

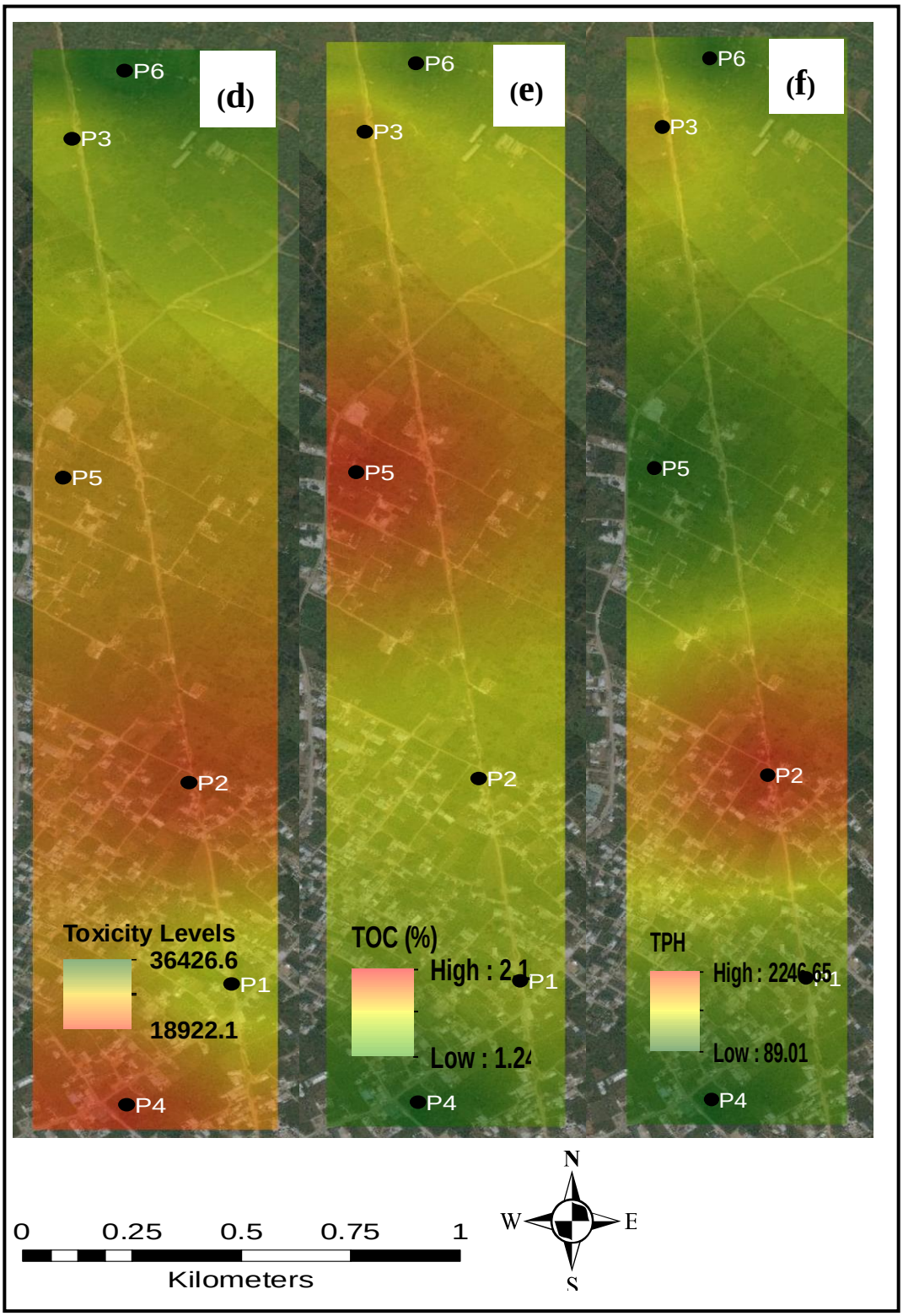

Figure 5.9:Soil hydrocarbon parameter content maps for the shoreline (a) toxicity (EC50), (b) TOC (%) and (c) TPH; and upland area (d) toxicity (EC50), (e) TOC (%) and (f) TPH.

5.5.1.3 Relationship between TPH and soil parameters

Figure 5.10 shows the correlation between TPH and TOC (%) and TPH and EC50 for dryland and mangrove land cover types. The correlation is between TPH and EC50 and TPH and TOC (%) for all samples (Figure 5.10a and b, respectively), TPH and EC50 and TPH and TOC (%) for mangroves (Figure 5.10c and d), as well as TPH and EC50, and TPH and TOC (%) dryland (Figure 5.10e and f). The results show a weak correlation between TPH and TOC (%) and TPH and EC50 for both the Pearson's and Spearman's correlation, except for the correlation between TPH and the EC50, which shows a moderate positive correlation for the dryland sample sites (R= -0.500). Note, the smaller the value of EC50 (i.e. EC50 <5000 mg L^{-1}), the more the toxicity, hence, a negative sign of correlation mean positive.

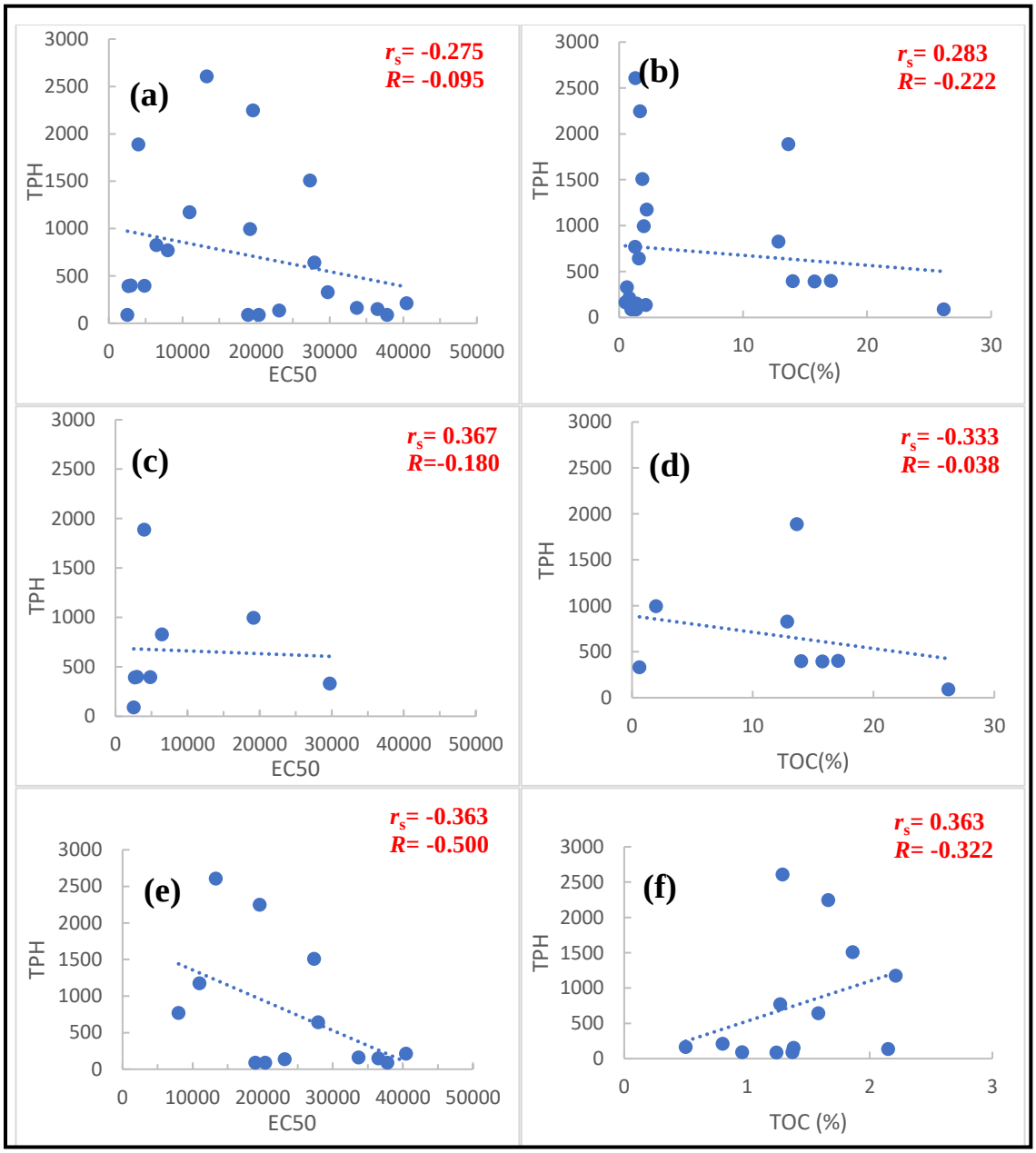

Figure 5.10:Relationship between TPH and soil parameters (a) TPH and EC50 for all samples, (b) TPH and TOC (%) for all samples, (c) TPH and EC50 for mangroves, (d) TPH and TOC (%) for mangroves (%), (e) TPH and EC50 for dryland, and (f) TPH and TOC (%) dryland.

5.5.2 Spectral analysis

5.5.2.1 Vegetation spectra

Figures 5.11 show each plant species' mean spectral reflectance curve for the dry land (upland and near the shoreline) and the mangrove sample plots from hyperspectral data (Figures 5.11a). Others are mean spectral reflectance hyperspectral data resample to Hyperion (Figure 5.11b), Sentinal 2 (Figure 5.11b) and Landsat 7 (Figure 5.11d). The

results show that the spectral reflection curve from Hyperion, a satellite-based hyperspectral sensor with more spectral bands than sentinel 2 and Landsat 7, looks similar to the spectral of in Figure 5.11a. Blue indicates mangrove vegetation, black indicates Awolowo, red indicates elephant grass, yellow indicates oil palm tree, green indicates mango tree, and blue indicates mangrove. Elephant grass has the highest reflectance in the near-infrared (NIR) region (700-1300 nm) of the electromagnetic spectrum, while mangrove grass has the lowest reflectance. The reflectance of mango trees and the Awolowo grass are almost the same within NIR, while the oil palm has the second-lowest reflectance after the Mangrove (Figure 5.11a). Additionally, the shape and the spectral curve were different for each plant group. While mango and oil palm trees have smooth curves around 977 nm, Awolowo grass, elephant grass, and mangrove have more variation due to deeper spectral absorption features in the same region.

Figure 5.12 shows the land and shoreline mean spectral reflectance for plants found on dryland, i.e., both upland land and shoreline in the NIR region, excluding the mangrove from hyperspectral data (Figure 5.12a). It can be observed that the upland plants have higher spectral reflectance than those of the same plant type.

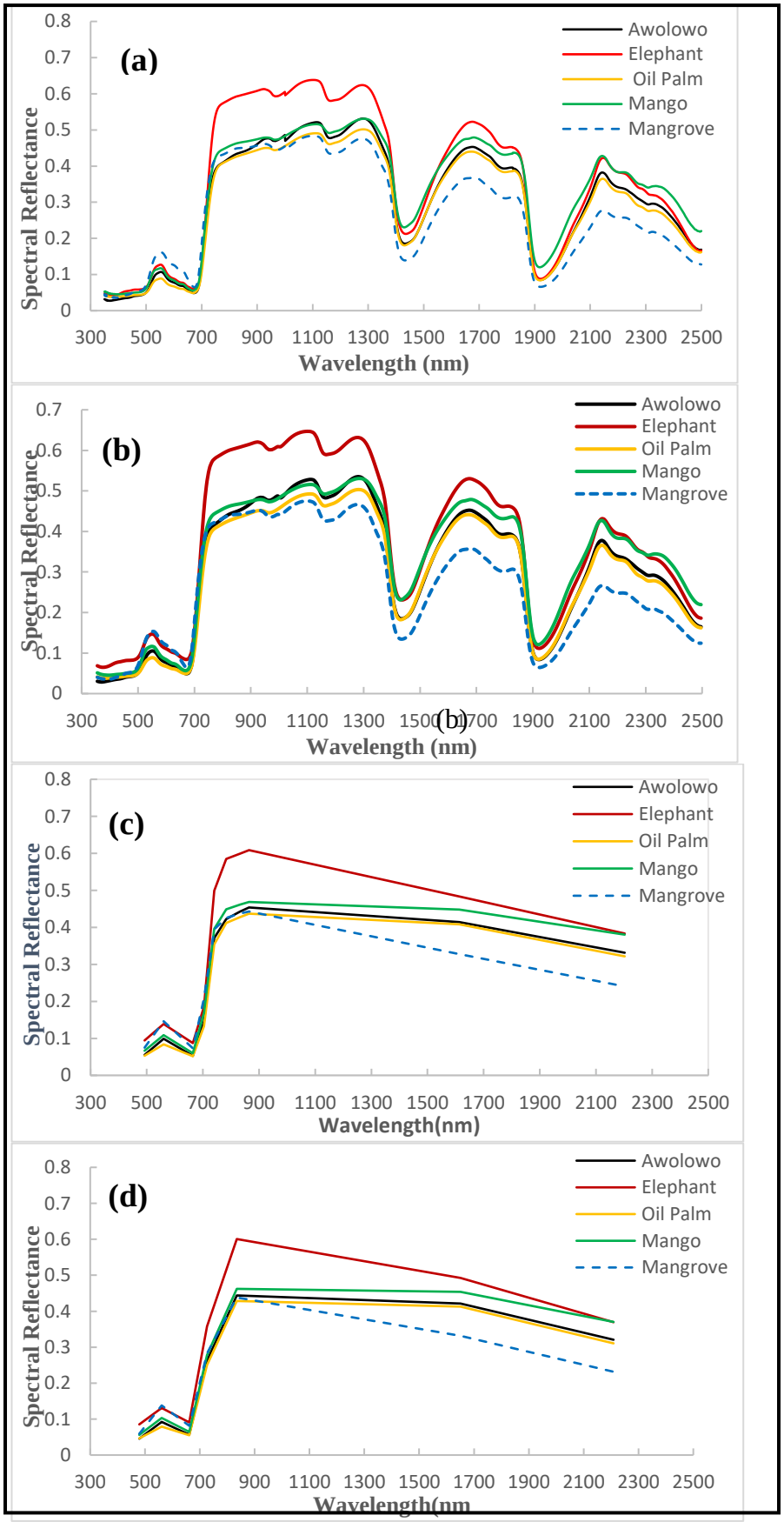

Figure 5.11:Mean spectral reflectance for each plant (a) hyperspectral data, and resampled reflectance to satellite sensors (b) Hyperion, (c) Sentinel 2 and (d) Landsat 7.

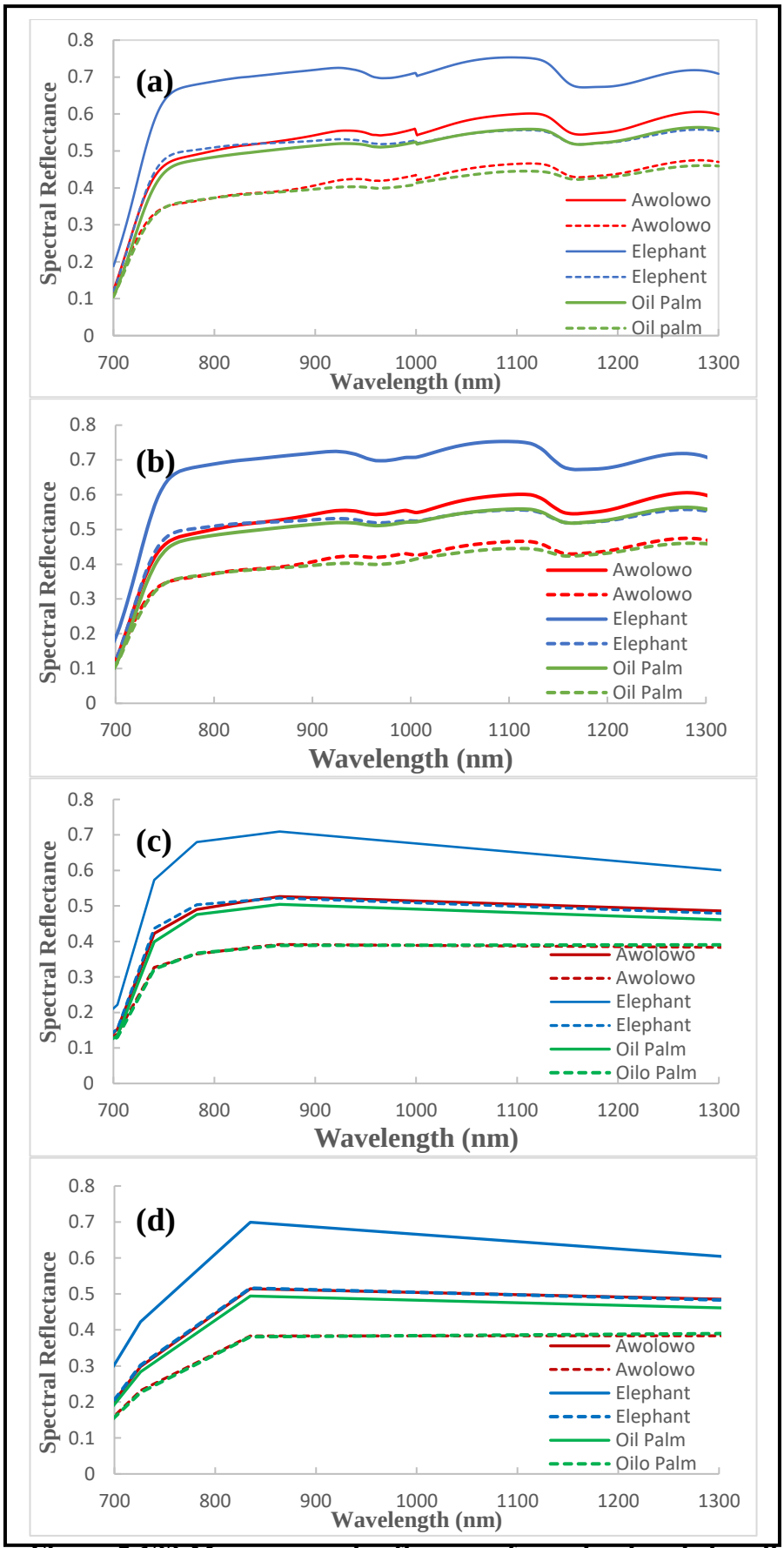

Figure 5.122:Mean spectral reflectance for upland and shoreline(broken lines) for land plants in Near-infrared region (a) hyperspectral data, and resampled reflectance to satellite sensors (b) Sentinel 2, (c) Landsat 7 and (d) Landsat 8.

Figure 5.13 shows the spectral reflectance curve for each plant type with varying TPH soil concentrations for Awolowo grass (Figure 5.13a), Elephant grass (Figure 5.13b), oil palm trees (Figure 5.13c), including upland and shoreline, mango trees (Figure 5.13d) and Mangrove (Figure 5.13e). For the three plant types found on dryland: upland (with the prefix "u" and a broken line) and shoreline (with a prefix "s") in Fig 5.13a-c, it is evident that the upland vegetations have higher spectral reflectance than those near the shorelines, even at similar or the same level of TPH concentration. Among the plant types, elephant grass (shoreline), oil palm (upland) and mango tree (shoreline) have the highest vegetation spectral reflectance (albedo), corresponding to the lowest TPH concentration of 89 mg kg^{-1} (Figure 5.13c and d). While the trend continues for oil palm trees with the overall spectral reflectance decreasing with the TPH concentration, the same thing could not be said of the elephant grass (shoreline) and mango trees. The corresponding highest reflectance curves to TPH concentration for the remaining plant species are at TPH 150 mg kg^{-1} upland and 1174 mg kg^{-1} shoreline (Awolowo), 136 mg kg^{-1} upland (Elephant grass) and 329 mg kg^{-1} (mangrove) instead of 89 mg kg^{-1}, respectively (Figure 5.13a-c and e). However, for mangroves, the lowest albedo corresponds to the highest TPH concentration (42,996 mg kg^{-1}).

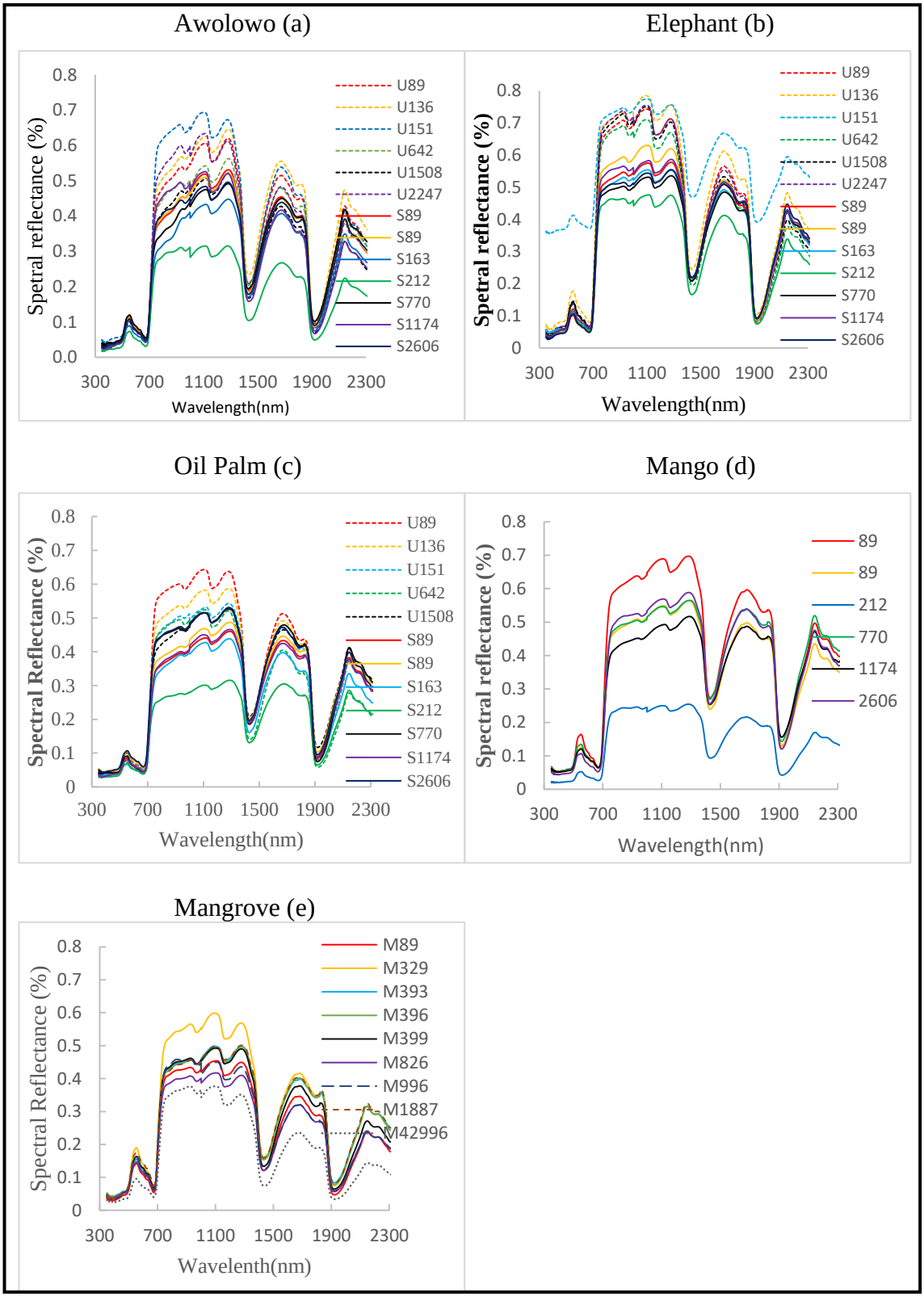

Figure 5.13:Spectral reflectance of different plant types exposed to varying TPH concentrations: (a) Awolowo, (b) elephant grass, (c) oil palm, (d) mango and (e) mangrove.

Prefixed to the to the TPH concentration; U=upland; S=shoreline; M=mangrove.

5.5.2.2 First derivative and Red Edge Position (REP)

Figure 5.14 shows the REP, the peak points of the 1st derivative and the TPH concentration. The number with a prefix corresponds to various TPH concentrations. The results show that different plant types have REPs at slightly different wavelengths. Generally, the first derivative peaks for plant samples located on the upland (labelled with the prefix "U" with broken lines) are higher than plants near the shoreline (labelled with the prefix "S" with continuous lines) for Awolowo grass, Elephant grass and oil palm trees (Figure 5.14 a-c). Additionally, the first derivative peaks show no obvious relationship to the TPH concentration for some plant species/types. For instance, the highest peak occurred for a TPH concentration of 2247 mg kg^{-1} (U2247) for both Awolowo and Elephant grass, while it occurred at the higher TPH (S2606) and lowest (S89) for shoreline samples of Awolowo grass and Elephant grass, respectively (Figure 5.14 a and b).

Table 5.3 shows the wavelengths at which REPs occur for the various plant types. It can be observed that REP has slightly different ranges for different plant types. The REP occurs at regions between 703-717 nm (Awolowo grass), 704-727 nm (Elephant grass), 703-714 nm (Mango trees), 703-724 nm (Oil Palm trees), and 696-704 nm (Mangrove). Among them, mangrove samples have the narrowest wavelength range, while elephant grass has the highest range. Figure 5.15 presents a boxplot summary of the REP for all plant samples. It shows that elephant grass has the highest REP among all plants. Furthermore, the oil palm tree has the highest interquartile range, whereas mangroves has the lowest interquartile range among all the plants.

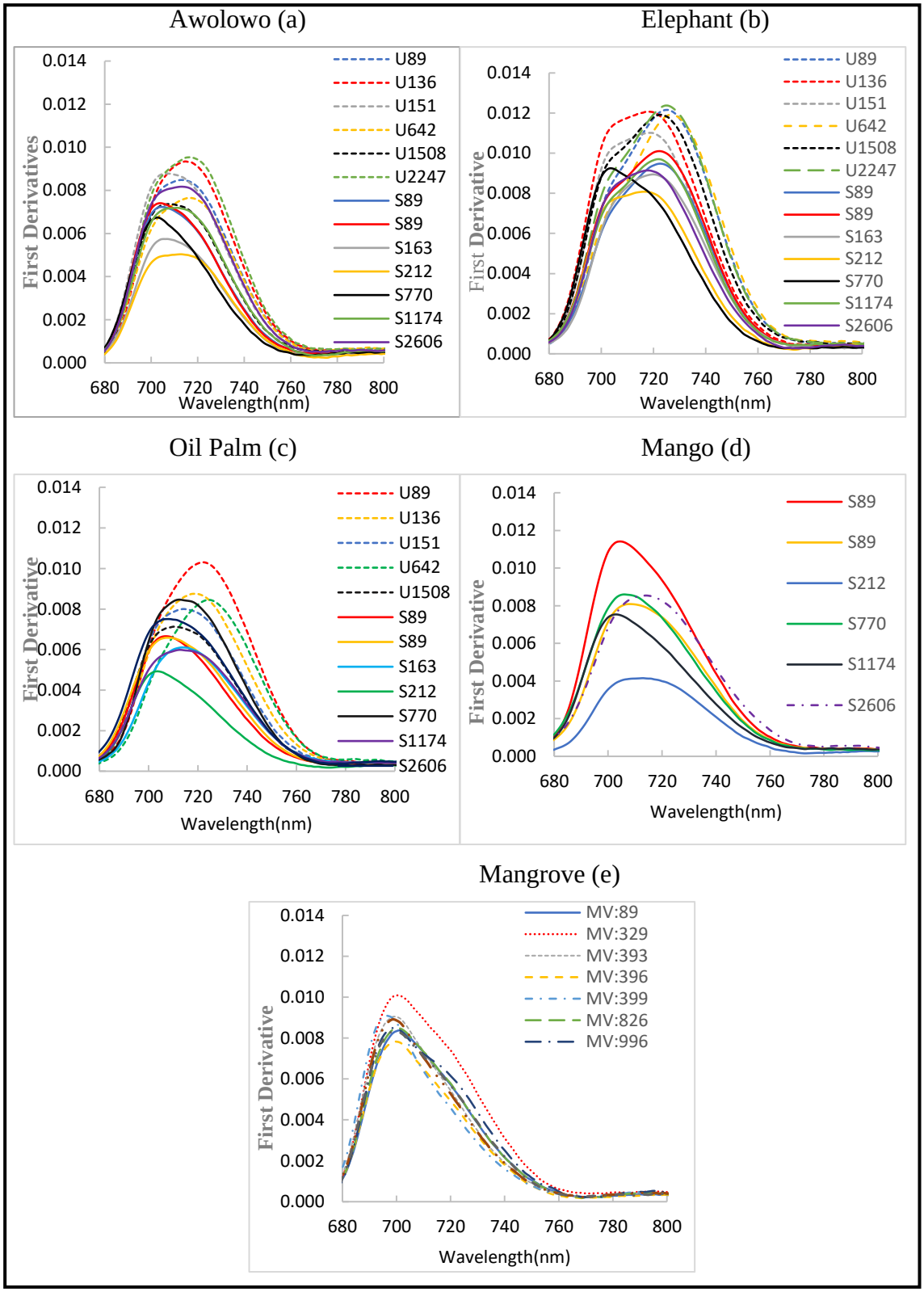

Figure 5.14:First derivative spectra of different plant species: (a) Awolowo grass, (b) elephant grass, (c) oil palm, (d) mango, and (e) mangrove.

Prefixed to the to the TPH concentration; U=upland; S=shoreline; M=mangrove.

Table 5.3 Red edge positions (nm) for various plant types.

Awolowo	Elephant	Oil Palm	Mango	Mangrove
703	704	703	703	696
704	717	707	704	699
705	718	708	706	699
707	718	708	708	699
707	719	710	713	699
707	720	712	714	699
711	722	713		700
713	722	714		701
713	723	714		704
713	723	718		
715	725	722		
716	725	724		
717	727			

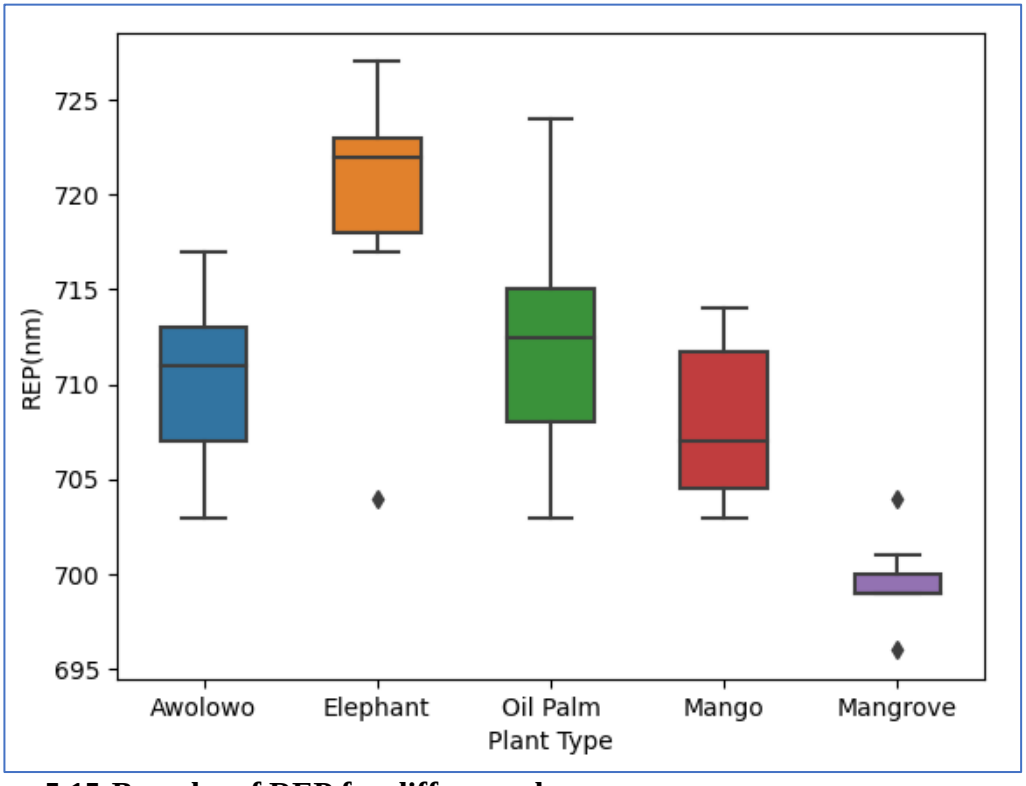

Figure 5.15:Box plot of REP for different plant types.

5.5.3 Statistical analysis of spectral properties

The statistical analysis of the relationship between the SHPs and plant types was performed based on the Spearman's (r_s) and Pearson's (R) correlations. The correlation is between the SHP, REP, and HVIs for different plant types/species. When $r_s > R$, the relationship between the variables is not linear but monotonic, and vice versa. For this research, the correlation is strong when $R \geq \pm 0.50$ and ± 1, moderate when R is between ± 0.30 and ± 0.49, weak when $R \leq \pm 0.29$, and no correlation when R = zero (Statisticssolutions.com, n.d.).

5.5.3.1 Red edge position and soil parameters

Figures 5.16-5.18 show graphs of the impact of TPH, EC50 and TOC (%) on the REP of awolowo grass**,** elephant grass**,** mango tree, oil palm trees, mangrove and all plant types combined using Spearman's and Pearson's correlations analysis. Figure 5.16 shows that the impact of TPH on REP is positive for Awolowo grass, elephant grass, oil palm and all plant types combined from Spearman's and Pearson's correlation with r_s and R <0.3 (Figure 5.16 a,b,d and f). However, the mango tree and mangrove are moderately positively and negatively impacted, with R= 0.398 (Figure 5.16c) and r_s = -0.456 (Figure 5.16e), respectively. This indicates that the Mangrove is the most impacted plant type in the Niger Delta, while the Mango is the most tolerant to THP content in the soil. Similarly, the impact of TOC (%) on REP is weak for Elephant grass and all plant types combined from both Spearman's and Pearson's correlation with r_s and R = <0.3 (Figure 5.17 b and f). For Awolowo, oil palm tree and mangrove, the impact is positive and moderate with r_s =0.456; R = 0.420, r_s = 0.302; R = 0.315 and R = 0.324 (Figure 5.17a, d and e) respectively, showing some level of the important of TOC (%) to their health. However, the mango tree's correlation is strong and negative, with r_s= -0.657*;* R= -0.650 (Figure 5.17c). This result was unexpected since TOC (%) is important to plant health. The implication is that Mango trees can grow on soil with low organic content. Similarly, Figure 5.18 shows Spearman's and Pearson's correlation between REP and EC50 for Awolowo grass, elephant grass, mangrove, and oil palm are weak with r_s and R <0.3. However, for the mango tree and all combined plants, the correlation is moderated and positive r_s= 0.429; R= 0.401 and r_s = 0.355; R= 0.337 (Figure 5.18 c and e), respectively. The result indicates that the mango tree is affected by pollutants in the soil.

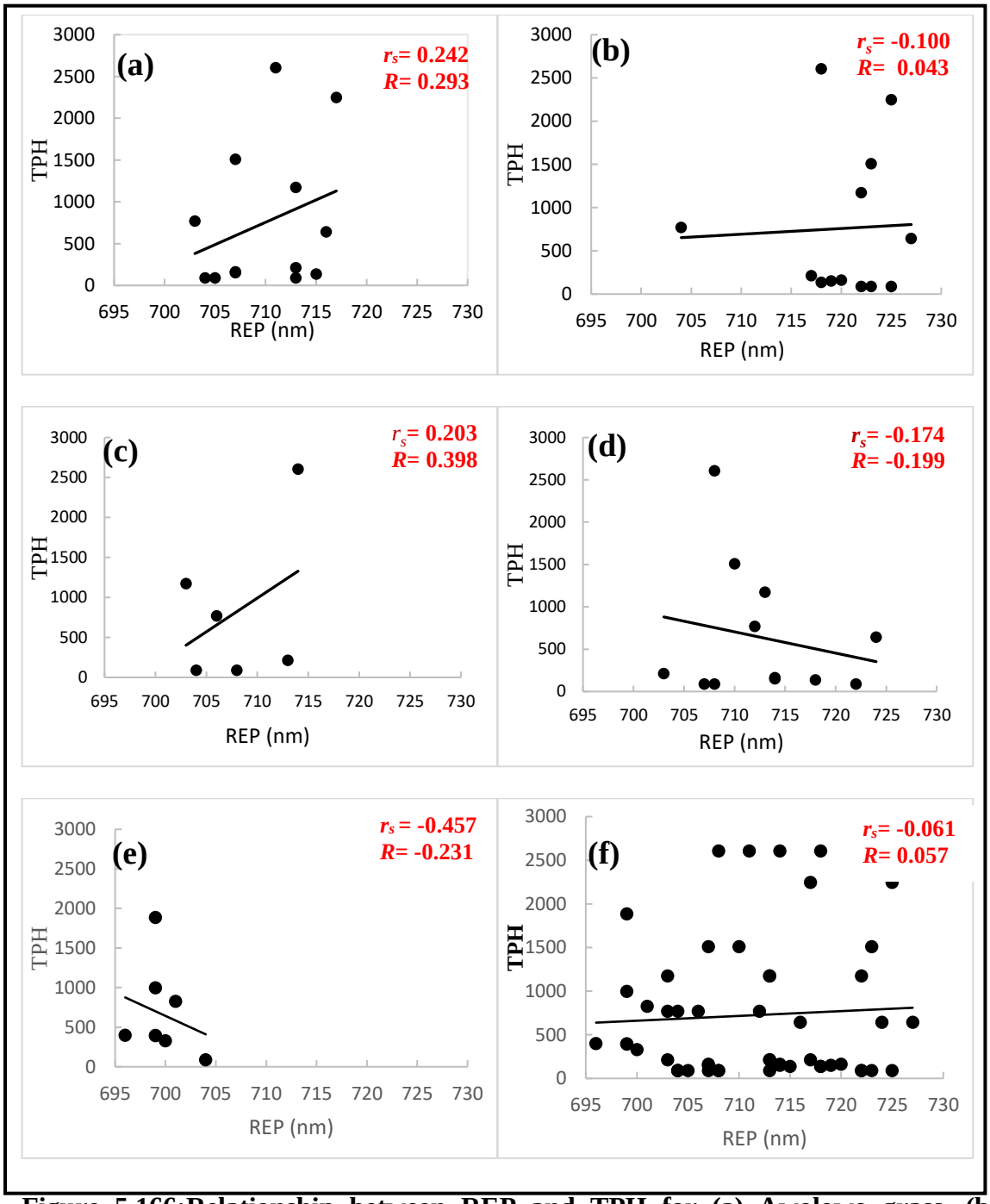

Figure 5.166:Relationship between REP and TPH for (a) Awolowo grass, (b) elephant grass, (c) mango tree, (d) oil palm tree, (e) mangrove tree and (f) all samples.

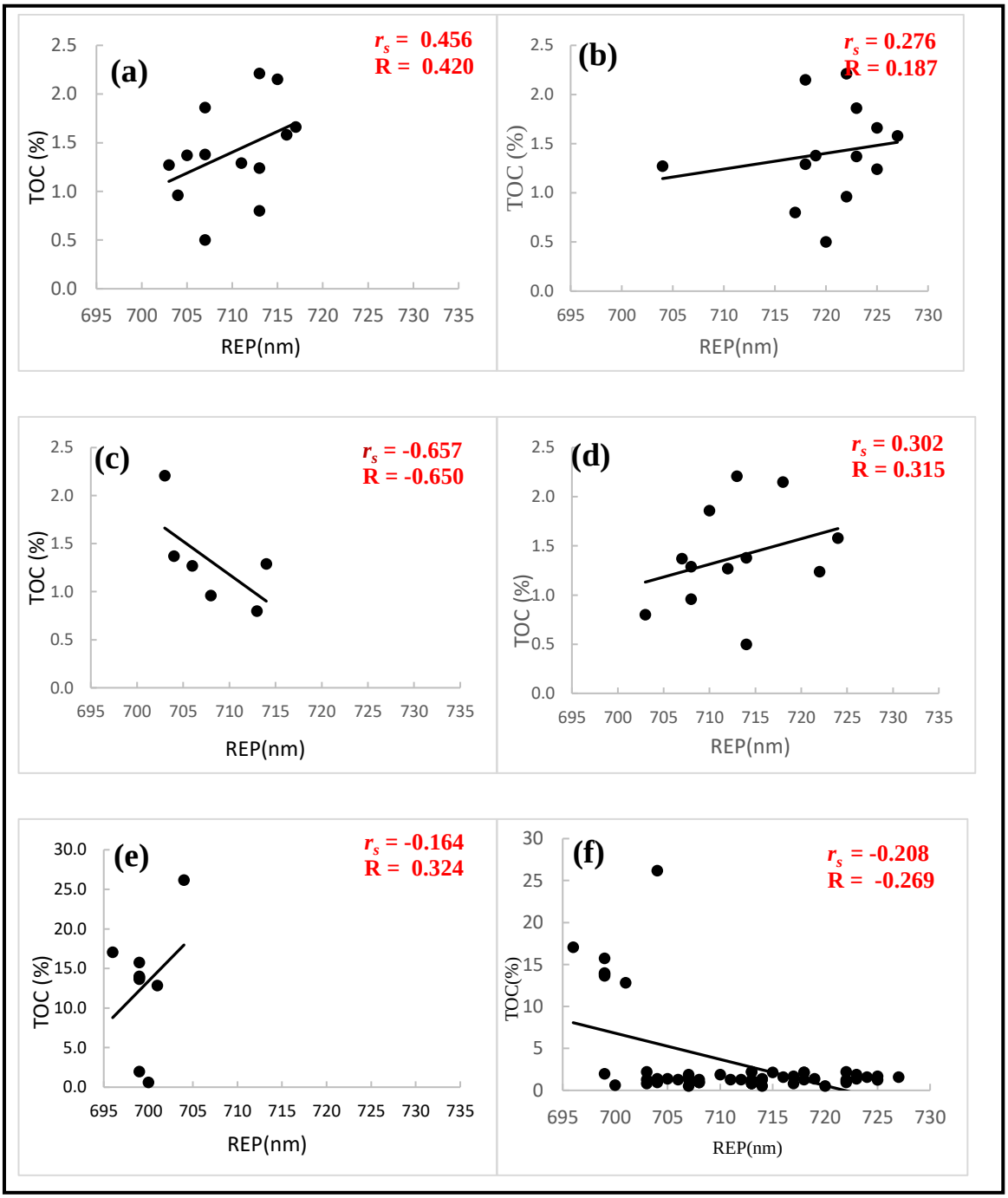

Figure 5.177: Relationship between REP and TOC (%) for (a) Awolowo grass, (b) elephant grass, (c) mango tree, (d) oil palm tree, and (e) mangrove tree and (f) all samples.

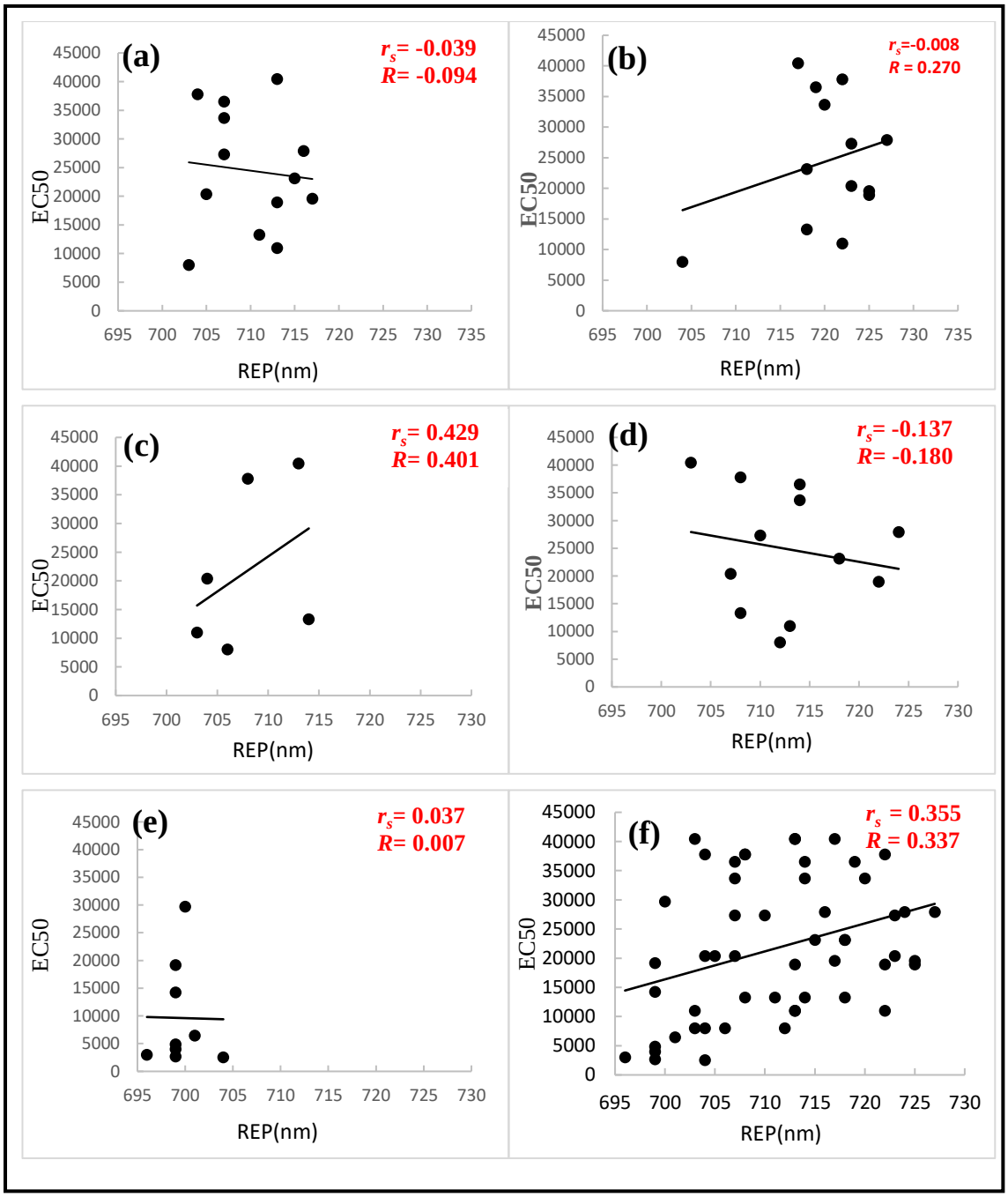

Figure 5.188: Relationship between REP and EC50 for (a) Awolowo grass, (b) elephant grass, (c) mango tree, (d) oil palm tree, (e) mangrove tree and (f) all samples.

5.5.3.2 Hyperspectral vegetation indices (HVIs) and soil parameters

Table 5.4 shows Spearman's and Pearson's correlations between the HVIs and SHPs for the individual vegetation types and all combined plants. It can be observed that each HVIs havr a different range of values (both negative and positive). Among the various HVIs, NDVVI844,447 has the highest value, followed by mND705, while the MDATT index and PRI have the lowest HVI values. While NDVVI844,447, mND705 and MDATT have

positive values ranging from 0 to 1, PRI, conversely, ranges from -1 to 1. Also, the MDATT index shows a negative correlation when other indices show a positive correlation.

The results show that the mangrove vegetation is the most impacted by TPH, having a strong negative correlation in terms of Spearman'swith R=-0.683 and rs = -0.500 (mND_{705}), respectively. However, the Awolowo is the least impacted. It has the s weakest correlation in terms of Spearman's and Pearson's correlation. At the same time, the correlation is moderate for elephant grass and oil palm tree in terms of Spearman with rs =-0.311(mND 705) and rs =-0.438 (PRI), respectively (Table 5.4a).

The impact of TOC (%) on the health of various plant types in Table 5.4b shows that the elephant grass is the least impacted by TOC (%) among all plant types, with R and r_s <0.3. However, the correlation is strong and negative for mango, all combined plants, and mangroves, with the highest values of R= -0.725 and R = -0.585 (mND_{705}) and R =0.654 (MDATT index), respectively. The Oil palm tree shows an interesting result. There is both positive and negative moderate correlation between TOC and the MDATT index (r_s= -0.483; R= -0.359) and PRI (r_s= -0.413; R= -0.324), a moderate and weak positive correlation for Spearman's with NDVVI844,447 (r_s= 0.315) but with highest r_s= -0.483 from (MDATT index) which indicate positive correlation since negative sign means positive for MDATT index. On the other hand, Awolowo has a strong positive correlation between TOC and HVIs, with the highest r_s = 0.621 (NDVVI844,447). The results show that only elephant grass is less responsive to the TOC (%) concentration among the plant types, with Awolowo grass being the most responsive plant type. Also, the presence of TOC (%) in the soil does not improve the health condition of mango and mangroves, but the health condition of Awolowo grass

The impact of EC50 in Table 5.4c shows that the mangrove and mango are the most impacted plant, with each having R =-0.870 (MDATT index) and r_s=0.600 (mND_{705}). The results show that awolowo grass and elephant grass are less responsive to toxicity in the soil among the plant types. However, oil palm is not affected. A negative correlation (which means positive) indicates resistance to pollutants since the higher the values of EC50, the less polluted the land.

Table 5.4. Correlation between SHP and HVIs

		mND 705		PRI		NDVVI844,447		MDATT index	
	Plant Types	***R***	***r_s***	**R**	***r_s***	***R***	***r_s***	***R***	***r_s***
(A)					**TPH**				
	All plant	-0.075	-0.153	-0.250	-0.205	0.071	0.022	0.091	0.106
	Awolowo	0.007	0.025	-0.135	-0.003	0.174	0.179	0.034	-0.091
	Elephant	-0.070	-0.311	0.106	-0.124	0.247	0.173	0.042	0.190
	Mango	0.312	0.058	0.265	0.232	0.143	0.058	-0.582	-0.116
	Palm Tree	-0.209	-0.095	-0.323	-0.438	-0.147	-0.105	0.051	0.046
	Mangrove	-0.683	-0.500	-0.351	-0.667	0.368	-0.476	0.275	0.524
(B)					**TOC**				
	All plant	-0.585	-0.227	-0.537	-0.459	-0.031	-0.027	0.510	0.170
	Awolowo	0.374	0.522	-0.017	0.016	0.486	***0.621***	-0.279	-0.500
	Elephant	-0.018	-0.011	-0.158	-0.225	0.032	0.110	-0.164	-0.286
	Mango	***-0.725***	-0.543	-0.339	-0.029	-0.564	P	0.437	0.371
	Palm Tree	0.218	0.273	-0.324	-0.413	0.289	0.315	-0.359	-0.483
	Mangrove	-0.276	-0.357	-0.240	-0.119	-0.252	-0.095	0.654	0.405
(C)					**EC50**				
	All plant	0.418	0.379	0.198	0.214	-0.099	0.182	-0.379	-0.363
	Awolowo	0.254	0.104	0.138	-0.115	0.107	-0.198	-0.301	-0.104
	Elephant	0.233	0.137	-0.240	-0.093	-0.344	-0.280	-0.217	-0.126
	Mango	0.416	0.600	-0.343	-0.314	0.335	0.543	-0.264	-0.657
	Palm Tree	-0.225	-0.336	-0.331	-0.098	-0.323	-0.371	0.200	0.210
	Mangrove	0.563	0.333	0.531	-0.024	0.627	0.190	-0.870	-0.381

5.6 Discussion

5.6.1 Soil hydrocarbon parameter (SHP) concentrations

To determine the impact of soil hydrocarbon parameters (SHP) on the health of plant types at the leaf scale using hyperspectral vegetation indices (HVIs), various soil hydrocarbon parameters (SHP) of varying concentrations in the soil for the two types of sample locations: upland and mangrove were analyse. From the results of the TPH concentration, a higher toxicity level was observed in the mangrove soil than in the land, with an average EC50 < 5000 mg L^{-1} (Figure 5.9a), while the land had many locations with EC50 > 10000 mg L^{-1}. For the land sample locations, none of the soils was characterised as having high toxicity. However, high toxicity was found in mangrove soils. Mangrove forests have become a dumping ground for waste due to overpopulation and poor waste management strategies (Numbere, 2019a). The establishment of open

waste disposal in coastal areas has also contributed to soil and water quality changes in mangroves (Numbere, 2019b). A significant amount of crude oil has been discharged into coastal environments, and mangroves are extremely responsive to oil and industrial waste (Onyena & Sam, 2020). The mangroves act as sinks, retaining pollutants from contaminated tidal water (TRCC, n.d.). Equally, most oil spills on land close to the shorelines are washed into the mangroves, contributing to the high toxicity of mangrove soil in the Niger Delta.

Similarly, the TOC (%) has a varying concentration for both the mangrove and the dryland soil samples, with the mangrove having a very high level of TOC (%) compared to land (Figure 5.9b). The average TOC (%) concentration for the combined soil samples is 6.10 wt%, while the mangrove and dryland have averages of 12.9 wt% and 1.40 wt%, respectively. The TOC (%) range is between 0.61 - 26.17 wt% for mangroves and 0.5-2.21 wt% for land. The minimum standard threshold value of source rock for hydrocarbon generation in the Niger Delta is 0.5 wt% (Fadiya et al., 2020; Oyonga, Itam, & Etete, 2019). The average values for all combined samples, mangrove and dryland, are above the minimum threshold. Additionally, all the results show that the TOC (%) in mangroves is above the threshold, while only one site (P8) is at the minimum threshold for dryland. Mangrove forests store five times more carbon per hectare than most other tropical forests around the world because their ability to store such large amounts of carbon is, in part, due to the deep, organic-rich soils in which they thrive (Onyena & Sam, 2020). Studies by Seiter et al. (2004) discovered that the world's highest TOC (%) contents are observed in the Atlantic Ocean along the West African continental margin, especially off Namibia, offshore the Congo mouth and along the West African margin. The implication of this result has revealed that the Niger Delta mangrove has one of the highest TOC (%) concentrations globally, rated as excellent with an average of 12.8 wt%. In comparison, dryland is rated good, with an average of 1.4 wt%, based on the rating of TOC (%) as poor (<0.5%), fair (0.5% - 1.0%), good (1.0% - 2.0%) or excellent (> 2.0%) (Onyena & Sam, 2020). The results from these studies recorded the highest TOC (%) compared to studies by Onyena & Sam (2020) of 6.97 wt%, Fadiya et al. (2020) 2.27 wt%, Umar et al. (2021) 8.11 wt% and Falebita et al. (2015) between 7.56 and 12.44 wt% in the Niger Delta.

In general, the TPH concentration in the study area was below the Environmental Guideline and Standards for the petroleum industry in Nigerian (EGASPIN) soil/sediment

intervention values for minerals (5000 mg/kg^{-1}), except for sample P20 (mangrove) (Figure 5.9c), which was above the EGASPIN intervention values by approximately 37000 mg/kg^{-1}. Previous measurements of TPH in the Niger Delta by Adeniji et al. (2017) and Alinnor & Nwachukwu (2013) were all below the EGASPIN intervention value limits. In contrast, Little et al. (2018) and UNEP (2011) had measurements both below and above the EGASPIN intervention value limits, similar to this study's findings. Different study locations could be the reason for the disparity with Adeniji et al. (2017) and Alinnor & Nwachukwu (2013) findings, who all had their TPH values below EGASPIN intervention value limits.

5.6.2 Relationship between TPH and other soil parameters

The presence of hydrocarbons in the soil could affect many soil properties (Egobueze et al., 2019), which could affect the vegetation's health. It is important to determine if the presence of one parameter affects the values of the other and how this could also affect the health condition of the vegetation. The increase in the concentration of TPH could lead to an increase or decrease in other soil parameters crucial for enhancing or diminishing plant health. The cause of toxicity present in the Niger Delta mangrove soil is not primarily from oil spills alone but from other sources, such as agricultural chemical, industrial and domestic waste. This is because the correlation between the TPH and EC50 for all vegetation and the mangrove is weak. However, a higher concentration of TPH might have led to an increase in the level of toxicity in the dryland soil, with the TPH and EC50 showing a moderate positive linear correlation for the dryland sample sites with R= -0.500 (Figure 5.10 e), given that lower EC50 values correspond to higher toxicity.

Similarly, the TPH has no significant impact on TOC (%) for all the sampled locations (mangrove and dryland combined and for mangrove and dryland, respectively). This finding agrees with Osuji & Adesiyanan (2005), who did not find any significant correlation between TPH and TOC (%) in an environment impacted by the 1997 leakage of the high-pressure crude oil pipeline in Isiokpo, in the Niger Delta in south-east Nigeria. But the studies by Wang et al. (2009) discovered a significantly positive correlation between TOC (%) and TPH contents in oilfields in Momoge Wetland, China, with R = 0.88, $p < 0.05$. The possible reason for the disparity in the findings between Wang et al. (2009) and Osuji & Adesiyanan (2005) and this study could be attributed to different geography, soil type and other environmental factors.

5.6.3 Health condition of plant types exposed to oil spills

The hyperspectral reflectance for each plant shows that elephant grass has the highest spectral reflectance in the NIR region. At the same time, mangrove has the lowest reflectance of each plant type within the NIR region (700-1300 nm) (Figure 5.11). This result agrees with Jensen et al. (2007), who discovered that the reflectance of healthy grass was higher than that of healthy mangroves, which could represent the diverse environment (sand, water, etc.) mangroves grow in. Additionally, the reflectance for the same plant type for the upland sites in the Igwuruta area of Port Harcourt is higher than those near the shoreline in Bodo for Awolowo, elephant grass and oil palm trees (Figure 5.12 a, b, and c), which suggests that they are healthier. Mango and mangrove were only found along the shoreline and could not be compared to upland and shoreline vegetation. This means that proximity to the sea could affect the spectral reflectance of vegetation. The mean spectral reflectance in the NIR region (700-1300 nm) for shoreline and upland vegetation shows that the highest range of spectral difference between shoreline and upland plant types is found in elephant grass. The shoreline vegetation in the Niger Delta is mostly flooded, which increases the chance of the upland being polluted more by the oil spill from the rivers, which could affect their reflectance. The marsh plant's spectral responses are predictably reduced in the near-infrared region as the canopies are progressively flooded (Kearney et al., 2009).

5.6.4 Leaf chlorophyll content of vegetation

One of the best remote sensing descriptors of chlorophyll concentration is the red edge (Filella & Peñuelas, 1994), whose shape and position are determined by chlorophyll content (Onisimo et al., 2007). The REP is based not on reflectance *per se* but rather on the wavelength position of the transition between low reflectance in the red region of the spectrum and high reflectance in the near-infrared region (Sims & Gamon, 2002), and it occurs between wavelengths of 680-750 nm. The results show that elephant grass and oil palm trees have the highest chlorophyll contents among all the sampled vegetation types, with the REP moving toward a longer wavelength (Figures 5.14 and 5.15). Similarly, the mangrove is the most stressed plant. It has the lowest chlorophyll concentration among all plants, followed by awolowo grass and mango trees with the REP moving toward a shorter wavelength. The movement of REP to a shorter wavelength is a sign of plant stress or low chlorophyll concentration. In comparison, the movement of REP to a longer wavelength indicates less vegetation stress and higher chlorophyll concentrations (Piro et

al., 2017). The implication is that the chlorophyll content could affect the ability of each plant type to withstand external stresses, especially from hydrocarbon. However, this result may not imply the effect of hydrocarbons since some plants naturally have higher chlorophyll contents than other plant types. However, since all the samples were taken on sites exposed to a similar soil and hydrocarbon concentration level, further research is required on plants not exposed to hydrocarbons to determine if the chlorophyll concentration is similar for different plant types.

5.6.5 Influence of soil hydrocarbon parameters on plant chlorophyll content

Physical changes in plants can be related to oil pollution and other environmental stresses, which may be responsible for a plant's spectral changes (Adamu, 2016). Therefore, analysing the impact of hydrocarbons at the species/type level will identify specific plant species/types sensitive to petroleum pollution and others that are more tolerant to pollution (Arellano et al., 2017). The REP has demonstrated to be one of the best remote sensing descriptors of chlorophyll concentration (Curran et al., 1995; Filella & Peñuelas, 1994). Based on the results presented in this chapter, despite some potential indications of the effect of TPH concentration on the chlorophyll content, overall, the TPH concentration did not significantly affect the chlorophyll content of any plants, except mangrove, which was negatively impacted to some extent. In fact, the chlorophyll content of Awolowo grass and mango trees was positively correlated. The reason for some impact on the mangrove could be due to lower chlorophyll content, which the impact of TPH might have caused.

Similarly, the TOC (%) has a moderate positive impact on the chlorophyll content of Awolowo grass, oil palm tree and mangrove (Pearson's), with Awowolo Awowolo being the most responsive. This was expected since a high TOC (%) concentration is generally good for plant growth. Despite the importance of TOC (%) to the plants, the chlorophyll of the mango trees shows an unusually strong negative correlation with TOC with r_s = -0.657 and R= -0.650 (Figure 5.17c). The mango trees may not require a high TOC (%) in the soil to maintain their health.

5.6.6 Impact of soil hydrocarbon parameters on vegetation

Remote sensing derived vegetation indices are evident in their use for effective detection and monitoring of the impacts of hydrocarbon spills on the health of vegetation (Kuppusamy & Ganesan, 2016). Similarly, Adamu et al. (2018) used broadband

vegetation spectral techniques to detect and monitor the impact of oil spills on vegetation in the Niger Delta using satellite-based indices. However, for this thesis, HVIs derived from field-based measurements were used to detect the impact of the SHP on common plant species in the Niger Delta. The HVIs have been developed and used to quantify the chlorophyll content and vegetation vigour, making them crucial in this study since field data on chlorophyll were not available. NDVVI844,447 was specifically developed for application on vegetation affected by oil pollution. The four HVIs, mND_{705} (Sims & Gamon, 2002), MDATT index (Lu et al., 2015), NDVVI844,447 (Onyia et al., 2018), and PRI (Gamon et al., 1997), have been used to estimate chlorophyll content in the leaves of the different vegetation types. The correlation between the TPH and all the HVIs for all combined plants is weak for Spearman's and Pearson's correlation (Table 5.4a). It indicates that the vegetation is not significantly affected by TPH, especially when no particular plant type is considered. It shows the level of tolerance by the plant to the level of TPH in the Niger Delta. However, the EC50 has a moderate positive correlation with the mND_{705} and MDATT indices for both Spearmen's and Pearson's correlation, which indicates that the health of the plants is somewhat affected by the level of toxicity in the soil. Additionally, the strong negative correlation between TOC (%) and the mND_{705}, MDATT index and PRI (Pearson's correlation) and the moderate negative correlation with PRI (Spearman's correlation) show that TOC (%) affects the health of the plant more than TPH and EC50, with the Pearson's correlation indicating that the TOC (%) has a linear effect on the plants (Table 5.4). This was not expected since TOC (%) is a soil property that enhances plant growth. However, a better understanding will come at the plant-specific level.

5.6.7 Impact of soil hydrocarbon parameters on the plant types

Based on the correlation between TPH and the HVIs in Table 5.4a, the health of the mangrove is the most impacted by TPH. The mangrove vegetation exhibited the strongest negative correlation between TPH and mND_{705}, MDATT index, PRI (Spearman's), and mND_{705} (Spearman's and Pearson's) with ($R>0.5$). This is anticipated as it is known that mangroves are very responsive to oil and industrial waste (Onyena & Sam, 2020). Similarly, the moderate negative correlation with PRI for oil palm (Spearman's and Pearson's) and mND_{705} for elephant grass (Spearman's) makes them the next most affected plants by TPH in the Niger Delta. The lack of impact of TPH on Mango trees and Awolowo grass indicates that some plants have successfully grown to be resistant to

soil contamination by petroleum hydrocarbons in the Niger Delta. However, there is no literature to support this hypothesis with regard to the vegetation types in the Niger Delta. Previous studies by Ikhajiagbe & Akindolor (2016) and Rahbar et al. (2012) have shown that Awolowo grass tolerates oil contamination in the soil. Awolowo grass can reduce the concentration of heavy metals in polluted soils (Ayesa et al., 2018). The sunflower family (to which Awolowo grass belongs) can survive soil hydrocarbon contamination of approximately 18,000 mg/kg by metabolic changes in chlorophyll a, total chlorophyll and carotenoids, showing no significant decrease under these conditions (Rahbar et al., 2012).

The strong positive correlation between the TOC (%) and HVIs for Awolowo grass with $R > 0.5$ for MDATT index, NDVVI844,447 and mND_{705} in Table 5.4b is an indication of the importance of TOC (%) to Awolowo grass. TOC (%) provides energy for soil microorganisms, affects plant growth as an energy source, and triggers nutrient availability through mineralisation (Https://spectralevolution.com/, n.d.). The weak and negative correlation between TOC (%) and the HVIs was not expected. Surprisingly, the mangrove and mango were indifferent to TOC (%), having a strong negative correlation with TOC (%), which might have been caused by their constant exposure to the oil spill.

The toxicity effect on the various vegetation types shows that each plant responds differently Table 5.4c. The level of toxicity might be responsible for the chlorophyll content in each plant type, as indicated in the REP in Figure 5.14, because mango and mangrove have the lowest chlorophyll content and are incidentally affected by toxic concentrations in the soil. The strong impact of EC50 on the health of mango and mangrove makes them the most vulnerable to soil toxicity among the plant types. Similarly, the moderate impact of toxicity on the health of Awolowo grass shows that it is not tolerant of toxic soil (though it is tolerant to TPH). In contrast, elephant grass and oil palm tree are not affected by soil toxicity (though they are moderately affected by TPH).

In the summary of the correlation analysis between soil hydrocarbon parameters (SHP) and HVIs for each vegetation type and the highest *R* values, the MDATT index correlated better than all the HVIs for at least each of the three correlations between the HVIs and SHP for each of the five plant types with four strong correlations. The MDATT index could be used for monitoring the health of mango trees and the mangrove since it correlates with the SHP for TPH and EC50 for the mango trees and EC50 and TOC (%) for the mangroves. The MDATT index has been developed to remotely estimate

chlorophyll content in plants with varying leaf surface structures (Lu et al., 2015). NDVVI844,447 is the next best performing index, having corrected better in four instances with one strong correlation (Awolowo grass) across three plant types between HVIs and SHP. It could be used for awolowo grass, with it having a better correlation with TPH and TOC (%). NDVVI844,447 was developed for monitoring biodiversity indicators in oil-polluted areas in the Niger Delta. Although mND_{705} has three strong correlations with SHP for elephant grass (TPH), mango (TOC (%)) and mangrove (TPH). Hence, it could not be recommended for any plant species except those SHPs correlated better. The PRI is the worst performing HVI. It correlated better with oil palm (TPH).

However, the lack of major impact of TPH and toxicity on the health/chlorophyll of different plant types apart from the mango (toxicity) and mangrove (TPH), which has a moderate correlation, could result from many factors, including the methodological and environmental. Assessing chlorophyll content in a diverse tropical forest is challenging due complex forest structure in the light interaction in the canopy and the resulting vertical photosynthesis gradient, the required rapid analysis of sampled leaves to preserve their biophysical and biochemical integrity (Arellano et al., 2017). But for this study, reasonable precautions were taken to minimise the effect of sampling and analyses method on the result. The leave samples were kept in a cooling box filled with an ice block, and all the leaves samples were analysed within two hours of collection. The light box was painted black and covered with black cloth to prevent interference from external sources. An alternative laboratory analysis will be direct field data capture. But this might be difficult to achieve for a place like the Niger Delta with a high-security risk. Similarly, a tree like a mango or oil palm might need climbing for spectral measurement, which might be difficult. Another factor, which is likely in the case of the study, is environmental. The constant exposure of the plants to industrial oil waste and oil spills might have made them develop some form of resistance to the impact of the oil spills and toxicity.

5.7 Conclusion

To determine the impact of soil hydrocarbon parameters (SHP) on the health of plant types at the leaf scale using hyperspectral vegetation indices (HVIs) in the Niger Delta, the Red edge position and five hyperspectral vegetation indices were used. The soil hydrocarbon parameters considered are Total petroleum hydrocarbon(TPH), Microtox (EC50 mg L^{-1}) and Total Organic Carbon (TOC (%)). For various concentrations of SHP,

the level of pollutant/toxicity in the soil in which plants are most affected is higher in the Mangrove soil than in dryland, which could have resulted in the low chlorophyll content in the mangrove. Also, the mangrove has a higher concentration of TOC (%), with an average concentration nine times higher than that of dryland soil, making it one of the soils with the highest concentration of TOC (%) in the world. The difference in TPH concentration between the dryland and the mangrove is small and falls within the permissible limit in Nigeria, except for one point in the mangrove. However, the TPH permissible limit in Nigeria is higher than in many countries.

For the impact of SHP on different plants, the mangrove vegetation is the most impacted plant by TPH and toxicity. In general, Awolowo grass is tolerant to all soil hydrocarbon properties. However, mango is the most tolerant to TPH but highly susceptible to toxicity. Therefore, there is a need for a policy that could reduce the quantity of pollutants in mangrove soil. The TPH and the toxicity in the mangrove might have led to the negative response of the mangrove to TOC (%), despite having nine times the average TOC (%) concentration than the dry land. The next plants impacted by TPH are oil palm trees and elephant grass.

Among the HVIs, the MDATT index performed strongest in detecting the impact of soil hydrocarbons on the various plant types in the Niger Delta. Therefore, it is recommended that a combination of field chlorophyll data with an HVIs study should be conducted to confirm the effectiveness of the MDATT index and other HVIs. The next chapter will discuss monitoring the impact of oil spills on different vegetation types at the plot scale, considering vegetation types, instead of being plant specific. This analysis will leverage the available spatiotemporal data from satellite based derived NDVI.

Chapter 6 Monitoring the impact of oil spills on vegetation at the plot scale.

Part of the work in this chapter has been presented as:

Kuta A. A., Grebby, S. and Boyd, D. S. (2019). Determining the impact of oil spills on vegetation in the Niger Delta using satellite imagery, AfricaGIS 2019 Innovations in Geospatial Technologies for Achieving Sustainable Development Goals in Africa, Kigali, Rwanda, 18 - 22 November 2019, Kigali Conference and Exhibition Village (KCEV).

6.1 Introduction

The effect of oil extraction activities on land cover, especially vegetation, could be devastating, leading to either the destruction or degradation of vegetation, depending on the type. Studying the impact of oil spills on vegetation on a plot scale in the Niger Delta region provides the practical/operational approach to detect and monitor the impact of oil spills on vegetation over a large, partially inaccessible area like the Niger Delta. Unlike the investigation at the leaf scale level, the vegetation study at the plot scale provides spatiotemporal data that enables monitoring vegetation health conditions before and after oil leakage or spill. Oil leakage or pollution may affect vegetation health and vigour (Adamu et al., 2015). Therefore, monitoring the health of vegetation is important in many ways and has diverse applications. For example, it can be used to forecast crop yield (Kogan & Salazar, 2012), assess natural forest expansion (Mancino et al., 2014), biodiversity and conservation (Ochege et al., 2017), to undertake drought monitoring (Amani et al., 2017; Kogan et al., 2017), and to detect oil pollution in vegetation (Adamu et al., 2015), among others. The two main approaches for assessing the health of vegetation are field-based and remote sensing. Some advantages of the field-based approach are data acquisition finer or leaf scale, allowing for under canopy data collection, and flexibility of acquiring data when needed. But despite the advantages of the field-based approach, its major disadvantage is that it requires considerable time, effort and budget, typically restricting their application to small areas and unsuitable for regional and global coverage (Tehrany, Kumar & Drielsma, 2017). Also, the field approach does not offer information on the health of the vegetation before the first field survey, limiting a spatiotemporal analysis. For places like Niger Delta, a field-based approach is unsuitable for other reasons, such as security concerns and difficult terrain.

Satellite remote sensing has become essential to the oil spill response (Fingas & Brown, 2014). Unlike field base approaches, satellite remote sensing provides a means of overcoming the limitations of field-based approaches. It has proven to be a useful tool in monitoring vegetation health and status over large, polluted areas (Adamu, 2016). A key advantage of this approach is that imagery is routinely acquired, which permits long-term spatiotemporal analysis of the vegetation canopy and limits the need for site visits. Other is it allows coverage of very large areas at a regional and global scale and collection of data over various scales and resolutions.

Vegetation indices (VIs) derived from airborne and satellite images represent a powerful and effective way of monitoring vegetation status, growth, and biophysical parameters (Villa et al., 2014). The derivation of VIs is based on using electromagnetic wave reflectance information from canopies obtained using passive sensors (Xue & Su, 2017). Choosing a VI for a particular application is a difficult task since there is currently no universally optimum VI because of the complexity of the different combinations of illumination conditions, waveband configurations, instrumentation, platforms and resolutions in each case (Xue & Su, 2017). Its value is used to quantify vegetation health or structure. Changes in vegetation reflectance spectra have been shown at visible (VIS: 400–700 nm), near-infrared (NIR: 700–1300 nm) and shortwave infrared (SWIR: 1300–2500 nm) ranges in response to oils and hydrocarbons (Khanna et al., 2013; Mishra et al., 2012; Pavanelli & Loch, 2018). Time series of the normalised difference vegetation index (NDVI) derived from satellite sensors are vital data to study vegetation dynamics (Guo et al., 2017) and have proven to be a robust indicator of terrestrial vegetation productivity (Wang et al., 2001). It can be used to estimate vegetation health and monitor changes in vegetation (Huang, Dai, Wang, & Han, 2014), especially in oil spill-impacted vegetation such as the Niger Delta region in Nigeria.

NDVI is a quantitative index often used for a quantitate proxy measure of vegetation health, cover and phenology (life cycle stage) over large areas (www.earthdatascience.org). Published studies on monitoring the impact of oil spills using satellite-derived VIs are scarce, especially in the Niger Delta region. Previous studies that examine the effect of oil spills on the health of vegetation in the Niger Delta region using satellite-derived VIs include Adamu (2016), Adamu et al. (2018) and Adamu (2015). These studies investigated the influence of oil spill volume and time gap (number of days between oil spill events and image acquisition date) using various VIs in the

mangroves of the Niger Delta region. In addition, Ozigis et al. (2019) identified oil-impacted land in the Niger Delta region of Nigeria by using a random forest classifier in conjunction with Landsat 8 OLI-derived vegetation health indices. Onyia, Balzter & Berrio (2018) monitored the impact of oil pollution and environmental pressure on biodiversity at a regional scale by integrating a Hyperion-derived normalised difference vegetation vigour index (NDVVI) and field data to develop a set of spectral metrics for biodiversity monitoring.

The studies by Adamu et al. (2016) revealed that five VIs (NDVI, SAVI, ARVI2, G/NIR and G-SWIR) detected oil spills, with NDVI producing better results than NDWI. However, the studies only focus on the mangrove vegetation and compare, in some cases, absolute NDVI values before and after spills. Furthermore, determining the change in NDVI before and after spills would be more appropriate to negate the impact of external factors on the NDVI, such as the soil nutrients and water content, among others, which may be higher at spill sites than at no-spill sites, which could lead to some spill sites having a higher NDVI value than no-spill sites. Hence, there is a need to look at the change in NDVI values at spill sites and compare them with no-spill sites for different types of vegetation in the Niger Delta to better understand the effect of oil spills. To fill the research gap identified in section 1.3, this chapter aims to assess the effects of oil spills on the health of different vegetation types at the plot scale using satellite-based Normalised Difference Vegetation Index (NDVI) from Landsat data. This will be achieved by (1) analysing the impact of oil spill volume and time after the oil spill spectral indices of various types of vegetation in an oil-polluted environment and (2) to undertake temporal monitoring of different types of vegetation to determine their medium- and long-term responses to oil spills. For this study, the vegetation types are divided into three categories: dense vegetation (DV), sparse vegetation (SV) and mangrove vegetation (MV).

6.2 Methodology

Figure 6.1 outlines the methodological approach taken in this chapter.

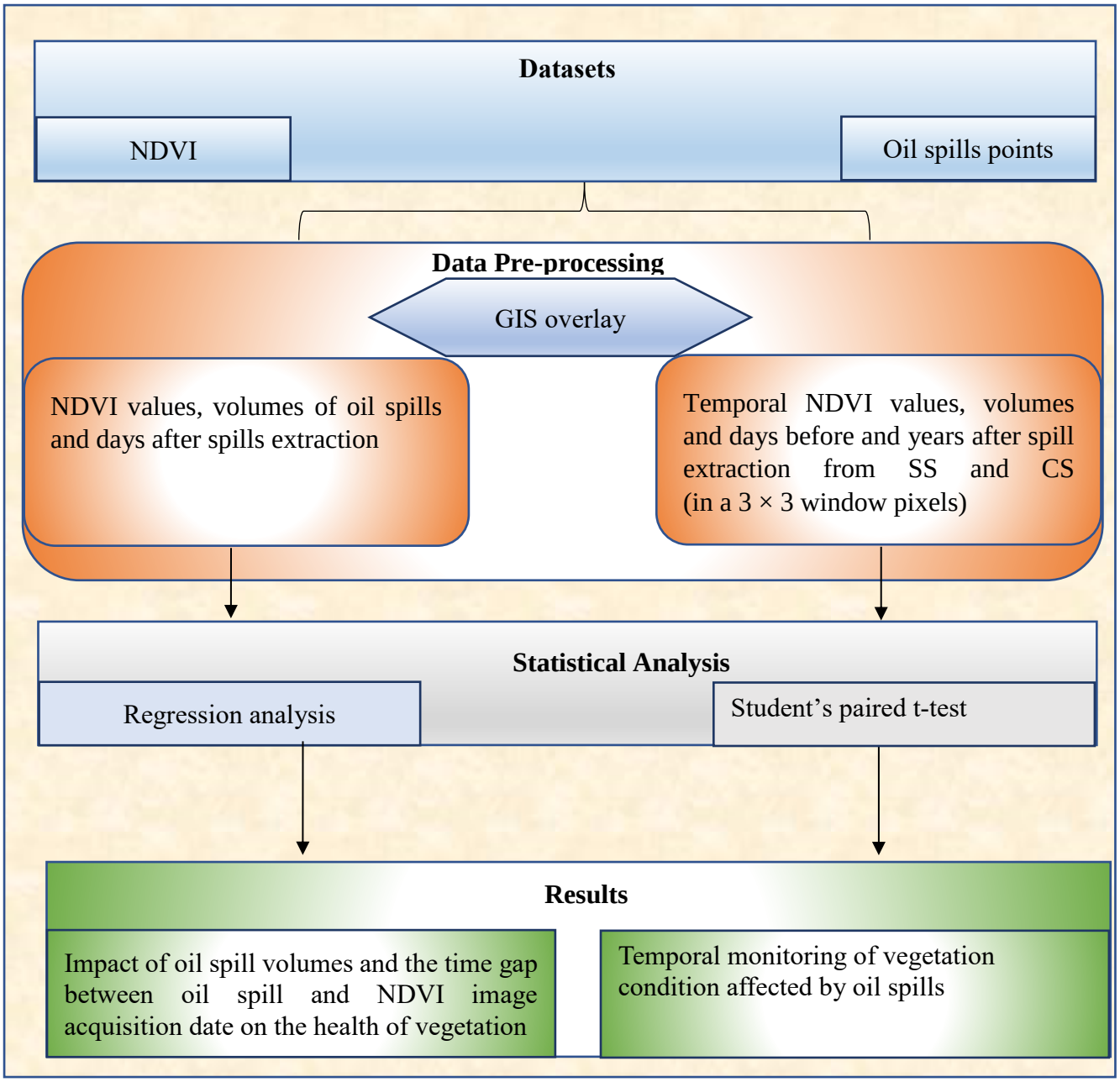

Figure 6.1: Methodology flow chart.

6.2.1 Data

6.2.1.1 Satellite-derived vegetation index (NDVI)

The health of vegetation was determined using Landsat 7 Enhanced Thematic Mapper Plus (ETM+) on-demand through EarthExplorer and ESPA satellite imagery level 2 for the period 2005–2018, which is a readily generated NDVI product from Landsat collection 1 data. All the satellite NDVI images were for the dry season from December to February to minimise cloud cover and temperature variability since the three months have almost the same weather conditions (with almost zero precipitation). NDVI was chosen because, from various studies, it has proven to be a robust VI in monitoring the impact of oil spills on the health of vegetation. The data comprise Landsat Surface Reflectance-derived spectral indices that are atmospherically corrected, orthorectified and downloaded from https://espa.cr.usgs.gov/. All the imageries are calibrated for time-series analysis, geometrically corrected and projected to WGS84 Universal Traverse Mercator Projection Zones 31 and 32 (Table 6.1).

Table 6.1: Landsat sensor platforms, paths/rows and pixel sizes.

Satellite	Sensor	Path/Row	Years of images acquisition	UTM Zone	Pixel sizes(m)
L7	ETM+	188/56	2006 to 2018	32	30
L7	ETM+	188/57		32	30
L7	ETM+	189/56		32	30
L7	ETM+	189/57		31	30
L7	ETM+	190/56		31	30

6.2.1.2 Oil spill data

The oil spill data downloaded from the Nigerian Oil Spill Monitor website (https://oilspillmonitor.ng/) in section 3.3.3 were used to analyse the oil spill incidences recorded in Nigeria from 2006 to 2018 with geographic coordinates. The data was compiled by the National Oil Spill Detection and Response Agency (NOSDRA) which relies on the voluntary support of oil companies to provide the spill data logistics, estimated spill volumes estimates etc. The oil spill volume is calculated through site visit by joint investigation team which includes representatives of regulatory agencies, the oil company, the affected community, and the security forces through a process called joint investigation visits (JIV). The report of JIV join provides information on the oil spill, its causes, scale and effects on the environment.

Figure 6.2 shows the distribution of oil spill occurrences used for extracting the NDVI values used to determine the effect of oil spills on vegetation. Figure 6.2a shows the oil spill points on the vegetation types used to investigate the factors (volumes of spills and time gap between oil spills and image acquisition date) influencing the detectability of oil spills using spectral indices. Figure 6.2b shows the oil spill points for temporal monitoring of different vegetation types affected by oil spills in the Niger Delta. The circle, square, and diamond shapes represent spill sites, and no-spill sites represent dense, sparse and mangrove vegetation. Green indicates no-spill sites (control), while red indicates spill sites.

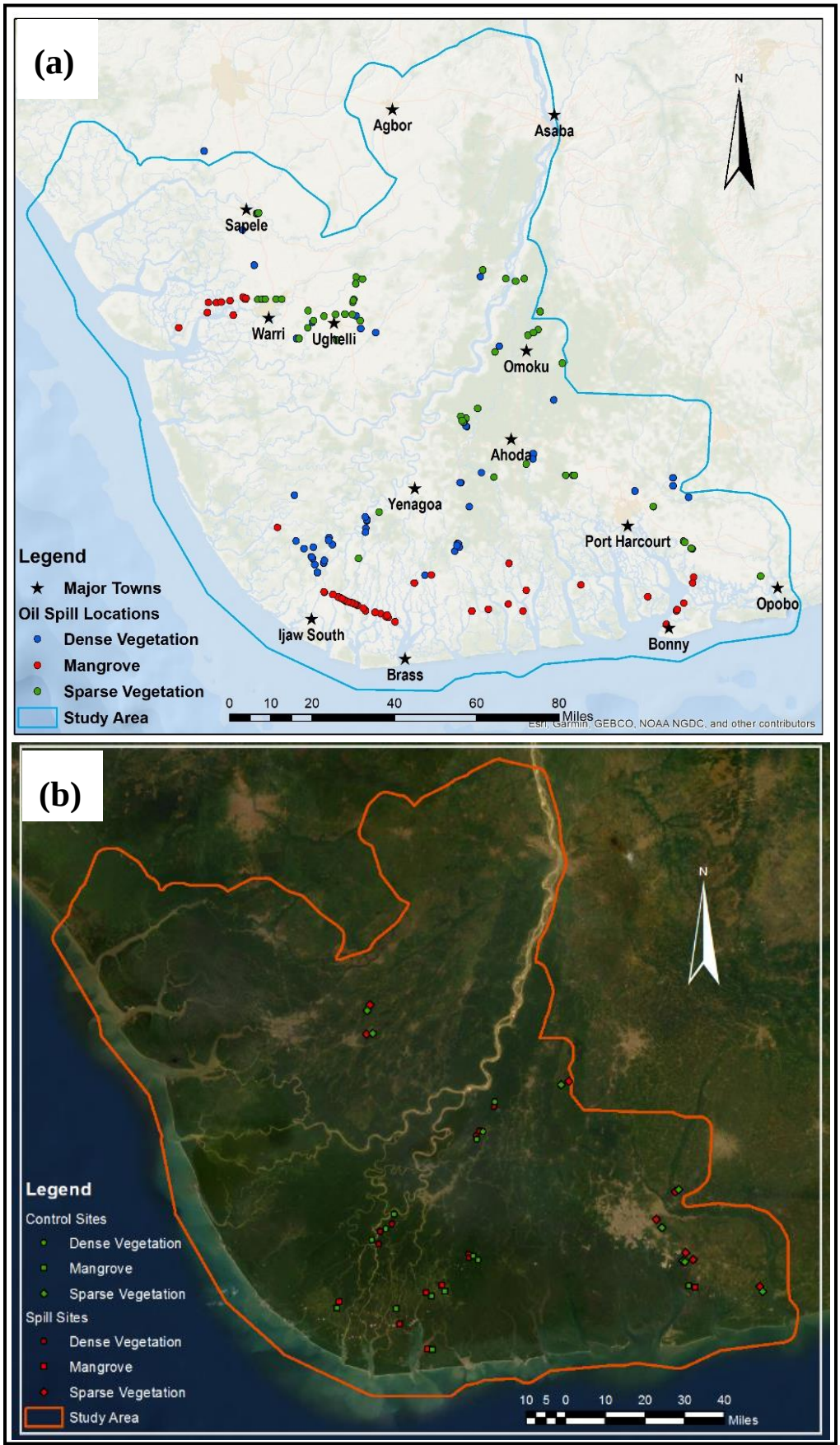

Figure 6.2. Spatial distribution of oil spills sample points for monitoring the effect of oil spills on vegetation (a) and location of spills and no spills sites for temporal monitoring of oil spill impacts on vegetation.

6.2.2 Methods

6.2.2.1 Analysis of the effect of oil spills on vegetation

The oil spill points within and around the study area were selected to extract NDVI values for the chosen spill sites for analysis. The total number of sample points used for determining the impact of oil spill volume, the time gap between oil spills and image acquisition date on the vegetation health are 55 for dense vegetation, 60 for sparse vegetation and 61 for mangrove vegetation (Table 6.2) out a total number of 8220 oil spill incidents points a subset of 8612 recorded oil spill incident with coordinate values. The shapefiles of oil spills with a minimum of 10 bbl were overlaid in GIS on the NDVI image. The time series Google world imagery served as a guide in identifying the correct vegetation types for selecting sites to extract NDVI values using a 1x1 pixel window before and after spills. The first available images acquired after the spills were used to derive the corresponding NDVI for comparison with spills volume and the time gap between oil spills dates and the image acquisition date. The time gap was computed between the recorded oil spills and the NDVI image acquisition dates.

The value of NDVI varied between − 1.0 and + 1.0, and the increasing amount of positive NDVI values indicates an increase in the amounts of green vegetation, while NDVI values near zero and decreasing negative values indicate non-vegetated features, such as barren surfaces (rock and soil), water, snow, ice, and clouds (Saravanan at el., 2019). The higher the value of NDVI, the healthier and dense the vegetation, while the lower the NDVI values are, the less healthy or dense the vegetation. Usually, if the traditional method is used, the NDVI is calculated as a ratio between the red (R) and near-infrared (NIR) sing equ1

$$\mathrm{NDVI} = \frac{\mathrm{NIR}-\mathrm{RED}}{\mathrm{NIR}+\mathrm{RED}} \qquad \text{Eq. 6.1}$$

The RED and NIR represent the spectral reflectance measurements acquired in the red (visible) and near-infrared regions.

The temporal monitoring of vegetation health following an oil spill involved comparing the NDVI values at spill sites (SS) with NDVI values at control sites (CS), where no spills had occurred. Spill sites were selected for each land cover type; 8 for dense vegetation and sparse vegetation and 6 for mangrove vegetation, and a time series of NDVI values were extracted to cover a period before spills and four to ten years after spills (Table 6.3)

to assess how the health of vegetation varied in comparison to sites not exposed to oil spills. Points with oil spill volumes above 225 bbl were selected for this analysis based on the minimum volume for which the impact of oil pollution on vegetation can be detected (Adamu et al., 2016). At each of the oil spill locations, average values of nine pixels around the polluted pixel (in a 3 × 3 window pixels) were sampled for extracting the vegetation indices because oil from spills may travel from the point of source, thereby affecting neighbouring surroundings (Adamu et al., 2018; Ozigis et al., 2019) The same sampling approach was also used for no-spill sites. The time ranges in years ranged from four to up to 10 years, depending on when the oil spills occurred. Instead of using the NDVI values for the analysis, the changes in NDVI for SS and CS were used, and the no-spill locations were proximal to reduce the effect of external factors on the NDVI, such as availability of water, sunlight, soil composition, variability in weather conditions, etc. Some oil spill sites may have an initial higher NDVI value than those at no-spill sites and may remain higher after the spill than the no-spill site if exposed to different external factors, which may affect the analysis. The values of change in NDVI were computed using the following equation:

$$\Delta NDVI = NDVI_{AS}^{1} \ldots\ldots NDVI_{AS}^{s} - NDVI_{BS} \quad \text{Eq. 6.2}$$

$\Delta NDVI$ and $NDVI_{BS}$ are changed in NDVI and NDVI before the oil spill, respectively, while $NDVI_{AS}^{1}$ and $NDVI_{AS}^{s}$ are the first and subsequence NDVI after a spill.

Table 6.2 shows the years of spills, the number of sample points per year for each type of vegetation, the NDVI image acquisition date for each year from 2006 to 2018, and the oil spill dates from 2006 to 2017. Table 6.3 shows the sample point spill dates, spill volumes, years after spills and NDVI date ranges for dense vegetation, sparse vegetation and mangrove vegetation. Minimum and maximum oil spills volumes for each vegetation type are 280 and 1500 bbl for dense vegetation, 228 and 1500 bbl for sparse vegetation and 264 and 2500 bbl for mangrove vegetation (Table 6.3).

Table 6.2: Year of oil spills, numbers of sample points, and NDVI acquisition dates used to assess the effect of oil spills on different vegetation types.

	Sample Points			NDVI acquisition Dates		
YOS	DV	SV	MV	DV	SV	MV
2006	1		1	09/12/2006		09/12/2006
2007	1	3	1	14/02/2008	14/02/2008	14/02/2008
2008	1	3	1	30/12/2008	07/12/2008, 30/12/2008	30/12/2008
2009		7	3		18/01/2010, 21/01/2011	02/01/2010, 21/01/2011
2010	6	9	4	21/01/2011	21/01/2011, 11/01/2011	14/01/2011, 21/01/2011
2011	2	6	4	17/01/2012	17/01/2012, 09/02/2012, 10/01/2013	09/02/2012, 10/01/2013
2012	2	5	5	10/01/2013	10/01/2013, 13/01/2014	10/01/2013, 13/01/2014
2013	2	3	10	21/12/2013	13/01/2014	13/01/2014, 27/12/2015
2014	11	4	18	16/01/2015 ,09/01/2015	09/01/2015, 16/01/2015	09/01/2015, 16/01/2015
2015	11	14	9	03/01/2016	03/01/2016, 05/01/2017	03/01/2016, 05/01/2017
2016	11	5	4	05/01/2017	29/12/2016, 05/01/2017, 08/01/2018	05/01/2017
2017	7	1	1	01/01/2018, 08/01/2018	08/01/2018	01/01/2018
Total	55	60	61			

Note: YOS=Year of Spill, DV=Dense vegetation, SV= sparse vegetation, MV=mangrove vegetation.

Table 6.3: Number of points, date and volumes of spills, number of years after spills for some selected spill points used to analyse the temporal effect of oil spill on change in NDVI values of spill sites.

Sample points	Spill date	Spill Volumes	Years after spill	NDVI date range
SSD1	01/10/2014	280.0	4	2014 to 2018
SSD2	13/10/2011	345.8	7	2012 to 2018
SSD3	25/06/2014	367.0	4	2014 to 2018
SSD4	14/11/2014	367.0	4	2014 to 2018
SSD5	09/04/2011	429	6	2012 to 2017
SSD6	25/04/2010	1000.0	6	2011 to 2018
SSD7	31/10/2011	1430.0	7	2012 to 2018
SSD8	25/04/2010	1500.0	7	2010 to 2018
SSS1	19/01/2014	228	4	2013 to 2017
SSS2	17/09/2013	235	5	2012 to 2017
SSS3	24/06/2010	260	8	2010 to 2017
SSS4	08/08/2008	440.3	10	2008 to 2018
SSS5	22/01/2012	529.5	7	2011 to 2018
SSS6	23/12/2010	802.5	7	2010 to 2017
SSS7	25/09/2010	1000	5	2010 to 2016
SSS8	05/05/2008	1500	10	2008 to 2017
SSM1	14/08/2013	264	4	2013 to 2018
SSM2	26/06/2010	800	7	2010 to 2018
SSM3	01/02/2010	1020	4	2010 to 2018
SSM4	05/08/2010	1510	8	2009 to 2018
SSM5	15/05/2009	1554	6	2008 to 2018
SSM6	15/06/2009	2500	6	2008 to 2018

SSD=sample site Dense; SSS=sample site Sparse; SSM=sample site mangrove.

6.2.2.2 Statistical analysis

Statistical methods provide tools for making quantitative decisions about a process or processes (Dahiru, 2011). Regression is a statistical technique used for prediction and causal inference to determine the linear relationship between two or more variables (Campbell & Campbell, 2008) and is used for forecasting and time-series modelling. Here, regression analysis was carried out to determine the impact of oil spill volume, the

time gap between oil spills and image acquisition date on vegetation health (i.e., NDVI), and the nature of any relationship between the variables and NDVI. For the temporal monitoring of vegetation health, students's paired t-tests were used to compare the change in NDVI values from spill sites with values from paired non-spill sites for several years to see how each vegetation type responds to being subjected to oil spills and to help understand the effect of time on vegetation health recovery. A paired t-test was used to compare the two population means of the two samples. Observations in one sample are paired with observations in the other sample (Shier, 2004) to determine the level of significance of any differences.

6.3 Results

6.3.1 NDVI values after spills, volumes of spill and time gap after the spill.

Table 6.4-6.7 shows the number of oil spill points, NDVI values after spills, volumes of spills in units of barrels, and the number of days (time gap) between the oil spill date and image acquisition date for dense, sparse and mangrove vegetation for various spill sites (ss). The highest spill volume for dense vegetation is 1894 bbl, 6866.16 bbl for sparse vegetation and 5000 bbl for mangrove vegetation. The lowest spill volume is 10 bbl for all vegetation types. Additionally, the volume of spills did not show a proportional effect on the NDVI values of some sites, especially the dense vegetation and sparse vegetation, i.e., There are sites with lower oil spill volumes having lower NDVI values. At the same time, others have large oil spill volumes and high NDVI values. The mangrove (Table 6.7) tends to have more sites with lower NDVI values at higher oil spill volumes than the remaining dense vegetation and sparse vegetation.

Tables 6.4-6.7 show the highest and lowest NVDI values in red and green bold text. It can be observed that dense vegetation has the highest NDVI value of 0.6611 at volume 108 bbl in Table 6.4 (DSS25), followed by sparse vegetation with 0.5825 at volume 22.15 in Table 6.5 (SSS12) and mangrove vegetation with 0.3913 at 53 in Table 6.6 (MSS25). Similarly, the mangrove vegetation has the lowest NDVI value of 0,0404 at 20 bbl (MSS15), followed by SS with 0.0428 at 14 bbl (SSS4) and dense vegetation with 0.1069 at 138 bbl (DSS 28), as shown in Tables 6.4, 6.5 and 6.6, respectively.

Table 6.4: Number of sample points, NDVI values after an oil spill, the volume of an oil spill, and the time gap between the oil spills and image dates for dense vegetation.

SS	NDVI	Volume (bbl)	DAS	SS	NDVI	Volume (bbl)	DAS
DSS1	0.2808	10	77	DSS29	0.5570	150	80
DSS2	0.2402	10	83	DSS30	0.3857	180	30
DSS3	0.3277	10	283	DSS31	0.2984	180	139
DSS4	0.267	10	153	DSS32	0.4110	182	80
DSS5	0.3485	10	108	DSS33	0.4339	202	65
DSS6	0.4405	14	10	DSS34	0.1790	204	286
DSS7	0.3323	15	187	DSS35	0.2553	221	256
DSS8	0.5988	15	51	DSS36	0.1393	251	239
DSS9	0.1429	17	55	DSS37	0.4879	266	151
DSS10	0.3115	20	74	DSS38	0.1528	280	107
DSS11	0.3619	23	187	DSS39	0.1922	311	19
DSS12	0.5878	25	198	DSS40	0.4496	344	303
DSS13	0.5726	27	51	DSS41	0.1650	367	205
DSS14	0.3264	29	283	DSS42	0.3802	461	129
DSS15	0.182	30	369	DSS43	0.2110	725	204
DSS16	0.4301	30	248	DSS44	0.3525	743	287
DSS17	0.1935	31	157	DSS45	0.5237	768	176
DSS18	0.579	41	85	DSS46	0.3559	797	135
DSS19	0.245	50	291	DSS47	0.3782	811	93
DSS20	0.5804	60	164	DSS48	0.5152	948	180
DSS21	0.3647	61	266	DSS49	0.3261	1000	271
DSS22	0.2889	70	286	DSS50	0.3938	1066	190
DSS23	0.2469	100	316	DSS51	0.3272	1100	360
DSS24	0.2091	100	196	DSS52	0.5524	1200	140
DSS25	**0.6011**	108	18	DSS53	0.2794	1455	93
DSS26	0.3854	127	49	DSS54	0.3000	1500	271
DSS27	0.4232	131	169	DSS55	0.2255	1894	167
DSS28	**0.1069**	138	174				

DSS=dense vegetation spill sites, DAS=days after a spill, red and green bold text=highest and lowest NDVI values.

Table 6.5: Number of sample points, NDVI values after an oil spill, the volume of an oil spill, and the time gap between the oil spills and image dates for sparse vegetation.

SS	NDVI	Volume (bbl)	DAS	SS	NDVI	Volume (bbl)	DAS
SSS1	0.0442	10	303	SSS32	0.4183	100	331
SSS2	0.5613	10	234	SSS33	0.1808	100	585
SSS3	0.1611	12	107	SSS34	0.2559	100	425
SSS4	**0.0428**	14	380	SSS35	0.3261	150	532
SSS5	0.3018	15	577	SSS36	0.2845	160	382
SSS6	0.3948	15	475	SSS37	0.3301	188.67	82
SSS7	0.5169	19.3	158	SSS38	0.0441	200	192
SSS8	0.3914	19.36	62	SSS39	0.5696	210	56
SSS9	0.2895	20	216	SSS40	0.3523	234	355
SSS10	0.5175	20	346	SSS41	0.2318	250	308
SSS11	0.0445	20	101	SSS42	0.1255	260	204
SSS12	**0.5825**	22.15	340	SSS43	0.3257	275	309
SSS13	0.3095	23	628	SSS44	0.3973	285	279
SSS14	0.4512	25	211	SSS45	0.3398	306.14	295
SSS15	0.4423	30.5	422	SSS46	0.1822	350	365
SSS16	0.339	32	155	SSS47	0.3488	440.3	144
SSS17	0.2923	34.84	338	SSS48	0.3615	500	305
SSS18	0.3424	35.33	36	SSS49	0.4545	529.5	354
SSS19	0.2481	40	548	SSS50	0.3394	630	118
SSS20	0.2786	45	613	SSS51	0.3946	637	114
SSS21	0.2633	47	178	SSS52	0.2873	802.5	22
SSS22	0.2724	50	180	SSS53	0.1786	862.6	217
SSS23	0.1104	53	135	SSS54	0.3018	864	106
SSS24	0.2804	64	101	SSS55	0.3004	946	118
SSS25	0.16	70	135	SSS56	0.2678	1000	118
SSS26	0.2616	70.5	130	SSS57	0.1630	1430	101
SSS27	0.3122	75	484	SSS58	0.2062	1500	216
SSS28	0.3293	75.5	184	SSS59	0.3622	2664	252
SSS29	0.2843	80	126	SSS60	0.3171	6866.16	330
SSS30	0.1987	90	47	SSS60	0.1573	1115	452
SSS31	0.337	92.8	497				

SSS=sparse vegetation spill sites, DAS=days after a spill, red and green bold text=highest and lowest NDVI values.

Table 6.6: Number of sample points, NDVI values after an oil spill, the volume of an oil spill, and the time gap between the oil spills and image dates for mangrove vegetation.

SS	NDVI	Volume (bbl)	DAS	SS	NDVI	Volume (bbl)	DAS
MSS1	0.1329	10	185	MSS32	0.1593	150	284
MSS2	0.1516	10	322	MSS33	0.0801	200	19
MSS3	0.1568	10	195	MSS34	0.2132	246	383
MSS4	0.1953	10	71	MSS35	0.0967	250	157
MSS5	0.3894	10	216	MSS36	0.2441	250	187
MSS6	0.1115	10	283	MSS37	0.3018	264	152
MSS7	0.2719	10	243	MSS38	0.0845	270	403
MSS8	0.1932	10	185	MSS39	0.2205	290	404
MSS9	0.1922	15	582	MSS40	0.1822	350	365
MSS10	0.2444	15	368	MSS41	0.1091	361	302
MSS11	0.182	15	142	MSS42	0.1586	400	22
MSS12	0.2373	17	66	MSS43	0.0601	479	176
MSS13	0.3379	19	301	MSS44	0.2494	561	586
MSS14	0.2458	20	262	MSS45	0.1592	570	282
MSS15	0.0404	20	46	MSS46	0.0899	634	1029
MSS16	0.1378	20	143	MSS47	0.2077	648	95
MSS17	0.1812	25	350	MSS48	0.1055	725	156
MSS18	0.229	26	293	MSS49	0.2116	800	209
MSS19	0.2487	30	92	MSS50	0.3319	1000	333
MSS20	0.2384	30	193	MSS51	0.2030	1020	354
MSS21	0.1598	38	79	MSS52	0.2979	1200	655
MSS22	0.214	45	268	MSS53	0.0594	1510	162
MSS23	0.2842	50	191	MSS54	0.1588	1900	321
MSS24	0.1887	50	61	MSS55	0.2294	2000	289
MSS25	0.3913	53	143	MSS56	0.1882	2450	313
MSS26	0.1199	60	313	MSS57	0.1547	2500	585
MSS27	0.0776	61	232	MSS58	0.0909	2699	185
MSS28	0.0731	61	307	MSS59	0.0573	3803	48
MSS29	0.1253	80	143	MSS60	0.1113	5000	52
MSS30	0.1707	130	51	MSS61	0.2957	5000	394
MSS31	0.13	150	53				

Note: MSS=Mangrove Vegetation Spill Sites, DAS=Days after a spill, red and green bold text=highest and lowest NDVI values.

6.3.2 Effect of oil spill volume on different types of vegetation

The regression analysis results on the relationship between NDVI values and oil spill volume and time interval after an oil spill are presented in Figures 6.3-6.8. Figure 6.3 shows the relationship between all volumes of the oil spill and NDVI. Also, Figure 6.4, Figure 6.5, Figure 6.6 and Figure 6.7 shows the corresponding relationship for volumes

above 225 bbl, volumes of 225–400 bbl, 401–1000 bbl and volumes >1000 bbl, respectively, for dense vegetation, sparse vegetation and mangrove vegetation. It can be observed that for all volumes of spills and up to volumes >225-400 bbl, there was a weak relationship between the oil spill volumes and NDVI values for all the vegetation types with R^2 <0.03 (Figure 6.3-6.5 a, b and c).

From the results, the sparse vegetation was affected by an oil spill at volumes between 401-1000 bbl with R^2 = 0.5(Figure 6.6b), while the dense vegetation was affected at volumes above 1000 bbl with R^2 =0.436 (Figure 6.7a). However, the mangrove was unaffected at any volume with R^2<0.3. The mangrove has the strongest positive correlation between the oil spill volume and NDVI values with R^2 =0.452 (Fig 6.6c). For the effect of time after spill, Figure 6.8 showed no strong correlation between the time after the spill and the NDVI value, with R^2 =0.088, R^2 = 0.003 and R^2 = 0.014 for dense, sparse and mangrove vegetation, respectively. However, the graph of dense vegetation showed signs of the effect of oil spills after a long time (Figure 6.8a) than sparse and mangrove vegetation.

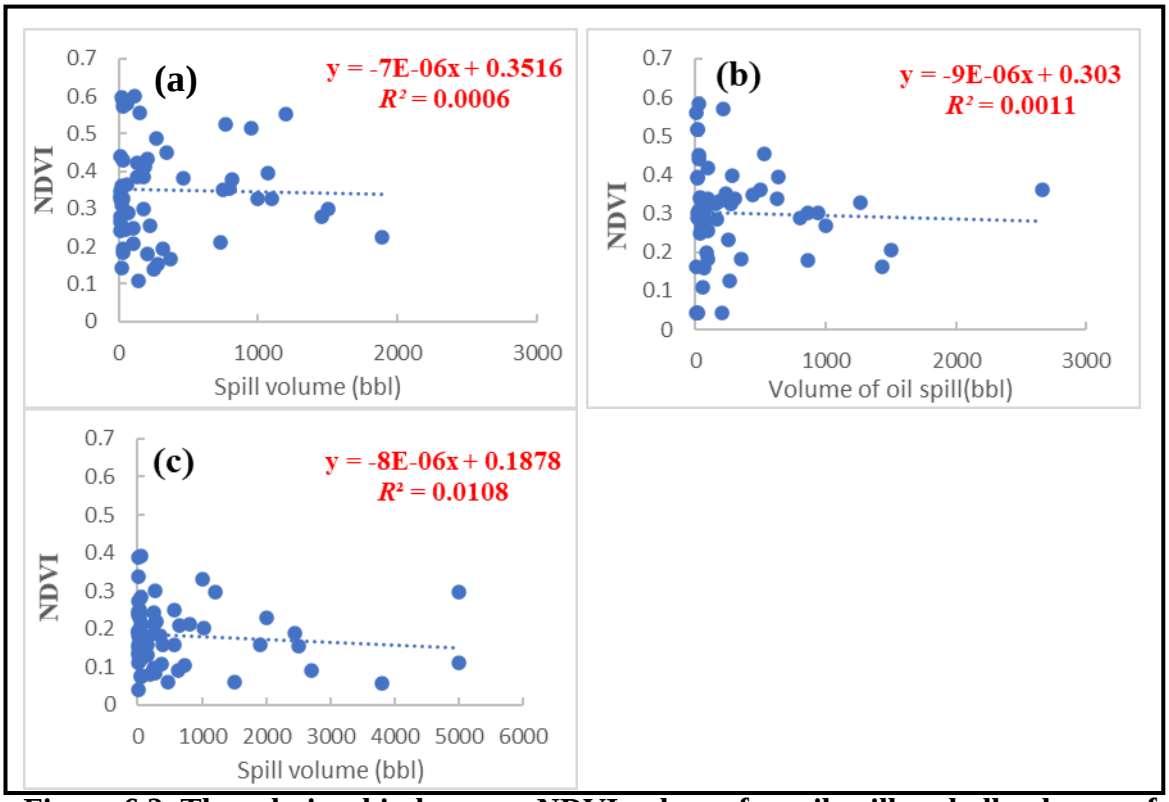

Figure 6.2. The relationship between NDVI values after oil spill and all volumes of the oil spill for (a) DV, (b) SV and (c) MV.

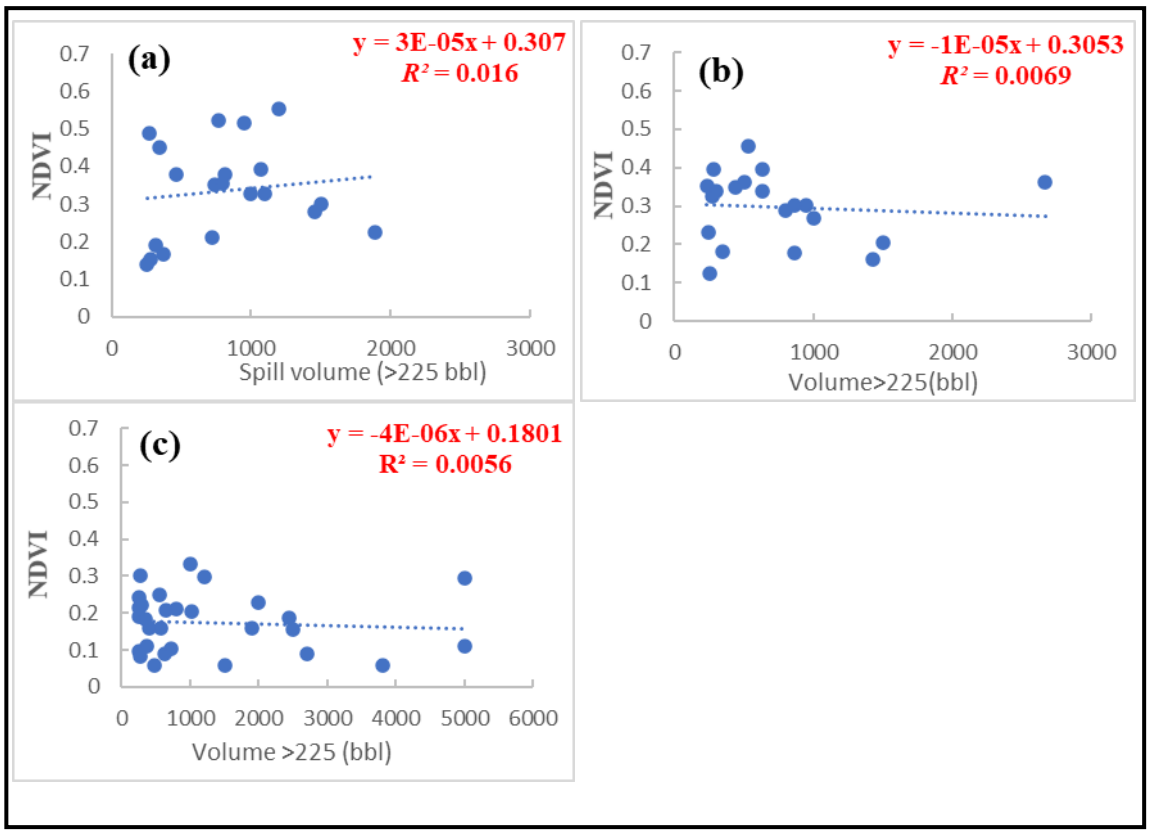

Figure 6.3. The relationship between NDVI and oil spills volumes above 225 bbl for (a) DV, (b) SV and (c) MV.

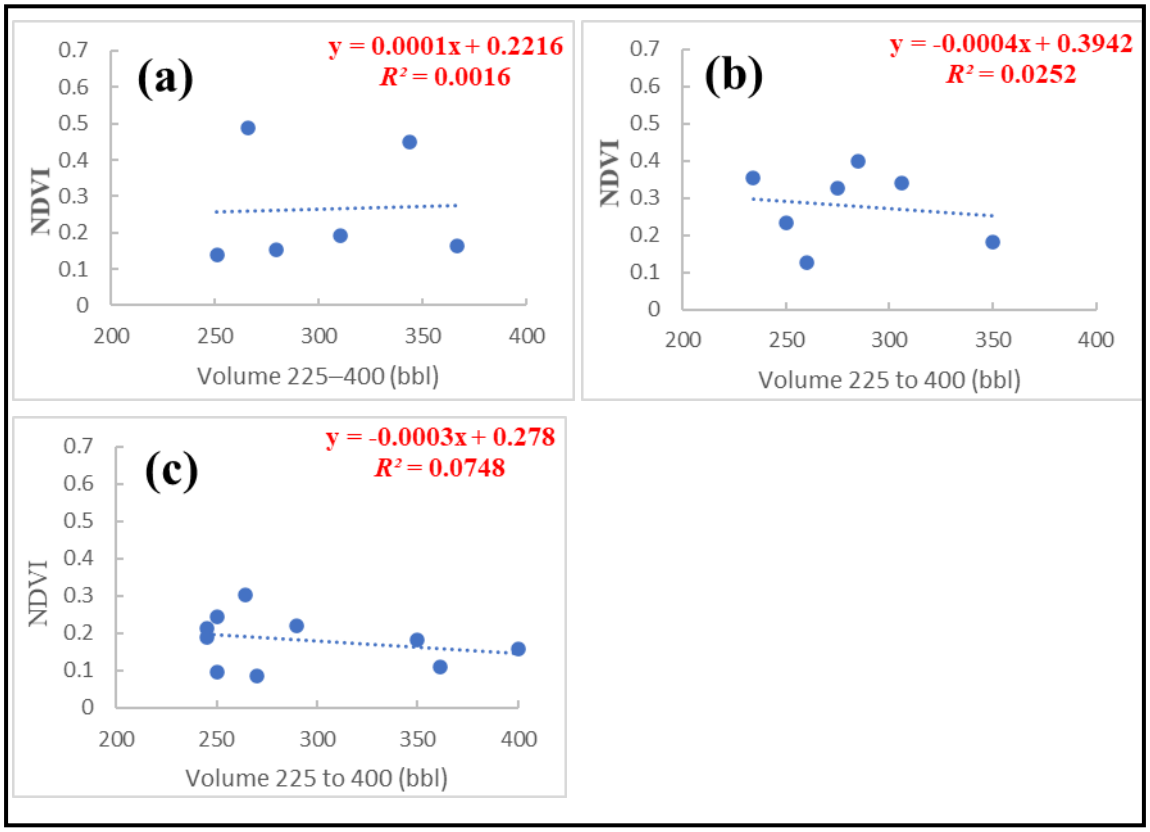

Figure 6.4. The relationship between NDVI and oil spill volumes of 225–400 bbl for (a) DV, (b) SV and (c) MV.

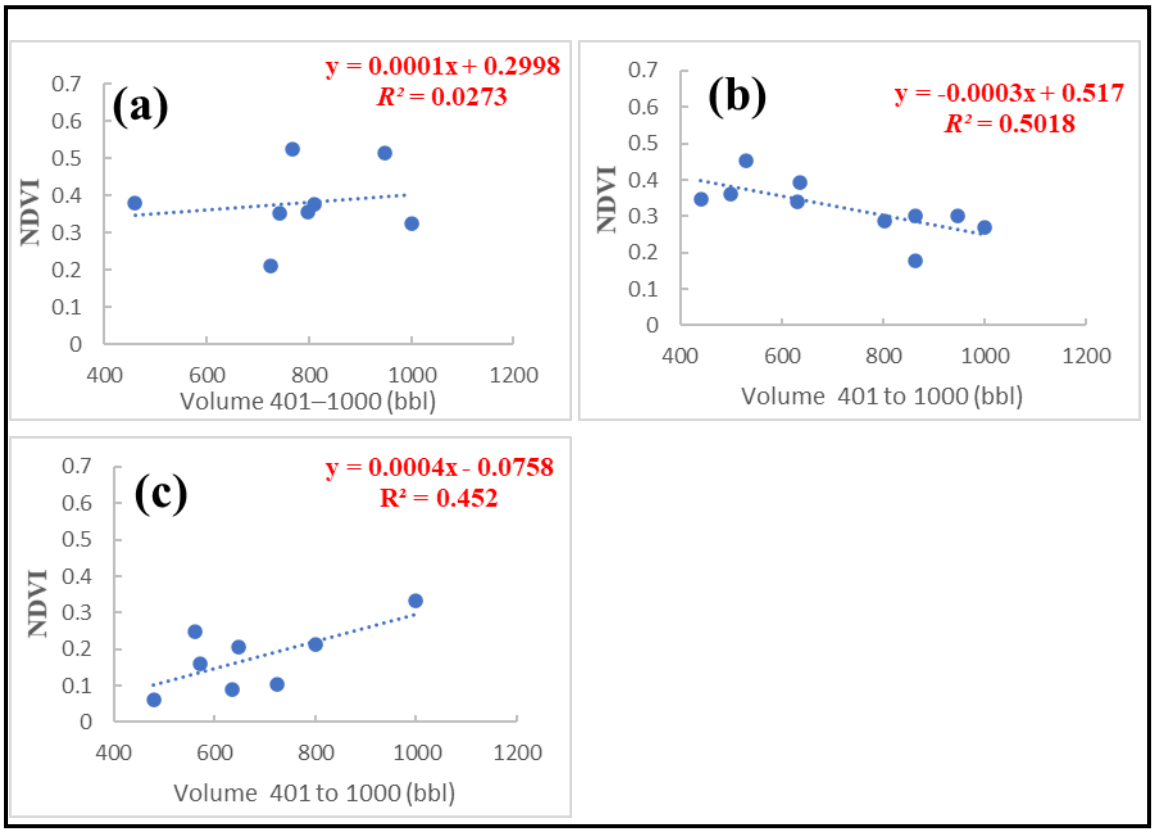

Figure 6.5. The relationship between NDVI and oil spill volumes of 401–1000 bbl for (a) DV, (b) SV and (c) MV.

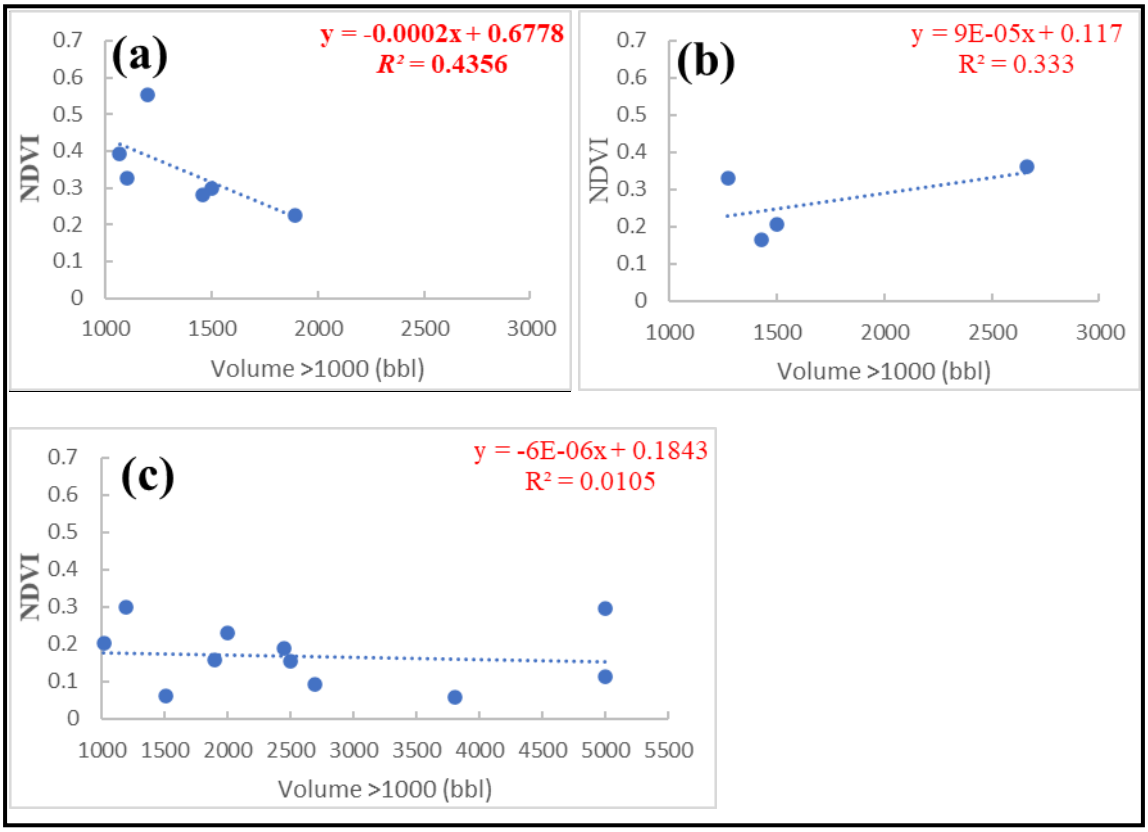

Figure 6.6. Relationship between NDVI and oil spill volumes greater than 1001 bb) for (a) DV, (b) SV and (c) MV.

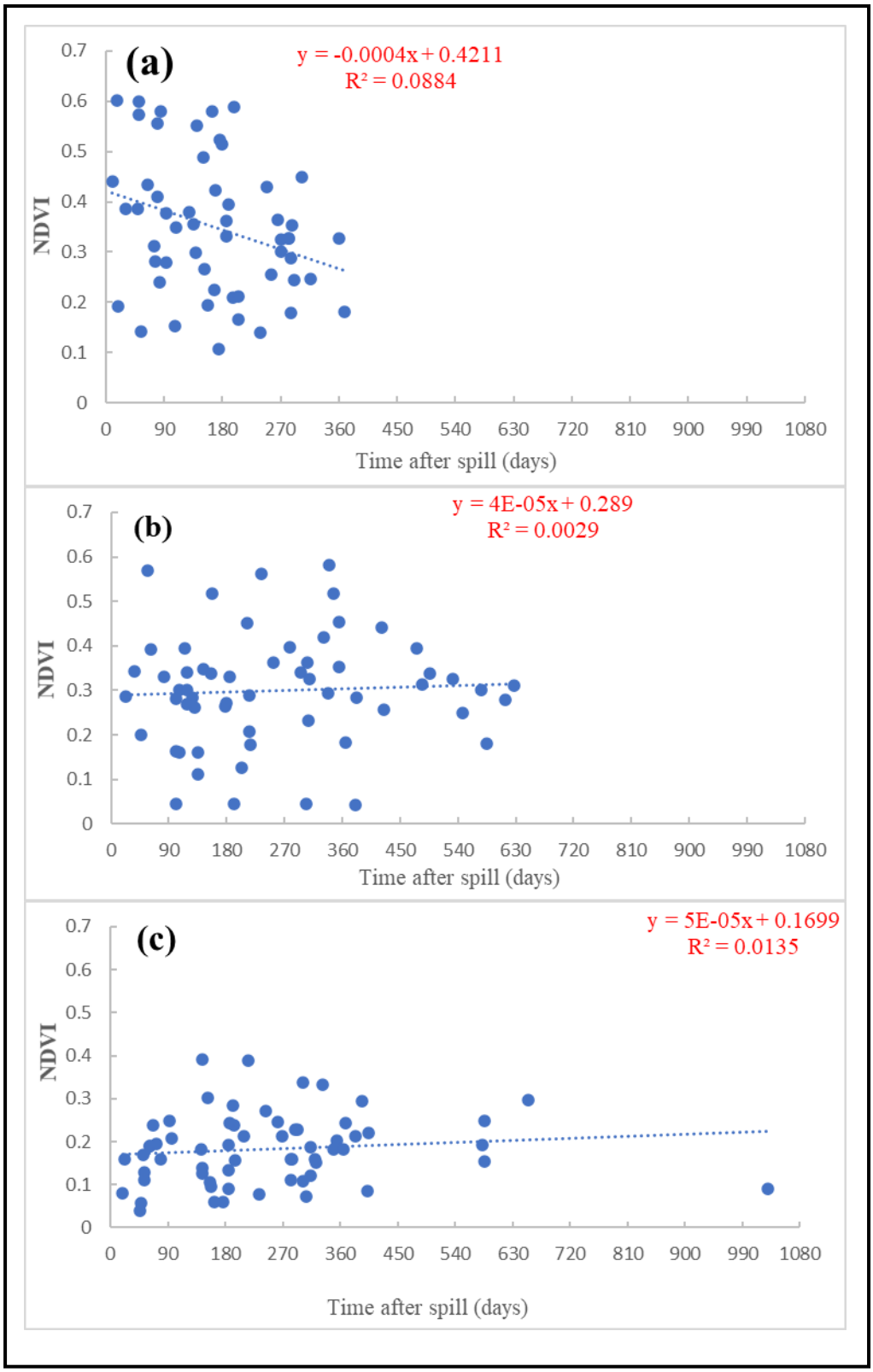

Figure 6.7. Relationship between NDVI and time after the spill for (a) DV, (b) SV and (c) MV.

6.3.3 Temporal analysis of the impact of oil spills on vegetation condition

6.3.3.1 NDVI and change in NDVI time series

Tables 6.7, 6.8 and 6.9 are the combined NDVI values for pre-and post-spill date**s** for both SS and CS used for temporal analysis of the effect of oil spill**s** on the health of vegetation and the change in NDVI time-series values for dense, sparse and mangrove vegetation for some selected points. The values in red represent NDVI observations acquired before the oil spill, while the black values correspond to NDVI values after the occurrence of a spill. The computed results of the change in NDVI time series values over many years after the spill for SS and CS are shown in light green (columns). The negative values indicate a decrease in NDVI relative to the NDVI value before the spill. A time-series dominated by negative values suggest that vegetation at that site failed to recover after being fully exposed to an oil spill. On the other hand, a positive NDVI value indicates that the vegetation recovered somewhat after exposure to an oil spill.

Table 6.7: NDVI values and change in NDVI time-series data for spill sites (SS) and control sites (CS) for dense vegetation.

ID	Volume(bbl)	Pre and Post spill days	NDVI Values		Change in NDVI	
			SS	CS	SS	CS
SD1	280	-261	0.4488	0.2925		
		107	0.1485	0.2106	-0.3003	-0.0819
		459	0.3318	0.2819	-0.1170	-0.0106
		827	0.3180	0.2734	-0.1309	-0.0191
		1195	0.3878	0.3561	-0.0610	0.0636
SD2	345.75	-265	0.3353	0.3081		
		119	0.4555	0.4006	0.1202	0.0925
		455	0.5229	0.5161	0.1876	0.2079
		823	0.6021	0.5714	0.2668	0.2633
		1191	0.6147	0.5681	0.2794	0.2599
		1543	0.5942	0.5729	0.2589	0.2648
		1911	0.4778	0.4382	0.1425	0.1300
		2279	0.4149	0.3962	0.0796	0.0881
SD3	367	-163	0.3111	0.3101		
		205	0.1658	0.1769	-0.1452	-0.1332
		557	0.4561	0.4488	0.1450	0.1387
		925	0.2787	0.3499	-0.0324	0.0398
		1293	0.3431	0.3568	0.0321	0.0467
SD4	367	-305	0.6049	0.6344		
		63	0.5277	0.6021	-0.0772	-0.0323
		415	0.5490	0.5919	-0.0559	-0.0425
		783	0.4467	0.4528	-0.1583	-0.1816
		1151	0.4092	0.4058	-0.1957	-0.2286
SD5	429	-78	0.3388	0.3569		
		306	0.4178	0.5085	0.0790	0.1516
		642	0.5453	0.5643	0.2065	0.2075
		1010	0.2897	0.1995	-0.0491	-0.1574
		1378	0.6102	0.6585	0.2714	0.3016
		1730	0.5757	0.5953	0.2368	0.2384
		2098	0.4434	0.4789	0.1046	0.1220
SD6	1000	-113	0.6785	0.6171		
		271	0.3199	0.3047	-0.3586	-0.3124
		655	0.2531	0.3176	-0.4254	-0.2995
		1359	0.3305	0.2980	-0.3480	-0.3191
		1727	0.4975	0.5042	-0.1810	-0.1129
		2447	0.3994	0.3448	-0.2791	-0.2723
		2815	0.3880	0.3179	-0.2905	-0.2992
SD7	1430	-283	0.2155	0.2646		
		101	0.1602	0.3466	-0.0553	0.0821
		437	0.3183	0.4549	0.1028	0.1903
		805	0.3713	0.3561	0.1557	0.0915
		1173	0.1154	0.1608	-0.1001	-0.1037
		1525	0.1844	0.2456	-0.0311	-0.0189
		1893	0.3721	0.4096	0.1566	0.1450
		2261	0.3562	0.4174	0.1406	0.1528
SD8	1500	-113	0.6074	0.5881		
		271	0.3069	0.3118	-0.3006	-0.2763
		655	0.2962	0.2303	-0.3112	-0.3578
		991	0.4654	0.4468	-0.1421	-0.1413
		1727	0.5051	0.4527	-0.1023	-0.1355
		2079	0.2546	0.2729	-0.3528	-0.3152
		2447	0.3611	0.3478	-0.2463	-0.2404
		2815	0.3588	0.3639	-0.2487	-0.2242

Note: red =NDVI values before oil spill date; red with negative values are the numbers of days before oil spill date, SD=sample site, light green =changes time-series changes in NDVI.

Table 6.8: NDVI values and change in NDVI time-series data for spill sites (SS) and control sites (CS) for sparse vegetation.

ID	Volume (bbl)	Pre and Post spill days	NDVI Values		Change in NDVI	
			SS	CS	SS	CS
SS1	234	-29	0.5074	0.5146		
		355	0.3240	0.3544	-0.1834	-0.1602
		707	0.3267	0.4068	-0.1807	-0.1079
		1075	0.1561	0.1882	-0.3514	-0.3264
		1443	0.2898	0.3333	-0.2176	-0.1813
SS2	235	-257	0.5050	0.5076		
		95	0.5131	0.5881	0.0082	0.0805
		479	0.3606	0.3995	-0.1444	-0.1081
		831	0.3888	0.3973	-0.1162	-0.1103
		1199	0.2081	0.2226	-0.2968	-0.2850
		1567	0.3476	0.3641	-0.1574	-0.1435
SS3	260	-180	0.3138	0.1845		
		204	0.1390	0.1580	-0.1748	-0.0265
		572	0.1221	0.1138	-0.1916	-0.0706
		924	0.3497	0.4820	0.0360	0.2976
		1276	0.4021	0.5472	0.0883	0.3628
		1660	0.2660	0.3513	-0.0478	0.1668
		2012	0.3190	0.4346	0.0053	0.2502
		2380	0.2061	0.1838	-0.1077	-0.0006
		2748	0.2607	0.3331	-0.0530	0.1486
SS4	440.3	-176	0.2742	0.3242		
		144	0.3529	0.4093	0.0787	0.0851
		528	0.1962	0.0857	-0.0779	-0.2385
		896	0.2782	0.3020	0.0040	-0.0222
		1280	0.1390	0.0948	-0.1351	-0.2294
		1616	0.3931	0.4209	0.1190	0.0966
		1984	0.4455	0.5027	0.1713	0.1785
		2352	0.3975	0.4317	0.1233	0.1075
		2704	0.3328	0.3741	0.0587	0.0499
		3072	0.3305	0.3670	0.0564	0.0428
		3440	0.2984	0.3259	0.0242	0.0016

Site ID	Volume (bbl)	Pre and Post spill days	NDVI Values		Change in NDVI	
			SS	CS	SS	CS
SS5	529.5	-366	0.3427	0.3422		
		18	0.2218	0.3114	-0.1209	-0.0308
		354	0.4613	0.4556	0.1186	0.1134
		722	0.5036	0.5133	0.1609	0.1712
		1090	0.4828	0.4980	0.1400	0.1558
		1442	0.4830	0.5012	0.1403	0.1590
		1810	0.3777	0.3877	0.0350	0.0455
		2178	0.3252	0.3381	-0.0175	-0.0041
SS6	802.5	-362	0.5372	0.1480		
		22	0.3071	0.3582	-0.2302	0.2103
		390	0.1895	0.2152	-0.3477	0.0672
		742	0.4758	0.5575	-0.0614	0.4095
		1094	0.5240	0.5699	-0.0132	0.4219
		1478	0.3460	0.4183	-0.1912	0.2704
		1830	0.3846	0.4829	-0.1527	0.3349
		2566	0.3701	0.4092	0.0274	0.0670
SS7	1000	-250	0.4881	0.4377		
		118	0.3017	0.2994	-0.1864	-0.1383
		502	0.3681	0.3562	-0.1200	-0.0815
		838	0.4462	0.4624	-0.0419	0.0247
		1206	0.5513	0.5944	0.0632	0.1567
		1926	0.4895	0.4851	0.0014	0.0473
SS8	1500	-136	0.5307	0.1918		
		216	0.2112	0.1702	-0.3195	-0.0215
		600	0.0510	0.1828	-0.4797	-0.0090
		984	0.2951	0.3628	-0.2356	0.1710
		1352	0.1402	0.1574	-0.3905	-0.0344
		1704	0.4668	0.5285	-0.0639	0.3367
		2056	0.5557	0.5822	0.0250	0.3904
		2440	0.3438	0.4024	-0.1869	0.2107
		2792	0.4210	0.4413	-0.1097	0.2495
		3160	0.2630	0.2934	-0.2677	0.1016
		3528	0.3844	0.4465	-0.1463	0.2547

Note: red =NDVI values before the oil spill date; red with negative values is the number of days before the oil spill date, SS=sample site sparse vegetation, light green = time-series changes in NDVI.

Table 6.9: NDVI values and change in NDVI time-series data for spill sites (SS) and control sites (CS) for mangrove vegetation.

ID	Volume (bbl)	Pre and Post spill days	NDVI Values		Change in NDVI		ID	Volume (bbl)	Pre and Post spill days	NDVI Values		Change in NDVI	
			SS	CS	SS	CS				SS	CS	SS	CS
SM1	264	-216	0.3529	0.3111			SM4	1510	-222	0.1403	0.0500		
		152	0.2922	0.3275	-0.0607	0.0164			162	0.0572	0.0563	-0.0831	0.0063
		520	0.2845	0.3368	-0.0684	0.0257			530	0.0389	0.0529	-0.1013	0.0029
		872	0.3927	0.4029	0.0398	0.0918			1234	0.1645	0.3586	0.0242	0.3086
		1240	0.2053	0.2002	-0.1475	-0.1109			1618	0.1018	0.2300	-0.0385	0.1800
		1608	0.2950	0.2498	-0.0579	-0.0613			1970	0.0814	0.2641	0.0589	-0.2141
SM2	800	-175	0.3113	0.3142					2338	0.0498	0.1229	0.0904	-0.0729
		209	0.2464	0.2976	-0.0649	-0.0166			2706	0.0931	0.2132	0.0472	-0.1632
		593	0.1899	0.2915	-0.1214	-0.0228	SM5	1554	-136	0.4212	0.4772		
		1665	0.3467	0.3943	0.0354	0.0801			232	0.2255	0.5384	-0.1957	0.0612
		2017	0.3236	0.3995	0.0123	0.0853			616	0.1343	0.2958	-0.2869	-0.1814
		2385	0.2029	0.2483	-0.1085	-0.0659			1000	0.1151	0.1939	-0.3061	-0.2833
		2753	0.2521	0.2949	0.0592	0.0193			1704	0.1846	0.2838	-0.2366	-0.1934
SM3	1020	-30	0.2994	0.3460					2072	0.1860	0.3803	-0.2352	-0.0969
		354	0.1988	0.2742	-0.1005	-0.0718			2424	0.1994	0.4786	-0.2218	0.0014
		1074	0.2551	0.3436	-0.0443	-0.0024			2792	0.0783	0.2272	-0.3429	-0.2500
		1442	0.2200	0.2341	-0.0794	-0.1119			3160	0.0974	0.2755	-0.3238	-0.2017
		1810	0.3053	0.3962	0.0059	0.0502	SM6	2500	-167	0.2933	0.2806		
		2530	0.2133	0.2436	-0.0861	-0.1024			585	0.1736	0.2071	-0.1196	-0.0735
									969	0.1648	0.1988	-0.1284	-0.0818
									1305	0.1536	0.2690	-0.1396	-0.0117
									1673	0.2096	0.3110	-0.0836	0.0304
									3129	0.1203	0.2432	-0.1729	-0.0374

Red =NDVI values before the oil spill date; red with negative values is the number of days before the oil spill date, SM=sample site mangrove vegetation, light green =time-series changes in NDVI.

6.3.3.2 The temporal effect of oil spills on the health of vegetation

Figures 6.9 a, b and c are the graphs that show the relationship between changes in NDVI values relative to pre-spill NDVI values for various times (number of days) after the spill for SS and CS for dense, sparse and mangrove vegetation, respectively. The result shows how the health of vegetation is affected after the spill for a more extended period and not just immediately after a spill. Figures 6.10a, b and c show how the oil spill volume affects only the change in NDVI at SS. Table 6.10 shows the paired t-test results computed to determine if there is a statistically significant difference between the changes in NDVI values after spills for SS and CS for dense, sparse and mangrove vegetation. Two observations can only be statistically significant if the *p*-value is <0.05, which means the null hypothesis states that there is no difference between changes in NDVI values after spills at SS and CS. For example, if the *p*-value of paired t-test results is >0.05, then there is no statistically significant difference between the change in NDVI after th**e** oil spill for some time (as shown in Table 6.3) at SS and CS. Table 6.10 shows a significant change in NDVI between SS and CS in Table 6.7-6.9 (i.e., the combined values), with sparse and mangrove vegetation being the most affected, with a *p*-value <0.001.

Table 6.10: Paired t-test analysis to determine the differences in the changes in NDVI values after spills for the SS and CS for dense, sparse and mangrove vegetation

Land cover type	*p*- values
Dense Vegetation	**
Sparse Vegetation	***
Mangrove vegetation	***

Levels of significance: * *p* -value < 0.001 (highly significant), ** *p* value < 0.01 (very significant), **p* -value < 0.05 (significant), ^{ns} *p*- value ≥ 0.05 (not significant).**

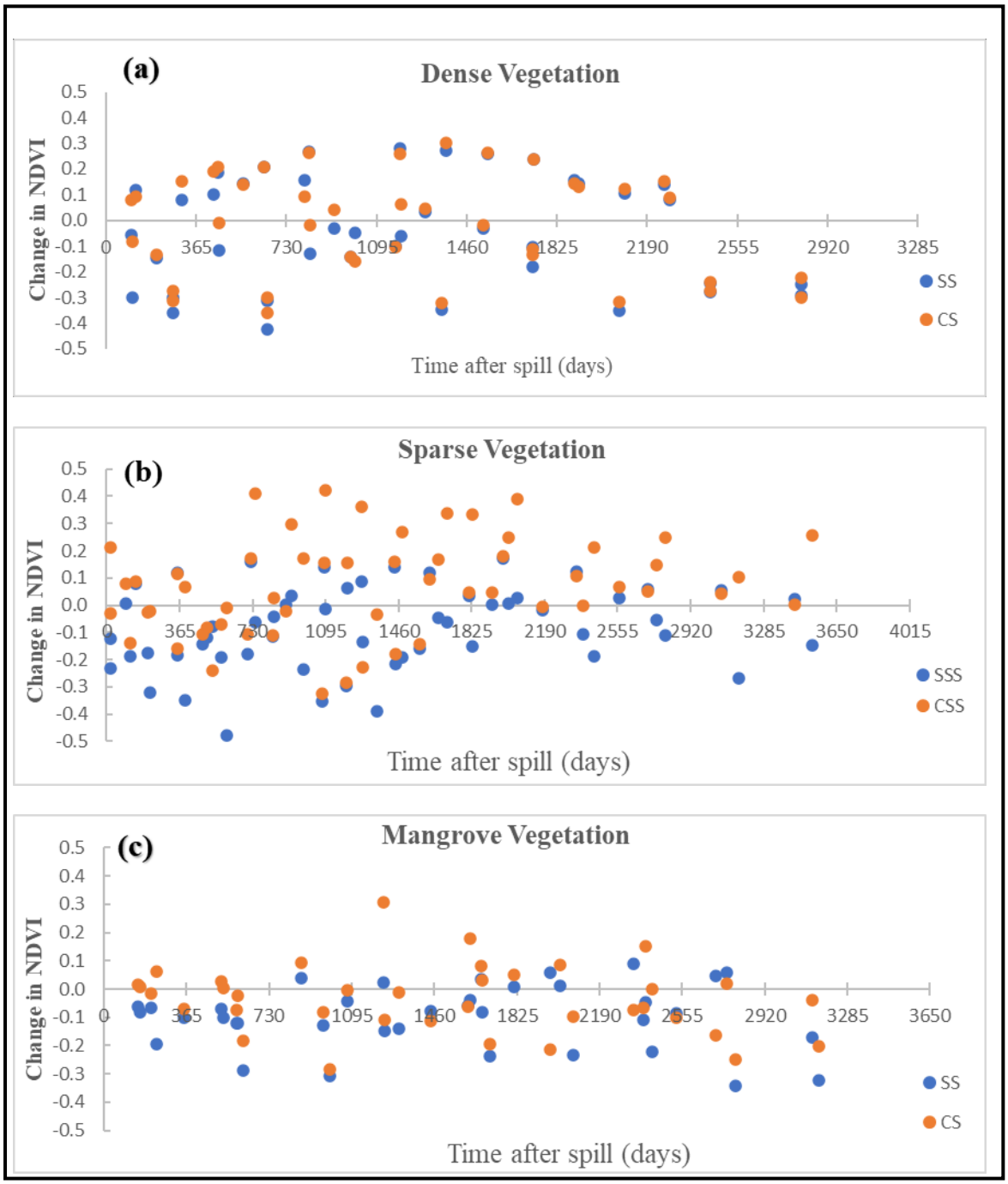

Figure 6.8: Relationship between change in NDVI and number of days after a spill for SS and CS for (a) DV, (b) SV and (c) MV.

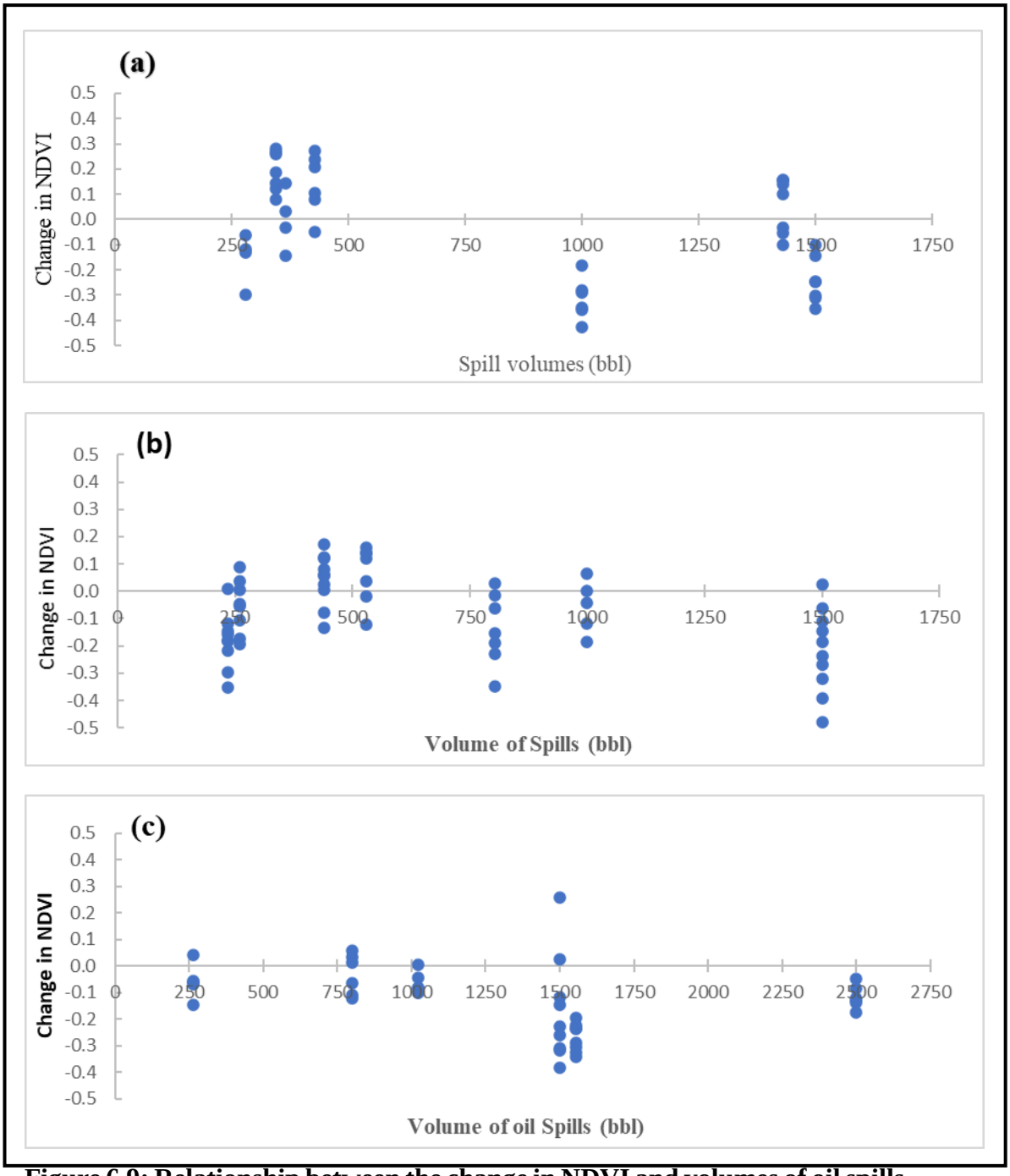

Figure 6.9: Relationship between the change in NDVI and volumes of oil spills on SS for (a) DV, (b) SV and (c) MV.

6.3.3.3 NDVI time series values analysis between spill sites and control sites

Table 6.11 shows the *p*-values from the student's t-test for changes in NDVI values after the spills for each SS and its corresponding CS for some years for dense, sparse and mangrove vegetation for different volumes of spills. Some *p*-values are very significant, while some are significant, with none having a highly significant p-value. A p-value of <0.05 means there is a statistically significant difference between a change in NDVI values after a spill for SS and CS. A p≥0.05

means the change in NDVI between SS and CS is not statistically significant. For example, it can be observed that for dense vegetation, the *p*- values are mostly >0.05, with only an oil spill volume of 280 bbl (SSD1) having a p-value of <0.05, while five out of eight sites for sparse vegetation have p<0.05 and mangrove vegetation having three out of six sites with p<0.05.

Figures 6.11, 6.12 and 6.13 illustrate the temporal changes in NDVI values of each spill site (SS) with its corresponding control sites (CS) from the values extracted from Tables 6.10–6.12 for dense vegetation, sparse vegetation and mangrove vegetation, respectively. The graphs show a visual representation of changes in NDVI values after an oil spill over some time to explain better the reason for various *p* values in Table 6.11 at SS and correspondent CS for dense vegetation, sparse vegetation and mangrove vegetation for different oil spill volumes. The graphs also show the possible recovery of vegetation from an oil spill after a certain period. Figure 6.11 a-h is the graph for dense vegetation having several years ranging from 0-4 years (Figure 6.11 a, c, d), 0-6 years (Figure 6.11 e and f) and 0-7 years (Figure 6.11 b, g and f) with the lowest and highest oil spill volumes of 280 and 1500 bbl, respectively, and with 4 and 7 years being the lowest and the highest number of years. The range of years for sparse vegetation in Figure 6.12a-h are 0-4 years (Figure 6.12 a), 0-5 years (Figure 6.12 b and g), 0-7 years (Figure 6.12 e and f), 0-8 years (Figure 6.12 c) and 0-10 years (Figure 6.12 d and h), with the lowest and highest oil spill volumes of 234 and 1500 bbl and with the lowest and highest numbers of years of 4 and 10 years, respectively. For mangrove vegetation in Figure 6.13 a-f, the years range from 0-5 years (Figure 6.13 a and d), 0-6 years (Figure 6.13 b and f) and 0-7 years (Figure 6.13 c and e), with the lowest and highest oil spill volumes of 264 and 2500 bbl and with both the lowest and highest numbers of years being 5 and 7 years, respectively.

From the graphs, a wider distance between the change in NDVI values between SS and CS indicates a significant difference in the condition/health of vegetation at SS and CS over the observed period. Additionally, a positive change in NDVI values means that the vegetation is recovering, while a negative change means that the vegetation's health is affected compared to the pre-spill condition. For almost all cases, the change in NDVI values is greater and negative at SS than CS within the first year after an oil spill for all the vegetation types. The only

exception is for SSD2 (Figure 6.11b), which has a greater positive change in NDVI within the first year than its corresponding CS.

The time-series line graph showing similar trends indicates that vegetation has similar conditions at these sites. The gap between the SS and SC line graph indicates the levels of significant differences in the health conditions of vegetation between SS and SC. A smaller gap shows that there is no significant difference in the health condition of the vegetation between SS and CS, while a larger gap means there is a significant difference compared to pre-spill. Where the line graph intersects and the SS line goes above the CS, it shows that the SS health condition of vegetation at that location has improved/recovered from the effect of an oil spill. From Figure 6.11 (dense vegetation), Figure 6.12 (sparse vegetation) and Figure 6.13 (mangrove vegetation), the sparse vegetation has a greater number of graphs whose lines between SS and CS are parallel, with wider gaps followed by the mangrove vegetation with dense vegetation, which has more intersecting lines between SS and CS. The graphs also show that all the CS are initially above the SS line except Figure 6.11 b (dense vegetation), although some SS later rise above CS, which shows recovery. This explains why dense vegetation has more sites with p>0.05 (Table 6.15).

Table 6.11: Paired t-test analysis of changes in NDVI values after a spill between each SS and CS at different volumes for DV, SV and MV.

VT	OSV	*p*- value	VT	OSV	*p* -value	VT	OSV	*p*- value
DV			SV			MV		
SSD1	280	*	SSS1	228	*	SSM1	264	*
SSD2	345.75	ns	SSS2	235	ns	SSM2	800	ns
SSD3	367	ns	SSS3	260	**	SSM3	1020	ns
SSD4	367	ns	SSS4	440.3	ns	SSM4	1510	ns
SSD5	429	ns	SSS5	529.5	ns	SSM5	1554	**
SSD6	1000	ns	SSS6	802.5	**	SSM6	2500	*
SSD7	1430	ns	SSS7	1000	*			
SSD8	1500	ns	SSS8	1500	**			

Note: VT=Vegetation type, OSV=Oil spill volume (bbl).
Levels of significance: * *p*- value < 0.001 (highly significant); ** *p*- value < 0.01 (very significant); **p* -value < 0.05 (significant), ns *p* -value ≥ 0.05 (not significant).**

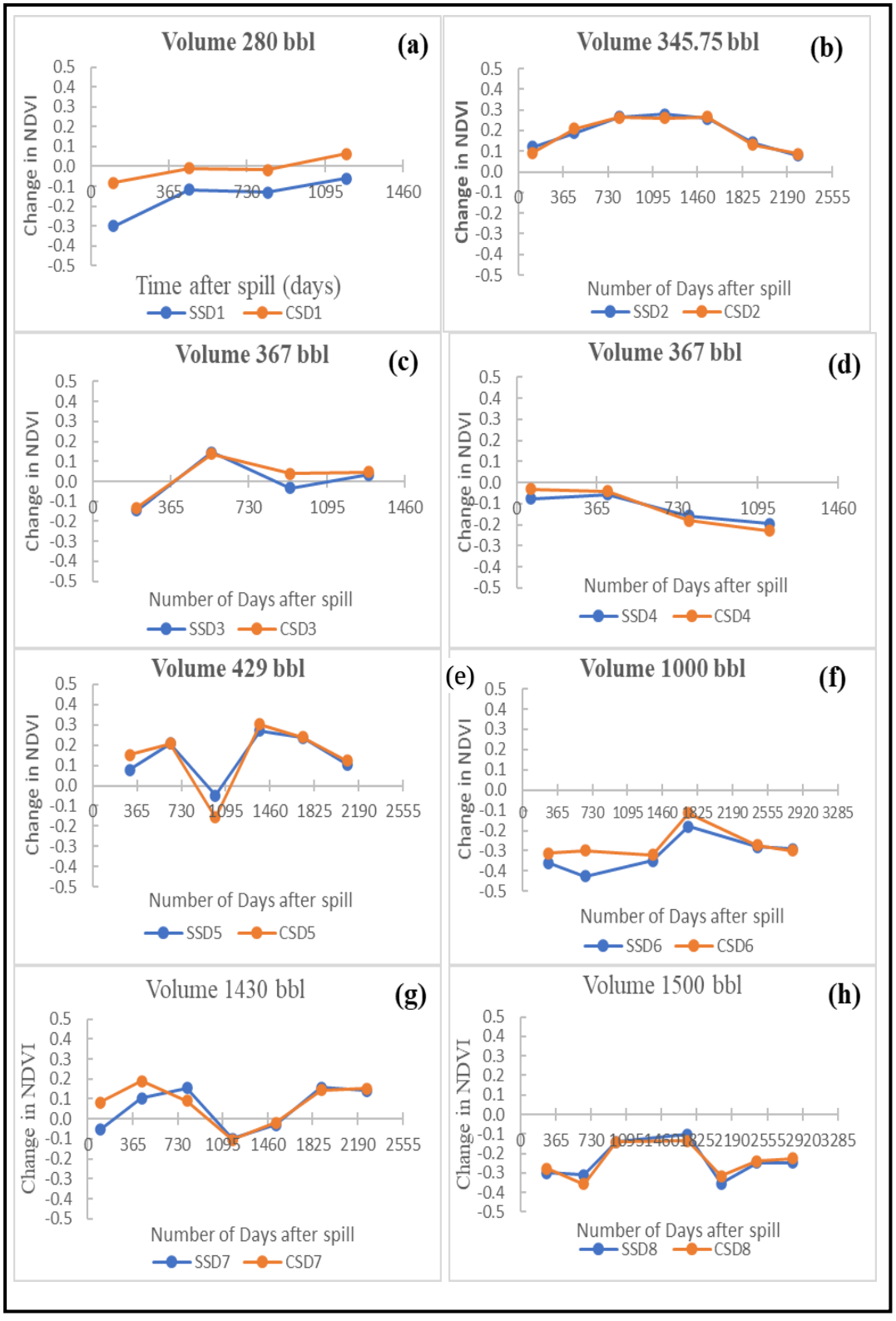

Figure 6.10: Temporal changes in NDVI values for each SS and CS for different oil spill volumes for dense vegetation.

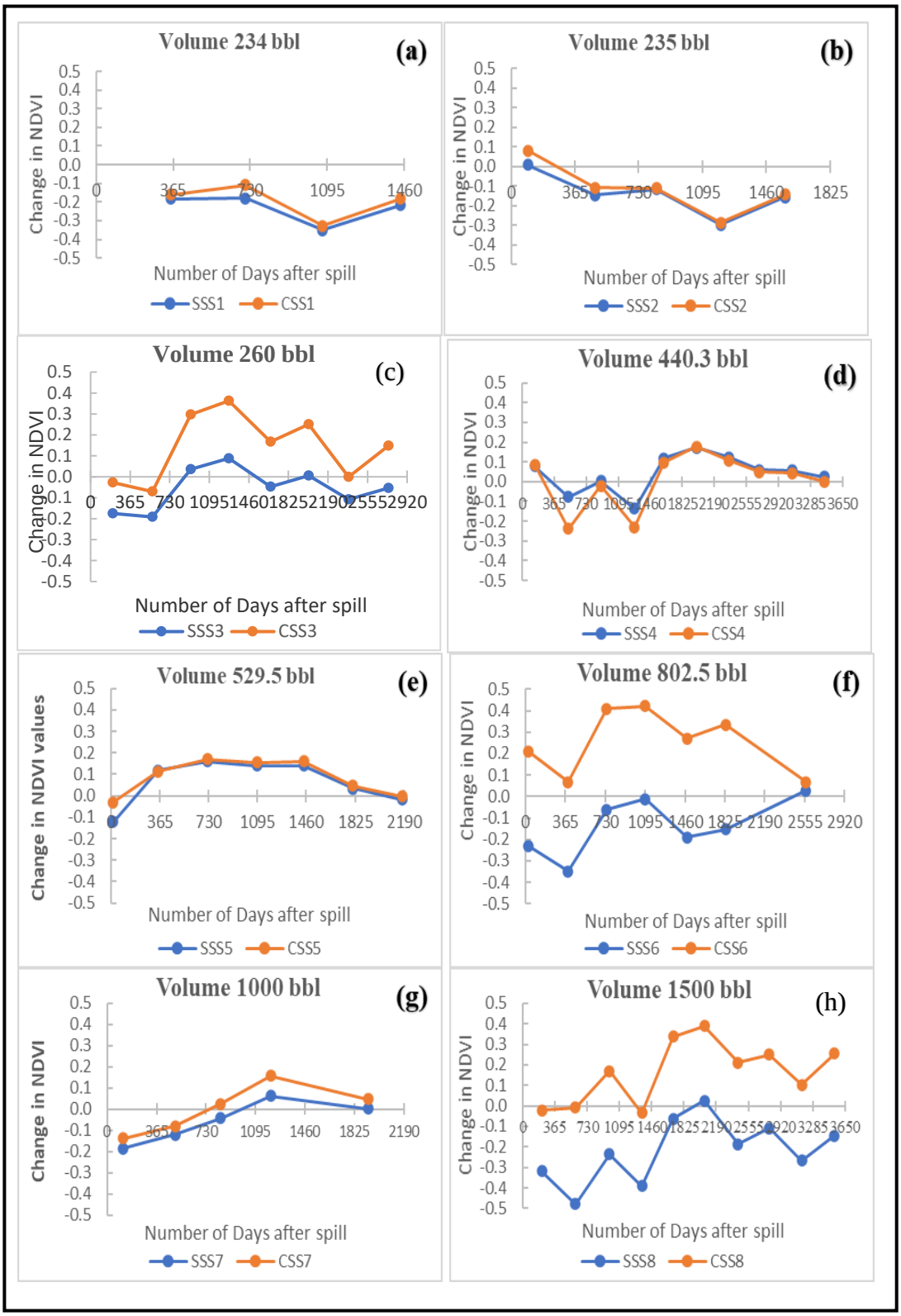

Figure 6.11: Temporal changes in NDVI values for each SS and CS for different oil spill volumes for sparse vegetation.

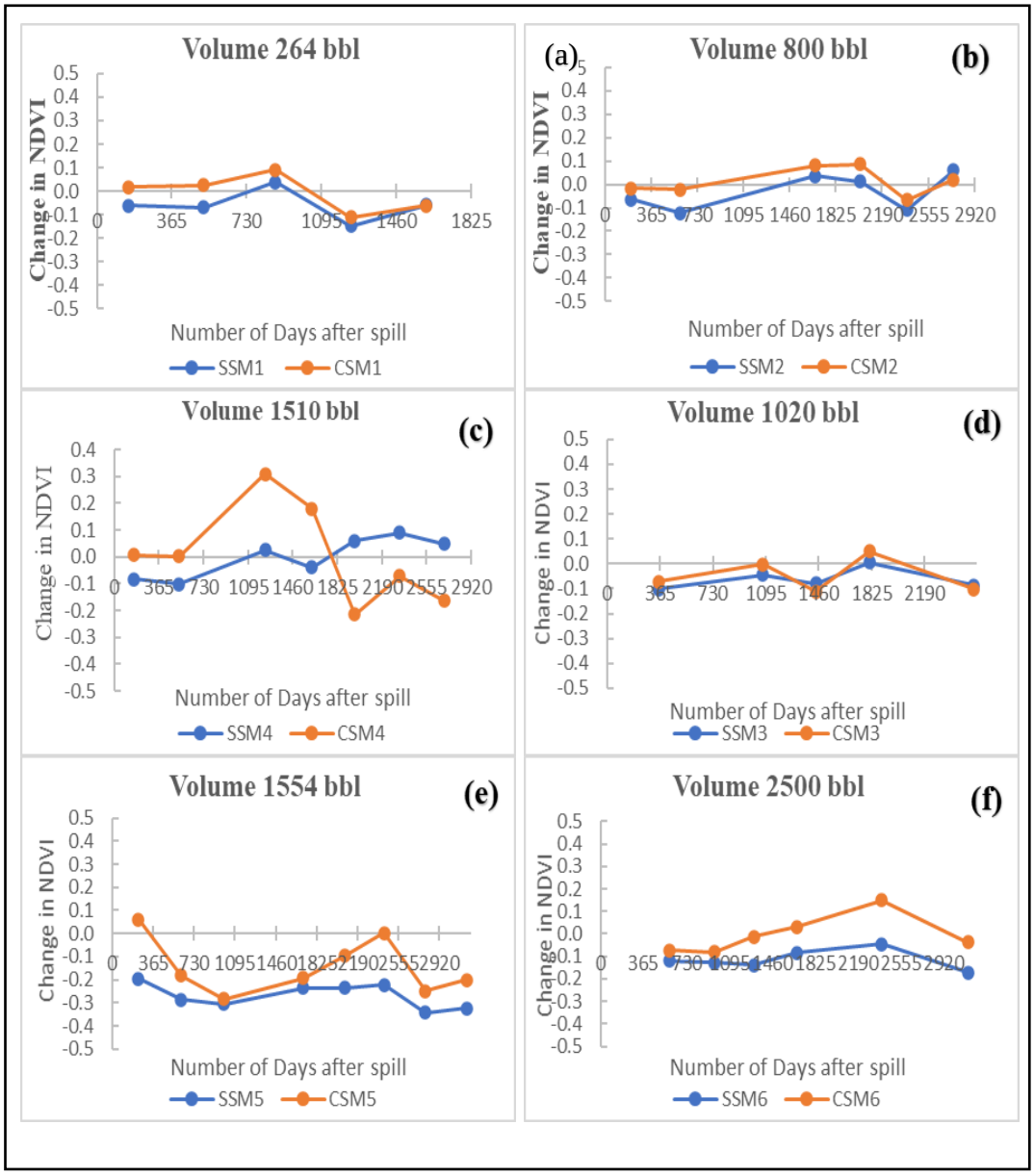

Figure 6.12: Temporal changes in NDVI values for SS and CS for different oil spill volumes for mangrove vegetation.

6.3.3.4 Some selected spill sites with their correspondent control sites for NDVI Time series

Figures 6.14, 6.15 and 6.16 show high-resolution satellite images of some selected spill sites and their corresponding control sites. The significant changes in NDVI values between the spill sites and their corresponding control sites for dense vegetation (SSD1), sparse vegetation (SSS8) and the mangrove (SSM 5) is because of the difference in the vegetation cover before and after the spill. For example, it can be observed that there is a difference in vegetation cover before and after spill of SSD1(Figures 6.14a and b), SSS8 (Figures 6.15a and b) and SSM5 (Figures 6.16 a and b). However, not much difference could be observed in

the vegetation cover of their control sites in the same period (Figures 6.14, 6.15, and 6.16 c and d). The spill years and volumes are SSD1 (2014, 280bbl) in Figure 6.14, SSS8(2008, 1500bbl) in Figure 6.15, and SSM5 (2009, 1554bbl) in Figure 6.16. The cloud cover means limited availability of reference images. For instance, the only available reference images before the oil spills for the mangrove were from 2004, while the spill happened in 2009, 5 years before the spill. However, the information provided is still important in understanding why there were significant differences between the spill sites and the corresponding control sites.

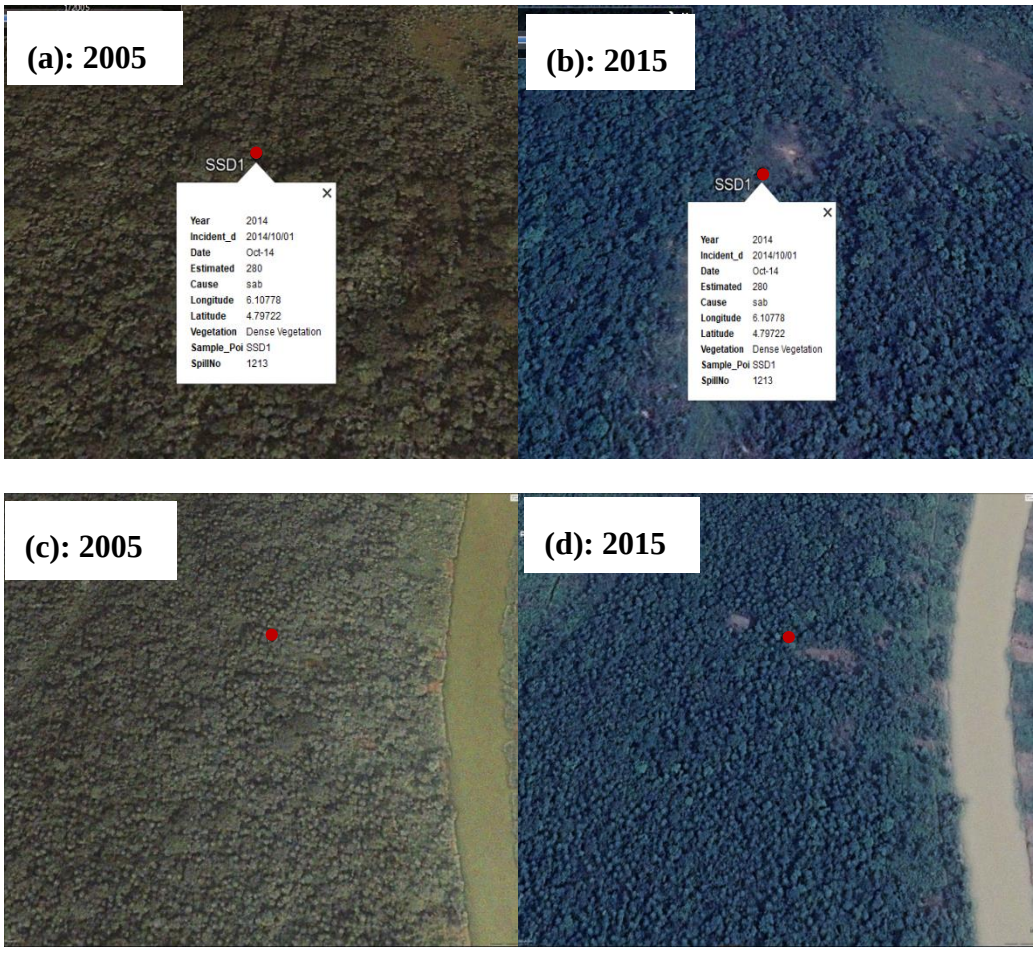

Figure 6.13:The dense vegetation spill site SSD1 in 2014 (a) before the spill in 2005, (b) after the spill in 2015, and control site (c) before the spill in 2005 and (d) after the spill in 2015.

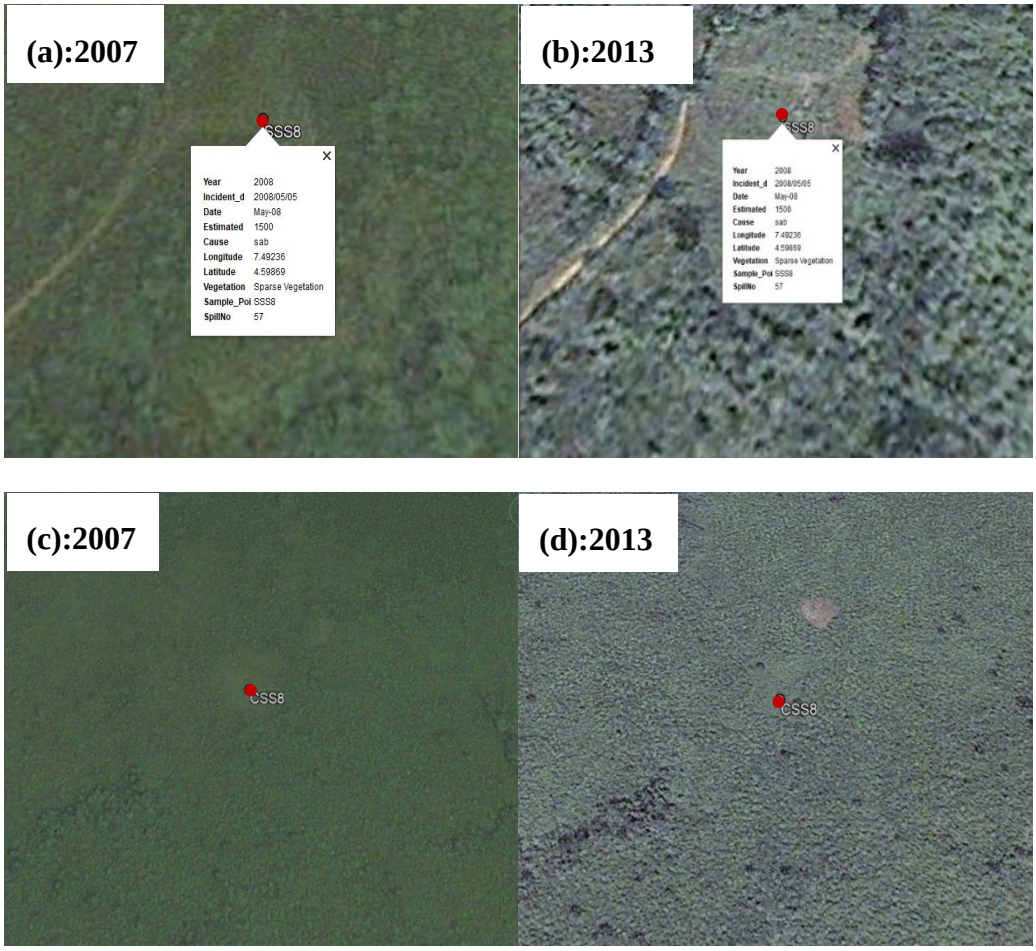

Figure 6.14:The sparse vegetation spill site SSS8 in 2008 (a) before the spill in 2007, (b) after the spill in 2013, and control sites (c) before the spill in 2007 and (d) after the spill in in 2013.

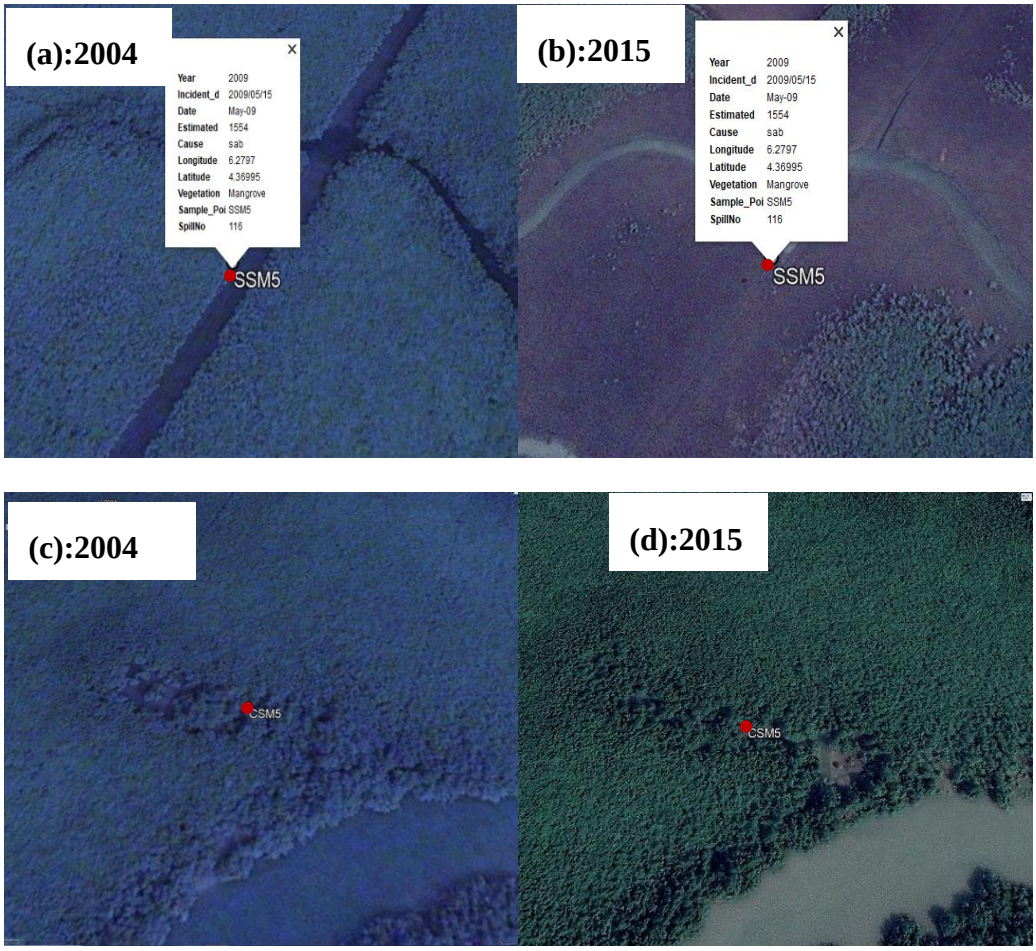

Figure 6.15:The mangrove spill site SSM 5 in 2009 (a) before the spill in 2004, (b) after the spill in 2015, and control sites (c) before the spill in 2004 and (d) after the spill in 2015.

.

6.4 Discussion

6.4.1 Impact of the volume of an oil spill and time gap on the spectral response of vegetation

Vegetation indices derived from remote-sensing images are an efficient tool to highlight the spectral differences due to changes in leaf pigments and internal leaf structure and can be used as indicators of plant health (Tote et al., 2014). The changes in vegetation health in oil polluted sites may depend on the volume of a given oil spill because it is assumed that larger-volume of oil spills may have a greater impact on the surrounding vegetation (Adamu, 2016)

The lack of a strong correlation between NDVI and all oil spill volumes on the different vegetation (R^2 <0.02) indicates that an oil spill can only affect the vegetation at a particular volume. A previous study by Adamu et al. (2016) suggested that changes in vegetation health were only detectable at the Landsat pixel scale (30 m × 30 m) if the oil spill volume exceeded 225 bbl. When different volumes were considered, the oil spill's impact on sparse vegetation was noticeable at a spill range between 401–1000 bbl and moderately impacted at volume >1000 bbl. This suggests that sparse vegetation is most affected by oil spills in the Niger Delta, within the range of 401–1000 bbl oil spill volume. Similarly, the next impacted vegetation is the dense vegetation which was impacted at a higher spill volume of >1000. The NDVI values decrease within the spill volume regions, with an increase in the oil spill volume. However, the lack of a negative correlation between the NDVI and the oil spill for the mangrove within all spills volume regions doesn't imply a lack of impact oil spill on the mangrove. Due to the mangrove vegetation being located within the swamp forest, where the oil spill could easily be washed out by ocean/sea currents, making it more unpredictable. The spill volume will not have much effect since waves and currents might propagate them to other locations. Oiling on marsh vegetation is more complex than just the chemical toxicity of oil because they are likely more prone to being saturated with oil and repeatedly reoiled during tidal cycles (Fingas, 2015).

For the relationship between the NDVI and the time after the oil spill, the dense vegetation shows more gradual signs of degradation, especially after 180 days (6

months) by decreasing in NDVI values following an oil spill in Figure 6.8 a. This is because the full extent of the oil damage on dense vegetation may not be obvious until 6-12 months after the spill incident (Bartha, 1976). The sparse vegetation and the mangrove vegetation seemed to show an earlier sign of degradation within 180 days and 90 days (Figure 6.8 c and c, respectively) and some sign of recovery after the first 90 days (for mangrove vegetation). This result suggests that different vegetation types respond differently to the oil spill volumes and the time gap between the spill and NDVI observations. On the other hand, mangrove vegetation shows earlier signs of degradation due to oil spills than dense vegetation and sparse vegetation within the first 90 days. Mangrove stress usually occurs within the first two weeks of an oil spill event, and these signs can be seen in several ways, such as chlorosis and defoliation to tree death (Omodanisi & Salami, 2014). Mangrove is very sensitive to oil, partly because oil films affect the breathing roots, which inhibit oxygen supply to the underground root system (IOM, 2010). Additionally, visible oil stress symptoms of vegetation depend upon the plant species type and degree of stress (Mohamadi et al., 2016). Each vegetation type has different biophysical properties, and the level of resistance varies.

6.4.2 Temporal monitoring of vegetation conditions affected by oil spills

The results show how oil spills impact vegetation health based on the change in NDVI values before and several years after spills and compare them with sites that have not been exposed to oil spills. The results provide a better understanding of the impact of the oil spill on the health condition of vegetation types over a period in the Niger Delta. Both graphical and statistical analyses using paired t-tests were used to determine oil spill-induced differences in the change in NDVI values of spill sites (SS) and control sites (CS) acquired on the same day. This was done because many factors could affect the level of change in NDVI, in addition to oil spills in both SS and CS. Some of these factors are the spill area size, impacted area environment, soil type, and size of the area burned by fire, among others (Mohamadi et al., 2016). From Tables 6.7–6.9, some SS have initial NDVI values higher than some CS. It means vegetation exposed to oil spills could be healthier (initially) than vegetation not exposed to a spill if all other conditions are consistent. Additionally, using only the absolute NDVI values could provide misleading results.

From the correlation between the change in NDVI and the number of years after a spill at SS and CS in Figure 6.9, each type of vegetation NDVI value changes over a period of some years for both the SS and CS. Both the SS and CS had negative changes in NDVI values, with sparse vegetation and mangrove vegetation having more negative changes. It would have been expected that the CS should not have negative changes. Nevertheless, other factors, such as weather conditions (such as temperature and rainfall), may not be the reason for CS having negative values since all the NDVI images were downloaded for the dry season, only between December and February, with almost the same weather conditions. The likely reason for this could be that some SS are located on more fertile soil than the CS.

Nevertheless, the changes are greater for SS, especially for sparse and mangrove vegetation. While dense vegetation SS had some NDVI higher than the NDVI before the spill within the first 730 days (2 years) after the spill, sparse vegetation had just a few, with mangrove vegetation having none above the NDVI before the spill within the first two years (Figure 6.9a, b and c). This makes the mangrove vegetation the most degraded vegetation in the Niger Delta impacted by oil spills, while the dense vegetation is more resistant to oil spills.

For the effect of oil spill volumes on the health of vegetation, the dense vegetation was less affected by a volume of spill between 225 and approximately 500 bbl but responded more to the oil spill at volumes of approximately 1000 bbl and 1500 bbl (Figure 6.10), similar to the results in Figure 6.4a and Figure 6.7a. The health condition of sparse vegetation is more affected at approximately 225 bbl to 300 bbl, 800 bbl and 1500 bbl. On the other hand, mangrove vegetation shows a greater negative change in the NDVI value at approximately 1500 bbl. The health of all vegetation types appears most affected by an oil spill at a volume of approximately 1500 bbl. The paired t-test in Table 6.10 shows that the health condition of vegetation at SS is affected by the impact of oil spills. The sparse and mangrove vegetation are the most affected, while the dense vegetation is the least affected. Mangroves are highly vulnerable to oil spills (Duke, 2016)

6.4.3 Temporal analysis of changes in NDVI values for each spill site with corresponding control sites

A temporal analysis was carried out on selected SS with varying volumes of oil spills and paired CS to determine the effect of oil spills on different vegetation types in the Niger Delta over a period of time to evaluate the level of recovery of the vegetation. As mentioned in section 6.4.2, the changes in NDVI values for SS and CS were used instead of the actual values. For example, the NDVI values for SSD6 in Table 6.7 before and immediately after the spill (0.6785 and 0.3199) are larger than the NDVI values for CS within the same period (0.6171 and 0.3047). This indicates that vegetation exposed to oil, depending on the volume of oil spilt, may still be healthier even after exposure to the spill, but it could be stressed sometime later. However, the changes in NDVI values for SS and CS for dense, sparse, and mangrove vegetation show that the negative changes over time are higher at SS than at CS. The negative change in NDVI values for both SS and CS shows signs of degradation in vegetation's health condition (a sign of stress) at a particular site. For most sites, the SS and CS had the same pattern of change in NDVI values, resulting from having the same environmental conditions, such as temperature and soil type, for each SS and its corresponding CS. Not all stressed vegetation may be related to oil spills (Adamu et al., 2018).Conversely, not all oil spills affect vegetation since other factors, such as annual rainfall (during the rainy season) and variability, could contribute to changes in NDVI values. However, it can be observed that the changes in NDVI values are greater at SS than at CS for all the dense, sparse and mangrove vegetation, which could be due to the impact of an oil spill. Although some spill sites' vegetation was able to recover after the oil spill, some could not recover for both SS and CS. However, CS tended to have smaller changes in NDVI values, which means that the oil spill still has some effect on the vegetation.

The statistical analysis in Table 6.11, which compares the difference between changes in NDVI values for each SS and CS at different oil spill volumes, shows that the impact of oil spills on the health condition of dense vegetation is less significant, with only one site having significant difference in NDVI values (SSD1 at spill volume 280 bbl). The most impacted vegetation is the sparse vegetation, with five out of eight locations having very significant and significant differences

with their CS, which indicated impacts on their health conditions. The nature of sparse vegetation, mostly grasses and smaller than the dense and mangrove vegetation, makes them more vulnerable to oil spills and other environmental factors. Similarly, the mangrove vegetation is the next affected vegetation, with three out of 6 locations having a very significant and significant impact on their health conditions. The results also show that the significance level difference in SS and CS is not directly proportional to the volumes of spills. For instance, the only significant impact of oil spill volume on dense vegetation is 280 bbl, the lowest spill volume. A similar scenario is also observed for the mangrove vegetation at a spill volume of 1554 bbl and a spill volume of 2500 bbl, with the CS NDVI values been significantly different with the SS. Some environmental condition variability in SS with its corresponding CS may be responsible for such results.

The oil spill has affected the recovery of some vegetation in the Niger Delta. Among all the vegetation, the dense vegetation recovers from the impact of oil spills faster than the sparse and mangrove vegetation. Apart from at volume 280 bbl, which shows that the change in NDVI from SS and CS are parallel without crossover at any point, every other point intersects at some point, showing a sign of recovery. For sparse and mangrove vegetation, the recovery is slower, with some locations never recovering within the study period, clearly showing that the sparse vegetation is the most impacted, with many graphs having a parallel line between the change in NDVI values for SS and CS. However, the mangrove vegetation is mostly affected within the first year of the spill, with none of the changes in NDVI values for CS larger than the changes in NDVI for SS (Figure 6.13), unlike dense vegetation and sparse vegetation, which have some changes in NDVI for CS larger than the NDVI for SS.

Similarly, the high-resolution satellite image of some selected spill sites before and after oil spills (Figure 6.14-6.16) with a statistically significant difference from their CS for the mangrove (SSM5) and the sparse vegetation (SSS8) show a visual difference between vegetation cover of SS and CS the vegetation dead around the mangrove SS. However, the sparse vegetation has more numbers of SS that are statistically significant from their CS. The nature of the dense vegetation

makes them less vulnerable to the impact of oil spills. Hence the small changes between the images before and after the oil spills.

6.5 Conclusion

The monitoring of oil spill impacts on vegetation using spectral indices (NDVIs) at the plot scale with statistical analysis was performed using linear regression and paired t-test analysis for different vegetation types. For the impact of volume on spectral indices of vegetation after a spill, the vegetation responded differently to various volumes of an oil spill, with sparse vegetation being the most affected among the three types of vegetation and dense vegetation responding more at a higher volume than the sparse vegetation the mangrove vegetation. The effect of the time gap after a spill also affects the spectral reflectance of each vegetation type, with the dense vegetation taking a longer time to show a sign of stress, unlike the sparse and mangrove vegetation, which show an earlier sign of stress.

The temporal analysis of changes in NDVI values for each spill site with corresponding control sites shows that sparse vegetation is also the most affected by an oil spill. The recovery rate from an oil spill is higher in dense vegetation and mangrove vegetation, with sparse vegetation being the slowest in recovery. Additionally, another factor, such as gas flaring, which increases the temperature and affects the soil quality around the flare site, seasonal changes in rainfall and weather conditions could affect the spectral response of the vegetation. This is because some of the sites never recovered during the studies for both SS and control sites. However, the SS has lower NDVI values in general, which indicates that the oil spill effect on the health of vegetation has a long-term impact depending on the types of vegetation, the volumes of the spill, and some environmental factors, among others. This result provides insight into how different types of vegetation respond to the effect of an oil spill, which could help in designing an oil spill clean-up program to reduce the impact on sparse vegetation in the Niger Delta by prioritising oil spill clean-up based on the vegetation type that is most affected by the impact of the oil spill. The next chapter will focus on detecting general land cover changes due to oil extraction activities at the landscape scale. It is important to understand other drivers that affect the vegetation apart from the oil spill, and also, the oil spill affect the other land cover, especially the vegetation spatially.

Chapter 7 Land cover change detection

Part of the work in this chapter has been presented and published in the book of proceedings volume 1 no 1 ISBN: 978- 978 – 55067 – 3 – 0 as:

Kuta, A. A., Grebby. S and Boyd, D. (2019). Land Cover Mapping using Combined Soft Classification and Geographic Object-Based Image Analysis (SGOBIA) in the Niger Delta Region of Nigeria, book of proceeding National Association of Surveying and geoinformatics Lecturers 1ST AGM/Conference Maiden Edition, Minna 2019

7.1 Introduction

Land use-land cover changes (LULCC) are directly or indirectly caused by factors playing out on the landscape (Zitta, Musa, & Muhammed, 2022). For many decades, the Niger Delta region has undergone severe environmental degradation and land cover change due to oil extraction activities (e.g., oil spills). While chapters 5 and 6 deal with the degradation of vegetation, in some cases, the effects of oil extraction activities on the vegetation are so severe that it dies off or is purposefully removed and completely changes the land cover. Hence the need to understand where changes have happened at a landscape scale. One way to detect land cover changes is through land cover maps derived from classified satellite images.

Classification is an important method used in remote sensing to relate pixel values to land cover classes present on the surface (Zhang & Roy, 2017). It is usually performed to retrieve land use/cover information using a range of statistical pattern recognition or clustering techniques (Sharma et al., 2016). There are two main classification outputs: soft (purely pixel-based) and hard classification (pixel- and object-based), with no single best method for all mapping problems (Lee et al., 2011), as each classifier has its advantages and disadvantages depending on the dataset used and the land cover types to be mapped. For example, some land cover types do not have a well-defined boundary or contain a mixture of land cover types within a single pixel (i.e., mixed pixels). Combined pixel-based, pixel grouping and object segmentation may offer greater potential for improved image classification (Al Fugara et al., 2009). However, this field has not been well explored (Costa et al., 2017; Lizarazo & Elsner, 2009), despite the inherent advantages it offers for overcoming several limitations of conventional approaches to land cover change mapping.

To use remote sensing to investigate land cover change, one must consider that land cover in the Niger Delta is complex and comprises mangroves, freshwater swamps, and a mixture of water with oil, giving rise to mixed pixels. Previous attempts at land cover mapping in the Niger Delta region have employed pixel-based hard classification techniques, which are not considered adequate for capturing the nature and complexity of land cover in the study area. Many authors have reported that object-based image classification methods are often more accurate than traditional pixel-based classification (Dornik et al., 2017; Frohn et al., 2011). But the parameterisation of crisp segmentation models commonly requires significant user interaction, making it difficult to employ such methods for the automated processing of large datasets in generating image objects with well-defined boundaries (Lizarazo & Elsner, 2009). Object-based classification also suffers from over- and under-segmentation of the land cover features and its inability to map vagueness in land cover due to the fuzziness of the classes to fill the research gap mentioned in section 1.3, the objective of this chapter was to test different classifiers and choose the best-performing classifier to map the land cover changes at the landscape scale, using Landsat data and integrating oil extraction activities data to determine their effect on the observed land cover changes. The result will provide a better understanding of landscape-scale changes to land cover, particularly the vegetation, that have occurred within the study area. Ultimately, the outcome could be used to map land cover changes in the whole Niger Delta region to determine the oil industry's impact on land cover.

Elsewhere, several studies have applied object-based soft classification to remote sensing datasets (Feizizadeh et al., 2017; Gudex-Cross et al., 2017; Wang et al., 2004). For example, using Landsat ETM 7+, Al Fugara et al. (2009) discovered that the classification results obtained using an object-oriented cum fuzzy logic approach to map land cover types in the Klang Valley, Malaysia, were superior to the pixel-based supervised classification, producing a higher overall accuracy of 89.78%, while the pixel-based classification had an overall accuracy of 70.24%. Other studies that have utilised Landsat datasets in conjunction with combined soft and object-based classification include Aksoy & Ercanoglu (2012), Asfour et al. (1995) and Yoon et al. (2003).

7.2 Methodology

Figure 7.1 outlines the methodological approach taken in this chapter.

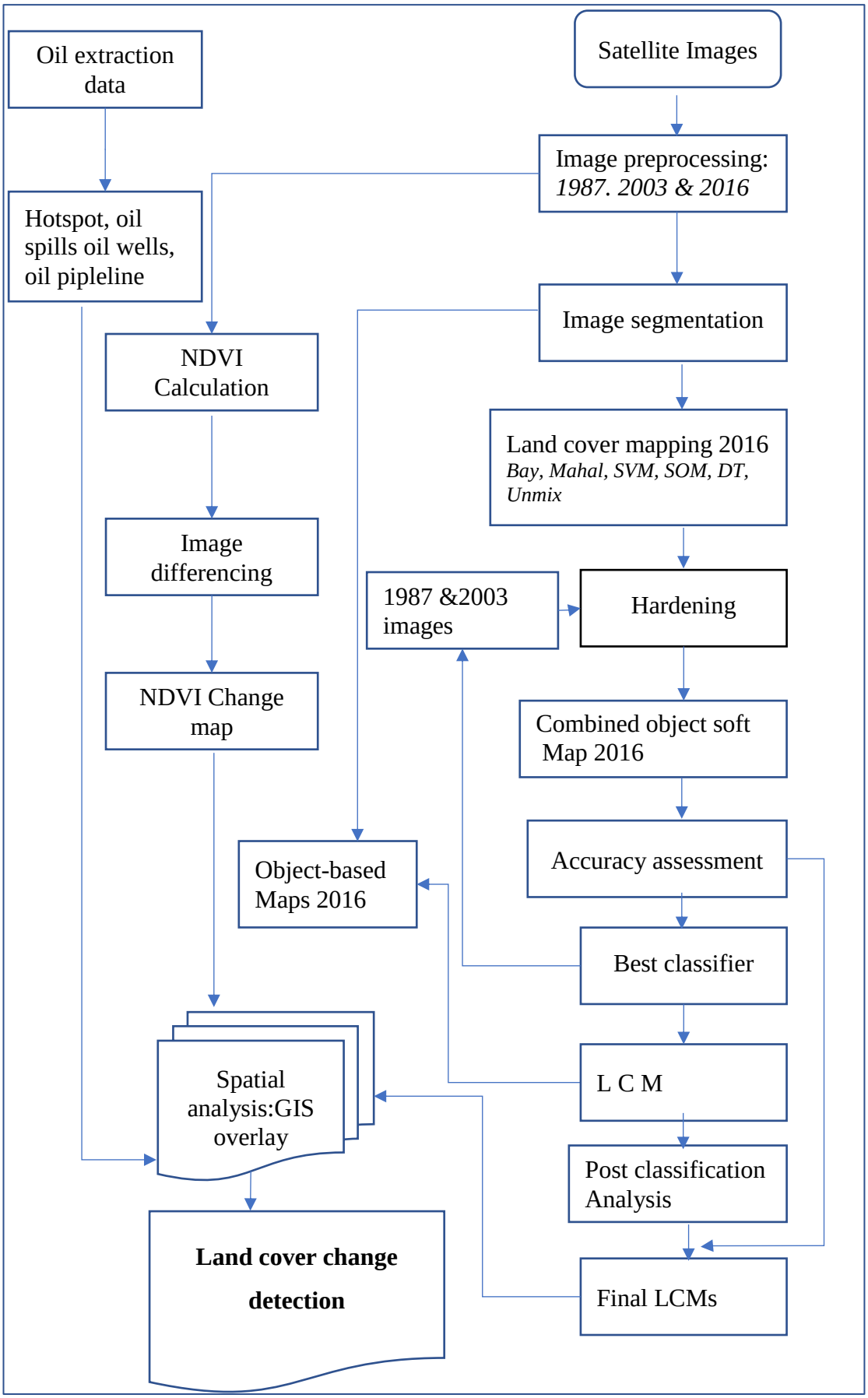

Figure 7.1:Methodology Flow Chart

7.2.1 Data

The oil extraction activities and satellite data, and the classifiers used in this chapter have been described in section 3.3.3 of the methodology chapter.

7.2.2 Methods

7.2.3 Land cover mapping

7.2.3.1 Image segmentation and training site development

The first step in land cover mapping was image segmentation. It involves dividing the satellite image into spatially partitioned contiguous groups of pixels (i.e., objects), used as the basic spatial unit of analysis (Costa et al., 2018). During land cover classification scheme development, seven land cover classes were identified for the study area: water, built-up, dense vegetation, sparse vegetation, mangrove, sand dune and bare soil (Table 7.1). The images were segmented using a scale of 30 to ensure that the segments were not too small or large after trying other scales. The training sites for the seven land cover classes were developed from the segmented images instead of screen digitising. One of the advantages of using objects for training samples is that it is more efficient than manually digitising the training sites. The classification was implemented using Terrset Geospatial Monitoring and Modelling System, 2020 software.

7.2.3.2 Land cover classification

Soft classification of the satellite images was performed using six soft classifiers available in Terrset 2020 on the 2016 satellite images using the developed training file of the segmented image as an input. The 2016 images were used because it is easier to assess the higher-resolution images from the Google Earth archive for the same period for ground truth for accuracy assessment instead of fieldwork. Soft classification, which reveals more land cover information and potentially a more accurate result, especially for coarse spatial resolution data (Choodarathnakara et al., 2012; Sharma, Goyal et al., 2016), was used to classify the satellite images. The output is not a single classified image, but a number of images are obtained as the classified output (Tiwari et al., 1999) of land cover information, which is very important for land resource management (Sharma et al., 2016). Finally, the hardener function in Terrset was used to produce a hard map for each classifier. The hardener uses the membership output images from the soft classifier to produce a hard decision image by selecting the class image that contains the maximum membership grade and assigning that class to the

image element (Eastman, 2016). The same hardened map from the two best classifiers was used to produce the object-based land cover map. The overall best classifier based on classification accuracy assessment and visual analysis was used to map the land cover for 1987 and 2002.

Many land cover classes were merged to minimise the effect of spectral similarities and to make the classification implementation more manageable. All water bodies were classified as water to avoid so many water classes. Every building: urban, rural, etc., was classified as built-up since the research interests are not on specific buildings. The vegetation class was based on the major vegetation types in the Niger Delta, which corresponded to the vegetation types in chapter 6. The vegetation in the Niger Delta comprises mangroves, which cover the coastal region of the Niger Delta, along with brackish lagoon and river systems, freshwater swamp forest, rainforest and derived savannah (Ayanlade & Howard, 2017). Agricultural and grassland were merged as sparse vegetation. Separating these classes poses difficulties, as the spectral separability between them is low (Nababa et al., 2020), and grassland is used for agricultural purposes. Sand deposits were given a class to minimise their influence on built-up, i.e. classified as built-up, which could greatly affect built-up accuracy. The bare soil was given a class since most of the consequence of oil spills on vegetation is anticipated to be converted to bare soil, making it an important land cover class.

Table 7.1: Land cover classes

Class	Group
Water (W)	River, pond, stream
Built-up (BU)	Urban, Rural etc
Dense Vegetation (DV)	Trees in general, oil palm, forest
Sparse vegetation (SV)	Shrubs, agriculture, grasses
Mangrove (M)	Tall and short and tall mangrove of all species.
Sand dune (SD	Beach, pure sand bars deposit
Bare soil (BS)	Mud, barren land, exposed soil

7.2.3.3 Land cover accuracy assessment

Accuracy assessment is a vital part of a program that maps land cover from remotely sensed imagery (Foody & Boyd, 2013). The value of the resulting map depends on the accuracy of the classification (Foody, 2002; Hashemian et al., 2004; Mahmon and Ya'acob, 2014). The stratified random sampling strategy was adopted among various

sampling methods to generate ground truth data for accuracy assessment, and at least 20 validation points per land cover class were selected. The minimum sample size should be 20 points per strata (Congalton & Green, 2008). Stratified random sampling using map classification to define strata is a simple but generally applicable design that typically satisfies most accuracy and reduces standard errors of class-specific accuracy estimates (Olofsson et al., 2014). It also ensures that even the least land cover class had some sample points. 400 ground truth sample locations were validated using high-resolution google earth images to determine the best-performing classifier. The following were reported: overall accuracy (OA), which measures how accurate the classified classes are; producer's accuracy (PA), which is the probability of how accurate each class was classified; and user's accuracy (UA), which is the probability that a certain class prediction belongs to that class. A test of statistical significance between the classification accuracy of the two best performing classifiers was computed using the McNemar test. For cases where the validation data are related, the McNemar test is more appropriate for testing the significance of any differences in classification accuracies. The McNemar test is based upon a Chi-squared ($\chi 2$) distribution, which involves a cross-tabulation of the number of validation pixels correctly and incorrectly classified through two algorithms (Grebby et al., 2011). The classifier that satisfied the visual accuracy of the 2016 map was used to classify the 1987 and 2003 satellite images. The 2016 classified map was chosen because it has the least cloud cover and has available reference data from Google Earth for ground truthing for classification accuracy assessment.

7.2.4 Post-classification map clean-up.

Post-processing is often carried out to reduce errors in the classified map (Townshend et al., 2012). Sometimes the only solution to achieve a highly accurate classification is to engage in manual clean-up (Eastman 2020). The land cover types in the Niger Delta, such as the built-up and bare soil, dense vegetation and mature mangrove, have similar spectral reflectance, which was corrected from the classified land cover map by reallocating the misclassified pixel to the right class by directly editing the pixel values beneath any region of interest (ROI) vector polygons. The post-classification ensured that the land cover maps were as accurate as possible. The second post-classification analysis was smoothing the pixels to reduce the "salt and pepper" effect due to some misclassification by reallocating a class to the predominant neighbours. The post-

classification clean-up was performed after the first accuracy assessment in order to compare the accuracies of the pre-cleanup with the post-clean-up map.

7.2.5 Land cover change detection and mapping

The following changes were detected: Magnitude of Change (MC), Nature of Change (NC), and Direction of Change (DC). The MC quantifies the amount of change that has occurred, or the gain and loss; NC compares each pixel of two classified images with a particular class of interests (inter-classes); DC takes the maximum of all the NCs based on the number of comparisons made, given that there were several predefined numbers of classes for this research.

The change analysis in the vegetation was performed using image differencing applied to the normalised vegetation index (NDVI) images of 1987 and 2016 using a raster calculator in ArcGIS. Many authors have used the NDVI to monitor vegetation quality in the Niger Delta, such as Adamu (2016); Fabiyi (2011). Before detecting the changes in NDVI (CNDVI), the NDVI values of ≥0.15 were extracted to ensure that non-vegetation features were removed, such as water and built-up area.

CNDVI, i.e., Gains and losses = $NDVI^{2}$–$NDVI^{1}$. Eq 7.1.

where $NDVI^{1}$ = first date NDVI (1987) and $NDVI^{2}$= second date NDVI (2016)

However, these returned results included pixels that have converted either from vegetation to other land cover or from other land covers to vegetation with values of 0. To obtain changes in vegetation for persistent vegetation in both periods, 1987 and 2016, first, the persistent vegetation (PV) was produced for the two dates using Eq2

PV =NDVI 2016*NDVI 1987 Eq. 7. 2

The PV produces a map of places that have retained vegetation in 1987 and 2016. To remove places that have been converted to other land covers from the CNDVI, the PV was reclassified to 1 and 0, with 1 representing persistent vegetation and 0 representing other land cover types.

Gain and losses in NDVI=PV*CNDVI Eq. 7.3

7.2.6 Spatial analysis of land cover changes.

Spatial analysis was conducted to determine how oil extraction activities affected the vegetation: dense, sparse, mangrove, and the entire vegetation using the NDVI map.

The analysis includes overlays of oil hotspots, pipelines, oil wells and oil spill points on the land cover/change maps and the NDVI map. The volume of oil spilt into each land cover was extracted using the extract function in QGIS, and the number and volumes of oil spilt into each land cover were quantified.

7.3 Results

7.3.1 Land cover accuracy assessment

Table 7.2 shows the overall and individual class accuracy for the six combined soft-object-based classifiers, object-based classifiers and the post-processed Bay map for 2016 and 1987. For the 1987 image, only the best two performing classifiers were used instead of the six since the 2 classifiers produced an acceptable accuracy for the land cover change detection. The 2002 map accuracy was not assessed due to cloud cover, which masked most validation sample points. As stated earlier, the 2016 images were used to determine the best two performing classifiers due to the available reference data from Google Earth. From the results in Table 7.2, different classifiers produced different levels of accuracy: overall (OA), producer (PA) and user accuracy (UA) for both the combined soft-object-based classifiers and object-based classifiers. Before the post-classification analysis on the Bay and Mahal map, the various OAs are Mahal=82.17%, Bay =81.56%, SVM=77.78%, UNMIX =74.73%, DT=74.34 and SOM= 55.83% and the 1987 bay 79.41%. The results of the object-based map from the two best performing classifiers show that BayObj has higher accuracy (77.87%) than MahalObj (76.41%).

Similarly, the results of 1987 in Table 7.2 show the OAs of Bay (79.41%) and BayPP (80.65%). The results show that the Mahal is the best performing classifier among the six, with Bay coming second and SOM the least performing classifier. BayObj and MahalObj also performed below their Bay and Mahal counterparts. However, for an individual class, the results of the UA and PA show that each classifier performed better in classifying some land cover types than even Mahal and Bay. For example, the water mapped better by Bay (UA= 90.74%) and SVM (UA=78.46%), Built-up by DT (UA=45.55%, PA=62.23%), Dense vegetation by SVM (PA=87.95%) and Unmix (UA=90.54%), Sparse vegetation by Mahal (PA=91.86%, UA=77.46), Mangrove by Bay (UA=91.18) and Mahal (PA=89.50%), Sand dune by Bay (PA=25.51), and both

DT/SVM (UA=100) and BS by DT (UA=70,97%) and Mahal (PA=49.30%). MahalObj performed below the six soft object classifiers except for the BayObj map sand dune, which performed better than all with PA=26.77%. Table 7.3 shows the per class confusion matrix from different classifiers for the 2016 map, including the object-based Table 7. 3a-i and 1987 map Table 7.3j and k.

The results of the McNemar test in Table 7.4 show that the accuracy between Mahal and Bay, the two most accurate classifiers, is not statistically significant, with a *p*-value = 0.82. From Table 7.4, 11 points were correctly classified in the Bay map but incorrectly classified in the Mahal map; 9 points were correctly classified in the Mahal map but incorrectly classified in the Bay map; 302 points were correctly classified in both the Bay map and the Mahal map, and 78 points were incorrectly classified in both the Bay map and the Mahal map. The second part of the accuracy assessment, which was visual, shows that the Bay class is less noisy compared to Mahal, and Mahal suffers more from "salt and pepper", especially for mangroves. Since the Bay and Mahal difference is not statistically significant, the Bay class was chosen for further post-classification clean up and land cover change mapping. From the results in table 7.2, it can be observed that the OA of the BayPP map of 2016 and Bay PP1987 increased from 81.56% to 83.06% and 79.41% to 80.65%, respectively.

Table 7.2: Land cover accuracy assessment of hardened soft maps from different classifiers.

Year	Classifiers	OA	Accuracies (%)	Water	Built-up	DV	SV	MG	SandDune	BS
			PA	72.68	48.24	85.52	87.40	88.70	**25.51**	45.67
	Bay	81.56	UA	**90.74**	50.00	84.00	76.06	**91.18**	96.00	62.79
			PA	67.08	**62.23**	87.89	68.23	75.80	22.39	32.23
	DT	74.34	UA	71.64	**54.55**	78.21	65.28	82.26	**100.00**	**70.97**
			PA	76.90	58.17	80.39	**91.86**	**89.50**	20.76	**49.30**
2016	Mahal	**82.17**	UA	85.25	53.97	87.88	**77.46**	89.71	100.00	56.25
			PA	74.72	42.44	86.17	27.15	64.55	13.08	5.07
	SOM	**55.83**	UA	68.06	42.67	56.76	47.37	60.49	94.74	25.00
			PA	**78.46**	46.20	**87.95**	69.56	89.00	23.02	40.24
	SVM	77.78	UA	85.25	44.62	79.27	72.22	86.84	**100.00**	65.00
			PA	78.93	22.06	**90.54**	71.03	77.15	14.07	35.22
	Unmix	74.73	UA	87.93	40.00	72.83	70.77	88.89	86.96	40.91
			PA	60.10	43.49	85.46	91.09	86.18	26.77	26.13
	Bay Obj	77.86	UA	86.79	58.93	80.26	72.50	83.56	96.00	61.11
			PA	61.34	45.33	78.02	89.79	88.44	21.78	34.34
	Mah OBJ	76.4148	UA	87.04	57.89	81.54	67.06	83.56	95.83	59.52
			PA	80.02	50.01	84.75	87.13	90.46	43.94	58.03
	BayPP	83.06	UA	91.07	62.75	84.93	76.06	92.65	92.86	66.04
			PA	30.96	11.57	88.18	85.06	76.73	99.00	30.06
	Bay	79.41	UA	91.84	35.71	80.95	80.88	89.66	76.74	67.44
			PA	63.06	75.85	90.50	81.71	84.22	18.62	45.29
1987	Bay PP	80.65	UA	89.80	51.28	82.28	76.47	83.82	77.08	67.35

Table 7.3: Confusion matrix from different classifiers for 2016/2017 (Table 7.3a-i) and 1987 (Table 7.3J and k) for different land cover types in the Niger Delta.

(a)				**Bay**				
Classes	**WT**	**BU**	**DV**	**SV**	**MG**	**SD**	**BS**	**Total**
WT	49	0	0	0	4	0	1	54
BU	3	32	1	7	0	6	15	64
DV	0	2	63	5	4	0	1	75
SV	0	3	12	54	0	0	2	71
MG	6	0	0	0	62	0	0	68
SD	0	1	0	0	0	24	0	25
BS	0	7	1	3	5	0	27	43
Total	58	45	77	69	75	30	46	400
(b)				**DT**				
WT	48	0	0	1	13	1	4	67
BU	3	36	3	6	0	4	14	66
DV	3	1	61	8	5	0	0	78
SV	2	3	9	47	6	0	5	72
MG	2	1	4	3	51	0	1	62
SD	0	0	0	0	0	24	0	24
BS	0	4	0	4	0	1	22	31
Total	58	45	77	69	75	30	46	400
(c)				**Mahal**				
WT	52	0	1	1	6	0	1	61
BU	1	34	1	6	0	5	16	63
DV	0	2	58	2	3	0	1	66
SV	0	1	14	55	0	0	1	71
MG	5	0	2	0	61	0	0	68
SD	0	0	0	0	0	23	0	23
BS	0	8	1	5	5	2	27	48
Total	58	45	77	69	75	30	46	400

Table 7.3 Confusion matrix from different classifiers cont.

(d)	SOM							
Classes	**WT**	**BU**	**DV**	**SV**	**MG**	**SD**	**BS**	**Total**
WT	49	4	0	4	8	1	6	72
BU	2	32	3	5	3	11	19	75
DV	1	3	63	36	6	0	2	111
SV	0	1	11	18	7	0	1	38
MG	5	4	0	6	49	0	17	81
SD	1	0	0	0	0	18	0	19
BS	0	1	0	0	2	0	1	4
Total	58	45	77	69	75	30	46	400
(e)	**SVM**							
WT	52	2	0	1	4	0	2	61
BU	0	29	1	15	0	8	12	65
DV	1	1	65	12	3	0	0	82
SV	0	2	7	39	2	0	4	54
MG	4	1	3	0	66	0	2	76
SD	0	0	0	0	0	22	0	22
BS	1	10	1	2	0	0	26	40
Total	58	45	77	69	75	30	46	400
(f)	**UNMIX**							
WT	51	0	0	0	6	0	1	58
BU	3	22	0	4	0	8	18	55
DV	1	2	67	11	10	0	1	92
SV	0	6	7	46	2	0	4	65
MG	3	0	2	1	56	0	1	63
SD	0	0	0	0	0	20	3	23
BS	0	15	1	7	1	2	18	44
Total	58	45	77	69	75	30	46	400

Table 7.3 Confusion matrix from different classifiers cont.

(g)				**BayOB**				
Classes	**WT**	**BU**	**DV**	**SV**	**MG**	**SD**	**BS**	**Total**
WT	46	0	0	0	5	0	2	53
BU	1	33	2	3	0	5	12	56
DV	2	3	61	3	4	0	3	76
SV	0	4	12	58	1	0	5	80
MG	9	1	1	0	61	0	1	73
SD	0	0	0	0	0	24	1	25
BS	0	4	1	5	4	0	22	36
Total	58	45	77	69	75	29	46	399
(h)				**MahalOB**				
WT	47	0	0	0	5	0	2	54
BU	1	33	2	4	0	6	11	57
DV	1	3	53	3	3	0	2	65
SV	2	3	19	57	0	0	4	85
MG	8	1	2	0	61	0	1	73
SD	0	0	0	0	0	23	1	24
BS	0	5	1	5	6	0	25	42
Total	59	45	77	69	75	29	46	400
(i)				**BayPP**				
Classes	**WT**	**BU**	**DV**	**SV**	**MG**	**SD**	**BS**	**Total**
WT	51	0	0	0	4	0	1	56
BU	2	32	0	7	0	3	7	51
DV	0	2	62	5	3	0	1	73
SV	0	3	12	54	0	0	2	71
MG	4	0	1	0	63	0	0	68
SD	0	2	0	0	0	26	0	28
BS	1	6	2	3	5	1	35	53
Total	58	45	77	69	75	30	46	400

Table 7.3 continued

1987

(j)				**Bay**				
Classes	**WT**	**BU**	**DV**	**SV**	**MG**	**SD**	**BS**	**Total**
WT	45	0	0	0	4	0	0	49
BU	3	20	0	2	5	13	13	56
DV	1	0	68	6	9	0	0	84
SV	2	0	6	55	0	0	5	68
MG	5	0	1	0	52	0	0	58
SD	5	3	1	0	0	33	1	43
BS	0	6	0	4	2	2	29	43
Total	61	29	76	67	72	48	48	401
(k)				**BayPP**				
WT	44	0	0	0	4	0	1	49
BU	1	20	1	3	1	5	8	39
DV	1	0	65	7	5	1	0	79
SV	2	0	8	52	0	0	6	68
MG	7	0	2	0	57	2	0	68
SD	6	5	0	0	0	37	0	48
BS	0	4	0	5	5	2	33	49
Total	61	29	76	67	72	47	48	400

Table 7.4: Extracted accuracy validation points for the McNemar test for statistically significant differences between Bay and Mahal. *p*-value =0.82

	Mahal		
Bay		+	-	Total
	+	302	11	313
	_	9	78	87
	Total	311	89	400

7.3.2 Land cover maps

Figure 7.2a-g shows the Bay 2016 soft classification maps, with each map representing a land cover class. The legend indicates the degree of the fuzzy membership function of each class; that is, black (0) indicates areas without fuzzy membership, while red (1) shows areas with full fuzzy membership rising from above 0 (Kuta 2012). Figure 7.3a-h shows the spatial extent of the land cover map from hardened soft object-based classifiers and the object-based map from hardened bay and mahal classifiers. Figure 7.3g-h. Figure 7.4a-c shows the subsets of the six classifiers mapped and two object-based maps showing some portions of the study area.

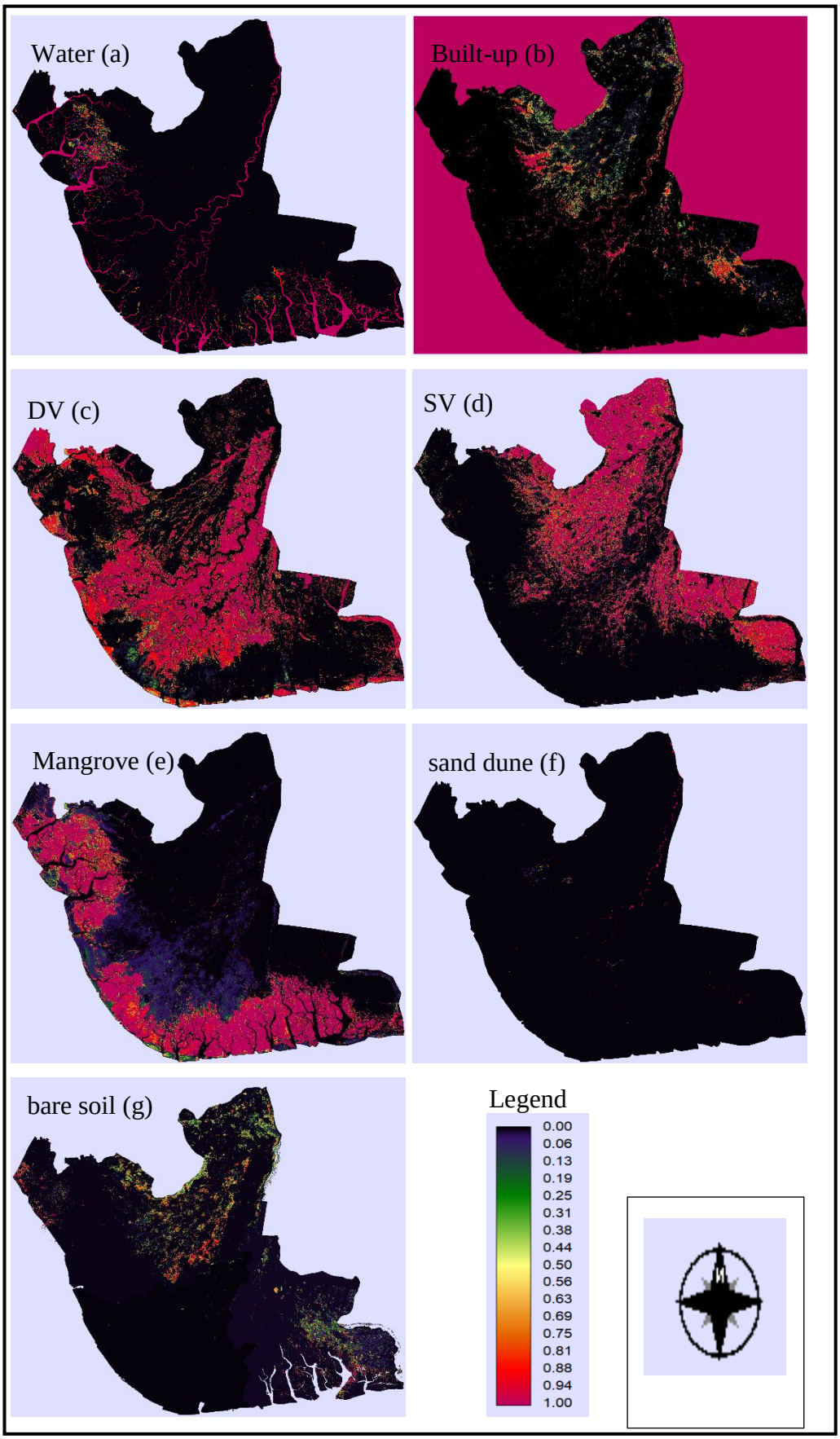

Figure 7.2:Bay soft land cover maps for 2016: (a) water, (b) built-up, (c) dense vegetation, (d) sparse vegetation, (e) mangrove, (f) sand dune and (g) bare soil.

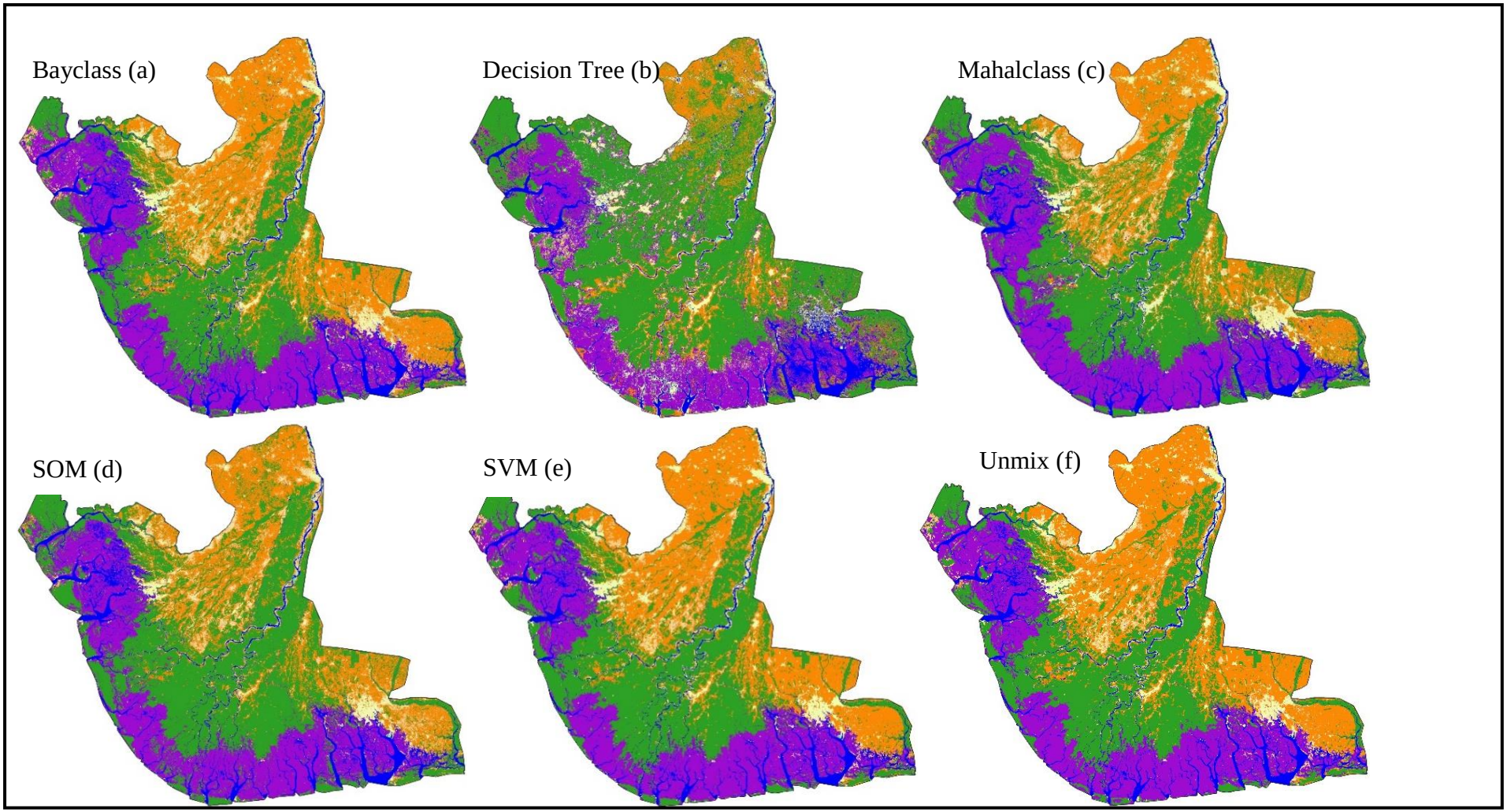

Figure 7.3: Hardened soft land cover maps cont.

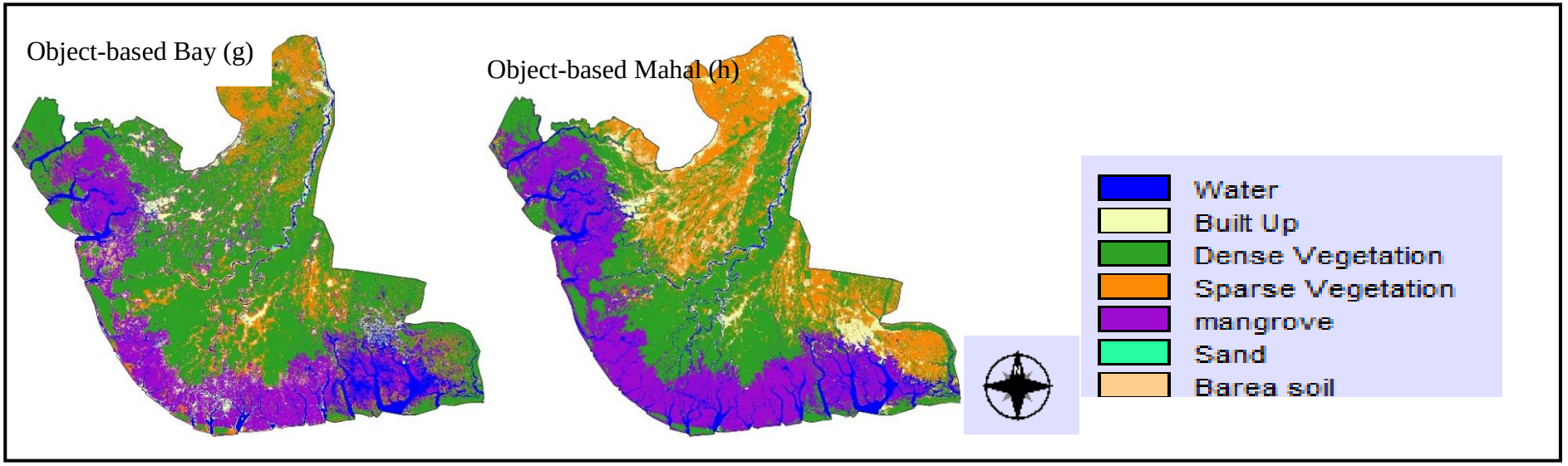

Figure 7.3:Hardened soft land cover maps (a) Bayclass, (b) Decision Tree, (c) Mahalclass, (d) SOM, (e) SVM and (f) Unmix, (g) Object-based Bay and (h) object-based Mahal.

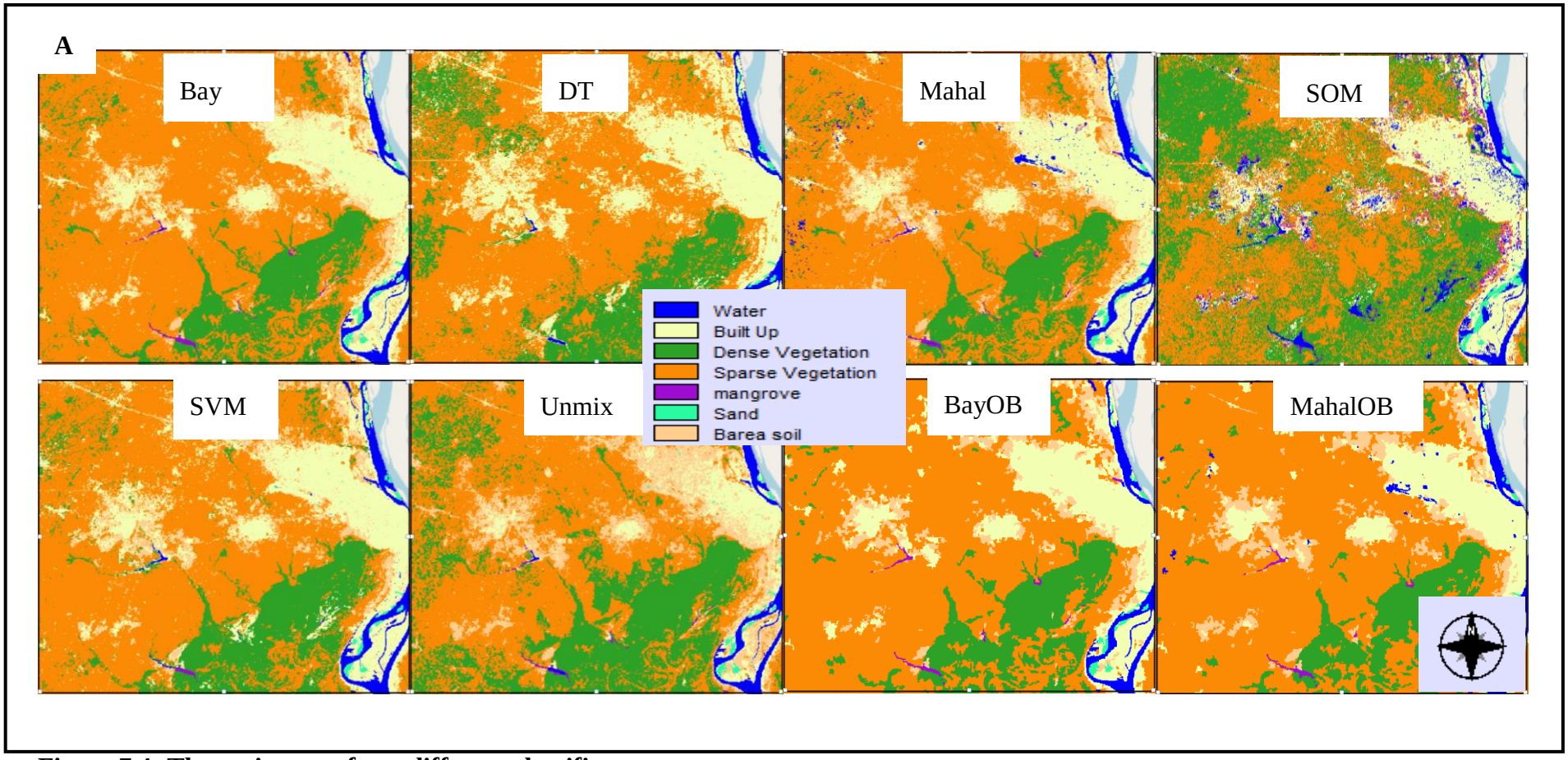

Figure 7.4: Thematic maps from different classifiers cont..

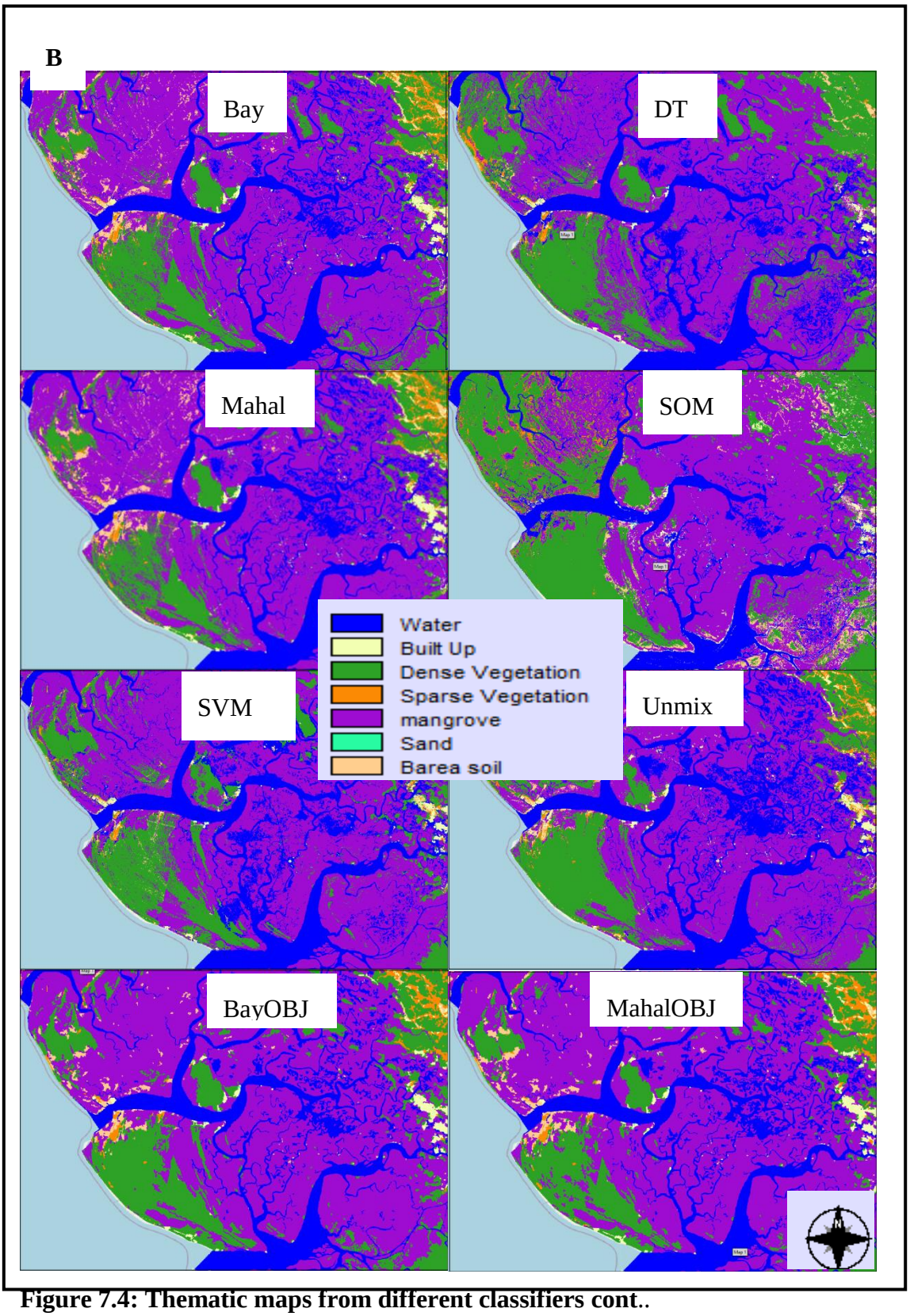

Figure 7.4: Thematic maps from different classifiers cont..

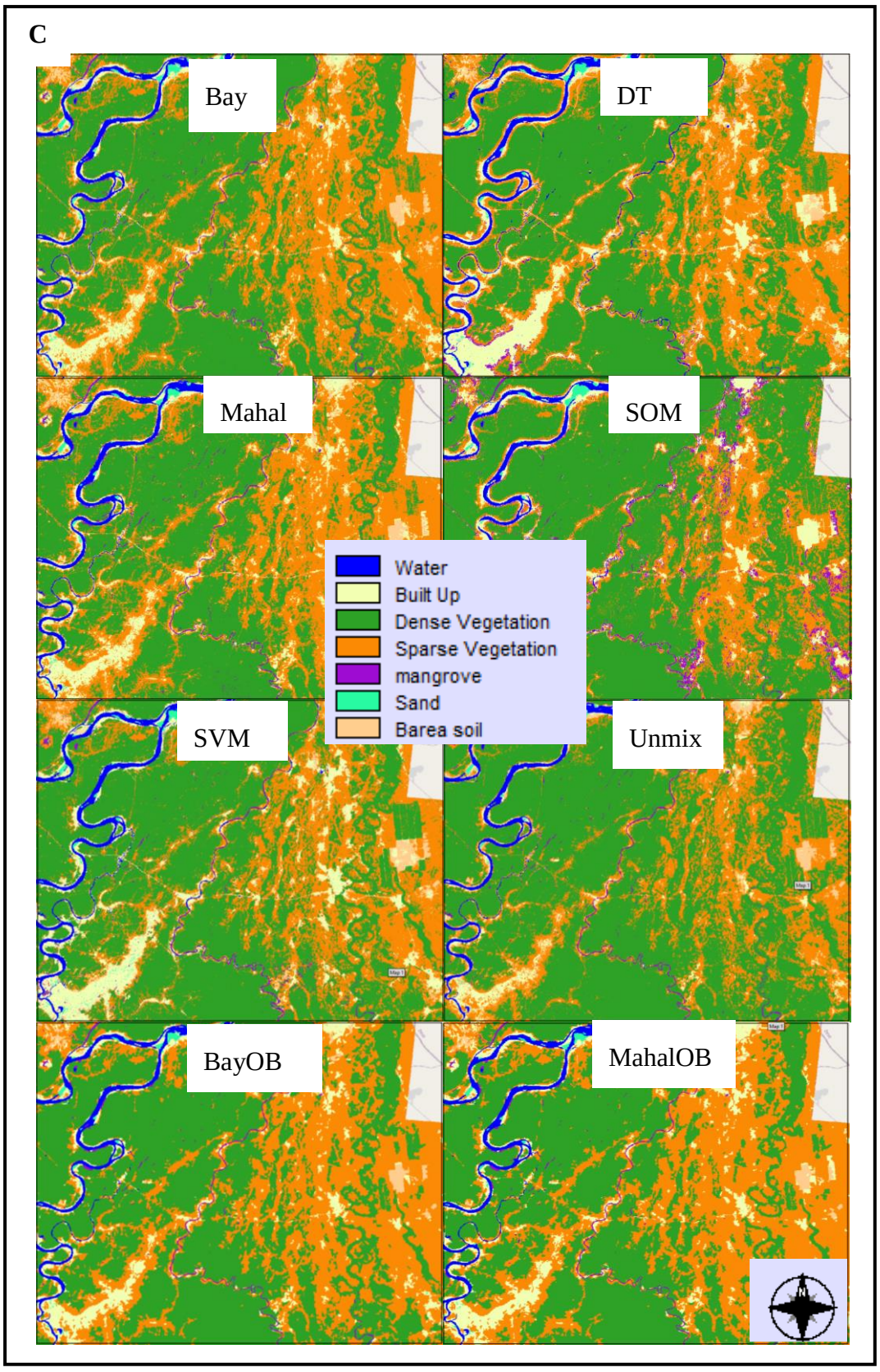

Figure 7.4:Thematic maps from different classifiers (A) shows BU, W, DV and SV in the northern Niger Delta around Asaba; (B) shows, primarily, M and DV in the eastern Niger Delta around Warri; and (C) shows water, DV, SV, etc., except for the mangroves in the central Niger Delta around Ahoada

7.3.3 Land cover extents.

Table 7.5 shows the land cover extents for various land cover types from the cleaned maps of 1987, 2002, and 2016. The proportion of land cover extents from the largest to the smallest in 1987, 2002 and 2016 are dense vegetation 15133.56 km^2 (41.03%), 13899.78 km^2 (37.68%) and 12470.3 km^2 (33.81%), followed by sparse vegetation 8972.74 km^2 (24.33%), 10036.24 km^2 (27.21%) and 10258.96 km^2 (27.81%), mangrove 8324.40 km^2 (22.57%), 8314.76 km^2 (22.54%) and 8592.85 km^2 (23.30%), with the least being sand dune. The results show continued net gains by built-up and sparse vegetation and net losses by dense vegetation and sand dunes from 1987-200 and 2002-2016. Mangrove and bare soil each had a net loss from 1987-2002 and net gains from 2002-2016, which were higher than the losses, while water had net gains from 1987-2002 and net losses from 2002-2016, which were lower than the net gains.

Figure 7.5 shows the graphical contributors of net changes experienced by each land cover class from the periods 1987-2002 in the first column, 2002-2016 in the second column and 1987-2016 in the third column. The rows are the net contribution to water in the first row, built up in the second row, dense vegetation in the third row, sparse vegetation in the fourth, mangrove in the fifth, sand dune in the sixth throw, and bare soil in the fifth, and seventh row. The results highlight that bare soil was the highest net contributor to built-up land between 1987 and 2002, while sparse vegetation became the highest net contributor in 2002-2016 and 1987-2016. It can be observed that the sparse vegetation and built-up are the highest negative net contributors to dense vegetation sand dunes, respectively. Others are shown in Figure 7.5. Figures 7.6a, b and c show the final (post-processed) land cover maps of 1987, 2002 and 2016, respectively, which were used to map the land cover changes in the Niger Delta. Some changes could be detected on the map, especially in built-up land and vegetation between 1987, 2002 and 2016. Figure 7.7 a-d show high-resolution satellite image a subset of some selected mixed land cover class which cause misclassifications in the land cover class. For example, urban built-up areas mixed with bare (Figure 7.7a), mangroves mixed with dense vegetation and bare soil (Figure 7.7b), rural built-up areas mixed with bare soil sparse vegetation and dense vegetation along a river (Figure 7.7c), built-up area mixed with sparse vegetation, dense vegetation and mangrove (Figure 7.7d), and mangrove mixed with bare soil and water (Figure 7.7e). These types

of land cover classes mixed within 30 by 30 metre pixels of Landsat make land cover mapping difficult in the Niger Delta using medium-resolution satellites like Landsat.

Figures 7.8a, b and c show the vegetation cover map derived from the NDVI for 1987, 2002, and 2016. The NDVI map of 2002 (7.8b) suffered from cloud cover, especially in the western and southern parts of the study area, which affected the quality of the NDVI map. The NDVI was reclassified to only the vegetation part by extracting values => 0.15, therefore removing no vegetation values. From the map in Figures 7.8 a b and c, the NDVI values decreased from 0.68 in 1987 to 0.58 in 2016, showing vegetation degradation signs. The loss of vegetation could be observed in the 2016 map around Warri-Sapele and the Port-Harcourt axis. The green areas have higher NDVI values.

Table 7.5: Areas of 1987 and 2016 land cover extents and net changes.

Land Covers	Area in Km^2			Area as %			NTC in Km^2			NTC in (%)		
	1987	2002	2016	1987	2002	2016	1987-2002	2002-2016	1987-2016	1987-2002	2002-2016	1987-2016
WT	2551.44	2666.27	2591.73	6.92	7.23	7.03	114.83	-74.54	40.29	4.50	-2.80	1.58
BU	644.23	810.68	1468.43	1.75	2.20	3.98	166.46	657.75	824.20	25.84	81.13	127.94
DV	15128.53	13899.78	12466.05	41.01	37.68	33.80	-1228.75	-1433.73	-2662.48	-8.12	-10.31	-17.60
SV	8969.12	10036.24	10254.49	24.32	27.21	27.80	1067.12	218.25	1285.37	11.90	2.17	14.33
M	8323.77	8314.76	8591.98	22.57	22.54	23.29	-9.01	277.22	268.21	-0.11	3.33	3.22
SD	160.74	124.13	96.14	0.44	0.34	0.26	-36.61	-27.98	-64.59	-22.78	-22.55	-40.19
BS	1095.40	1021.37	1404.41	2.97	2.77	3.81	-74.02	383.04	309.01	-6.76	37.50	28.21
Total	36873.23	36873.23	36873.23	100	100	100						

NTC=Net Changes in Km^2, WT=water, BU=built-up, DV=dense vegetation, SV=sparse vegetation, M= mangrove, SD=sand dunes and BS=bare soil.

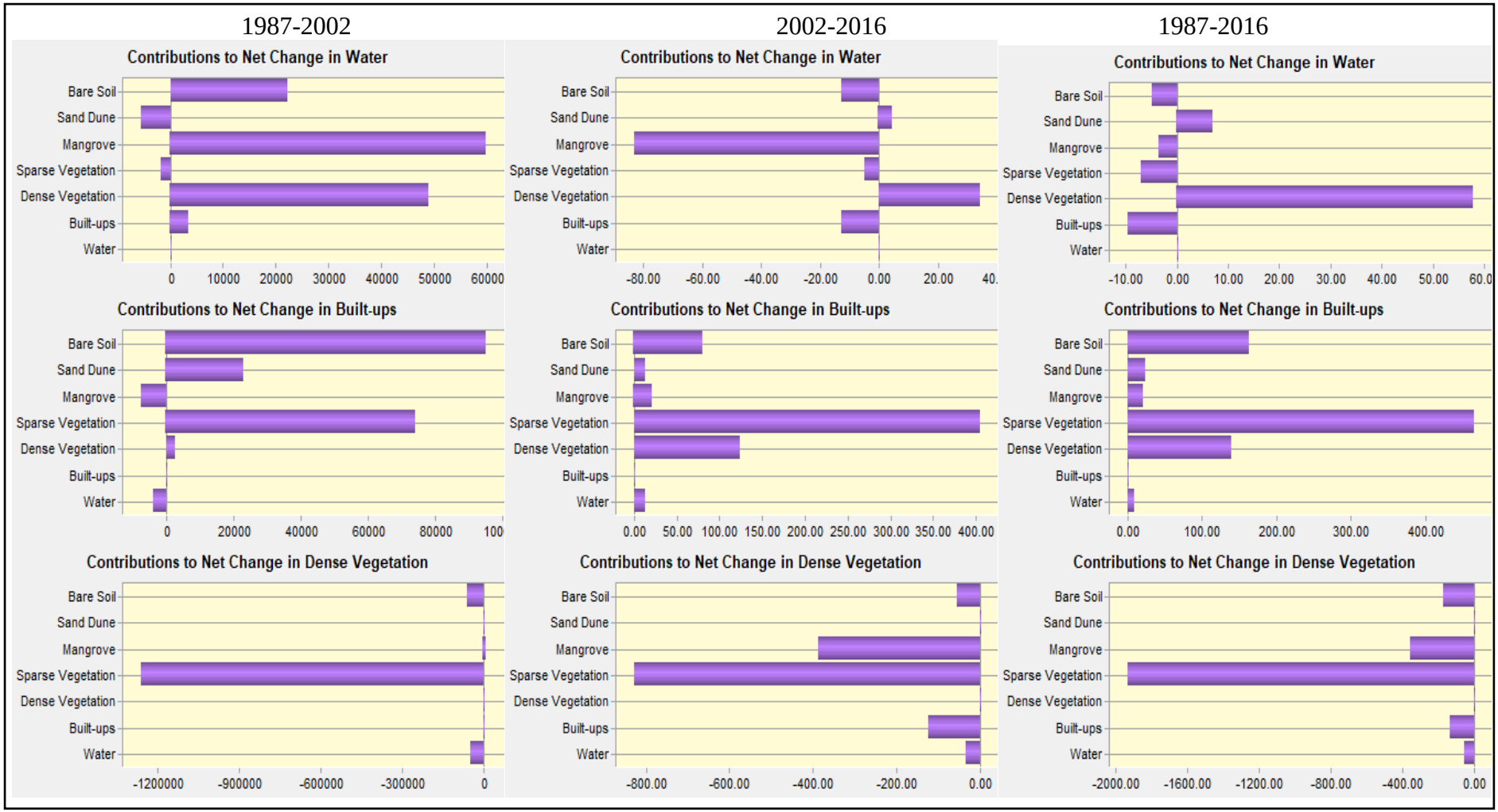

Figure 7.5: Contributor to net changes cont..

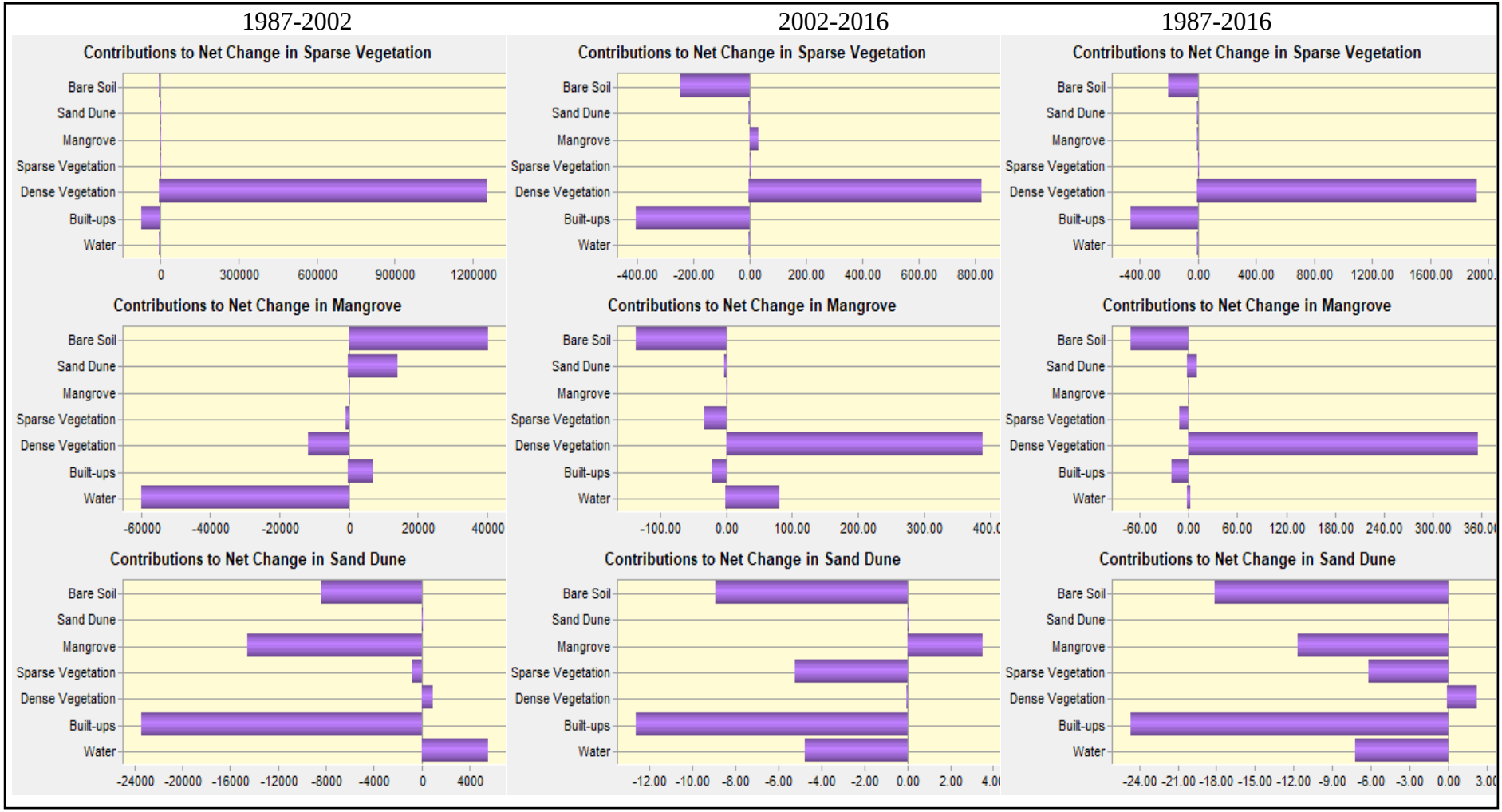

Figure 7.5: Contributor to net changes cont..

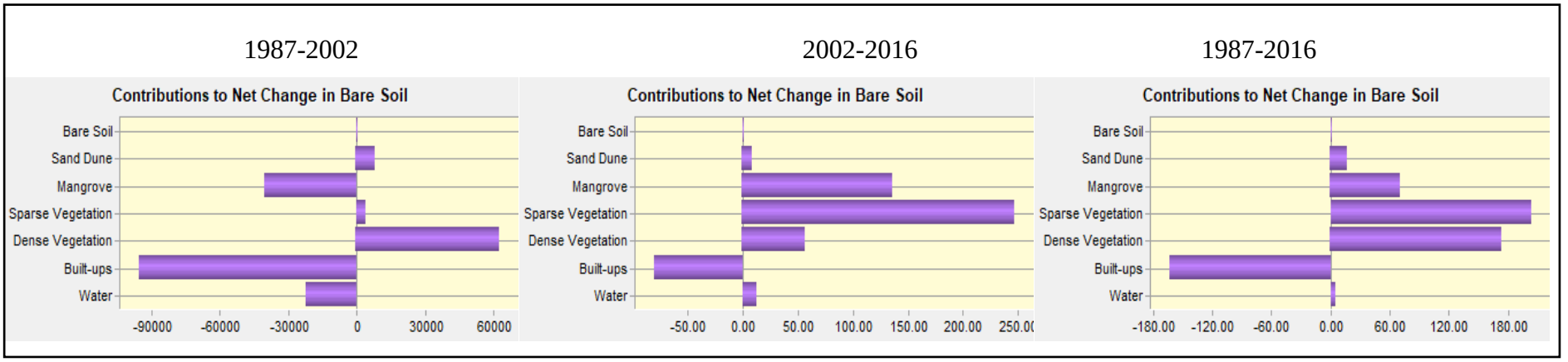

Figure 7.5:Contributor to net changes experienced by each land cover type in km^2.

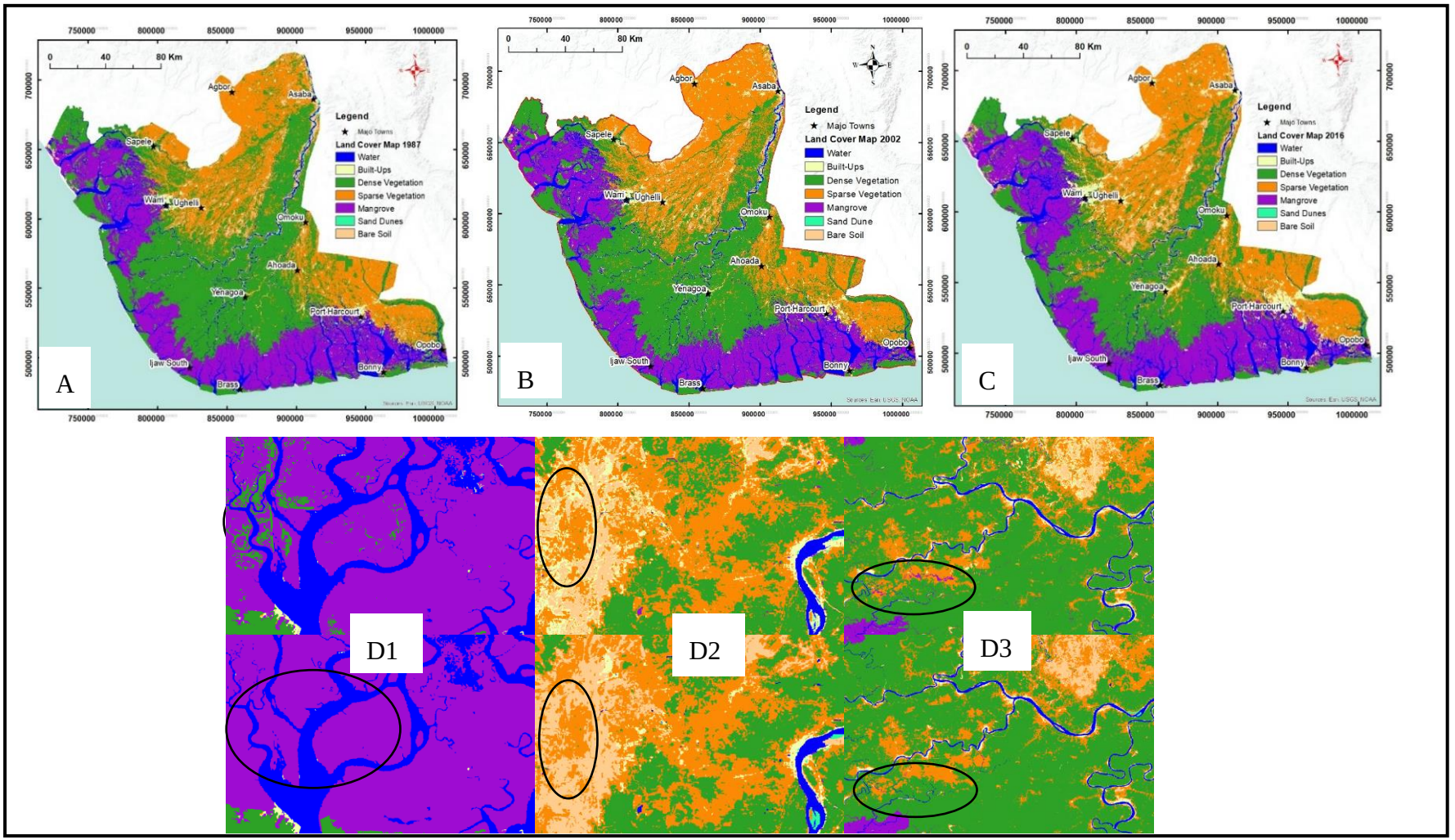

Figure 7.6:Land cover maps of (a) 1987, (b) 2002, (c) 2016 and (d1-3) show a comparison between a subset of the classified map (first row) and post-classified cleaned map (second row) for the 2016 land cover map.

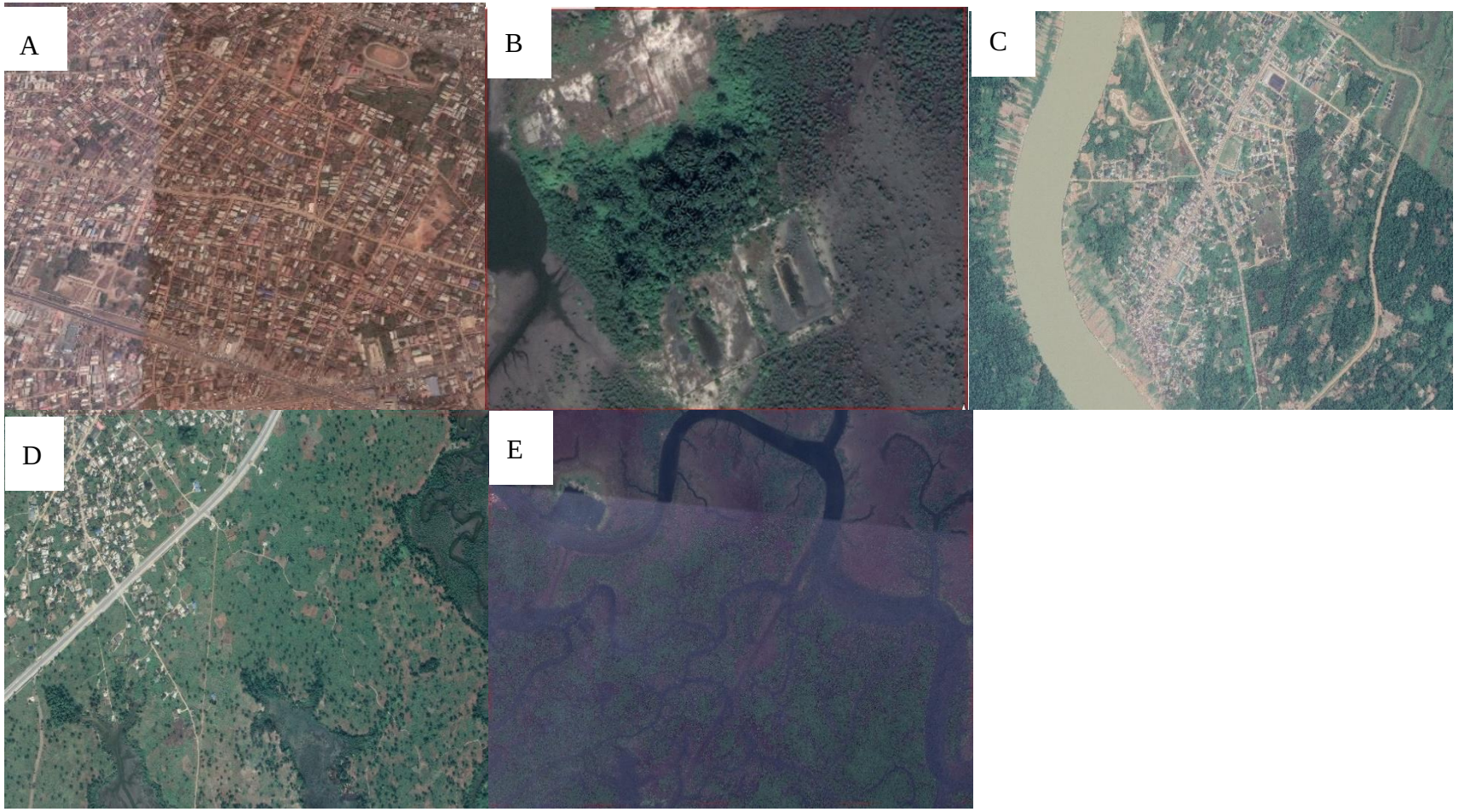

Figure 7.7:High-resolution satellite image of some subset of the study area showing causes of mixed pixel in the land cover map

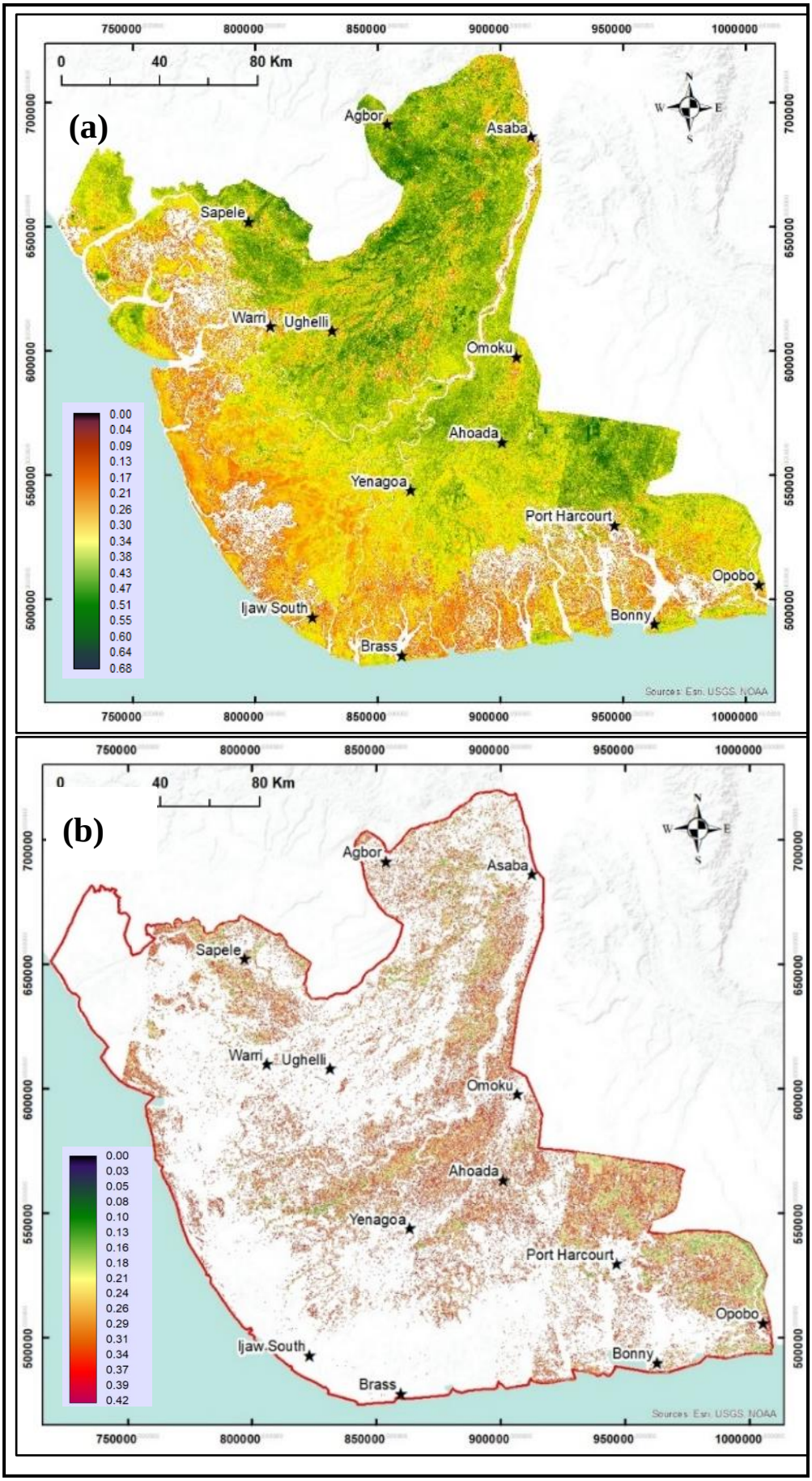

Figure 7.8: Vegetation map (NDVI) cont..

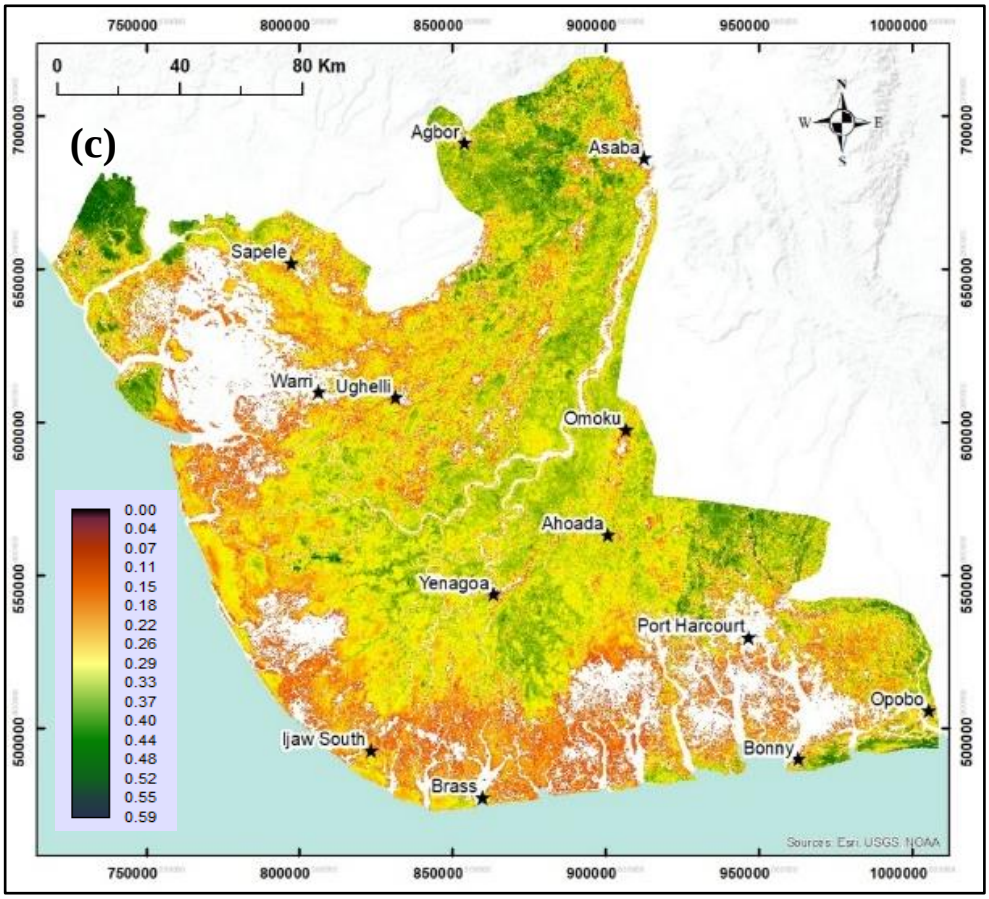

Figure 7.8:Vegetation map (NDVI) for (a) 1987, (b) 2002 and (c) 2016.

Note: Figure 7.8b is affected by cloud cover

7.3.4 Land Cover Change Detection

7.3.4.1 The magnitude of change in land cover: gains and losses

Table 7.6 shows the gains and losses for each land cover type from 1987-2002 and 2002-2016. Bult-up area is the highest gainer in proportion to its total size in both 1987-2002 and 2002-2016 and overall, from 1987-2016, having gained 484.85 km^2 (75.26%), 939.53 km^2 (115.89%) and 1067.19 km^2 (165.65%). On the other hand, the sand dune is the highest loser for all periods, having lost 139.98 Km^2 (86.50%) in 2016. Dense vegetation and mangroves were the least gained and lost, respectively, at 1032.67 km^2 (6.82%) and 740.13 (8.89%). The full extent of gains and losses are shown in Table 7.6. The spatial extent of gain and losses for each land cover class from 1987 to 2016 is shown in Figure 7.9. Green indicates gains, while red indicates losses. The land cover classes are water (7.9a), built-up area (Figure 7.9b), dense vegetation (7.9c), sparse vegetation (7.9d), mangrove (7.9e), sand dune (7.9f) and bare soil (7.9 g). The maps show that built-up area and sparse vegetation are the highest gainers in

spatial extent (Figure 7.9b and c), while dense vegetation is the highest loser. The gains and losses for 1987-2002 and 2002-2016 are in appendix B.

The degradation in vegetation in the Niger Delta region of Nigeria is high. Figure 7.10 a and b shows the gain and losses in NDVI from 1987-2016, covering the entire study period. The periods of 1987-2002 and 2002-2016 were not calculated due to the poor quality (cloud cover) of the 2002 images. It can be observed from the gain and losses that the vegetation only gained 0.28 in 2016 and lost 0.48 in the same year. The value of 0 or close to 0 is the location with little change.

Table 7.6: Gains and losses of land cover extent between 1987 and 2016 in km2 and as a percentage.

Land cover classes	1987-2002				2002-2016				1987-2016			
	Area in km^2		Area in (%)		Area in km^2		Area in (%)		Area in Km^2		Area in (%)	
	Gains	losses	Gains	losses	Gains	losses	Gains	losses	Gains	Losses	Gains	Losses
WT	632.52	517.69	24.79	20.29	579.15	653.69	21.72	24.52	559.92	519.70	21.95	20.37
BU	484.85	318.40	75.26	49.42	939.53	281.78	115.89	34.76	1067.19	242.74	165.65	37.68
DV	1621.05	2849.80	10.72	18.84	1405.27	2839.00	10.11	20.42	1032.67	3695.93	6.83	24.43
SV	2748.73	1681.61	30.65	18.75	2446.22	2227.97	24.37	22.20	3173.82	1887.60	35.39	21.05
M	943.28	952.29	11.33	11.44	1173.94	896.72	14.12	10.78	1008.58	740.13	12.12	8.89
SD	92.31	128.92	57.43	80.21	67.71	95.69	54.55	77.09	74.48	139.98	46.34	87.09
BS	680.46	754.49	62.12	68.88	1013.01	629.97	99.18	61.68	1035.71	726.28	94.55	66.30

Note: WT=water, BU=built-up, DV=dense vegetation, SV=sparse vegetation, M= mangrove, SD=sand dunes and BS=bare soil

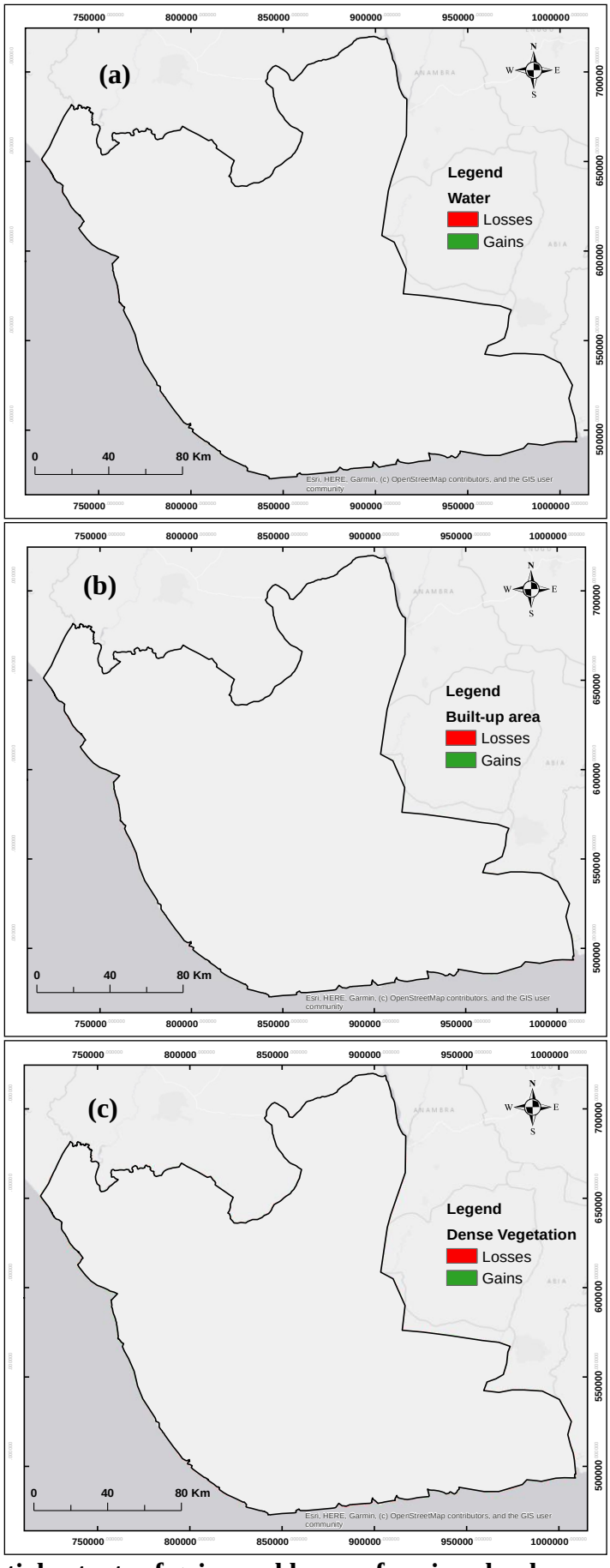

Figure 7.9: Spatial extents of gains and losses of various land cover classes cont..

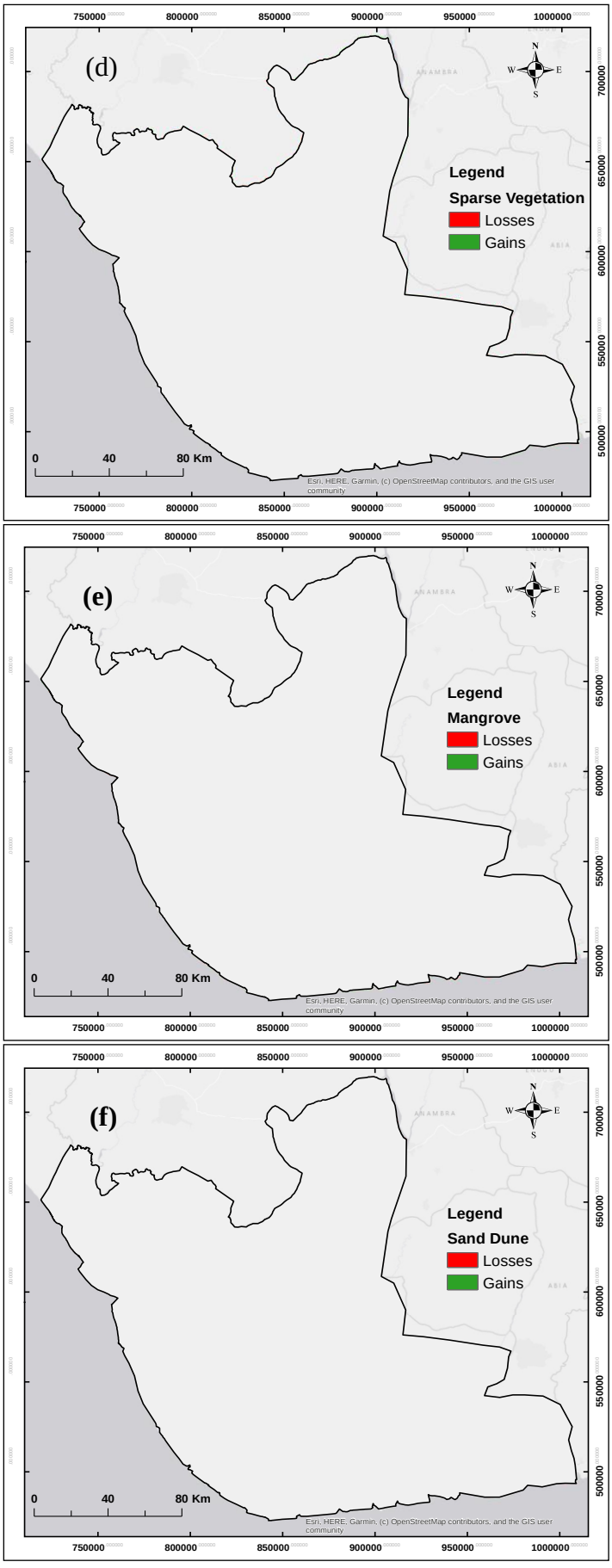

Figure 7.9: Spatial extents of gains and losses of various land cover classes cont..

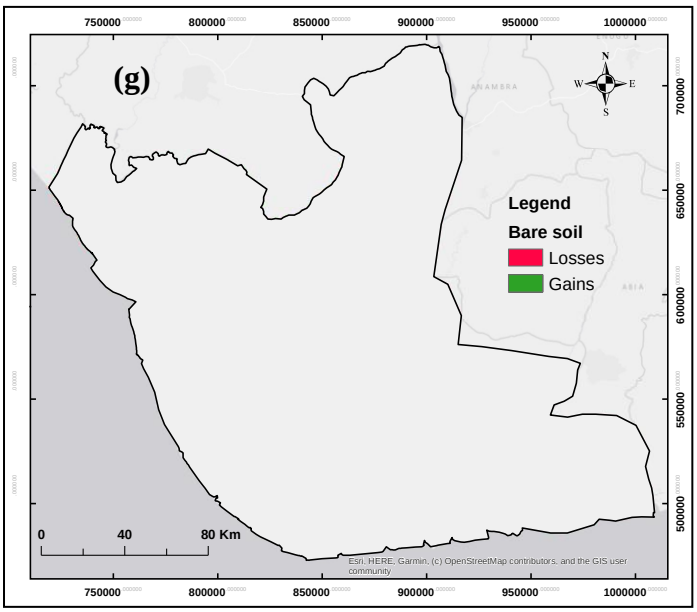

Figure 7.9:Spatial extents of gains and losses of various land cover classes between 1987 and 2016 (a) Water, (b) Built-up areas, (c) Dense vegetation, (d) Sparse vegetation, (e) Mangrove, (f) Sand dunes and (g) Bare soil.

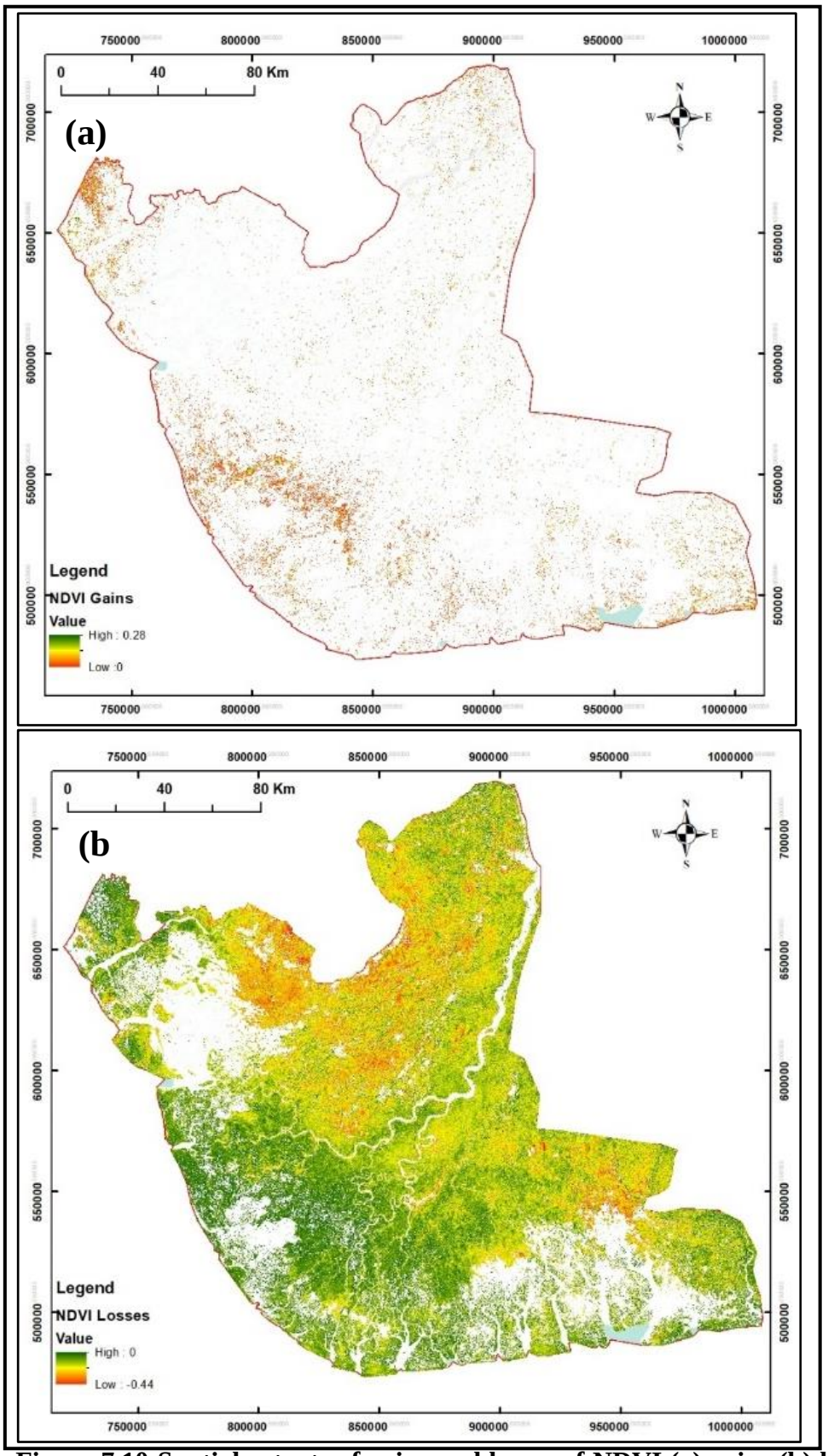

Figure 7.10:Spatial extents of gains and losses of NDVI (a) gains (b) loss between 1987 and 2016.

7.3.4.2 Nature of land cover changes and direction of change: Conversions between various land cover classes.

Table 7.7a-c shows the land cover conversion for 1987-2002, 2002-2016 and 1987-2016 calculated using three land cover maps of 1987, 2002 and 2016. For the three periods, the table summarises the area that has remained unchanged, and the types of change observed for each class from 1987-2002, 2002-2016 and 1987-2016. The rows are the conversions from a particular land cover to all other land covers, while the columns are the conversion from other land covers to a particular land cover. For example, Water lost 18.02 km^2 in row 1, column 2 to build up but gained 21.35 km^2 in row 2, column 1 between 1987 and 2002 (Table 7.7a).

Table 7.7: Land cover conversions extend in km^2 from (a) 1987 to 2002, (b) 2002 to 2016 and (c) 1987 to 2016 with no change in red bold.

Land cover classes		**To 2002 (a)**						
		WT	BU	DV	SV	M	SD	BS
From 1987	WT	2033.75	18.02	86.15	13.89	339.19	43.78	16.66
	BU	21.35	325.83	58.93	172.66	25.09	7.87	32.50
	DV	130.41	61.44	12278.45	2068.85	474.57	12.22	102.31
	SV	12.25	239.69	933.96	7287.51	15.08	10.23	470.41
	M	393.19	18.33	485.17	15.75	7371.48	3.52	36.32
	SD	38.75	28.95	11.35	10.98	16.63	31.81	22.26
	BS	36.57	118.41	45.49	466.61	72.72	14.69	340.91
To 2016				**(b)**				
From 2002	WT	2012.57	29.63	87.01	21.89	448.05	31.17	35.93
	BU	16.87	528.90	19.88	156.20	14.14	6.01	68.68
	DV	121.40	144.18	11060.78	1840.11	649.72	4.56	79.03
	SV	16.97	561.47	1011.55	7808.27	12.52	4.57	620.89
	M	364.89	35.98	260.62	45.22	7418.04	5.93	184.07
	SD	35.95	18.66	4.47	9.80	2.40	28.44	24.41
	BS	23.07	149.61	21.73	373.00	47.10	15.46	391.40
To 2016				(c)				
From 1987	WT	2033.27	27.01	60.87	18.01	335.40	39.02	39.40
	BU	17.35	401.96	31.80	134.24	18.53	2.66	38.16
	DV	118.93	171.01	11437.63	2617.50	571.43	6.99	210.06
	SV	10.93	600.59	685.03	7085.14	6.03	3.33	581.69
	M	331.88	39.28	214.82	16.89	7584.27	5.71	131.55
	SD	46.23	27.35	4.62	9.53	17.39	21.85	34.85
	BS	34.59	201.94	35.54	377.64	59.81	16.77	369.48

NOTE: WT=water, BU=built-up, DV=dense vegetation, SV=sparse vegetation, M=mangrove, SD=sand dunes and BS=bare soil

Figure 7.11 a-f shows the spatial conversions (changes) from a particular land cover class to all other land cover classes. The maps are the conversion from a particular land cover type to all. The conversions are from water to all (Figure 7.11a), built-up area to all (Figure 7.11 b), dense vegetation to all (Figure 7.11 c), sparse vegetation to all (Figure 7.11 c), mangrove to all (Figure 7.11 d), sand dunes to all (Figure 7.11e) and bare soil to all (Figure 7.11f).

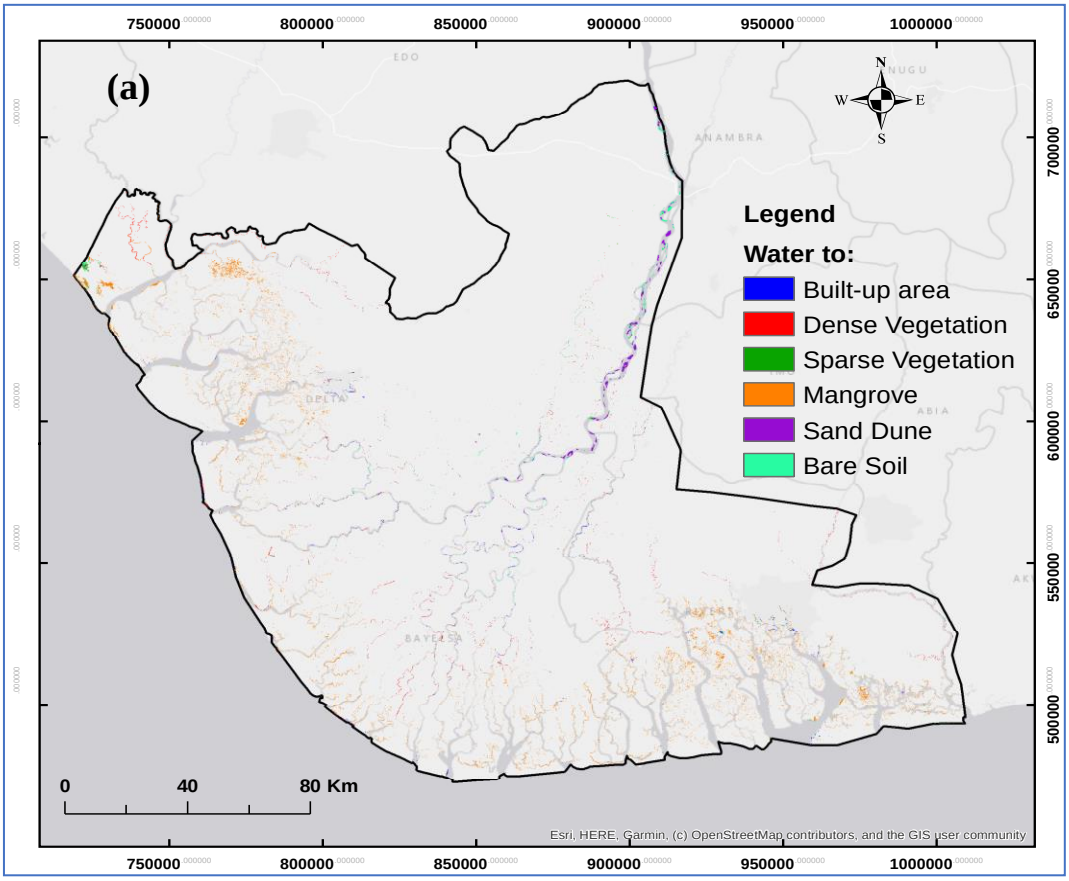

Figure 7.11:Land cover conversion cont..

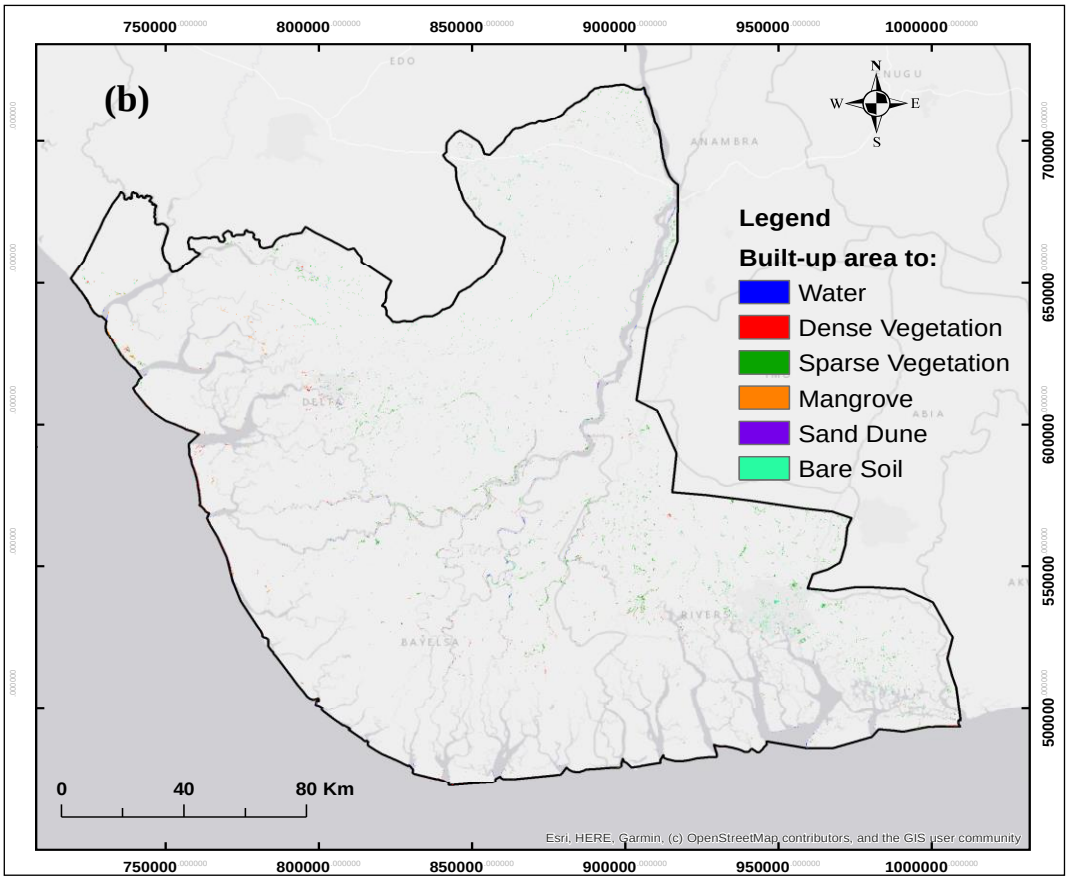

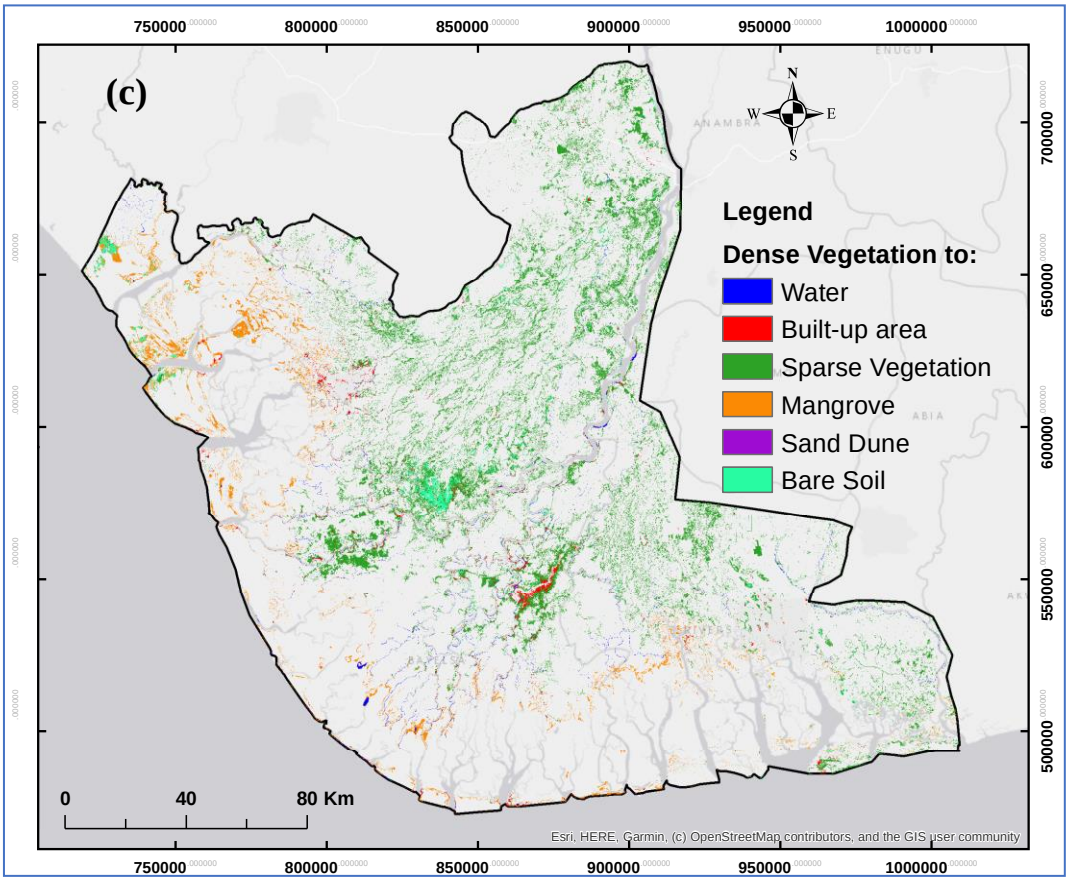

Figure 7.11: Land cover conversion cont..

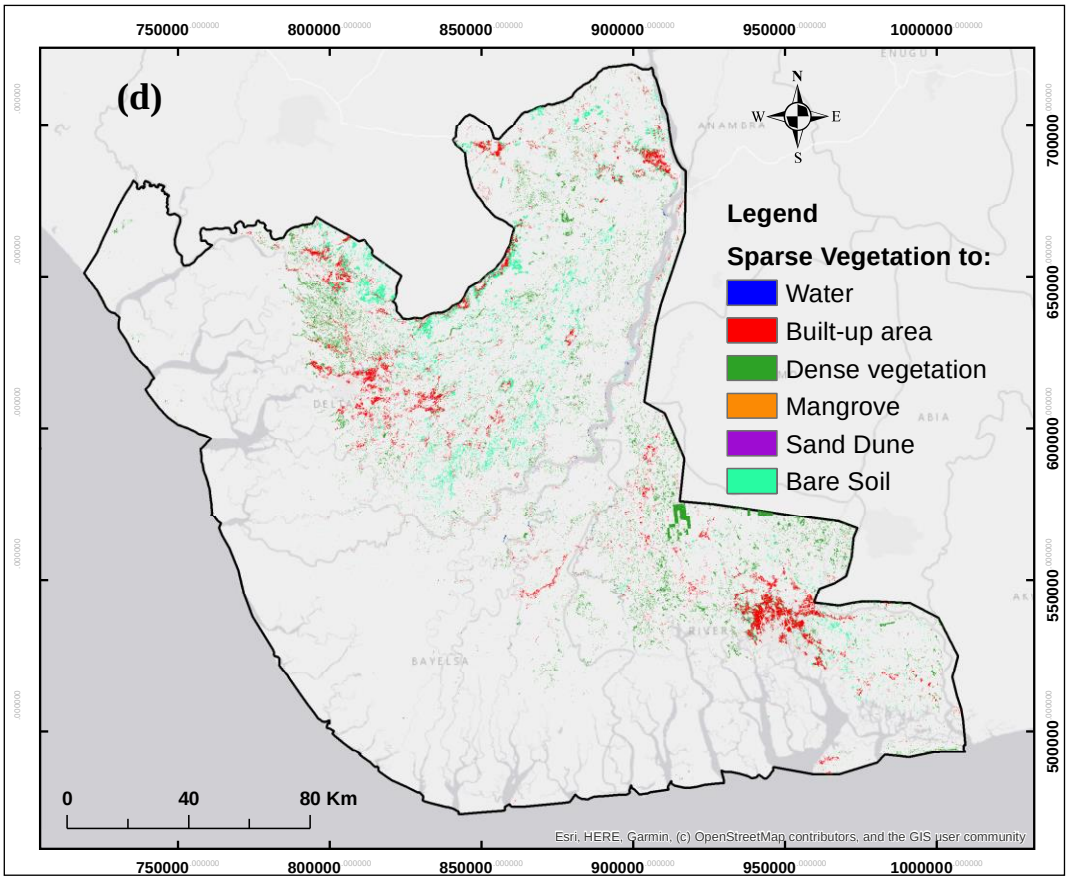

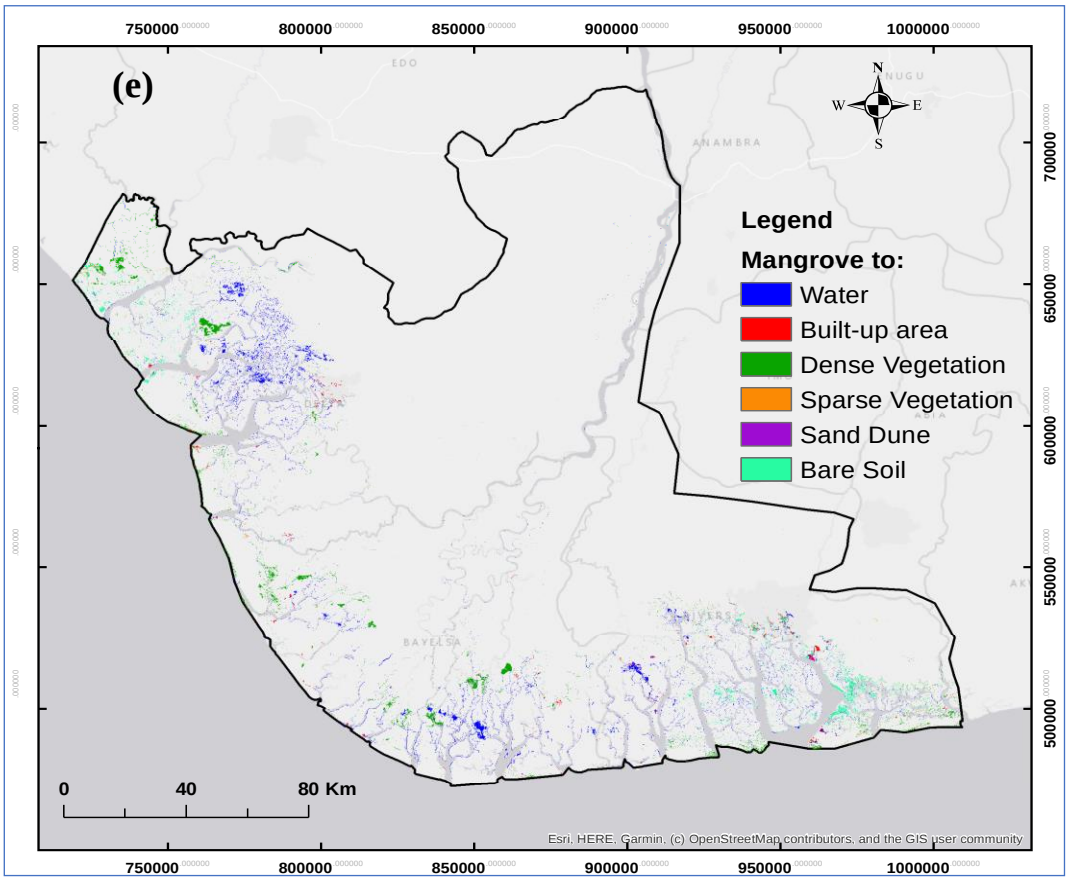

Figure 7.11: Land cover conversion cont..

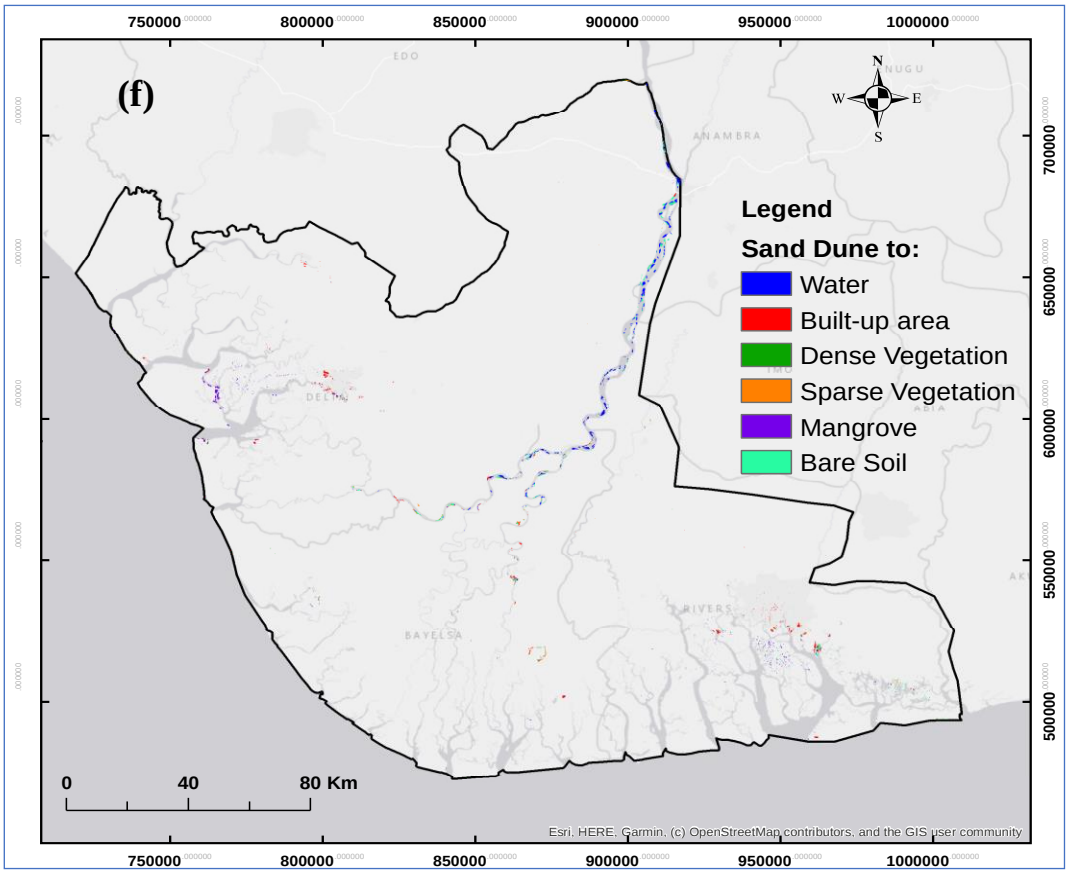

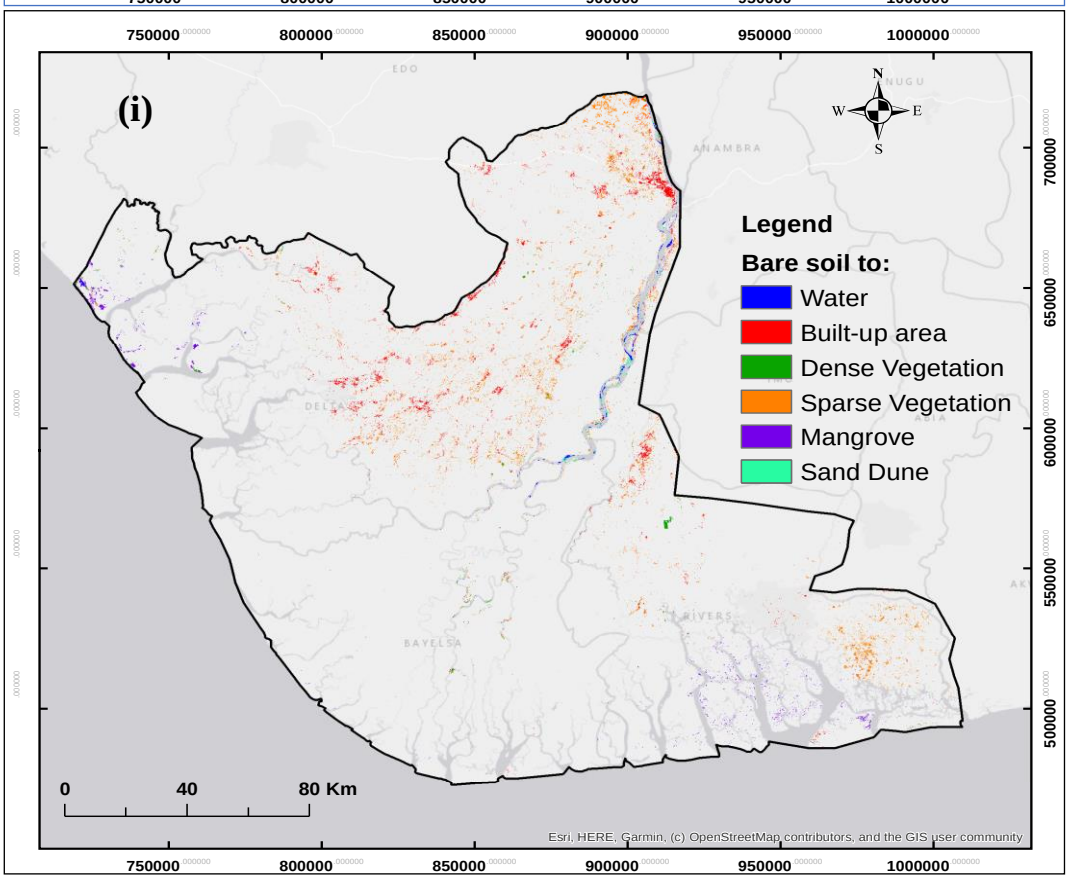

Figure 7.11:Land cover conversion from (a) water, (b) built-up area, (c) dense vegetation, (d) sparse vegetation, (e) mangrove, (f) sand dunes and (g) bare soil to all other land cover types.

7.3.5 Impact of oil extraction on land cover changes.

The number and volume of oil spills in each land cover class in 2016 are shown in Table 7.8. From Table 7.8, there have been 6698 oil spills, and 354906.13 barrels (bbl) spills into the land cover in the study area. The results show that sparse and dense vegetation have the highest number of spills and volume, respectively, with sand dune having the least number and volume of spills. Figure 7.12 is the overlay of oil facilities on the land cover maps of 2016. The oil spills are located along the oil pipeline since most of them are from sabotage and vandalization, with a few cases occurring due to equipment failure and others.

Table 7.8: Numbers of spills and volumes of oil spills per barrel in land cover. NS=number of spills, V=Volumes of spills and bbl=barrel

Land cover Classes	NS	V in bbl	NS as %	V as %
WT	860	34777.12	12.84	9.80
BU	439	40009.534	6.55	11.27
DV	1589	98656.14	23.72	27.80
SV	1789	96000.42	26.71	27.05
M	1655	59077.45	24.71	16.65
SD	24	691.33	0.36	0.19
BS	342	25694.143	5.11	7.24
Total	**6698**	**354906.13**	**100.00**	100.00

NS=number of spills, V=Volumes of spills, bbl=barrel, WT=water, BU=built-up, DV=dense vegetation, SV=sparse vegetation, M=mangrove, SD=sand dunes and BS=bare soil

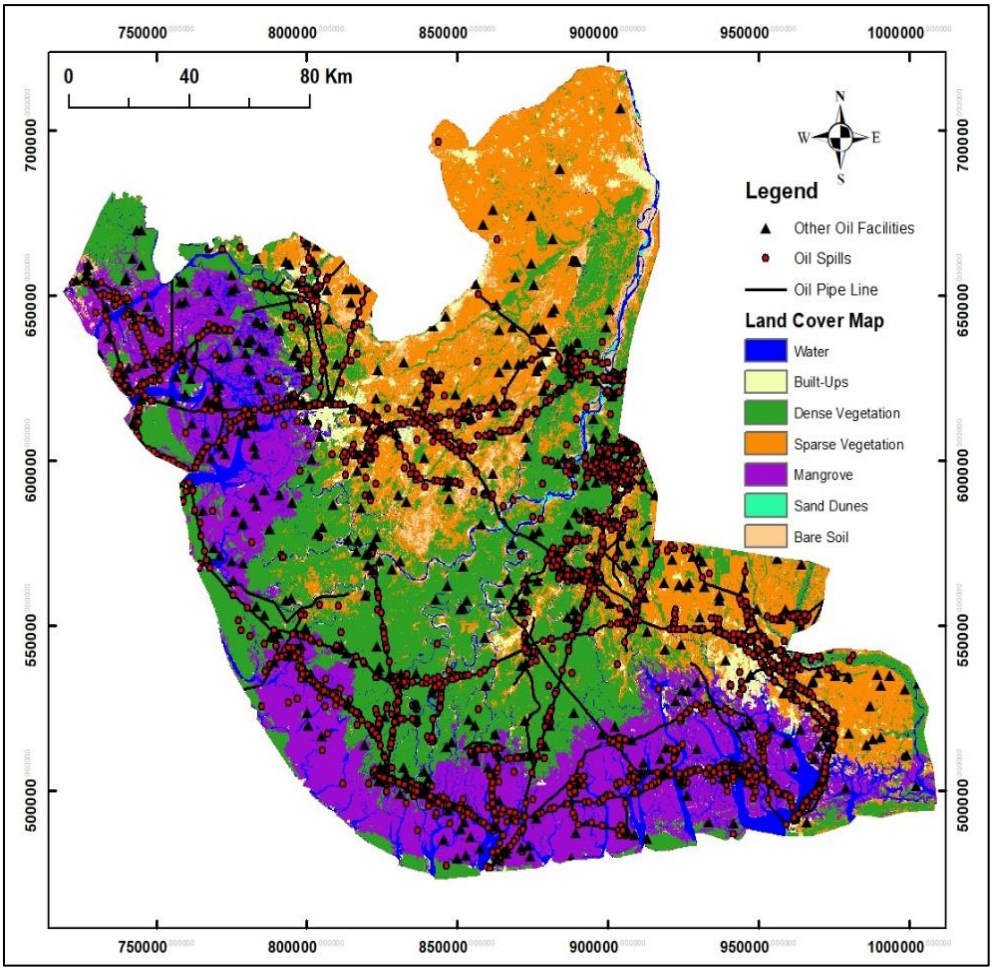

Figure 7.12:Distribution of oil spills and facilities on various land cover classes.

Figures 7.13-7.15 show the distribution of oil facilities and oil spill hot spots overlaid on land cover changes in dense vegetation, sparse vegetation and mangrove from 1987 to 2016, instead of from 1987-2002 and 2002-2016. The main interest is to map the changes from 1987-2016. The vegetation map shows the conversion of each vegetation to other land cover types and the gains by each vegetation in light blue. For example, Figure 7.13 shows the conversion of dense vegetation to water, built-up land, sparse vegetation, mangroves, sand dunes and bare soil. It can also be observed from the map that the dense vegetation lost more to other land cover types than it gained, although some gained could be seen northeast of Warri and northwest of Ahoada

Figure 7.16 shows the distribution of oil facilities and oil-spill hot spot areas from 2008 to 2019 overlaid on vegetation's gain and loss map (NDVI). The map shows the relationship between vegetation degradation and oil extraction activities in the Niger Delta. It can be observed, for example, that the places that experience high loss are close to the oil pipelines and spills, especially around the central part of the study area.

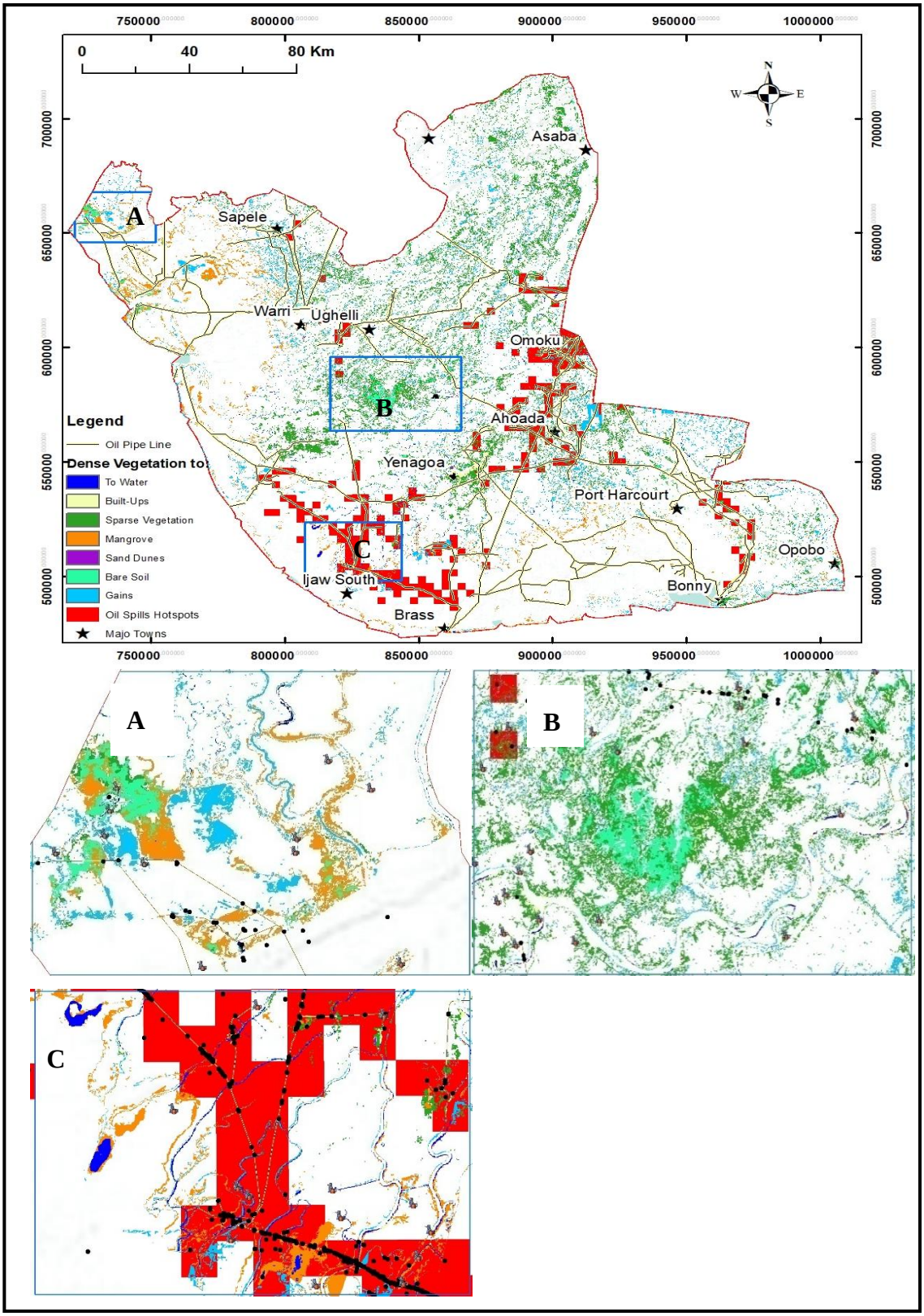

Figure 7.13:Land cover losses from DV to all and DV gain from 1987 to 2016 overlaid on oil spill hotspots, pipelines and oil wells (A) western Niger Delta, west of Sapele, (B) the central Niger Delta and (C) the southern Niger Delta.

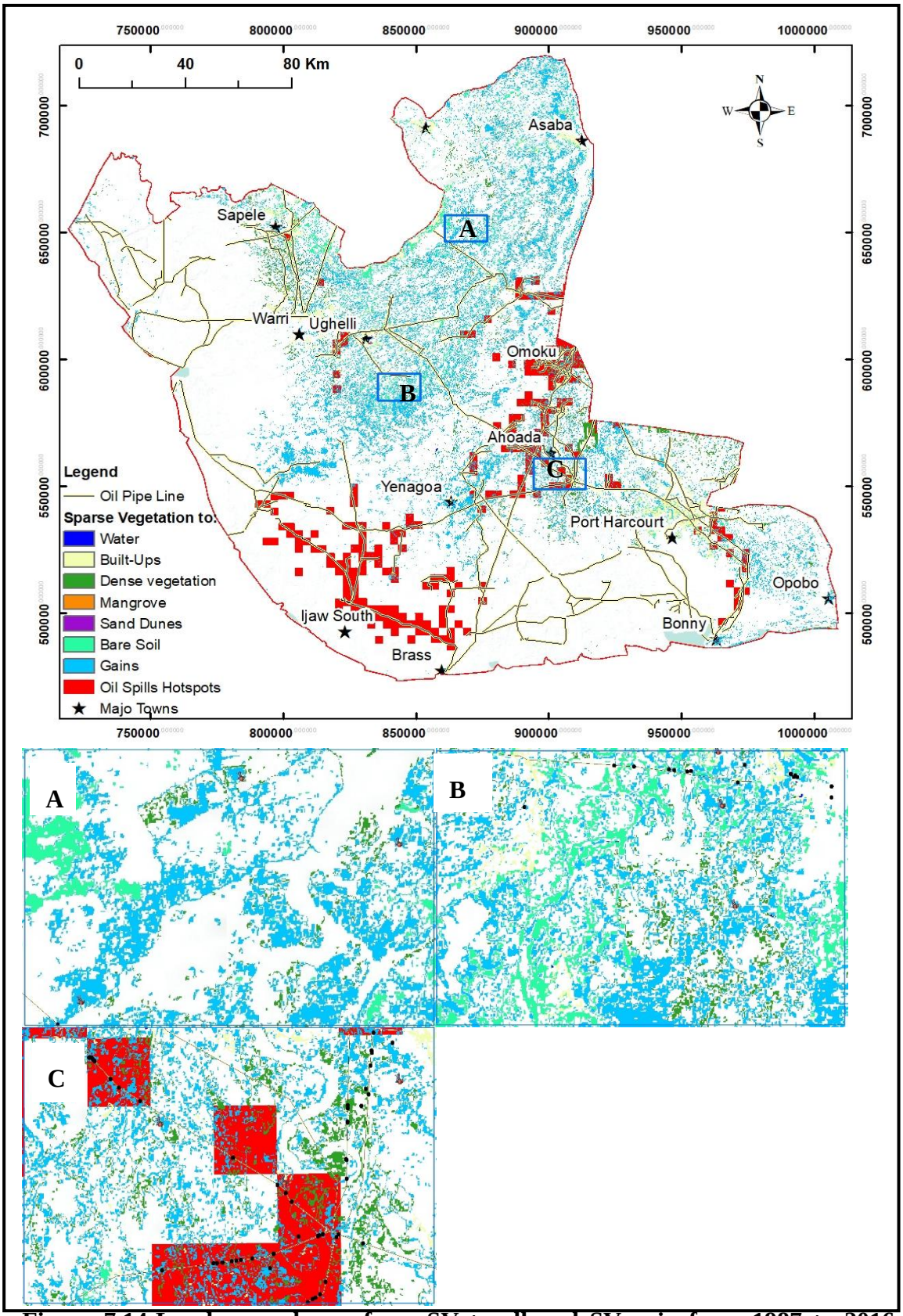

Figure 7.14:Land cover losses from SV to all and SV gain from 1987 to 2016 overlaid on oil spill hotspots, pipelines and oil wells (A) in the northern Niger Delta, (B) in the central Niger Delta and (C) toward the eastern Niger Delta

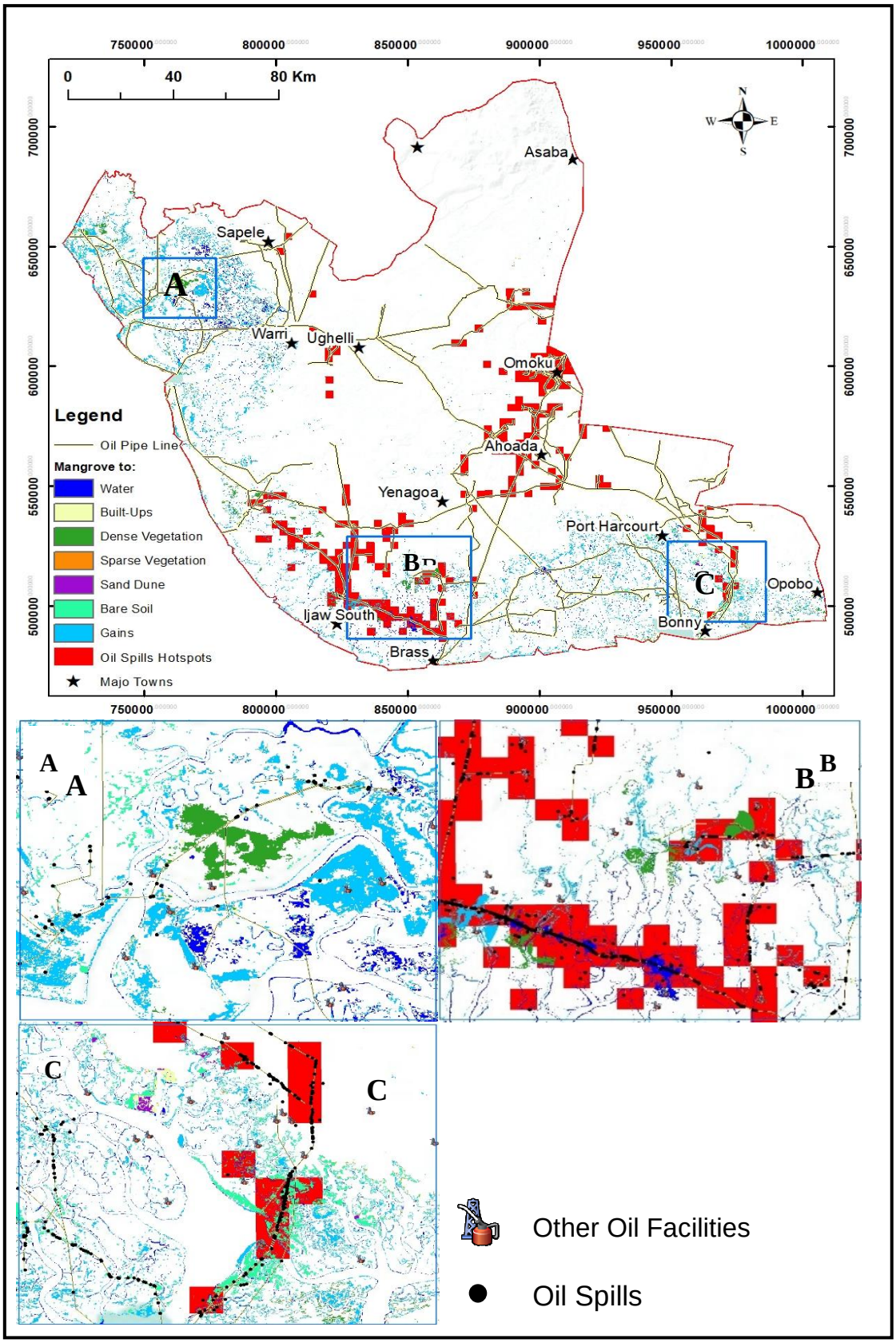

Figure 7.15:Land cover losses from M to all and M gain from 1987 to 2016 overlaid on oil spill hotspots, pipelines and other oil facilities (A) in the western Niger Delta, west of Sapele, (B) in the southern Niger Delta and (C) in the eastern Niger Delta.

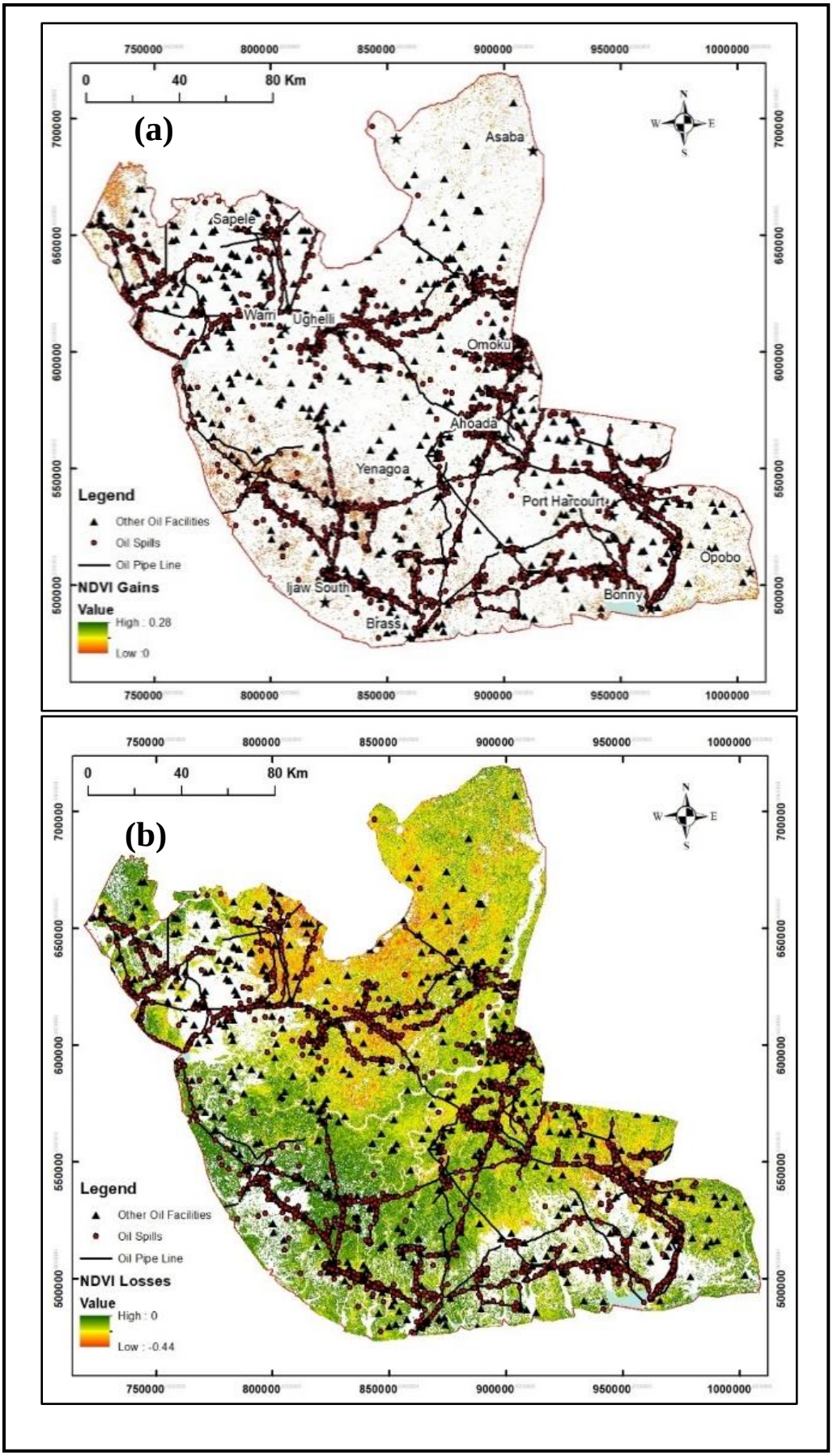

Figure 7.16:Gains and losses in vegetation conditions between 1987 and 2016 from NDVI (a and d).

7.4 Discussion

7.4.1 Challenges of land cover mapping in the Niger Delta

The Niger Delta region is one of the most affected worldwide by Landsat archive gaps and consistent cloud cover (Nababa et al., 2020). The first challenge for remotely sensing the Niger Delta is frequent cloud coverage (Kuenzer et al., 2014). The limited availability of cloud-free data, especially from optical sensors such as Landsat for land cover mapping and change detection, is a challenge. The second problem is mixed pixels among the land cover classes in the Niger Delta, water mixed with mangroves and mangroves mixed with dense vegetation, sparse vegetation with dense vegetation and even water mixed with built-up, etc., partly due to the land cover types and the spatial resolution of the images. Mapping mangrove forests and other land cover types, in particular, is challenging, as they are affected by seasonal and intertidal effects, pixels often mixed with vegetation, soil, and water due to their location between land and sea and the average tidal range in the Niger Delta being 1.5 m (Nababa et al., 2020). The last challenge is the issue of spectral similarities among different land cover classes. Spectral similarities were discovered between mangrove and dense vegetation, bare soil, sand dunes and built-up areas, water bodies and mangroves, etc. Even the water bodies have similar spectral reflectance to the built-up due to oil spills, making them brighter in reflections. The problem of spectral similarities in the Niger Delta land cover was not overcome using soft classifiers since they were not developed to solve this problem. All six classifiers used in this research had the same challenges. Incidentally, none of the authors who have carried out land cover classification in the Niger Delta ever noted this problem. Heumann (2011) encountered the same challenges when mapping fringe mangroves on Isabela Island in the Galapagos Archipelago, Ecuador, using remote sensing data due to the spectral similarity of mangroves with associated species and the lack of clear zonation between species. A post-classification analysis was used to reallocate the land cover classes to their original pixels to reduce the impact of spectral similarities on the land cover classes.

7.4.2 Soft maps

Despite the challenges of mapping land cover in the Niger Delta, seven different land cover classes were mapped for 1987, 2002 and 2016 using the Bay classifier, which was more visually accurate and less "noisy" than the Mahal, which had higher overall

accuracy. For a soft map of 2016 from the Bay land cover map (Figure 7.2), both the extent and intensity of each land cover type are similar to a "hotspot" map. The dense and sparse vegetation are the most extensive land cover types located around the central part of the study area, with the sparse vegetation located toward the northern part of the study area. The soft maps and changes detected by them could be used to prioritise interventions related to land cover changes, especially when resources are scarce. Unlike the hard map, each soft land cover class has a map, which can be used to analyse land cover changes and monitoring; since they show places with more intense land cover types or changes, they could help policy makers identify the locations requiring more urgent attention since the degree of change is mapped. Unfortunately, for this research, the problem of spectral similarity among some land cover types could not allow further analysis using the maps.

7.4.3 Hard maps

All the classifiers used were carefully chosen to include some that have been used before in the Niger Delta and those that have not been used**.** The classifiers that have been used for land cover mapping in the Niger Delta are maximum likelihood (Ayanlade & Howard, 2017; Eyoh & Okwuashi, 2016; Omo-Irabor & Oduyemi, 2007 etc.), the SVM method under the radial basis function kernel type (Nwobi et al., 2020) and random forest (Nababa et al., 2020; Ozigis et al., 2019). The Bayes, Mahal, SOM and Unmix classifiers have not been used in the Niger Delta before. Also, from previous studies, only two authors have compared two classifiers for mapping land cover in the Niger Delta. Nwobi et al. (2020) compared SVM and Maximum likelihood classifiers to map land cover in the Niger Delta, while Ozigis et al. (2019) compared the fuzzy forest (FF) and random forest (RF) methods in detecting and mapping oil-impacted vegetation from post-spill using multispectral data in the Niger Delta. From this study, Mahal performed better, with an overall of 82.17%, followed by Bay with 81.56%, with the least being SOM with 55.83% (Table 7.3). The overall accuracy is different from Nwobi et al. (2020), who achieved better accuracy with SVM than the maximum likelihood classifier in the Niger Delta. Although he did not compare it with the same classifiers used in this study, his study area's extent was also larger. Similarly, the object-based classifier for Bay and Mahal, the two best classifiers, did not perform well; they also suffered from spectral similarities**.** Object-based classification using medium resolution remotely sensed images may be relatively low in accuracy when the objects are over- or under

segmented due to spectral confusion and over- or underemphasis of spectral variations within/between large objects (Wang et al., 2018). Although Mahal was the best overall classifier, it was discovered that it has more issues with spectral misclassification; it has more "noise" than Bay, especially for vegetation, which tends to be the most important land cover for this study. Hence, Mahal did not meet the visual accuracy, and Bay was chosen as the best classifier. The result of McNemar also shows that the difference between the Mahal and Bay classifiers is not statistically significant, $p>0.05$.

For per-class accuracy from Bayes, water, dense vegetation, sparse vegetation and mangrove were mapped to higher accuracy by all classifiers ranging from PA=64%-78% and UA 60%-91%, in 2016 and 1987, including the object-based except for SOM despite all the land cover classes suffering from spectral similarities. For instant, all classifiers classified some water as mangrove, apart from DT (Figure 7.5). However, the built-up was the less accurately mapped land cover, thought the DT classifier produced a better PA and UA for the built-up. From the analysis of the high-resolution satellite image in Figure 7.7, various land cover classes are mixed, and the built-up area was confused by bare soil for all classifiers except SOM due to spectral similarities. Most of the buildings in the Niger Delta, especially in the rural area, are built haphazardly using thatch, mud, timber etc., without recourse to town planning rules and are located along the banks of creeks and rivers (Amasuomo & Japo, 2016). The buildings have a lot of space, even in the urban built-up area between the blocks having bare soil, making it difficult for the classifier to map. However, the results by (Ayanlade & Howard, 2017; Nababa et al., 2020; Nwobi et al., 2020; Omo-Irabor & Oduyemi, 2007) all achieved high accuracy in the built-up. The high accuracies achieved in built-up areas by these authors could be that some did not consider spectral similarities among various land covers, and they assumed some bare soil and sand dunes as built-up, with some not having bare soil as a class. For instance, Ayanlade and Howard (2017) did not have bare soil as a class, while Omo-Irabor and Oduyemi (2007) had built-up and bare soil as one class. The misclassification of dense vegetation as sparse vegetation and the mangrove as either water or dense vegetation was expected since dense vegetation is also found within sparse vegetation and vis versa. The mangrove is located in the water with some dense vegetation, resulting in mixed pixels. The proximity of sparse vegetation was also the reason for it being misclassified as built-up, especially in the rural area where farming activities are around the houses. Overall, this accuracy

achieved is satisfactory for the objective of this work since the most important land cover is vegetation in general.

7.4.4 Post-classification analysis

Any change detection can only be as good as the individual classification (Kuenzer et al., 2014). The problem of spectral similarities and the "salt and pepper" effect was reduced using post-classification or postprocessing. Spectral similarities among objects within the parcel can misclassify certain land-cover types (Li et al., 2014). The classification accuracy for Bay increased from 81.56% to 83.06% after post-classification analysis, and the visual quality of the map improved, as shown in Figure 7.6. For the land cover to be used for change mapping, one must ensure that the land cover map is produced with high accuracy. The advantage of post-classification analysis is that it improves the classified map's accuracy and allows for more interaction between the classifier and the analyst (human). The analyst can intervene in the classification when the classifier cannot distinguish between objects with similar reflectance. The major disadvantage is that it may be labour-intensive for a large study area. Wang et al. (2018) also had an improved accuracy between 5% and 14.1% after post-classification analysis of four study areas of Cixi, Yinchuan and Maanshan in China and Hartford in the USA using the Markov chain random field (MCRF) post-classification method to improve object-based land use/cover classifications on different landscapes.

7.4.5 Qualitative and quantitative land cover extents

Despite the challenges of mapping land cover in the Niger Delta, seven different land cover classes were mapped from the Bay classifier for 1987, 2002 and 2016. This study discovered that the dense vegetation occupied the largest portion of the study area 15133.56 km^2 in 1987, 13899.78 km^2 in 2002 and 12470.30 km^2 in 2016 and experienced a continuous net loss of 8.12% (1228.75 km^2) and 10.31% (1433.73 km^2) for the first and second periods, respectively. However, the high net gain by the built-up area for both the first and the second periods makes it the main net contributor to the net losses in all land cover classes. The gain is caused by oil extraction activities, such as building oil facilities and shelters to meet the growing demand for shelter to accommodate both the locals and workers working for various national multination oil companies, which mostly involve clearing and felling trees. The results of Eyoh and Okwuashi (2016); Nababa et al. (2020); Nwobi et al. (2020); Omo-Irabor and Oduyemi

(2007) also show that the built-up area is the highest net gainer at all times, while the dense vegetation (forest) is the highest loser and possible the main net contributor to the net gain in all land cover classes.

However, unlike the dense vegetation, the net gain recorded by sparse vegetation for the two periods, with the first period being higher with 11.90% and 2.17% in the second, is a pointer that the sparse vegetation is the main gainer from the loss experienced by dense vegetation. Similarly, the net loss in the first period of 0.11% and a net gain of 3.33% in the second period for the mangroves shows a sign of either recovery of the mangrove or the conversion of other land cover classes to mangrove. This could have a positive impact on the animal and people of the Niger Delta since the mangrove is important to both animals and the inhabitants of the Niger Delta. However, the net gain in the second period for the mangrove did not agree with most of the authors who reported a consistent net loss in mangroves, except for the study by Eyoh and Okwuashi (2016), who recorded a net increase in a mangrove from 3.03% to 10.34% in 2016 from 2002. Similarly, Kuenzer et al. (2014) discovered that the mangrove forest (overall, combining all mangrove classes) had remained more or less the same, with 10,311 km^2 in 1986/87 and 10,072 km^2 in 2013, just a small loss. Comparing this study with others shows that the spatial and temporal scales are different. Some authors cover the entire political Niger delta, while some cover a section of this study area. At the same time, some cover a shorter time.

From the NDVI map, the vegetation in the Niger Delta has been seriously affected by urban growth, especially around Port Harcourt and Sapele-Warri, as seen in the 2016 map (Figure 7.8). The mangrove vegetation in the southern part of the study area is the most degraded vegetation, with lower NDVI values in 1987, 2002 and 2016. The NDVI value in 1987 was higher than the NDVI value in 2002, while the NDVI value in 2002 was lower than the NDVI value in 2016 (Figure 7.8a-c), which shows that the vegetation degraded with an NDVI value of 0.68 in 1987, decreased to 0.48 in 2002 and increased to 0.58 in 2016 from 2002. The increase in NDVI in 2016 from 2002 could be attributed to the influence of natural forces and the ability of some plant types to develop tolerance to the impact of oil spills and other hazardous materials. For example, during the fieldwork, some mangroves were regenerating after being destroyed by oil spills. Vegetation resources in the Niger Delta have been under stress conditions due to human-induced impacts arising from oil and gas activities (Ochege et al., 2017), especially in

the central part of the Niger Delta. The results by Ayanlade and Howard (2017) also show severe deforestation, especially in the north-western and north-eastern parts of the delta, with the mean NDVI decreasing from 0.61 in 1987 to 0.55 in 2001 and decreasing further to 0.48 in 2011. Ochege et al. (2017) also discovered a severe decline in healthy forests and vegetation in the Sagbama oil field from an NDVI of 0.55 in 1987 to 0.32 in 2002 and later rose to 0.44 in 2013. However, it was still lower than the initial NDVI in 1987.

7.4.6 Land cover change analysis

7.4.6.1 Gains and Loses: Landscape

Each land cover is expected to gain and lose in land cover changes. Unlike the net losses and gains, the gross gain and losses show what each land cover gives and takes. From Table 7.6, the gain and losses of water are not high; 24.79% and 21.71% in the first and second periods and 20.29% and 24.52% within the same period. The built-up area gained 75% (484.85 km^2), lost 49.42% (318.40^2) in the first period, gained 115.89%, and lost just 34.76% in the second period, which was the highest gain. The rapid expansion in the built-up area in the second period could be partly attributed to the increase in population from both the locals and the workers working with many multinational oil companies, the building of new oil facilities and an increase in wealth in the hands of some people due to the increased affluence resulting from increased individual income earning/employment opportunities, activities of oil theft, illegal refineries, etc., which put more money into the hands of the local people. Although most land cover change studies did not report the gross gain and losses, Eyoh and Okwuashi (2016) and Nababa et al. (2020) also recorded losses in the built-up area. The loss in the built-up could result from some buildings destroyed by the militant activities or spectral similarity with other land cover types, especially in the first period. On the other hand, dense vegetation experienced continuous loss. It was the least gainer, with 10.72% (1621.05 km^2) gain and 18.84% (2849.80 km^2) loss and 10.1% (1405.27 km^2) and 20.40 (2839.00 km^2) loss in the first and second period, making it the largest loser and the most vulnerable land cover undergoing massive destruction. The forest in the Niger Delta suffered heavy depletion throughout the 30 years at a rate of approximately 1% per year (Eyoh & Okwuashi, 2016). The massive destruction of dense vegetation is expected due to massive pressure. Forest loss/degradation has increased over the years due to crude oil activities, urbanisation/developments, population increases, agricultural

activities and natural causes such as flooding, which vary from community to community, with agricultural activities and population growth being responsible for most of the losses across the landscape (Igu, 2017). Unlike the dense vegetation, the sparse vegetation gained more than what it lost in the two periods: 30.65% (2748.73 km^2) gain and 18.75% (1681.61 km^2) lost, and 24.37% (2446.22 km^2) and 22.20% (2227.97 km^2). The gain and loss in the second period are minimal. Eyoh and Okwuashi (2016) also recorded a 1.85% loss and 2.40% gain in their study between 1986 and 2016. Sparse vegetation could gain some loss from dense vegetation since any destruction of dense vegetation could also be because farming activities could contribute to the sparse vegetation gaining more in the two periods.

Although the mangrove lost more than it gained in the first period and gained more than it lost in the second period, the difference was small in the first period (11.33% gain and 11.44% loss). The difference between gain and loss is greater in the second period (12.12% gain and 8.89% lost). Only Eyoh and Okwuashi (2016) recorded a gain of 7.87% against the loss of 2.17% from mangroves in the Niger Delta. Sand dune lost more than what it gained in both 2002 and 2016. The loss of sand dunes in both periods is because beaches and pure sand bars are highly dynamic at short time scales (Kuenzer et al., 2014). Many of them were located in mangroves during the construction of massive oil facilities, such as the Warri refinery and pipelines in the Niger Delta, which have now been converted to either mangroves or built-up areas.

The spatial extent for gain and losses covering the entire period; 1987-2016 in Figure 7.9 shows that the built-up area gained more around Asaba (north-east), Warri (north-west), Yenegoa (central) and Port-Harcourt (south-east) of the Niger Delta. The reason is that Asaba, Yenegoa and Port-Harcourt are the state capitals of Delta, Bayelsa and Rivers states and are homes to many multinational oil companies. At the same time, Warri also hosts the Warri refinery. Other spatial locations of the remaining land cover gains and losses are shown in Figure 7.9a-f. The spatial extent of gains and losses could identify the exact location of land cover change to implement policies to mitigate land cover changes such as forest depletion.

7.4.6.2 Gains and losses: Normalised difference vegetation index analysis

While oil extraction activities have a devastating consequence on ecosystems, studies on the spatiotemporal monitoring of vegetation are scarce in the Niger Delta region.

Thus, the use of NDVI data to quantify the gains and losses over time is one method of monitoring land degradation, specifically in ascertaining the health and status of vegetation. In this study, the analysed NDVI data show that the vegetation in the Niger Delta from 1987-2016 has been significantly degraded. It only gained approximately 0.28 NDVI value in 2016 and lost approximately 0.44 within the same period. The degradation in the quality of vegetation is more severe around Warri-Sapele (northwest), the centre of the study area around Ughelli and the southwest around Port-Harcourt. The Niger Delta is home to many oil refineries and facilities, which results in gass flaring into the environment. The presence of oil refineries and oil wells could be one of the factors responsible for the high degradation of vegetation in the region.

7.4.6.3 Directions of land cover changes

While oil extraction activities have devastating consequences on ecosystems, studies on the spatiotemporal monitoring of vegetation are scarce in the Niger Delta region. Thus, the use of NDVI data to quantify the gains and losses over time is one method of monitoring land degradation, specifically in ascertaining the health and status of vegetation. In this study, the analysed NDVI data show that the vegetation in the Niger Delta from 1987-2016 has been significantly degraded. It only gained approximately 0.28 NDVI value in 2016 and lost approximately 0.44 within the same period. The degradation in the quality of vegetation is more severe around Warri-Sapele (northwest), the centre of the study area around Ughelli and the southwest around Port-Harcourt. The Niger Delta is home to many oil refineries and facilities, which results in gas flaring into the environment. The presence of oil refineries and oil wells could be one of the factors responsible for the high degradation of vegetation in the region.

7.4.6.4 Directions of land cover changes

The directions of land cover changes; the net contributor to changes in each land cover class could help to tell the conversion from one land cover class to another land cover type. This may be of interest to policy making in the Niger Delta since the net gains and losses and gross gains and losses did not give such information on interclass conversion. For sparse vegetation, dense vegetation is the most targeted land cover for the period, leading to the conversion of 2068.85 km^2 and 1840.11 km^2 in 2002 and 2016 of dense vegetation to sparse vegetation. Sparse vegetation is the major change driver for dense vegetation; the conversion could be due to clearing or felling trees for farming, illegal

lumbering, etc. Mangroves and water also targeted dense vegetation in the first period, while mangroves and built-up areas targeted dense vegetation in the second period. Similarly, sparse vegetation was the most targeted by dense vegetation in the same period, with 933.96 km^2 and 1011.55 km^2 of sparse vegetation converted to dense vegetation. However, the conversion from dense vegetation to sparse vegetation was more than twice in the first period and almost three times the conversion from sparse to dense vegetation in the second period. Other drivers of conversion from sparse vegetation in the first and second periods are bare soil and built-up land, 470.41 km^2 and 239.69 km^2 in the first period and 561.47 km^2 and 620.89 km^2 in the second period. The conversion from sparse vegetation to built-up is almost four times that of dense vegetation to built-up area (Table 7.7). The possible reason for the high rate of conversion from sparse vegetation to built-up land could be the ease of building houses and other infrastructure, which requires less clearing and the preparation of the land. The dense vegetation /forest is more difficult and costly to build on. The high conversion of sparse vegetation to bare soil indicates land degradation since they are areas with very little or no vegetation cover.

For mangroves, dense vegetation and water are the most targeted land cover in the first and second periods, leading to the conversion of 485.17 km^2 and 364.89 km^2 to dense vegetation and water, respectively. The conversion of mangroves to dense vegetation could result from the invasion of oil palm tree species since they were all classified as dense vegetation. The mangroves of the Niger Delta are endangered by the invasive Nipa Palm (Numbere, 2019a; Nwobi et al., 2020; Onyena & Sam, 2020).

Similarly, the second most targeted land cover in the first and second periods was dense vegetation and water. Other land cover conversions are shown in Table 7.7. Additionally, mangroves are the most targeted land cover by water in the first and second periods, with 339.19 km^2 and 448.05 km^2 converted to water. When mangroves die, most locations are converted to water since they are mixed with water.

From the maps of spatial conversion from 1987 to 2016 in Figure 7.11a-g, the conversions from dense vegetation to sparse vegetation are more intense and extensive around the northern part of the study area down to the central and south-eastern regions. The conversion from sparse vegetation also shows that the built-up area bare soil and dense vegetation cover the largest extent of the map Figure 7.11 d. The derived

nature/direction of changes map has provided the necessary information that could help in locating a particular place of interest for any land cover change programs.

7.4.7 Effect of oil extraction activities on land cover

7.4.7.1 The volume of oil spilt into land cover

From various studies, none has quantified the number of oil spills into the land cover in the Niger Delta. The high number of oil spills into the sparse vegetation (26.71% of the total oil spill) and the high volumes of oil spills into dense vegetation (27.80% of the total volume of the spill) will have a devastating effect on them and the inhabitant of Niger delta. The high conversion from sparse vegetation to bare soil could be because of the oil spill, which easily destroys the sparse vegetation leading to land degradation, unlike the dense vegetation, which is not easily affected by the oil spill. The oil spill's impact, especially on sparse vegetation, could have health implications for the human who consume food (especially vegetables) from such contaminated land. Sparse vegetation is highly cultivated in the Niger Delta. The spill could affect even the fruit from some dense vegetation, such as oil palm, mango fruit, etc. An oil spill-induced conversion of sparse vegetation to bare soil will expose the land to other environmental problems, such as soil erosion. Similarly, the mangrove, with the second-largest number of spill incidences (24.71%) and third-largest spill volumes, has caused the degradation of the mangrove despite the lack of net loss in its spatial extent for the period of the study. This called for an investigation to ascertain whether foods produced on such oil-contaminated land are safe for human consumption

7.4.7.2 Spatial analysis: impact of oil spills on vegetation

The responses of different vegetation types throughout 1987-2016 to the impact of oil spills and oil extraction activities in the Niger Delta differ. The result is the validation of the previous chapters, five and six, which looked at vegetation at leaf and plot scales using hyperspectral and satellite-derived normalised vegetation indices. The oil facilities in the Niger Delta are mostly located in the central Niger Delta, Southwest and Southeast. They are mostly located within dense vegetation, sparse vegetation, and mangrove. Only a few oil wells are in the northern part of the study area, with the oil spills mostly found along the oil pipelines. Most of the losses in dense vegetation are within oil spill, pipeline or oil spill hotspot locations. Some changes are from dense

vegetation to mangroves and bare soil in the southern part of the study area (Figure 7.13a). Although the loss of dense vegetation to mainly sparse vegetation and bare soil in the central part of the Niger delta is not particularly close to oil facilities, it may still result from oil extraction activities. Multidirectional water flow enables the spread of oil within the extensive tidal river network and mangrove swamps in the Niger Delta, which has become a persistent sink of oil that is redistributed instead of being removed (Obida et al., 2021). However, the changes from dense vegetation to mangrove and water in the south around Ijaw south are mostly within oil spill hotspots, pipelines and spills. The dense vegetation near the mangrove is more vulnerable to the impact of oil extraction activities, especially oil spills, since mangrove spills stay longer.

For most sparse vegetation, the loss toward the north of the study area is not close to oil facilities, hotspots, or spills (Figure 7.14). However, the loss to the bare soil around the central part of the Niger Delta is found close to the oil pipeline, unlike some losses in the southern part of the study area, which are farther away from the oil facilities. As a low-lying region, approximately 2 m to 4 m above sea level (Adamu 2016) with a flow direction from north to south, the vegetation south of the oil spills could be affected kilometres away from the spill location. In the rainy season, rivers, surface water and tributaries flow towards the Atlantic Ocean in the south just as the water table tilts towards the same direction, providing many opportunities for trapped oil to migrate freely along the southward flow direction without major restriction from inundated surfaces (Shittu, 2014). The losses of sparse vegetation to dense vegetation in the south-eastern study area are mostly near the oil spill hotspot, pipeline and spill location. The gain in sparse vegetation could result from the resistance of some sparse vegetation to the impact of oil spills, although there are some conversions to built-up. Among all the vegetation types, mangroves are the most vulnerable to the impact of oil extraction activities in the Niger Delta. The loss of mangroves to water and bare soil was mostly found close to oil pipelines, hotspots and spills (Figure 7.15a, b and c). Mangroves are extremely responsive to contamination by oil and industrial waste. Once oil and marine tar residues are deposited on or around mangroves, they stick to plant surfaces, absorbing to oleophilic surfaces of flora and fauna (Onyena & Sam, 2020). Oil exploration/exploitation activities affect Mangrove forests, and some portions have been converted to farmlands (TRCC, n.d.).

7.4.7.3 Land degradation due to oil extraction activities

Vegetation degradation is one of the consequences of oil extraction activities that affect vegetation health. This study shows that the vegetation in the Niger Delta has been highly degraded within the past 30 years. The gain from the NDVI values is just an average of 0.28, with just a few areas showing vegetation with values close to that. The major gains in NDVI, around the extreme northwest region of the study area, west of Sapele, especially the dense vegetation, as shown from the land cover map, have a few oil facilities, with oil pipelines and spills below it (Figure 7.15a). The proximity of the dense vegetation to water could have caused the gains. The mangrove between Yenogoa and Ijaw South also experienced gains within the pipeline and oils pills corridor. At the same time, the sparse vegetation did not show any appreciable gain, especially in the northwest and southeast of the study area around Ugelli and Opobo. The high losses in the NDVI are highly related to oil extraction activities, especially in the northwest, around Warri-Ugehelli, northeast, around Port-Harcourt and the central part of the Niger Delta, covered by dense vegetation and sparse vegetation. The losses are less intense in the mangrove. The study by Ayanlade and Howard (2017) NDVI shows that forests are mostly degraded, especially in the north-west and north-east part of the map, with lowland rainforest being degraded, which is more intense than freshwater swamp forests and mangroves.

7.5 Conclusion

Qualitative and quantitative spatiotemporal land cover change mapping was carried out in the Niger Delta using three-date satellite images and combining the data with oil extraction data to assess the impact of oil extraction activities on land cover changes at both temporal and spatial scales, specifically, the vegetation. From the six classifiers (Bayes, DT, Mahal, SOM, SVM and Unmix) tested, Mahal and Bayes's classifier performed best, with Bayes being less affected by mixed pixels. The land cover changes at the landscape scale and the effect of oil extraction activities on the observed changes was assessed using the best performing land cover mapping classifier, the Bayes classifier. While the results of land cover mapping were used to assess land cover changes in terms of conversions, the NDVI data were used to assess the degradation in vegetation. The research has provided valuable results that can be useful in mitigating the impact of oil extraction activities, especially vegetation, on the land cover in the Niger Delta. The summary of the results is as follows:

- The largest land cover is the dense vegetation, and the best performing classifier that meets both the statistical and visual accuracy is the Bayesian classifier (Bay), with an OA of 83.06%.
- The land cover in the Niger Delta, especially the dense vegetation (Forest), is under pressure mostly from the SV, including agriculture.
- The build-up has experienced a substantial increase for the two periods and has the largest net gain of 127.94%.
- Mangrove is more vulnerable to the impact of oil extraction activities in terms of conversion.
- Land cover and vegetation are affected by oil extraction activities in the Niger Delta, with many conversions from vegetation to no vegetation occurring in proximity to oil extraction activities.
- Where there has not been a conversion from other land cover types, the vegetation is highly degraded and influenced by oil extraction activities, as shown by the NDVI data.

There is an urgent need to restore vegetation before it deteriorates further. These results can be used to develop an intervention program to restore the quantity and quality of vegetation and take steps to mitigate the impact of oil spills, and conduct proper environmental impact assessments before siting any oil infrastructure or carrying out exploration activities.

Chapter 8 Synthesis and conclusions

8.1 Discussion

This research aimed to comprehensively characterise the impact of oil extraction activities on the land cover change in the Niger Delta at different scales using multispectral and hyperspectral remote sensing data. This study analysed the spatiotemporal oil spill hotspot and oil facilities hotspot, the relationships between oil extraction activities/facilities and the observed land cover changes in quality (degradation) and quantity (conversions from one land cover type to another) by integrating oil spill and facilities data with land cover change information derived from remote sensing. The general discussion summarised the main findings from the four objectives chapters (4, 5, 6, and 7), which addressed the following objectives and research questions.

8.1.1 Where and how frequently have oil spills occurred over the past 13 years, and where are the oil facilities located in the Niger Delta?

Since the oil discovery, environmental pollution from oil exploration and exploitation has plagued the Niger Delta region for over five decades (Umar et al., 2019). Oil spills and resultant land contamination have destroyed rural economies and social livelihood in the Niger Delta, and due to the inadequacy of the oil companies, together with the destruction of livelihood, led the people to vandalise and steal from the oil infrastructure as a way of obtaining compensation (Sam, 2016). To achieve the aim of this thesis, the first objective was to examine the spatiotemporal evolution of oil spill hotspots from 2007-2019 and oil facility hotspots in the Niger Delta using spatial statistic hotspot analysis. The Gestis-Ord General G and The Getis-Ord Gi* local statistic a were used to examine the spatiotemporal evolution of oil spills from 2017 to 2019 in the Niger Delta, while the oil facilities hotspot map was produced using Kernel Density Estimation in chapter 4**.** Understanding the historical and geographical distribution of oil spills will help in adopting an appropriate remediation strategy and prevent further spills in the area (Umar et al., 2021). Detecting oil spills also forms the basis for establishing the total area affected by oil pollution, facilitating remediation efforts and recovery after oil spills, and monitoring the impacts of oil pollution on plant life (Ozigis et al., 2019).

- Where and how frequently have oil spills occurred over the past 13 years?

The oil spills in the Niger Delta are located along the oil pipelines spread across the study area. This is not surprising since the sabotage of oil pipelines is the major cause of oil spills in the Niger Delta. Between 2007 and 2019, the average annual oil spill incidents were approximately 586. However, May and November recorded the highest number of oil spills within the study period in many years, while April had the lowest number of oil spill incidents in the Niger Delta. The year 2014 was the worst year for oil spill incidence in the Niger Delta, while 2007 recorded the fewest spills, according to the NOSDRA. However, the incidence of oil spills in the Niger Delta decreased after the peak year in 2014. Nevertheless, the frequency of oil spills is high and will adversely affect the environment and land cover changes

From the consistent oil spill hotspot map, the location in the southern part of the study area, around Ijaw south, has a more consistent hotspot for seven years along a major pipeline, while Ahoada-Omoku, in the south-eastern part has a consistent hotspot of up to six years. These results agree with Obida et al. (2018), whose results show that the southern Ijaw-Nembe-Brass axis of the pipeline is by far the most contaminated area in terms of oil spill intensity based on the oil spill volume due to it remote and inaccessible location, making policing a hard task. Incidentally, unlike Ahoada-Omoku, which primarily falls within the medium and high density of oil wells and pipelines, Ijaw south, with the most consistent oil spill hotspot, falls within the low density of oil wells and pipelines. Also, the mangrove close to the sea makes it difficult for the activities of the oil pipeline vandal to be spotted.

The oil spill incidence may continue to occur in the Niger Delta; the extent of occurrence will depend on the peace and stability in the region since most of the oil spills are caused by sabotage. This study has answered some questions, such as the spatiotemporal pattern of oil spill concentrations and the frequencies. This provided information that could help mitigate the oil spill due to sabotage. The security agencies could prioritise their surveillance around hotspots by sabotage, accounting for 81% of oil spill incidents in the study area between 2007 and 2019. From the autocorrelation of annual spills, 2013 and 2015 have the most clustered oil spill incidences, while 2019 has the most random spill incidence despite 2013 having the highest number of oil spill incidents. Additionally, the spatiotemporal pattern of oil spill hotspots in the Niger Delta is

inconsistent in most locations throughout the year, which shows how dynamic the vandal activities are.

- Where are the oil facilities located in the Niger Delta?

The three states of the traditional Niger Delta, namely Bayelsa, Rivers, and Delta, have the highest number of oil spill occurrences and oil facility distributions (Umar et al., 2019), accounting for 88% of recorded oil spills in Nigeria from 2007-2019. The implication is that the land cover, especially the vegetation, is the most affected by oil extraction activities in these states. The oil facilities, pipelines and wells are distributed across the study area. The oil pipeline network is extensive, covering almost the entire extent, except for the northern part of the study around Agbor and Asaba. These towns are not oil-producing areas of the Niger Delta, hence, the lack of pipeline networks. The oil well also follows the same pattern as the oil pipelines, spread across the study area except for the north. For the density of oil facilities, i.e., the oil pipeline and well, Ahoada and Omoku, southeast of the study area, have the densest oil pipeline and oil wells, which is also the location with the most consistent oil spill hotspots. These locations require a comprehensive land cover study to assess the impact of oil extraction on vegetation. The result of the hotspot analysis also provided data for further analysis in chapter 7 to assess the impact of oil spills on land cover changes (conversion and degradation).

8.1.2 What are the responses of plant types to various concentrations of soil hydrocarbon properties?

The Niger Delta region has experienced petroleum hydrocarbon contamination of different magnitudes for several decades, making the soil highly hydrocarbon-contaminated, toxic and unproductive in some cases. The presence of TPH in soil may affect vegetation and other soil properties, such as the level of toxicity (EC50) and total organic content (TOC%) in the soil, which could affect the health conditions of different plant types. Plants depend mostly on soil quality for growth and survival. Oil seepage influences the soil and the vegetation around hydrocarbon seeps (Omodanisi & Salami, 2014). To achieve the aim of this thesis, the second objective was to analyse the impact of soil hydrocarbon parameters (SHP):Total petroleum hydrocarbons(TPH), Microtox (EC50 mg L^{-1}) and Total Organic Carbon (TOC (%)) on the health of plant types at the leaf scale using hyperspectral vegetation indices (HVIs). The red edge parameters and

four hyperspectral vegetation indices HVIs were used to determine each plant's spectral response to SHPs using Spearman's and Pearson's correlation analysis. It was done to test the hypothesis that various plant types are affected by the SHPs, leading to reduced leaf chlorophyll content in plant families. From the results, the responses of spectral reflectance of plant types to various concentrations of soil hydrocarbon properties differ from individual plant types. Spectral reflectance is a source of information on vegetation's chemical-physical status and physiological properties (Piro et al., 2017). The results show that TPH most impacts the mangrove. Most reported oil spillages have occurred in the mangrove swamp forest in the Niger Delta (Kadafa, 2012a), and even those that occurred on land sometimes get washed into the mangrove. Mangroves are the most vulnerable to large-scale and chronic oil spills (Onyena & Sam, 2020), mainly because spilt oils are stored in the soil and rereleased annually during inundation (Adelana & Adeosun, 2011). Hydrocarbon has been trapped in mangroves for many years and remains circulating by waves and currents since the mangroves are in the water. However, the Mango is the most tolerant among all the plant types to TPH. Being a larger plant, Mango could withstand the oil spill's impact more than the mangrove and other plant types.

On the other hand, oil palm is the plant most affected by the amount of soil toxicity, followed by elephant grass. Interestingly, mangroves and mangoes are the most tolerant to the impact of soil toxicity and are positively correlated. Mangroves are trees or large shrubs that have adapted to harsh environmental conditions and have developed unique survival features (Onyena & Sam, 2020). Due to oil extraction activities, pollutants from industrial waste have been trapped in mangroves for many years, making them tolerant to the impact of pollutants despite having a higher toxicity concentration than the land where the mango plants were located.

Additionally, Mango is the most affected by TOC (%), having a higher negative correlation, while Awolowo is the least affected. The implication is that mangoes can survive on soil without many soil nutrients, unlike Awolowo grass. The plant needs TOC (%), which is not harmful, unlike the hydrocarbons and pollutants present in the soil. Having information on plant-specific responses to the impact of soil hydrocarbons could help understand how each plant is tolerant to the impact of oil extraction and other soil parameters.

This result has shown that TPH does not significantly correlate with TOC (%) and toxicity in the soil in the Niger Delta. Each plant responds differently to the impact of soil hydrocarbon parameters. This result is important to the government and other stakeholders interested in restoring the environment affected by the oil spill in the Niger Delta. For instance, the mango tree could be used in the locations that have been affected by the oil spill, which has killed some trees that are not tolerant of the impact of THH. The tolerance of mangroves to toxicity also means that they can survive in the Niger Delta despite being the most vulnerable to TPH.

8.1.3 What is the effect of oil on the health of different types of plants?

The impacts of hydrocarbon seepage pollution in vegetation are reducing the plant transpiration rate, levels of chlorophyll content, higher levels of foliar water content and leaf structural changes (Susantoro et al., 2018). Hence, the need to investigate the effect of spill volume and time gap after oil spills on vegetation health and how health changes over a period spanning before and after the occurrence of spills by way of the NDVI for dense vegetation, mangrove vegetation and sparse vegetation. To achieve the aim of this thesis, the third objective was to assess the effects of oil spills on the health of different vegetation types at the plot scale using satellite-based Normalised Difference Vegetation Index (NDVI) from Landsat data. Regression analysis was carried out to determine the impact of oil spill volume, the time gap between oil spills and image acquisition date on vegetation health as indicated by NDVI values. For the temporal monitoring of vegetation health, a student's paired t-test was used to compare the change in NDVI values from spill sites with values from non-spill sites for all sites combined and for each spill site for several years. It was done to determine each vegetation type's response after being subjected to oil spills and to help understand the effect of time on vegetation health recovery.

From the results, different vegetation types respond differently to the oil spill volume, and the time interval between the oil spill dates affects them. When all the spill volumes were used, the relationship between the NDVI and the volume of oil spills was weak for all the vegetation types, with the highest R^2=0.0108 for mangroves. These results show a weak or no relationship and agree with Adamu et al. (2016), with R^2=0.0001 when all spill volumes were used. The dense vegetation responded more to oil spill volumes above 1000 bbl (R^2=0.4356), and sparse vegetation responded more to oil spill volumes between 400 and 1000 bbl (R^2=0.5018). In contrast, the mangrove vegetation has the

weakest relationship at a volume between 225 and 400 bbl with R^2=0.0748), although it has a strong inverse relationship within 401 to 1000 bbl with $\underline{R^2}$=0.452. This result differs from Adamu et al. (2016), which had a positive R^2=0.5944. The lack of oil spill volume impact on the mangrove does not indicate that the oil spill does not impact the mangrove. The possible reason is the dynamic nature of the location of the mangrove in the water bodies, which makes it difficult to quantify the volume of the oil spills. When oil spills into the mangrove, it could propagate to places with less or without oil spills. Also, the constant exposure of mangroves from oil spills from the land, which gets washed into the mangrove, could contaminate the mangrove site not, which may make it have more volume of the spill than what was originally spilt. It can be observed from the leaf scale that the health condition of the mangrove was the most affected among all plant types when the hydrocarbon was correlated for each sample site for the mangrove. Studying the oil volume's impact on mangroves from the plot scale might not give the best result.

In terms of the influence of time after the oil spill on the vegetation, a weak relationship exists for all the vegetation. However, the oil spill's effect was more visible within 90 days for both sparse vegetation and mangrove vegetation than for dense vegetation. Depending on plant species and hydrocarbon type, chlorophyll may decrease differently in polluted hydrocarbon environments (Serrano-Calvo et al., 2021). The results by Adamu et al. (2016) showed a general decrease in the NDVI values of mangroves in the first year, which implied the impacts of oil pollution on vegetation. Still, the NDVI values increased after a year, which implies vegetation recovery.

Similarly, the comparison results of all the changes in NDVI values of SS and CS show a highly significant difference between the change in NDVI values before and after the spill for sparse vegetation and mangrove vegetation and a very significant difference for dense vegetation. The dense vegetation is less affected by the impact of oil spills, as indicated by the significance level. The results agree with some authors. For example, the results by Onyia et al. (2018) show a significant difference in vascular plant species richness and diversity from non-polluted and oil-polluted vegetation in the Niger Delta. Similarly, Adamu et al. (2018) also show a significant difference between vegetation at the spill site and non-spill sites in mangrove vegetation in the Niger Delta. From the statistical analysis comparing the difference between changes in NDVI values for each SS and CS at different oil spill volumes, the impact of oil spills on the health condition

of dense vegetation is less significant, with only one site having a *p*-value <0.05 (SSD1 at spill volume 280 bbl). The impact of oil spills on health conditions is greater on sparse vegetation and mangrove vegetation at various spill volumes, with sparse vegetation being the most impacted, with five out of eight locations having very significant differences (at volumes 260, 802.5 and 1500 bbl) and significant (at volumes 228 and 1000 bbl) impacts on their health conditions, respectively.

In summary:

- The volume and time after spills have different effects on the vegetation types in the Niger Delta, with dense vegetation responding to the impact of oil spills at a higher volume than sparse vegetation and mangrove vegetation.
- The impact of the oil spill is felt within the first 90 days after the spill for sparse vegetation and mangrove vegetation.
- There is a significant difference in the change in NDVI values between SS, with their corresponding CS, with sparse vegetation being the most affected and dense vegetation being the least affected.

The next discussion will provide more information in map form about the impact of oil extraction on vegetation at the landscape scale, conversion, and degradation.

8.1.4 What are the observed pattern of land cover changes and what land cover types are more affected by extraction activities in the Niger Delta?

Monitoring the locations and distributions of land cover changes is vital for establishing links between policy decisions, regulatory actions and subsequent land use activities (Ahmad, 2012). In the Niger Delta, more than 1000 km^2 of land has been contaminated by oil pollution, with broadleaved forest, mangroves and agricultural land being the most impacted land cover types (Obida et al., 2018). The land cover in the Niger Delta has undergone many changes over the past 30 years due to the construction of oil facilities and oil spills. The objective of this chapter was to test different classifiers and choose the best-performing classifier to map the land cover changes at the landscape scale using multispectral Landsat data and integrate oil extraction activities data to determine their effect on the observed land cover changes. Six different combined soft and object-based classifiers were used to map land cover classes in the Niger Delta using the 2006 Landsat image to determine the best classifier that would satisfy both statistical

and visual accuracy. The classification results show that Bayclass performed better than the other classifiers. The accuracy improved after post-classification correction, and the Bayclass was used for land cover mapping of the two satellite images and change detection.

Many factors were identified during the land cover classification that affects land cover mapping in the Niger Delta using a medium-resolution image, such as Landsat. From all six classifications, it was discovered that the problem of land cover mapping in the Niger Delta goes beyond mixed pixels. Rather, the main problem was what Nababa et al.(2020) described as spectral similarities in the land cover types. The built-up area has spectral similarities with the bare soil, sand dunes and even water bodies affected by oil spills. However, despite the effect such spectral similarities have on the land cover in the Niger Delta, no author has taken any step to reduce its impact on the accuracy of land cover classes in the Niger Delta. For this thesis, the problem of spectral similarities was reduced through post-classification analysis. The correct land cover class was manually edited to improve the visual and statistical accuracy with 1.5% and 1.24% in the 2016 and 1987 Bayclass maps, respectively. Although the effect on the accuracy was small, the visual accuracy improved greatly. The overall improvement in the classification accuracy of the land cover maps through post-classification analysis is significant in their potential use for land change modelling (Manandhar et al., 2009).

The result of land cover change mapping shows different patterns of land cover changes: from 1987-2016, there was a net increase of 1.58% by water, 127% by built-up land, 14.33% by sparse vegetation, 3.22% by mangroves and 28.21% by bare soil, with a decrease of 17.60% by dense vegetation. The astronomical increase in built-up area points to the fact that more infrastructure has been built, including oil facilities, in the past 30 years in the Niger Delta, while the loss of dense vegetation and the increase in sparse vegetation and bare soil is a pointer that the forest in the Niger Delta is being destroyed. The forest is very important to the region because it is a source of food, a habitat for various types of animals, etc. Generally, vegetation is the most affected by oil extraction activities. The most affected land cover by oil spill volume and the numbers of spills are dense vegetation and sparse vegetation, respectively. Similarly, land degradation in dense and sparse vegetation is highly related to oil extraction activities, especially in the northwest, around Warri-Ugehelli, northeast, around Port-Harcourt and the central part of the Niger Delta, unlike the mangrove. The proximity of

the vegetation to oil facilities caused great damage to them in the form of destruction or degradation.

8.1.5 At what scale (i.e., leaf, plot, landscape) are these effects manifested?

The effect of oil extraction affected the land cover differently on a different scale. The vegetation grouping for the plot and landscape scale differs from the leaf scale except for the mangrove. At the leaf scale, the oil spill's impact is more manifested on the mangrove vegetation/plant, while the impact is more manifested on sparse vegetation at the plot scale. The difference in vegetation most affected by oil spill between the leaf and plot scale could be because more than one species are included in sparse vegetation at the plot scale. For example, Awolowo and Elephant grass etc., are jointly called sparse vegetation, with different levels of resistance to the impact of oil spills within the 30 by 30-metre pixels of the Landsat image. Similarly, the same reason stated in section 8.1.3 could be the major reason why the mangrove seems not impacted by oil spill volumes at the plot scale

For the impact of oil at the landscape scale, dense vegetation is the most affected land cover type in terms of oil spill volume, followed by sparse vegetation and mangrove. In contrast, sparse vegetation is the most affected land cover, followed by mangrove and dense vegetation in terms of the number of oil spill incidences. Obida et al. (2018) also reported broadleaved tropical rainforest (dense vegetation) as the most contaminated land cover type in terms of oil spill volume, followed by mangroves and cropland (sparse vegetation), which agree with dense vegetation for this research. The difference in results for sparse and mangrove vegetation could be attributed to the difference in the spatial extent of the study area. In general, vegetation is the most affected land cover by the oil extraction activities in the Niger Delta, with over 70% of oil spilt in terms of incidence and quantity (volume).

Similarly, the impact of oil extraction is manifested in all the vegetation types at the landscape scale. The conversions to non-vegetation land cover are within oil extraction activities, especially the dense and sparse vegetation. The degradation in vegetation is more manifest in dense and sparse vegetation than in the mangrove, mostly found around oil extraction activities. Compared to the plot scale, the oil spill's impact on the mangrove manifests more at the landscape scale. The reason stated in section 8.1.3 (i.e. the dynamic nature of the mangrove, which is located in the water body, makes it

difficult to assess the impact of oil spill volume on it since an oil spill in a particular location could propagate to other locations). The multi-scale characterisation of the impact of oil extraction on land cover change, especially the vegetation, has provided information on how each vegetation is affected by the impact of oil extraction activities in the Niger Delta.

In summary, oil extraction activities contribute to land cover changes in the Niger Delta both in quantity(conversions) and quality (degradation). Land cover changes and conversion from dense, sparse, and mangroves are close to oil spill hotspots, locations, and facilities. The spatial analysis between observed changes from NDVI and oil extraction activities shows that the quality of the vegetation in the Niger Delta from 1987-2016 has degraded.

While land cover mapping, it was discovered that:

- Object-based land cover classification using optical medium resolution satellite images such as Landsat in the Niger Delta is unsuitable for mapping land cover classes.
- The spectral similarities of land cover classes make soft classifications unsuitable for mapping land cover such as the Niger Delta.

The problem of spectral similarities among the land cover classes: dense vegetation and mangrove, bare soil, sand dune and built-up etc., was reduced through post-classification analysis, and it is recommended for future land cover mapping in the Niger Delta.

8.2 The implication of the results

Like any production activity, oil extraction activities have a lot of implications for the health of the inhabitants of the Niger Delta. The quality of vegetation that has been degraded and killed means the Niger Delta will be more vulnerable to environmental disasters such as flooding, global warming, etc., due to vegetation's role in providing habitat, converting solar energy to biomass, and being a source of oxygen etc.

The spatiotemporal evolution of the oil spill hotspots means that the land cover will be affected differently depending on the consistency of the oil spills at a particular place. For those locations with less consistent oil spill hotspots, the land cover, especially the

vegetation, might recover more quickly. In contrast, those locations with more consistent spills may either die (depending on the types of vegetation or plant types), degrade or develop resistance to the impact of oil spills depending on the impacted area size, spilt oil volume, residual oil volume on-site, impacted area environment, and response, recovery, and clean-up. The degradation of mangroves from oil contamination and high toxicity in the soil will affect the quality of flora and fauna, which are sources of food for the region's inhabitants. The food from the contaminated and toxic mangroves could have health implications for the inhabitant.

Similarly, the loss of forests and the astronomical increase in the built-up areas is not sustainable in the long run due to its part in the carbon cycle. The stakeholders in the Niger Delta have to formulate policies to reduce the rate at which the dense vegetation is being destroyed. At the same time, the little increase in mangroves shows that some are recovering from the oil spill's impact, which could restore some of the lost species that live in mangroves though some have suffered irreversible damage. The result of this research can help policymakers make policies that could alleviate the impact of oil spills on the environment.

8.3 Limitations

Although this research has achieved its aims, some limitations affect the studies in one way or the other.

- For the analysis of oil spill hotspots and the spatial analysis of oil facilities, the oil spill data are from 2007, which did not cover the same land cover change modelling period. The oil well map was produced in 2007, which may not include some current oil facilities. Many oil spill data were not complete, spill data without coordinates made them unusable, and in most cases, the cause of the spill was not recorded. These challenges could affect the analysis.
- To determine the effect of soil hydrocarbon properties on vegetation: Leaf Scale, access to sample collection sites was limited due to security challenges. Samples were collected only from locations the locals were willing to allow access to, which made the samples collected in River's state only instead of the three states covering the study area. Additionally, there were no data on chlorophyll in the

leaf samples to validate the potency of the HVIs. The chlorophyll of the leaf sample would have enabled the validation of the suitability of HVIs in detecting the impact of soil hydrocarbon properties on different plant species.

- For monitoring the impact of oil spills on vegetation at the plot scale using the normalised difference vegetation index (NDVI), most satellite derived NDVIs have Landsat GAP errors and cloud cover, limiting the temporal analysis of the impact of oil spills on vegetation. Additionally, some oil spill data used lack the oil spill volume attribute.
- Cloud cover and spectral similarities were limitations for land cover change modelling, although they have already been mentioned in chapter seven. Data on gas flaring and illegal oil refineries were not available to determine their effect on land cover changes. The absence of socioeconomic data on farming activities and lumbering could affect land cover change modelling.

8.4 Future work and replication of the study

This study could be applied to the whole state in the Niger Delta and other oil spill-impacted locations worldwide. Therefore, future research should focus on the following.

- The oil spill hotspot analysis should include the volume of spills. It could help better understand the impact of oil spills on land cover changes. Unlike the oil spill point, the volume, depending on topography and proximity to the water body, could travel a longer distance from the spill point, affecting vegetation kilometres away from the oil spill point. Some of the observed changes in the land cover, far away from oil-extracted activities, might have been affected by the propagated oil spill that travelled from the spill point.
- A field chlorophyll measurement should accompany the spectral measurement of the leaf sample to validate the HVI in future studies, which could also be used to develop plant specific HVIs in the Niger Delta. Additionally, plant DNA should be used to determine the level of tolerance and resistance that some plants might have developed to the impact of hydrocarbons, especially for plants exposed to continuous hydrocarbon contamination for several years.
- Some observed changes not close to the oil extraction could result from other activities. For instance, an illegal oil refinery could cause environmental damage than spills from known oil facilities. The activities of illegal refineries are not

regulated and cause soot (a mass of impure carbon particles that result from the incomplete burning of hydrocarbons, especially from illegal refineries and gas flaring), which also affects the vegetation. This variable could also have some impact on the land cover. Therefore, socioeconomic data, gas flaring locations, and illegal oil refinery data should be used to model their impact on land cover changes.

- Higher-resolution satellite images should be explored for land cover mapping to minimise spectral similarities in the Niger Delta. Similarly, RADAR sensors can be used for land cover mapping to overcome the cloud problem, although the temporal resolution is low compared to the Landsat archives. Another alternative is using a hyperspectral satellite image (Hyperion), especially for determining the effect of oil spills on vegetation at plot scale and land cover mapping to overcome the problem of cloud cover. It offers more spectral bands than Landsat, which could be used to develop satellite-based Hyperspectral Vegetation indices(HVIs). But the problem is that it has a low temporal resolution and the same spatial resolution as Landsat. Also, it might not be suitable for land cover mapping of a large area like the Niger Delta due to its standard scene having a width of 7.7 kilometres and a length of 42 kilometres.
- A study on the impact of oil spills on the land surface temperature, especially the vegetation in the Niger Delta, should be carried out. The derived surface temperature map can be integrated with oil extraction data and NDVI map to determine the influence of oil extracted on the surface temperature of vegetation.

The success of this research could be replicated to study the impact of both natural and manmade environmental factors. Among them are:

- Characterisation of the impact of climate changes on the land cover change or land degradation, especially vegetation in North East Nigeria or any part of the world facing desertification. The rainfall and temperature data could be used instead of the oil spill data to correlate them with the vegetation map health map (e.g. NDVI) and urban heat island to determine the extent of their relationship.

- The impact of mining activities such as gold and coal mines on the land cover changes at leaf, plot and landscape scale. The soil sample could examine the

amount of lead and other toxic substances and how that impacts the vegetation's health. The NDVI of vegetation near the mine could be analysed as well, and the land cover change map would reveal general changes in the land cover around the mine.

8.5 Conclusion

The oil extraction activities in the Niger Delta have impacted the land cover through oil spills, clearing and destroying the vegetation to construct oil facilities such as pipelines and oil wells. This research has characterised the impact of oil extraction activities on land change, especially the vegetation in the Niger Delta at multi-scale levels. The land cover, especially the vegetation in the Niger Delta, is seriously affected by oil extraction activities. All three vegetation studies show that oil spill extraction activities affect land cover, especially vegetation.

The results of the oil spill hotspot show that 88% of oil spill incidences in Nigeria occurred in the traditional Niger Delta: Bayelsa, Rivers, and Delta states, with highly statistically significant oil spill clusters and oil facilities on some parts of the Niger Delta.

For leaf-scale analysis, among the plant species/types, mangroves are the most affected plant by the impact of hydrocarbons and toxicity in the Niger Delta, while Mango is the most tolerant plant to TPH. The oil palm trees are the most tolerant to soil pollutants. Additionally, Mango can withstand a harsher environment than the other plant types in the Niger Delta by growing even on soil with low total organic carbon, unlike Awolowo grass. However, for monitoring the impact of oil spills at the plot scale using vegetation groups instead of plane species, sparse vegetation is the vegetation type most affected by the volume of spill and the time it takes to recover from an oil spill. The sparse vegetation includes the Awolowo grass and the Elephant grass.

The land cover change detection shows that dense vegetation (natural forest) is continuously depleting, while the built-up areas are experiencing a significant increase. This is important because the natural forest serves as a home to diverse wildlife, trees, etc. The economic importance of such forests to the inhabitants of the Niger Delta cannot be overemphasised. There is a need for stakeholders to design a program to mitigate the depletion of forests through afforestation.

Last, to minimise the problem of spectral similarities on the classified map, post-classification cleaning is recommended. This research could help address the environmental problems in the Niger Delta, such as land pollution, degradation and land cover change, prioritising programs such as oil spill cleans up or remediation, among others.

References

Abam, T. K. S. (1999a). Impact of dams on the hydrology of the Niger Delta. *Bulletin of Engineering Geology and the Environment*, *57*(3), 239–251. https://doi.org/10.1007/s100640050041

Abam, T. K. S. (1999b). Modification o f Niger Delta physical ecology : the role of dams and reservoirs. *Hydro-Ecology: Linking Hydrology and Aquatic Ecology (Proceedings of Workshop IIW2 Held at Lïinuinallam. UK. July 1999). I AI IS Publ. No. 266.2001*, (2).

Abam, T. K. S. (2001). Perspectives de la recherche hydrologique régionale dans le delta du Niger. *Hydrological Sciences Journal*, *46*(1), 13–25. https://doi.org/10.1080/02626660109492797

Abbas, I. I. (2012). An Assessment of Land Use/Land Cover Changes in a Section of Niger Delta, Nigeria. *Frontiers in Science*, *2*(6), 137–143. https://doi.org/10.5923/j.fs.20120206.02

Abbasi, M., Darvishsefat, A. A., & Schaepman, M. E. (2010). Spectral reflectance of rice canopy and red edge position (REP) as indicator of high-yielding variety. *International Archives of the Photogrammetry, Remote Sensing and Spatial Information Sciences - ISPRS Archives*, *38*(January), 1–5. https://doi.org/10.5167/uzh-38633

Abdullah, H., Darvishzadeh, R., Skidmore, A. K., Groen, T. A., & Heurich, M. (2018). European spruce bark beetle (Ips typographus, L.) green attack affects foliar reflectance and biochemical properties. *International Journal of Applied Earth Observation and Geoinformation*, *64*(July 2017), 199–209. https://doi.org/10.1016/j.jag.2017.09.009

Adamu, B. (2016). *Broadband multispectral indices for remote sensing of vegetation affected by oil spills in the mangrove forest of the Niger Delta , Nigeria.Thesis submitted for the degree of Doctor of Philosophy at the University of Leicester*. University of Leicester.

Adamu, B., Tansey, K., & Ogutu, B. (2015). Using vegetation spectral indices to detect oil pollution in the Niger Delta. *Remote Sensing Letters*, *6*(2), 145–154. https://doi.org/10.1080/2150704X.2015.1015656

Adamu, B., Tansey, K., & Ogutu, B. (2016). An investigation into the factors influencing the detectability of oil spills using spectral indices in an oil-polluted environment. *International Journal of Remote Sensing*, *37*(10), 2338–2357. https://doi.org/10.1080/01431161.2016.1176271

Adamu, B., Tansey, K., & Ogutu, B. (2018). Remote sensing for detection and monitoring of vegetation affected by oil spills. *International Journal of Remote Sensing*, *39*(11), 3628–3645. https://doi.org/10.1080/01431161.2018.1448483

Adedeji, O., Ibeh, L., & Oyebanji, F. (2011). Sustainable Management of Mangrove Coastal Environments in the Niger Delta Region of Nigeria: Role of Remote Sensing and GIS. *Proceedings of the Environmental Management Conference, Federal University of Agriculture, Abeokuta, Nigeria*, 308–326. Retrieved from http://journal.unaab.edu.ng/index.php/COLERM/article/view/251

Adelana, S., & Adeosun, T. (2011). Environmental pollution and remediation: challenges and management of oil Spillage in the Nigerian coastal areas. *American Journal of Scientific and Industrial Research*, *2*(6), 834–845. https://doi.org/10.5251/ajsir.2011.2.6.834.845

Adeniji, A. O., Okoh, O. O., & Okoh, A. I. (2017). Petroleum hydrocarbon fingerprints of water and sediment samples of buffalo river estuary in the Eastern Cape Province, South Africa. *Journal of Analytical Methods in Chemistry*, *2017*. https://doi.org/10.1155/2017/2629365

Adoki, A. (2013). Trends in vegetation cover changes in Bonny area of the Niger Delta Trends in vegetation. *J. Appl. Sci. Environ. Manage.*, *17*(March), 89–103.

Afify, H. A. (2011). Evaluation of change detection techniques for monitoring land-cover changes: A case study in new Burg El-Arab area. *Alexandria Engineering Journal*, *50*(2), 187–195. https://doi.org/10.1016/j.aej.2011.06.001

Agbonifo, P. (2016). Oil Spills Injustices in the Niger Delta Region: Reflections on Oil Industry Failure in Relation to the United Nations Environment Programme (UNEP) Report. *International Journal of Petroleum and Gas Exploration Management*, *2*(1), 26–37.

Aghalino, S. O. (2000). British Colonial Policies and the Oil Palm Industry in the Niger

Delta Region of Nigeria, 1900-1960. *AFrican Study Monographs*, *21*(1), 19–33.

Ahmad, F. (2012). Detection of change in vegetation cover using multi-spectral and multi-temporal information for district Sargodha, Pakistan. *Sociedade & Natureza*, *24*(3), 557–571. https://doi.org/10.1590/S1982-45132012000300014

Ahmad, P. T., Sinha, P. D. K., & Chakraborty, P. P. P. (2019). *GEOLOGY Module : Remote Sensing Platforms and Sensors Table of Content GEOLOGY Module : Remote Sensing Platforms and Sensors*. (January). Retrieved from https://www.researchgate.net/publication/330212930_Remote_Sensing_Platforms_and_Sensors

Ahmad, W. A., Ahmed, M. A., & Al-sharia, G. H. (2017). Using normalized difference vegetation index (NDVI) to identify hydrocarbon seepage in Kifl Oil Field and adjacent areas South of Iraq. *Journal of Environment and Earth Science*, *7*(1), 16–27. Retrieved from www.iiste.org

Ajayi, O. G., Palmer, M., & Salubi, A. A. (2018). Modelling farmland topography for suitable site selection of dam construction using unmanned aerial vehicle (UAV) photogrammetry. *Remote Sensing Applications: Society and Environment*, *11*(March), 220–230. https://doi.org/10.1016/j.rsase.2018.07.007

Ajayi, O. G., Salubi, A. A., Angbas, A. F., & Odigure, M. G. (2017). Generation of accurate digital elevation models from UAV acquired low percentage overlapping images. *International Journal of Remote Sensing*, *38*(8–10), 3113–3134. https://doi.org/10.1080/01431161.2017.1285085

Akani, G. C., Luiselli, L., & Politano, E. (1999). Ecological and conservation considerations on the reptile fauna of the eastern Niger Delta (Nigeria). *Herpetozoa*, *11*(3/4), 141–153.

Akpoborie, O. O., & Akporhonor, I. A. (2008). Bioline International Official Site (site up - dated regularly) The Oil and Gas Industry and the Niger Delta : Implications for the Environment. *Journal of Applied Sciences and Environmental Management*, *Vol. 12*(No. 3), 29–37.

Aksoy, B., & Ercanoglu, M. (2012). Landslide identification and classification by object-based image analysis and fuzzy logic: An example from the Azdavay region

(Kastamonu, Turkey). *Computers and Geosciences*, *38*(1), 87–98. https://doi.org/10.1016/j.cageo.2011.05.010

Akujuru, V. A. (2014). *A framework for determining the compensable value of damages due to contamination to wetlands in the Niger Delta of Nigeria, A Thesis submitted in partial fulfilment of the requirements for the award of the Degree of Doctor of Philosophy of the University*.

Al Fugara, A. M., Pradhan, B., & Mohamed, T. A. (2009). Improvement of land-use classification using object-oriented and fuzzy logic approach. *Applied Geomatics*, *1*(4), 111–120. https://doi.org/10.1007/s12518-009-0011-3

Alagoa, E. J. (2005). *A History of the Niger Delta. an Historical Interpretation of Ijo Oral Tradition*. Port Harcourt: Onyoma Research Publications.

Alinnor, I. J., & Nwachukwu, M. a. (2013). Determination of total petroleum hydrocarbon in soil and groundwater samples in some communities in some communities in River State, Nigeria. *Journal of Environmental Chemistry and Ecotoxicology*, *5*(11), 292–297. https://doi.org/10.5897/JECE2013.0298

Amani, M., Salehi, B., Mahdavi, S., Masjedi, A., & Dehnavi, S. (2017). Temperature-Vegetation-soil Moisture Dryness Index (TVMDI). *Remote Sensing of Environment*, *197*, 1–14. https://doi.org/10.1016/j.rse.2017.05.026

Amasuomo, T. A., & Japo, O. (2016). Improving Durability of Rural Buildings in Riverine Niger Delta Region: a Case Study on Need To Utilize Appropriate Technology. *International Journal of African Society, Cultures and Traditions*, *4*(1), 17–43.

Amevor, R. (2016). *Renewed militancy exacerbates the complex peace process in the Niger Delta* (12 October). 12 October. Retrieved from https://www.iiss.org/en/iiss voices/blogsections/iiss-voices-2016-9143/october-d6b6/niger-delta-militancy-72c9

Amini Parsa, V., & Salehi, E. (2016). Spatio-temporal analysis and simulation pattern of land use/cover changes, case study: Naghadeh, Iran. *Journal of Urban Management*. https://doi.org/10.1016/j.jum.2016.11.001

Amiri, A. M., Imaninasab, R., & Nadimi, N. (2018). Hotspot Identification in an Urban

Network: A Comparison Among Four Different Techniques Transportation Equity Calculation View project Impact of different factors on popularity of public transit among women in Tehran View project. *Transportation Research Board 97th Annual Meeting*, (January), 1–19. Retrieved from https://www.researchgate.net/publication/333261531

Ana, K. F. V., Tatiane, da C. B., Rogerio, F. D., Janeo, E. A. F., Roberta, S. N. de L., Rafael, S. F., … Sabrina, C. (2017). Production potential and chemical composition of elephant grass (Pennisetum purpureum Schum.) at different ages for energy purposes. *African Journal of Biotechnology*, *16*(25), 1428–1433. https://doi.org/10.5897/ajb2017.16014

Anejionu, O. C. D., Ahiarammunnah, P. A. N., & Nri-ezedi, C. J. (2015). Hydrocarbon pollution in the Niger Delta: Geographies of impacts and appraisal of lapses in extant legal framework. *Resources Policy*, *45*, 65–77. https://doi.org/10.1016/j.resourpol.2015.03.012

Arellano, P., Tansey, K., Balzter, H., & Boyd, D. S. (2015). Detecting the effects of hydrocarbon pollution in the Amazon forest using hyperspectral satellite images. *Environmental Pollution*, *205*, 225–239. https://doi.org/10.1016/j.envpol.2015.05.041

Arellano, P., Tansey, K., Balzter, H., & Tellkamp, M. (2017). Plant family-specific impacts of petroleum pollution on biodiversity and leaf chlorophyll content in the Amazon rainforest of Ecuador. *PLoS ONE*, *12*(1), 1–18. https://doi.org/10.1371/journal.pone.0169867

Asanebi, H. (2016). A Concise View of Niger Delta Region of Nigeria : An Interpretation of a Nigeria Historian. *International Research Journal of Interdisciplinary & Multidisciplinary Studies (IRJIMS)*, *II*(X), 56–63. Retrieved from http://oaji.net/articles/2016/1707-1480920397.pdf

ASD. (2008). ViewSpec Pro ™ User Manual. *ASD Document 600555 Rev. A*.

Asfour, Y. R., Carpenter, G. A., & Grossberg, S. (1995). *Landsat Satellite Image Segmentation Using the Fuzzy ARTMAP Neural Network*. (February).

Asri, N. A. M., Sakidin, H., Othman, M., Matori, A. N., & Ahmad, A. (2020). Analysis

of the hydrocarbon seepage detection in oil palm vegetation stress using unmanned aerial vehicle (UAV) multispectral data. *Proceedings of International Conference on Advances in Materials Research (Icamr - 2019)*, *2274*, 050007. https://doi.org/10.1063/5.0018054

Ayanlade, A. (2014). *Remote Sensing of Environmental Change in the Niger Delta , Nigeria*. King ' s College London , UKKing ' s College London , University of London, UK.

Ayanlade, A., & Howard, M. T. (2017). Understanding changes in a Tropical Delta: A multi-method narrative of landuse/landcover change in the Niger Delta. *Ecological Modelling*, *364*, 53–65. https://doi.org/10.1016/j.ecolmodel.2017.09.012

Ayesa, S. A., Chukwuka, K. S., & Odeyemi, O. O. (2018). Tolerance of Tithonia diversifolia and Chromolaena odorata in heavy metal simulated-polluted soils and three selected dumpsites. *Toxicology Reports*, *5*(November), 1134–1139. https://doi.org/10.1016/j.toxrep.2018.11.007

Bailey, K. M., McCleery, R. A., Binford, M. W., & Zweig, C. (2016). Land-cover change within and around protected areas in a biodiversity hotspot. *Journal of Land Use Science*, *11*(2), 154–176. https://doi.org/10.1080/1747423X.2015.1086905

Bally, I. S. E. (2006). Mangifera indica (mango), ver. 3.1. *Species Profiles for Pacific Island Agroforestry*, (April), 25.

Baranoski, G. V. G., & Rokne, J. G. (2005). A practical approach for estimating the red edge position of plant leaf reflectance. *International Journal of Remote Sensing*, *26*(3), 503–521. https://doi.org/10.1080/01431160512331314029

Barcelos, E., De Almeida Rios, S., Cunha, R. N. V., Lopes, R., Motoike, S. Y., Babiychuk, E., … Kushnir, S. (2015). Oil palm natural diversity and the potential for yield improvement. *Frontiers in Plant Science*, *6*(MAR), 1–16. https://doi.org/10.3389/fpls.2015.00190

Barnsley, M. (1999). Digital remotely-sensed data and their characteristics. *Geographical Information Systems*, *1*(1), 451–466. Retrieved from http://www.scielo.br/pdf/cr/v38n9/a11v38n9.pdf%5Cnhttp://www.scielo.br/scielo.php?script=sci_abstract&pid=S0103-

84782008000900011&lng=pt&nrm=iso&tlng=pt%5Cnhttp://dx.doi.org/10.1016/j.geomorph.2011.08.020%5Cnhttp://dx.doi.org/10.1016/j.geomorph.2009.03.00

Bartha, R. (1976). The effect of oil spills on trees. *J. Arboriculture*, (December), 180.

Berrett, C., & Calder, C. A. (2016). Bayesian spatial binary classification. *Spatial Statistics*, *16*, 72–102. https://doi.org/10.1016/j.spasta.2016.01.004

Blackburn, G. A. (1998). Quantifying chlorophylls and carotenoids at leaf and canopy scales: An evaluation of some hyperspectral approaches. *Remote Sensing of Environment*, *66*(3), 273–285. https://doi.org/10.1016/S0034-4257(98)00059-5

Briottet, X., Marion, R., Carrere, V., Jacquemoud, S., Chevrel, S., Prastault, P., … Bourguignon, A. (2011). HYPXIM: A new hyperspectral sensor combining science/defence applications. *2011 3rd Workshop on Hyperspectral Image and Signal Processing: Evolution in Remote Sensing (WHISPERS)*, 1–4. https://doi.org/10.1109/WHISPERS.2011.6080957

Brock, J. (2013). Nigeria's stolen oil is sold and laundered abroad - report. Retrieved June 11, 2020, from Reuters website: https://www.reuters.com/article/nigeria-oil-theft/nigerias-stolen-oil-is-sold-and-laundered-abroad-report-idUSL5N0HE2RC20130919

Burian, J., Zapletal, J., & Pászto, V. (2022). Disaggregator – a tool for the aggregation and disaggregation of spatial data. *Earth Science Informatics*, (0123456789). https://doi.org/10.1007/s12145-021-00737-9

Campbell, D., & Campbell, S. (2008). *Statlab Workshop Introduction to Regression and Data Analysis with*.

Carincotte, C., Derrode, S., & Bourennane, S. (2006). Unsupervised change detection on SAR images using fuzzy hidden Markov chains. *IEEE Transactions on Geoscience and Remote Sensing*, *44*(2), 432–441. https://doi.org/10.1109/TGRS.2005.861007

Chainey, S. (2013). Examining the influence of cell size and bandwidth size on kernel density estimation crime hotspot maps for predicting spatial patterns of crime. *BSGLg*, *60*(1), 7–19.

Chen, J., Gong, P., He, C., Pu, R., & Shi, P. (2003). Land-Use / Land-Cover Change

Detection Using Improved Change-Vector Analysis. *Photogrammetric Engineering Remote Sensing*, *69*(4), 369–379. https://doi.org/10.14358/PERS.69.4.369

Chen, J., Zhu, X., Vogelmann, J. E., Gao, F., & Jin, S. (2011). A simple and effective method for filling gaps in Landsat ETM+ SLC-off images. *Remote Sensing of Environment*, *115*(4), 1053–1064. https://doi.org/10.1016/j.rse.2010.12.010

Chen, M., & Ludwing, S. (2017). Color Image Segmentation using Fuzzy C-Regression Model. *Hindawi*, *2017*, 1–15.

Cheng, Z., Zu, Z., & Lu, J. (2018). Traffic crash evolution characteristic analysis and spatiotemporal hotspot identification of urban road intersections. *Sustainability (Switzerland)*, *11*(1). https://doi.org/10.3390/su11010160

Chika, C., & Ndidi, A. F. (2022). ILLEGAL OIL BUNKERING SABOTAGE AND VANDALISM IN NIGER DELTA AREA ILLEGAL OIL BUNKERING SABOTAGE AND VANDALISM IN NIGER DELTA AREA OF NIGERIA Chibuzor Chika and Alete Favour Ndidi. *Academic Journal of Current Research*, *Vol.9*, *No.*(September), 90–99.

Choodarathnakara, A. L., Kumar, T. A., Shivaprakash, K., & Patil, C. G. (2012). Soft Classification Techniques for RS Data 1. *Ijcset*, *2*(11), 1468–1471.

Congalton, R. G. (1988). A comparison of sampling schemes used in generating error matrices for assessing the accuracy of maps generated from remotely sensed data. *Photogrammetric Engineering and Remote Sensing*, *54*, 593–600. Retrieved from http://www.csa.com/partners/viewrecord.php?requester=gs&collection=TRD&recid=A8839098AH

Congalton, R. G., & Green, K. (2008). *Assessing the Accuracy of Remotely Sensed Data: Principles and Practices* (2nd ed.). https://doi.org/https://doi.org/10.1201/9781420055139

Cook, D., & Swayne, D. F. (2007). Supervised Classification. *Interactive and Dynamic Graphics for Data Analysis: With R and GGobi (Use R!)*, 188. Retrieved from http://www.ggobi.org/book/

Costa, H., Foody, G. M., & Boyd, D. S. (2017). Using mixed objects in the training of

object-based image classifications. *Remote Sensing of Environment*, *190*, 188–197. https://doi.org/10.1016/j.rse.2016.12.017

Costa, H., Foody, G. M., & Boyd, D. S. (2018). Supervised methods of image segmentation accuracy assessment in land cover mapping. *Remote Sensing of Environment*, *205*(December 2017), 338–351. https://doi.org/10.1016/j.rse.2017.11.024

Cotrozzi, L., Peron, R., Tuinstra, M. R., Mickelbart, M. V., & Couture, J. J. (2020). Spectral phenotyping of physiological and anatomical leaf traits related with maize water status1[open]. *Plant Physiology*, *184*(3), 1363–1377. https://doi.org/10.1104/pp.20.00577

Coulter, L. L., Stow, D. A., Tsai, Y. H., Ibanez, N., Shih, H. chien, Kerr, A., … Mensah, F. (2016). Classification and assessment of land cover and land use change in southern Ghana using dense stacks of Landsat 7 ETM+ imagery. *Remote Sensing of Environment*, *184*, 396–409. https://doi.org/10.1016/j.rse.2016.07.016

Curran, P. J., Windham, W. R., & Gholz, H. L. (1995). Exploring the relationship between reflectance red edge and chlorophyll concentration in slash pine leaves. *Tree Physiology*, *15*(3), 203–206. https://doi.org/10.1093/treephys/15.3.203

Dahiru, T. (2011). P-Value, a true test of statistical significance? a cautionary note. *Annals of Ibadan Postgraduate Medicine*, *6*(1), 21–26. https://doi.org/10.4314/aipm.v6i1.64038

Dana, R. H., & Cooper, G. W. (1964). Susceptibility to Hypnosis and T.A.T. Card 12M. *American Journal of Clinical Hypnosis*, *6*(3), 208-210file:///c:/program%20files%20(x86)/arcgis/d. https://doi.org/10.1080/00029157.1964.10402344

Danquah, J. A., Roberts, C. O., & Appiah, M. (2018). Elephant Grass (Pennisetum purpureum): A Potential Source of Biomass for Power Generation in Ghana. *Current Journal of Applied Science and Technology*, *30*(6), 1–12. https://doi.org/10.9734/cjast/2018/45224

Dash, J. P., Watt, M. S., Pearse, G. D., Heaphy, M., & Dungey, H. S. (2017). Assessing very high resolution UAV imagery for monitoring forest health during a simulated

disease outbreak. *ISPRS Journal of Photogrammetry and Remote Sensing*, *131*, 1–14. https://doi.org/10.1016/j.isprsjprs.2017.07.007

Deligiorgi, D., & Philippopoulos, K. (2011). Spatial Interpolation Methodologies in Urban Air Pollution Modeling: Application for the Greater Area of Metropolitan Athens, Greece. *Advanced Air Pollution*, (August). https://doi.org/10.5772/17734

Deng, R.-J., Deng, Y.-H., Yu, S., & Hou, D. (2008). Hydrocarbon geology and reservoir formation characteristics of Niger Delta Basin. *Shiyou Kantan Yu Kaifa/Petroleum Exploration and Development*, *35*, 755–762.

Dessalegn, Y., Assefa, H., Derso, T., & Tefera, M. (2014). Mango Production Knowledge and Technological Gaps of Smallholder Farmers in Amhara Region , Ethiopia. *American Scientific Research Journal for Engineering, Technology, and Sciences*, *10*(1), 28–39. Retrieved from http://ccs.infospace.com/ClickHandler.ashx?encp=ld=20161024&app=1&c=govome4&s=govome&rc=govome4&dc=&euip=197.156.133.81&pvaid=add3505b338e4e2093bcfd0155ca9a57&dt=Desktop&fct.uid=ac35c511700a4fc0ac5ad55c5b263ed5&en=DC7CWTeowf1v0Hk3zSVE+PPimCiN6qqIvV7SiWv

Devi, R. N., & Jiji, G. W. (2015). Change Detection Techniques - A Survey. *International Journal on Computational Science & Applications*, *5*(2), 45–57. https://doi.org/10.5121/ijcsa.2015.5205

Dim, C. I. P. (2017). Hydrocarbon Prospectivity in the Eastern Coastal Swamp Depo-belt of the Niger Delta Basin - Stratigraphic Framework and Structural Styles. *SpringerBriefs in Earth Sciences*, 9–17. https://doi.org/10.1007/978-3-319-44627-1

Ding, L., Chen, K. L., Liu, T., Cheng, S. G., & Wang, X. (2015). Spatial-temporal hotspot pattern analysis of provincial environmental pollution incidents and related regional sustainable management in China in the period 1995-2012. *Sustainability (Switzerland)*, *7*(10), 14385–14407. https://doi.org/10.3390/su71014385

Dornik, A., Drâguţ, L., & Urdea, P. (2017). Classification of soil types using geographic object-based image analysis and Random Forest. *Pedosphere*, *0160*. https://doi.org/10.1016/S1002-0160(17)60377-1

Doust, H. (1990). Petroleum geology of the Niger Delta. *Geological Society, London, Special Publications*, *50*(1), 365. https://doi.org/10.1144/GSL.SP.1990.050.01.21

Dragut, L., Csillik, O., Eisank, C., & Tiede, D. (2014). Automated parameterisation for multi-scale image segmentation on multiple layers. *ISPRS Journal of Photogrammetry and Remote Sensing*, *88*, 119–127. https://doi.org/10.1016/j.isprsjprs.2013.11.018

Duke, N. C. (2016). Oil spill impacts on mangroves: Recommendations for operational planning and action based on a global review. *Marine Pollution Bulletin*, *109*(2), 700–715. https://doi.org/10.1016/j.marpolbul.2016.06.082

Duro, D. C., Franklin, S. E., & Dubé, M. G. (2012). Multi-scale object-based image analysis and feature selection of multi-sensor earth observation imagery using random forests. *International Journal of Remote Sensing*, *33*(14), 4502–4526. https://doi.org/10.1080/01431161.2011.649864

Dyring, E. (1973). Principles of Remote Sensing. *Ambio*, *11*(3), 57–69. https://doi.org/10.4324/9780203714522-9

E&P Forum/UNEP. (1997). Environmental management in oil and gas exploration and production. In *Industry And Environment*. https://doi.org/10.65/Jss2003.09.085.

Eastman, J. R. (2016). *TerrSet Tutorial: Geospatial Monitoring and Modeling System*. 470. Retrieved from https://clarklabs.org/wp-content/uploads/2016/03/TerrSet18-2_Brochure_WEB.pdf

Egberongbe, F., Nwilo, P., & Badejo, O. (2006). Oil Spill Disaster Monitoring along Nigerian Coastline". Paper presented at. *5th FIG Regional Conference: …*, 1–23. Retrieved from http://citeseerx.ist.psu.edu/viewdoc/summary?doi=10.1.1.510.3507

Egobueze, F. E., Ayotamuno, J. M., Iwegbue, C. M. A., Eze, C., & Okparanma, R. N. (2019). Effects of organic amendment on some soil physicochemical characteristics and vegetative properties of Zea mays in wetland soils of the Niger Delta impacted with crude oil. *International Journal of Recycling of Organic Waste in Agriculture*, *8*(s1), 423–435. https://doi.org/10.1007/s40093-019-00315-6

Egorov, A. V., Hansen, M. C., Roy, D. P., Kommareddy, A., & Potapov, P. V. (2015). Image interpretation-guided supervised classification using nested segmentation. *Remote Sensing of Environment*, *165*, 135–147. https://doi.org/10.1016/j.rse.2015.04.022

Egwu, S. a. (2012). Oil Spill Control and Management. *Petroleum Technology Development Journal (PTDF)*, *1*(January), 1–6. https://doi.org/1595-9104

El Hassan, I. M. (2004). Desertification Monitoring Using Remote Sensing Technology. *International Conference on Water Resources & Arid Environment*, 15. Retrieved from http://www.psipw.org/English_PDF/3_Distance/E3-3.pdf

ESRI. (2002). *Using ArGis Spatial Analyst*. 238.

Everitt, J. H., Yang, C., & Davis, M. R. (2010). Mapping an annual weed with colour-infrared aerial photography and image analysis. *Geocarto International*, *25*(1), 45–52. https://doi.org/10.1080/10106040802677037

Eyoh, A., & Okwuashi, O. (2016). *Spatial and Temporal Evaluation of Land Use / Land Cover Change of the Niger Delta Region of Nigeria from 1986-2016*. *3*(6), 15–23.

Fabiyi, O. (2011). Change actors analysis and vegetation loss from remote sensing data in parts of the Niger Delta region. *Journal of Ecology and The Natural Environment*, *3*(12), 381–391. Retrieved from http://www.academicjournals.org/journal/JENE/article-abstract/FF5765910157

Fadiya, S. L., Adekola, S. A., Oyebamiji, B. M., & Akinsanpe, O. T. (2020). Source rock geochemistry of shale samples from Ege-1 and Ege-2 wells, Niger Delta, Nigeria. *Journal of Petroleum Exploration and Production Technology*, *11*(2), 579–586. https://doi.org/10.1007/s13202-020-01038-5

Falebita, D. E., Ayeni, O. Z., Bayowa, O. G., & Anukwu, G. C. (2015). Study of the Organic Richness and Petrophysical Characteristics of Selected Shales from the Analysis of Wireline Logs: A Case of "Neya" Field, Niger Delta. *Ife Journal of Science Vol.*, *17*(1), 41–52.

Farhana Ahmad, S. S., & Hazrina Idris, N. (2022). *Oil Spill Impacts on Mangrove Forest from Satellite Remote Sensing*. 60–64. https://doi.org/10.1109/iconspace53224.2021.9768774

Feizizadeh, B., Blaschke, T., Tiede, D., & Moghaddam, M. H. R. (2017). Evaluating fuzzy operators of an object-based image analysis for detecting landslides and their changes. *Geomorphology*, *293*(November 2015), 240–254. https://doi.org/10.1016/j.geomorph.2017.06.002

Filella, I., & Peñuelas, J. (1994). The red edge position and shape as indicators of plant chlorophyll content, biomass and hydric status. *International Journal of Remote Sensing*, *15*(7), 1459–1470. https://doi.org/10.1080/01431169408954177

Fingas, M. (2017). *Oil Spills : Causes , Consequences , Prevention , and Countermeasures Oil Spills : Causes , Consequences , Prevention ,*. https://doi.org/10.1142/9789814699983

Foody, G M. (2002). The role of soft classification techniques in the refinement of estimates of ground control point location. *Photogrammetric Engineering and Remote Sensing*, *68*(9), 897–903.

Foody, Giles M. (2002). Status of land cover classification accuracy assessment. *Remote Sensing of Environment*, *80*(1), 185–201. https://doi.org/10.1016/S0034-4257(01)00295-4

Foody, Giles M., & Boyd, D. S. (2013). Using volunteered data in land cover map validation: Mapping west African forests. *IEEE Journal of Selected Topics in Applied Earth Observations and Remote Sensing*, *6*(3), 1305–1312. https://doi.org/10.1109/JSTARS.2013.2250257

Frohn, R. C., Autrey, B. C., Lane, C. R., & Reif, M. (2011). Segmentation and object-oriented classification of wetlands in a karst Florida landscape using multi-season Landsat-7 ETM+ imagery. *International Journal of Remote Sensing*, *32*(5), 1471–1489. https://doi.org/10.1080/01431160903559762

Fuentes, R., León-Muñoz, J., & Echeverría, C. (2017). Spatially explicit modelling of the impacts of land-use and land-cover change on nutrient inputs to an oligotrophic lake. *International Journal of Remote Sensing*, *00*(00), 1–20. https://doi.org/10.1080/01431161.2017.1339928

Gamon, J. A., Penuelas, J., & Field, C. B. (1992). A Narrow-Waveband Spectral Index That Tracks Diurnal Changes in Photosynthetic Efficiency. *REMOTE SENS.*

ENVIRON., *41*(1), 35–44. https://doi.org/10.1088/0305-4470/24/13/001

Gamon, J. A., Serrano, L., & Surfus, J. S. (1997). The photochemical reflectance index: An optical indicator of photosynthetic radiation use efficiency across species, functional types, and nutrient levels. *Oecologia*, *112*(4), 492–501. https://doi.org/10.1007/s004420050337

Ganguly, K., Kumar, R., Mruthyunjaya Reddy, K., Jagadeeswara Rao, P., Raj Saxena, M., & Ravi Shankar, G. (2016). Optimization of spatial statistical approaches to identify land use/land cover change hot spots of Pune region of Maharashtra using remote sensing and GIS techniques. *Geocarto International*, *6049*(May), 1–20. https://doi.org/10.1080/10106049.2016.1178813

Geneletti, D., & Gorte, B. G. H. (2003). A method for object-oriented land cover classification combining Landsat TM data and aerial photographs. *International Journal of Remote Sensing*, *24*(6), 1273–1286. https://doi.org/10.1080/01431160210144499

George, R., Padalia, H., Sinha, S. K., & Kumar, A. S. (2018). Evaluation of the use of hyperspectral vegetation indices for estimating mangrove leaf area index in middle Andaman Island, India. *Remote Sensing Letters*, *9*(11), 1099–1108. https://doi.org/10.1080/2150704X.2018.1508910

Getis, a. (2005). Spatial statistics. *Geographical Information Systems Volume 1*, 239–252.

Giziakis, K., Kanellopoulos, N., & Gialoutsi, S. (2013). Spatial Analysis of Oil Spills from Marine Accidents in Greek Waters. *Spoudai*, *63*(3–4), 60–74. Retrieved from https://search.proquest.com/docview/1924866022?accountid=14495%0Ahttp://fp5qq3tk5q.search.serialssolutions.com/directLink?&atitle=Spatial+Analysis+of+Oil+Spills+from+Marine+Accidents+in+Greek+Waters&author=Giziakis%252C+Kostantinos%253BKanellopoulos%252C+

Grebby, S., Naden, J., Cunningham, D., & Tansey, K. (2011). Integrating airborne multispectral imagery and airborne LiDAR data for enhanced lithological mapping in vegetated terrain. *Remote Sensing of Environment*, *115*(1), 214–226. https://doi.org/10.1016/j.rse.2010.08.019

Gu, J., Congalton, R. G., & Pan, Y. (2015). The impact of positional errors on soft classification accuracy assessment: A simulation analysis. *Remote Sensing*, *7*(1), 579–599. https://doi.org/10.3390/rs70100579

Gudex-Cross, D., Pontius, J., & Adams, A. (2017). Enhanced forest cover mapping using spectral unmixing and object-based classification of multi-temporal Landsat imagery. *Remote Sensing of Environment*, *196*, 193–204. https://doi.org/10.1016/j.rse.2017.05.006

Gunderson, J. (2006). *the Effect of Hydrocarbon Contamination and Mycorrhizal*.

Guo, X., Zhang, H., Wu, Z., Zhao, J., & Zhang, Z. (2017). Comparison and evaluation of annual NDVI time series in China derived from the NOAA AVHRR LTDR and terra MODIS MOD13C1 products. *Sensors (Switzerland)*, *17*(6), 1–18. https://doi.org/10.3390/s17061298

Gyawali, B., Fraser, R., Wang, Y., & Bukenya, J. (2004). *Land Cover and Socio-economic Characteristics in the Eight Counties of Alabama : A Spatial Analysis*. 1–13.

Haack, R. C., Sundararaman, P., Diedjomahor, J. O., Xiao, H., Gant, N. J., May, E. D., & Kelsch, K. (2000). Niger delta petroleum systems, Nigeria. *AAPG Memoir*, *73*, 213–231.

Harcourt, P. (2012). *Socio Economic Importance of Red Mangrove (Rhizophora Racemosa L) To Rural Dwellers in Southern Nigeria*. *2*(8), 182–186.

Harris, N. L., Goldman, E., Gabris, C., Nordling, J., Minnemeyer, S., Ansari, S., … Potapov, P. (2017). Using spatial statistics to identify emerging hot spots of forest loss. *Environmental Research Letters*, *12*(2). https://doi.org/10.1088/1748-9326/aa5a2f

Hashemian, M. S., Abakar, A. A., & Fatemi, S. B. (2004). Study of sampling methods for accuracy assessment of classified remotely sensed data. *20th International Society for Photogrammetry and Remote Sensing Congress*, 12–23.

Hester, D. B., Nelson, S. A. C., Cakir, H. I., Khorram, S., & Cheshire, H. (2010). High-resolution land cover change detection based on fuzzy uncertainty analysis and change reasoning. *International Journal of Remote Sensing*, *31*(2), 455–475.

https://doi.org/10.1080/01431160902893493

Heumann, B. W. (2011). An object-based classification of mangroves using a hybrid decision tree-support vector machine approach. *Remote Sensing*, *3*(11), 2440–2460. https://doi.org/10.3390/rs3112440

Hill, J., Jarmer, T., Udelhoven, T., & Stellmes, M. (2006). Remote Sensing and Geomatics Applications for Desertification and Land Degradation Monitoring and Assessment. *Geometrics for Land and Water Management: Achievements and Challenges in the Euromed Context*, 15–22.

Houborg, R., Fisher, J. B., & Skidmore, A. K. (2015). Advances in remote sensing of vegetation function and traits. *International Journal of Applied Earth Observation and Geoinformation*, *43*, 1–6. https://doi.org/10.1016/j.jag.2015.06.001

https://fsf.nerc.ac.uk/instruments/asd_fieldspec.shtml. (n.d.). ASD FieldSpec Pro System. Retrieved September 1, 2018, from NERC Field Spectroscopy Facility (FSF) website: https://fsf.nerc.ac.uk/instruments/asd_fieldspec.shtml

Https://spectralevolution.com/. (n.d.). *Spectral Evolution:Measuring Total Organic Carbon in Soil Total* (pp. 1–2). pp. 1–2. Retrieved from www.spectralevolution.com

Hu, T., Wu, W., & Liu, L. (2014). COMBINATION OF HARD AND SOFT CLASSIFICATION METHOD BASED ON ADAPTIVE THRESHOLD. *Geoscience and Remote Sensing Symposium (IGARSS), 2014 IEEE International*, 4180–4183.

Huang, J., Dai, Q., Wang, H., & Han, D. (2014). Empirical Regression Model Using Ndvi, Meteorological Factors For Estimation Of Wheat Yield In Yunnan, China. *International Conference on Hydroinformatics*, 1–9.

Ibrahim, E., Adam, S., Wal, D. Van Der, Wever, A. De, & Sabbe, K. (2009). *Assessment of Unsupervised Classification Techniques*. 158–179.

Ibrahim, S., Hamisu, I., & Lawal, U. (2015). Spatial Pattern of Tuberculosis Prevalence in Nigeria: A Comparative Analysis of Spatial Autocorrelation Indices. *American Journal of Geographic Information System*, *4*(3), 87–94. https://doi.org/10.5923/j.ajgis.20150403.01

Igboh, M. N., Ikewchi, C. J., & Ikewuchi, C. C. (2009). Chemical profile of chromolaena odorata leaves.pdf. *Pakistan Journal of Nutrition*, Vol. 8, pp. 521–524.

Igu, N. (2016). *Freshwater Swamp Forest Ecosystem in the Niger Delta: Ecology, Disturbance and Ecosystem Services*. University of York PhD thesis.

Igu, N. I. (2017). Swamp Forest Use and Loss in the Niger Delta: Contextual and Underlying Issues. *Open Journal of Forestry*, *07*(01), 34–47. https://doi.org/10.4236/ojf.2017.71003

Ikhajiagbe, B., & Akindolor, A. (2016). Comparative effects of pretreatment of stem cuttings of Chromolaena odorata (Siam weed) with sodium azide and hydroxylamide on the survival and phyoremediative performance in an oil-polluted soil. *Nigerian Journal of Biotechnology*, *31*(1), 27. https://doi.org/10.4314/njb.v31i1.5

Inampudi, R. B. (1998). Image mosaicing. *IGARSS '98. Sensing and Managing the Environment. 1998 IEEE International Geoscience and Remote Sensing. Symposium Proceedings. (Cat. No.98CH36174)*, (91), 2363–2365 vol.5. https://doi.org/10.1109/IGARSS.1998.702214

Inglada, J., Vincent, A., Arias, M., Tardy, B., Morin, D., & Rodes, I. (2017). Operational High Resolution Land Cover Map Production at the Country Scale Using Satellite Image Time Series. *Remote Sensing*, *9*(1), 95. https://doi.org/10.3390/rs9010095

Ite, A. E., Ibok, U. J., Ite, M. U., & Petters, S. W. (2013). Petroleum Exploration and Production: Past and Present Environmental Issues in the Nigeria's Niger Delta. *American Journal of Environmental Protection*, *1*(4), 78–90. https://doi.org/10.12691/env-1-4-2

Ivanov, A., & Zatyagalova, V. (2008). A GIS approach to mapping oil spills in a marine environment. *International Journal of Remote …*, (1). Retrieved from http://www.tandfonline.com/doi/abs/10.1080/01431160802175587

Jafarbiglu, H., & Pourreza, A. (2022). A comprehensive review of remote sensing platforms, sensors, and applications in nut crops. *Computers and Electronics in Agriculture*, *197*(July 2021), 106844. https://doi.org/10.1016/j.compag.2022.106844

Jana, M., & Sar, N. (2016). Modeling of hotspot detection using cluster outlier analysis and Getis-Ord Gi* statistic of educational development in upper-primary level, India. *Modeling Earth Systems and Environment*, *2*(2), 1–10. https://doi.org/10.1007/s40808-016-0122-x

Jensen, R., Mausel, P., Dias, N., Gonser, R., Yang, C., Everitt, J., & Fletcher, R. (2007). Spectral analysis of coastal vegetation and land cover using AISA + hyperspectral data. *Geocarto International*, *22*(1), 17–28. https://doi.org/10.1080/10106040701204354

Jia, L. J., Zheng, X. Q., & Miao, J. L. (2018). Research progress and hotspot analysis of spatial interpolation. *IOP Conference Series: Earth and Environmental Science*, *113*(1). https://doi.org/10.1088/1755-1315/113/1/012079

Jiang, C., Chen, Y., Wu, H., Li, W., Zhou, H., Bo, Y., … Hyyppä, J. (2019). Study of a high spectral resolution hyperspectral LiDAR in vegetation red edge parameters extraction. *Remote Sensing*, *11*(17), 1–14. https://doi.org/10.3390/rs11172007

Jong, Steven Michael De. (2007). *Chapter 1 Basics of Remote Sensing*. https://doi.org/10.1007/978-1-4020-2560-0

Jong, Steven M., Meer, F. D., & Clevers, J. G. P. W. (2006). Basics of Remote Sensing. *Remote Sensing Image Analysis: Including the Spatial Domain*, 1–15. https://doi.org/10.1007/1-4020-2560-2_1

Joshi, N., Baumann, M., Ehammer, A., Fensholt, R., Grogan, K., Hostert, P., … Waske, B. (2016). A review of the application of optical and radar remote sensing data fusion to land use mapping and monitoring. *Remote Sensing*, *8*(1), 1–23. https://doi.org/10.3390/rs8010070

Kadafa, A. A. (2012a). Environmental Impacts of Oil Exploration and Exploitation inthe Niger Delta of Nigeria. *Global Journal of Science Frontier Research Environmnet & Earth Sciences*, *12*(3), 1–11.

Kadafa, A. A. (2012b). Oil Exploration and Spillage in the Niger Delta of Nigeria. *Civil and Environmental Research*, *2*(3), 38–51.

Kalinic, M. (2018). Kernel Density Estimation (KDE) vs . Hot-Spot Analysis - Detecting Criminal Hot Spots in the City of San Francisco. *21st International*

Conference on Geographic Information Science (AGILE 2018), (June), 1–5.

Karan, S. K., & Samadder, S. R. (2018). A comparison of different land-use classification techniques for accurate monitoring of degraded coal-mining areas. *Environmental Earth Sciences*, *77*(20), 1–15. https://doi.org/10.1007/s12665-018-7893-5

Karsidi, A. (2004). Spatial Analysis Of Land Use / Land Cover Change Dynamics Using Remote Sensing And Geographic Information Sytems : A Case Study In The Down Stream And Surroundings Of The Ci Tarum Watershed [Disertasi]. *Thesis*, (May), 243.

Kato, A., Morgenroth, J., Kelbe, D., Gomez, C., & Van Aardt, J. (2013). Ground truth measurement of trees using terrestrial laser for satellite remote sensing. *International Geoscience and Remote Sensing Symposium (IGARSS)*, 2106–2109. https://doi.org/10.1109/IGARSS.2013.6723228

Kearney, M. S., Stutzer, D., Turpie, K., & Stevenson, J. C. (2009). The effects of tidal inundation on the reflectance characteristics of coastal marsh vegetation. *Journal of Coastal Research*, *25*(6), 1177–1186. https://doi.org/10.2112/08-1080.1

Khanna, S., Santos, M. J., Ustin, S. L., Koltunov, A., Kokaly, R. F., & Roberts, D. A. (2013). Detection of salt marsh vegetation stress and recovery after the Deepwater Horizon Oil Spill in Barataria Bay, Gulf of Mexico using AVIRIS data. *PLoS ONE*, *8*(11). https://doi.org/10.1371/journal.pone.0078989

Kharaka, Y. K., & Dorsey, N. S. (2005). Environmental issues of petroleum exploration and production: Introduction. *Environmental Geosciences*, *12*(2), 61–63. https://doi.org/10.1306/eg.intro0605020205

Kleemann, J., Baysal, G., Bulley, H. N. N., & Fürst, C. (2017). Assessing driving forces of land use and land cover change by a mixed-method approach in north-eastern Ghana, West Africa. *Journal of Environmental Management*, *196*, 411–442. https://doi.org/10.1016/j.jenvman.2017.01.053

Kochubey, S. M., & Kazantsev, T. A. (2012). Derivative vegetation indices as a new approach in remote sensing of vegetation. *Frontiers of Earth Science*, *6*(2), 188–195. https://doi.org/10.1007/s11707-012-0325-z

Kogan, F., Guo, W., & Yang, W. (2017). SNPP/VIIRS vegetation health to assess 500 California drought. *Geomatics, Natural Hazards and Risk*, *5705*(August), 1–13. https://doi.org/10.1080/19475705.2017.1337654

Kogan, F., & Salazar, L. (2012). Forecasting crop production using satellite-based vegetation health indices in Kansas, USA. *International Journal of Remote Sensing*, *33*(9), 2798–2814. https://doi.org/10.1080/01431161.2011.621464

Kohonen, T. (1982). Self-organized formation of topologically correct feature maps. *Biological Cybernetics*, *43*(1), 59–69. https://doi.org/10.1007/BF00337288

Koutika, L. S., & Rainey, H. J. (2010). Chromolaena odorata in different ecosystems: Weed or fallow plant? *Applied Ecology and Environmental Research*, *8*(2), 131–142. https://doi.org/10.15666/aeer/0802_131142

Kuenzer, C., van Beijma, S., Gessner, U., & Dech, S. (2014). Land surface dynamics and environmental challenges of the Niger Delta, Africa: Remote sensing-based analyses spanning three decades (1986-2013). *Applied Geography*, *53*, 354–368. https://doi.org/10.1016/j.apgeog.2014.07.002

Kumar, K. S., Bhaskar, P. U., & Padmakumari, K. (2015). Application of Land Change Modeler for Prediction of Future Land Use Land Cover a Case Study of Vijayawada City. *International Journal of Advanced Technology in Engineering and Science*, 2571–2581.

Kumar, L., Schmidt, K., Dury, S., & Skidmore, A. (2002). Imaging Spectrometry and Vegetation Science. *Imaging Spectrometry. Remote Sensing and Digital Image Processing*, 111–155. https://doi.org/10.1007/978-0-306-47578-8_5

Kumar, M., Saurabh, V., Tomar, M., Hasan, M., Changan, S., Sasi, M., … Mekhemar, M. (2021). Mango (Mangifera indica l.) leaves: Nutritional composition, phytochemical profile, and health-promoting bioactivities. *Antioxidants*, *10*(2), 1–23. https://doi.org/10.3390/antiox10020299

Kumar, S., & Arya, S. (2021). Change Detection Techniques for Land Cover Change Analysis Using Spatial Datasets: a Review. *Remote Sensing in Earth Systems Sciences*, *4*(3), 172–185. https://doi.org/10.1007/s41976-021-00056-z

Kundu, A., & Dutta, D. (2011). Monitoring desertification risk through climate change

and human interference using Remote sensing and GIS. *International Journal of Geomatics and Geosciences*, *2*(1), 21–33.

Kuppusamy, J., & Ganesan, J. (2016). *International Journal of Advanced and Applied Sciences*. *3*(6), 24–26. Retrieved from http://science-gate.com/IJAAS/Articles/2016-3-12/14 2016-3-12-pp.106-112.pdf

Kuta, A. A. (2012). *A Fuzzy approach to modelling land cover changes in north-eastern Nigeria* (Vol. 6). University of Leicester.

Kuta, A. A., & Comber, A. J. (2015). *A Fuzzy approach to modelling land cover changes in north-eastern Nigeria*. *6*(2).

Landsat-Missions. (n.d.). Calibration & Validation.

Langeveld, J. W. A., & Delany, S. (2014). *The impact of oil exploration, extraction and transport on mangrove vegetation and carbon stocks in nigeria*.

Lawley, V., Lewis, M., Clarke, K., & Ostendorf, B. (2016). Site-based and remote sensing methods for monitoring indicators of vegetation condition: An Australian review. *Ecological Indicators*, *60*, 1273–1283. https://doi.org/10.1016/j.ecolind.2015.03.021

Lee, T. F., Mak, K. I. M., Rackovsky, O. R. I., Lin, Y., Allison, J., Loke, J. C., & Friedman, S. L. (2011). *NIH Public Access*. *223*(3), 648–657. https://doi.org/10.1002/jcp.22063.Downregulation

Levine, N. (2007). ‘ Hot Spot ’ Analysis I Statistical Approaches to the Measurement of ‘ Hot Spots .’ *Manual for CrimeStat: A Spatial Statistics Program for the Analysis of Crime Incident Locations*.

Li, F., Miao, Y., Hennig, S. D., Gnyp, M. L., Chen, X., Jia, L., & Bareth, G. (2010). Evaluating hyperspectral vegetation indices for estimating nitrogen concentration of winter wheat at different growth stages. *Precision Agriculture*, *11*(4), 335–357. https://doi.org/10.1007/s11119-010-9165-6

Li, M., Blaschke, T., Cheng, L., & Tiede, D. (2016). A systematic comparison of different object-based classification techniques using high spatial resolution imagery in agricultural environments. *International Journal of Applied Earth Observation and Geoinformation*, *49*, 87–98.

https://doi.org/10.1016/j.jag.2016.01.011

Li, S., Wang, W., Ganguly, S., & Nemani, R. R. (2018). Radiometric Characteristics of the Landsat Collection 1 Dataset. *Advances in Remote Sensing*, *07*(03), 203–217. https://doi.org/10.4236/ars.2018.73014

Li, X., Myint, S. W., Zhang, Y., Galletti, C., Zhang, X., & Turner, B. L. (2014). Object-based land-cover classification for metropolitan Phoenix, Arizona, using aerial photography. *International Journal of Applied Earth Observation and Geoinformation*, *33*(1), 321–330. https://doi.org/10.1016/j.jag.2014.04.018

Li, Z., & Eastman, J. R. (2010). Commitment and typicality measures for the Self-Organizing Map. *International Journal of Remote Sensing*, *31*(16), 4265–4280. https://doi.org/10.1080/01431160903246725

Lillesand, T., Kiefer, R. W., & Chipman, J. (2008). *Remote Sensing and Image Interpretation* (6th ed.). New York: John Wiley & Sons.

Lin, Y.-P., Chu, H.-J., Wu, C.-F., Chang, T.-K., & Chen, C.-Y. (2011). Hotspot analysis of spatial environmental pollutants using kernel density estimation and geostatistical techniques. *International Journal of Environmental Research and Public Health*, *8*(1), 75–88. https://doi.org/10.3390/ijerph8010075

Ling, F., Foody, G. M., Li, X., Zhang, Y., & Du, Y. (2016). Assessing a temporal change strategy for sub-pixel land cover change mapping from multi-scale remote sensing imagery. *Remote Sensing*, *8*(8). https://doi.org/10.3390/rs8080642

Liping, C., Yujun, S., & Saeed, S. (2018). Monitoring and predicting land use and land cover changes using remote sensing and GIS techniques—A case study of a hilly area, Jiangle, China. *PLoS ONE*, *13*(7), 1–23. https://doi.org/10.1371/journal.pone.0200493

Little, D. I., Holtzmann, K., Gundlach, E. R., & Galperin, Y. (2018). Sediment hydrocarbons in former mangrove areas, southern ogoniland, eastern niger delta, nigeria. *Coastal Research Library*, *25*, 323–342. https://doi.org/10.1007/978-3-319-73016-5_14

Liu, L., Feng, J., Rivard, B., Xu, X., Zhou, J., Han, L., … Ren, G. (2018). Mapping alteration using imagery from the Tiangong-1 hyperspectral spaceborne system:

Example for the Jintanzi gold province, China. *International Journal of Applied Earth Observation and Geoinformation*, *64*, 275–286. https://doi.org/10.1016/j.jag.2017.03.013

Lizarazo, I., & Elsner, P. (2009). Fuzzy segmentation for object-based image classification. *International Journal of Remote Sensing*, *30*(January 2015), 1643–1649. https://doi.org/10.1080/01431160802460062

Lola, S., Natalia, R.-C., Andreas, H., & Laurie, C. (2015). *A technical handbook supporting calibration and*.

Longley, P. (2002). Geographical Information Systems: will developments in urban remote sensing and GIS lead to "better" urban geography? *Progress in Human Geography*, *26*(2), 231–239. https://doi.org/10.1191/0309132502ph366pr

Lu, D., Mausel, P., Brondízios, E. e, & Moran, E. (2003). Change detection techniques. *International Journal of Remote Sensing*, *25*(12), 2365–2407. https://doi.org/10.1080/0143116031000139863

Lu, D., & Weng, Q. (2007). A survey of image classification methods and techniques for improving classification performance. *International Journal of Remote Sensing*, *28*(5), 823–870. https://doi.org/10.1080/01431160600746456

Lu, S., Lu, X., Zhao, W., Liu, Y., Wang, Z., & Omasa, K. (2015). Comparing vegetation indices for remote chlorophyll measurement of white poplar and Chinese elm leaves with different adaxial and abaxial surfaces. *Journal of Experimental Botany*, *66*(18), 5625–5637. https://doi.org/10.1093/jxb/erv270

Lucieer, A., Stein, A., & Fisher, P. (2003). Texture-based segmentation of high-resolution remotely sensed imagery for identification of fuzzy objects. *Proceedings of GeoComputation*. Retrieved from http://www.geocomputation.org/2003/Papers/Lucieer_Paper.pdf

Luiselli, L., Amori, G., Akani, G. C., & Eniang, E. A. (2015). Ecological diversity, community structure and conservation of Niger Delta mammals. *Biodiversity and Conservation*, *24*(11), 2809–2830. https://doi.org/10.1007/s10531-015-0975-8

Lv, Z., Shi, W., Benediktsson, J. A., & Ning, X. (2016). Novel object-based filter for improving land-cover classification of aerial imagery with very high spatial

resolution. *Remote Sensing*, *8*(12). https://doi.org/10.3390/rs8121023

Ma, L., Li, M., Ma, X., Cheng, L., Du, P., & Liu, Y. (2017). A review of supervised object-based land-cover image classification. *ISPRS Journal of Photogrammetry and Remote Sensing*, *130*, 277–293. https://doi.org/10.1016/j.isprsjprs.2017.06.001

MacLean, M. G., Campbell, M. J., Maynard, D. S., Ducey, M. J., & Congalton, R. G. (2013). Requirements for labelling forest polygons in an object-based image analysis classification. *International Journal of Remote Sensing*, *34*(7), 2531–2547. https://doi.org/10.1080/01431161.2012.747017

Madanian, M., Soffianian, A., & Fakheran, S. (2012). Monitoring Land Use/Cover Changes Using Different Change Detection Techniques (Case Study: Falavarjan Area, Isfahan, Iran). *International Conference on Applied Life Sciences*, (1998), 155–160. Retrieved from http://cdn.intechopen.com/pdfs/39888/InTech-Monitoring_land_use_cover_changes_using_different_change_detection_techniques_case_study_falavarjan_area_isfahan_iran_.pdf

Mahmon, N. A., & Ya'acob, N. (2014). A review on classification of satellite image using Artificial Neural Network (ANN). *2014 IEEE 5th Control and System Graduate Research Colloquium*, 153–157. https://doi.org/10.1109/ICSGRC.2014.6908713

Maimaitiyiming, M., Ghulam, A., Bozzolo, A., Wilkins, J. L., & Kwasniewski, M. T. (2017). Early detection of plant physiological responses to different levels of water stress using reflectance spectroscopy. *Remote Sensing*, *9*(7), 1–23. https://doi.org/10.3390/rs9070745

Manandhar, R., Odehi, I. O. A., & Ancevt, T. (2009). Improving the accuracy of land use and land cover classification of landsat data using post-classification enhancement. *Remote Sensing*, *1*(3), 330–344. https://doi.org/10.3390/rs1030330

Mancino, G., Nolè, A., Ripullone, F., & Ferrara, A. (2014). Landsat TM imagery and NDVI differencing to detect vegetation change: Assessing natural forest expansion in Basilicata, southern Italy. *IForest*, *7*(2), 75–84. https://doi.org/10.3832/ifor0909-007

Mas, J.-F. (1999). Monitoring land-cover changes: a com parison of change detection techniques. *International Journal of Remote Sensing*, *20*(1), 139–152. https://doi.org/10.1080/014311699213659

Mba, I. C., Mba, E. I., Ogbuabor, J. E., & Arazu, W. O. (2019). Causes and terrain of oil spillage in Niger delta region of Nigeria: The analysis of variance approach. *International Journal of Energy Economics and Policy*, *9*(2), 283–287. https://doi.org/10.32479/ijeep.7332

Milton, E. J., Fox, N. P., & Schaepman, M. E. (2006). Progress in field spectroscopy. *International Geoscience and Remote Sensing Symposium (IGARSS)*, *113*, 1966–1968. https://doi.org/10.1109/IGARSS.2006.509

Mirkatouli, J., Hosseini, A., & Neshat, A. (2015). Analysis of land use and land cover spatial pattern based on Markov chains modelling. *City, Territory and Architecture*, *2*(1), 4. https://doi.org/10.1186/s40410-015-0023-8

Mishra, D. R., Cho, H. J., Ghosh, S., Fox, A., Downs, C., Merani, P. B. T., … Mishra, S. (2012). Post-spill state of the marsh: Remote estimation of the ecological impact of the Gulf of Mexico oil spill on Louisiana Salt Marshes. *Remote Sensing of Environment*, *118*, 176–185. https://doi.org/10.1016/j.rse.2011.11.007

Mohamadi, B., Liu, F., & Xie, Z. (2016). Oil spill influence on vegetation in Nigeria and its determinants. *Polish Journal of Environmental Studies*, *25*(6), 2533–2540. https://doi.org/10.15244/pjoes/63666

Mohamadi, B., Xie, Z., & Liu, F. (2015). GIS Based Oil Spill Risk Assessment Model for the Niger Delta's Vegetation. *Nature Environment & Pollution Technology*, *14*(3), 545–552. Retrieved from http://search.ebscohost.com/login.aspx?direct=true&db=eih&AN=109417969&site=ehost-live

Mueller-Warrant, G. W., Whittaker, G. W., & Young, W. C. (2008). GIS Analysis of Spatial Clustering and Temporal Change in Weeds of Grass Seed Crops. *Weed Science*, *56*(05), 647–669. https://doi.org/10.1614/WS-07-032.1

Musa, Z. N., Popescu, I. I., & Mynett, A. (2016a). Approach on Modeling Complex Deltas in Data Scarce Areas: A Case Study of the Lower Niger Delta. *Procedia*

Engineering, *154*, 656–664. https://doi.org/10.1016/j.proeng.2016.07.566

Musa, Z. N., Popescu, I., & Mynett, A. (2016b). Assessing the sustainability of local resilience practices against sea level rise impacts on the lower Niger delta. *Ocean and Coastal Management*, *130*, 221–228. https://doi.org/10.1016/j.ocecoaman.2016.06.016

Mutanga, O., Dube, T., & Ahmed, F. (2016). Progress in remote sensing: vegetation monitoring in South Africa. *South African Geographical Journal*, *98*(3), 461–471. https://doi.org/10.1080/03736245.2016.1208586

Mutanga, Onisimo, & Skidmore, A. K. (2007). Red edge shift and biochemical content in grass canopies. *ISPRS Journal of Photogrammetry and Remote Sensing*, *62*(1), 34–42. https://doi.org/10.1016/j.isprsjprs.2007.02.001

Mwalusepo, S., Muli, E., Faki, A., & Raina, S. (2017). Land use and land cover data changes in Indian Ocean Islands: Case study of Unguja in Zanzibar Island. *Data in Brief*, *11*, 117–121. https://doi.org/10.1016/j.dib.2017.01.010

Myint, S. W., Wentz, E. a, & Purkis, S. J. (2007). Employing spatial metrics in urban land-use/land-cover mapping: Comparing the Getis and Geary indices. *Photogrammetric Engineering and Remote Sensing*, *73*(12), 1403–1415.

Nababa, I. I., Symeonakis, E., Koukoulas, S., Higginbottom, T. P., Cavan, G., & Marsden, S. (2020). Land cover dynamics and mangrove degradation in the niger delta region. *Remote Sensing*, *12*(21), 1–22. https://doi.org/10.3390/rs12213619

Naboureh, A., Rezaei Moghaddam, M. H., Feizizadeh, B., & Blaschke, T. (2017). An integrated object-based image analysis and CA-Markov model approach for modeling land use/land cover trends in the Sarab plain. *Arabian Journal of Geosciences*, *10*(12). https://doi.org/10.1007/s12517-017-3012-2

NDRDMP. (2006). Niger Delta Region Land and People. In *Niger Delta Regional Development Master Plan, Chapter 1*. Port Harcourt, Nigeria.

Nelson, J. R., & Grubesic, T. H. (2017). Oil spill modeling. *Progress in Physical Geography*, 030913331774473. https://doi.org/10.1177/0309133317744737

Niger Delta Region: Land and People. (n.d.). *Development*.

Numbere, A. O. (2019a). *Impact of Invasive Nypa Palm (Nypa Fruticans) on Mangroves in Coastal Areas of the Niger Delta Region, Nigeria BT - Impacts of Invasive Species on Coastal Environments: Coasts in Crisis* (C. Makowski & C. W. Finkl, Eds.). https://doi.org/10.1007/978-3-319-91382-7_13

Numbere, A. O. (2019b). Municipal Solid Waste Disposal in Mangrove Forest: Environmental Implication and Management Strategies in the Niger Delta, Nigeria. In H. E.-D. M. Saleh (Ed.), *Municipal Solid Waste Management*. https://doi.org/https://doi.org/10.5772/intechopen.83809

Nwobi, C., Williams, M., & Mitchard, E. T. (2020). Rapid Mangrove forest loss and Nipa Palm (Nypa fruticans) expansion in the Niger Delta, 2007-2017. *Remote Sensing*, *12*(14), 2007–2017. https://doi.org/10.3390/rs12142344

Nwogwugwu, N., Alao, E., & Egwuonwu, C. (2012). Militancy and Insecurity in the Niger Delta: impact on the inflow of foreign direct investment to Nigeria. *Kuwait Chapter of Arabian Journal of Business and Management*, *2*(1), 23–37.

Obi, C. (2014). Oil and conflict in Nigeria's Niger Delta region: Between the barrel and the trigger. *Extractive Industries and Society*, *1*(2), 147–153. https://doi.org/10.1016/j.exis.2014.03.001

Obida, C B, Whyatt, J. D., Blackburn, A. G., & Semple, K. T. (2017). *Spatial Analysis along a Network : Human and Environmental Exposure to Pipeline Hydrocarbon Pollution in the Niger Delta*. 1–6. Retrieved from http://huckg.is/gisruk2017/GISRUK_2017_paper_32.pdf

Obida, Christopher B., Blackburn, A. G., Whyatt, D. J., & Semple, K. T. (2018). Quantifying the exposure of humans and the environment to oil pollution in the Niger Delta using advanced geostatistical techniques. *Environment International*, *111*(October 2017), 32–42. https://doi.org/10.1016/j.envint.2017.11.009

Obida, Christopher B., Blackburn, G. A., Whyatt, J. D., & Semple, K. T. (2021). Counting the cost of the Niger Delta's largest oil spills: Satellite remote sensing reveals extensive environmental damage with >1million people in the impact zone. *Science of the Total Environment*, *775*, 145854. https://doi.org/10.1016/j.scitotenv.2021.145854

Ochege, F. U., George, R. T., Dike, E. C., & Okpala-Okaka, C. (2017). Geospatial assessment of vegetation status in Sagbama oilfield environment in the Niger Delta region, Nigeria. *Egyptian Journal of Remote Sensing and Space Science*, *20*(2), 211–221. https://doi.org/10.1016/j.ejrs.2017.05.001

Odudu, O. O. (2017). *COMPENSATION ISSUES IN THE NIGER-DELTA – A CASE STUDY OF BOBOROKU, JESSE, DELTA STATE, NIGERIA C.O. Odudu, Ph.D, Department of Estate Management, University of Benin, Benin City, Nigeria*. *5*(4), 21–43.

Ogon, P. (2003). Land and forest resource use in the Niger Delta: issues in regulation and sustainable management. *Http://Globetrotter.Berkeley.Edu/GreenGovernance/Papers/Ogon2006.Pdf*, 1–13.

Ohimain, E. I. (2003). Environmental impacts of oil mining activities in the Niger Delta Mangrove Ecosystem. *8th International Congress on Mine Water & the Environment*, 503–517.

Ohimain, E. I. (2007). Environmental Impacts of oil mining activities in the Niger Delta Mangrove Ecosystem. *P8th International Congress on Mine Water & the Environment, Johannesburg, South Africa*, (LC), 7. https://doi.org/10.1080/01431161.2016.1176271

Okoro, S. U., Schickhoff, U., Böhner, J., & Schneider, U. A. (2016). A novel approach in monitoring land-cover change in the tropics: oil palm cultivation in the Niger Delta, Nigeria. *DIE ERDE–Journal of the Geographical Society of Berlin*, *147*(1), 40–52. https://doi.org/10.12854/erde-147-3

Okoye, C. O. &, & Okunrobo, L. A. (2014). Impact of Oil Spill on Land and Water and Its Health Implications in Odu- Gboro Community, Sagamu, Ogun State, Nigeria. *World Journal of Environmental Sciences & Engineering*, *1*(1), 1–211. Retrieved from http://scenrp.com/Journals.php

Olmanson, L. G., Brezonik, P. L., & Bauer, M. E. (2013). Airborne hyperspectral remote sensing to assess spatial distribution of water quality characteristics in large rivers: The Mississippi River and its tributaries in Minnesota. *Remote Sensing of Environment*, *130*, 254–265. https://doi.org/10.1016/j.rse.2012.11.023

Olofsson, P., Foody, G. M., Herold, M., Stehman, S. V., Woodcock, C. E., & Wulder, M. A. (2014). Good practices for estimating area and assessing accuracy of land change. *Remote Sensing of Environment*, *148*, 42–57. https://doi.org/10.1016/j.rse.2014.02.015

Olujobi, O. J., Olarinde, E. S., & Yebisi, T. E. (2022). *The Conundrums of Illicit Crude Oil Refineries in Nigeria and Its Debilitating Effects on Nigeria ' s Economy : A Legal Approach*. (4), 1–15.

Omo-Irabor, O. O., & Oduyemi, K. (2007). A hybrid image classification approach for the systematic analysis of land cover (LC) changes in the Niger Delta region. *Proceedings of the I5th International Symposium on Spatial Data Quality, Enschede, The Netherlands*, (LC), 7. Retrieved from www.isprs.org/proceedings/XXXVI/2-C43/Session2/paper_omoleomo.pdf

Omodanisi, E. O., & Salami, A. T. (2014). An Assessment of the Spectra Characteristics of Vegetation in South Western Nigeria. *IERI Procedia*, *9*, 26–32. https://doi.org/10.1016/j.ieri.2014.09.036

Onyena, A. P., & Sam, K. (2020). A review of the threat of oil exploitation to mangrove ecosystem: Insights from Niger Delta, Nigeria. *Global Ecology and Conservation*, *22*, e00961. https://doi.org/10.1016/j.gecco.2020.e00961

Onyia, N. N., Balzter, H., & Berrio, J. C. (2018). Detecting vegetation response to oil pollution using hyperspectral indices. *International Geoscience and Remote Sensing Symposium (IGARSS)*, *2018-July*, 3963–3966. https://doi.org/10.1109/IGARSS.2018.8519398

Onyia, Nkeiruka Nneti, Balzter, H., & Berrio, J. C. (2018). Normalized difference vegetation vigour index: A new remote sensing approach to biodiversity monitoring in oil polluted regions. In *Remote Sensing* (Vol. 10). https://doi.org/10.3390/rs10060897

Ooi, W. S., & Lim, C. P. (2006). Hybrid Image Segmentation based on Fuzzy Clustering Algorithm for Satellite Imagery Searching and Retrieval. In A. Abraham, B. de Baets, M. Köppen, & B. Nickolay (Eds.), *Applied Soft Computing Technologies: The Challenge of Complexity* (pp. 355–372). https://doi.org/10.1007/3-540-31662-0_28

Osuagwu, A. N., Okigbo, A. U., Ekpo, I. A., Chukwurah, P. N., Agbor, R. B., & Bessong Agbor, R. (2013). Effect of Crude Oil Pollution on Growth Parameters , Chlorophyll Content and Bulbils Yield in Air Potato (Dioscorea bulbifera L .). *International Journal of Applied Science and Technology*, *3*(4), 37–42. Retrieved from www.ijastnet.com

Osuji, L. C., & Adesiyanan, S. O. (2005). he Isiokpo oil-pipeline leakage: total organic carbon/organic matter contents of affected soils. *Chemistry & Biodiversity*, *2*(8), 1079–1085.

Oyonga, O. A., Itam, A. E., & Etete, E. N. (2019). *Petrophysical Evaluation of Total Organic Carbon Content (TOC) in Gbada Formation, Niger D Elta Basin*. (October).

Ozigis, M. S., Kaduk, J. D., & Jarvis, C. H. (2019). Mapping terrestrial oil spill impact using machine learning random forest and Landsat 8 OLI imagery: a case site within the Niger Delta region of Nigeria. *Environmental Science and Pollution Research*, *26*(4), 3621–3635. https://doi.org/10.1007/s11356-018-3824-y

Ozigis, M. S., Kaduk, J. D., Jarvis, C. H., da Conceição Bispo, P., & Balzter, H. (2019). Detection of oil pollution impacts on vegetation using multifrequency SAR, multispectral images with fuzzy forest and random forest methods. *Environmental Pollution*, *256*, 1–17. https://doi.org/10.1016/j.envpol.2019.113360

Paramasivam, C. R., & Venkatramanan, S. (2019). An introduction to various spatial analysis techniques. *GIS and Geostatistical Techniques for Groundwater Science*, (June), 23–30. https://doi.org/10.1016/B978-0-12-815413-7.00003-1

Park, Y., Al-Qublan, H., Lee, E., & Egilmez, G. (2016). Interactive Spatiotemporal Analysis of Oil Spills Using Comap in North Dakota. *Informatics*, *3*(2), 4. https://doi.org/10.3390/informatics3020004

Pathak, S. (2014). New Change Detection Techniques to monitor land cover dynamics in mine environment. *International Archives of the Photogrammetry, Remote Sensing and Spatial Information Sciences - ISPRS Archives*, *40*(8), 875–879. https://doi.org/10.5194/isprsarchives-XL-8-875-2014

Pavanelli, D. D., & Loch, C. (2018). Mangrove spectra changes induced by oil spills

monitored by image differencing of normalised indices: Tools to assist delimitation of impacted areas. *Remote Sensing Applications: Society and Environment*, *12*(October), 78–88. https://doi.org/10.1016/j.rsase.2018.10.001

Pegg, S., & Zabbey, N. (2013). Oil and water: The Bodo spills and the destruction of traditional livelihood structures in the Niger Delta. *Community Development Journal*, *48*(3), 391–405. https://doi.org/10.1093/cdj/bst021

Pei, W., Yao, S., Knight, J. F., Dong, S., Pelletier, K., Rampi, L. P., … Klassen, J. (2017). Mapping and detection of land use change in a coal mining area using object-based image analysis. *Environmental Earth Sciences*, *76*(3), 1–16. https://doi.org/10.1007/s12665-017-6444-9

Phiri, D., & Morgenroth, J. (2017). Developments in Landsat Land Cover Classification Methods: A Review. *Remote Sensing*, *9*(9), 967. https://doi.org/10.3390/rs9090967

Piro, P., Porti, M., Veltri, S., Lupo, E., & Moroni, M. (2017). Hyperspectral monitoring of green roof vegetation health state in sub-mediterranean climate: Preliminary results. *Sensors (Switzerland)*, *17*(4), 1–17. https://doi.org/10.3390/s17040662

Press, A. (2010, May 5). Shell reports record oil spillages in. *Theguardian.Com*, pp. 2009–2010. Retrieved from https://www.theguardian.com/environment/2010/may/05/shell-oil-spill-niger-delta

Prins, E. (2009). *Satellite Mapping of Land Cover and Use in relation to Oil Exploitation in Concession Block 5A in Southern Sudan 1987 – 2006*.

Prudente, V. H. R., Mercante, E., Johann, J. A., Souza, C. H. W. de, Cattani, C. E. V., Mendes, I. S., & Caon, I. L. (2021). Use of terrestrial remote sensing to estimate soybeans and beans biophysical parameters. *Geocarto International*, *36*(7), 773–790. https://doi.org/10.1080/10106049.2019.1624982

Punnuri, S. M., & Singh, B. P. (2013). Oil palm. *Biofuel Crops: Production, Physiology and Genetics*, 392–414.

Pyagbara, L. S. (2007). The Adverse Impacts of Oil Pollution on the Environment and Wellbeing of a Local Indigenous Community: The Experience of the Ogoni People of Nigeria. *United Nations Department of Economic and Social Affairs, Division*

for Social Policy and Development, International Expert Group Meeting on Indigenous Peoples and Protection of the Environment, Khabarovsk, Russian Federation, August 27-29, 2007.

Qian, S. E. (2021). Hyperspectral Satellites, Evolution, and Development History. *IEEE Journal of Selected Topics in Applied Earth Observations and Remote Sensing*, *14*, 7032–7056. https://doi.org/10.1109/JSTARS.2021.3090256

Qin, Y., Niu, Z., Chen, F., Li, B., & Ban, Y. (2013). Object-based land cover change detection for cross-sensor images. *International Journal of Remote Sensing*, *34*(19), 6723–6737. https://doi.org/10.1080/01431161.2013.805282

Rahbar, F. G., Kiarostami, K., & Shirdam, R. (2012). Effects of petroleum hydrocarbons on growth, photosynthetic pigments and carbohydrate levels of sunflower. *Journal of Food, Agriculture and Environment*, *10*(1), 773–776.

Rama, M. C., Mahendran, D. S., & Kumar, T. C. R. (2016). *A Survey on Land Cover Change Detection*. 13655–13661. https://doi.org/10.15680/IJIRSET.2016.0507143

Ramachandra, T. V., & Kumar, U. (2004). *GRDSS for Land use , land cover analysis*. (January 2004).

Rawat, J. S., Biswas, V., & Kumar, M. (2013). Changes in land use/cover using geospatial techniques: A case study of Ramnagar town area, district Nainital, Uttarakhand, India. *The Egyptian Journal of Remote Sensing and Space Science*, *16*(1), 111–117. https://doi.org/10.1016/j.ejrs.2013.04.002

Rawat, J. S., & Kumar, M. (2015). Monitoring land use/cover change using remote sensing and GIS techniques: A case study of Hawalbagh block, district Almora, Uttarakhand, India. *The Egyptian Journal of Remote Sensing and Space Science*. https://doi.org/10.1016/j.ejrs.2015.02.002

Reyes, A., Solla, M., & Lorenzo, H. (2017). Comparison of different object-based classifications in LandsatTM images for the analysis of heterogeneous landscapes. *Measurement: Journal of the International Measurement Confederation*, *97*, 29–37. https://doi.org/10.1016/j.measurement.2016.11.012

Richards, J. A. (2013). Supervised Classification Techniques. In *Remote Sensing Digital*

Image Analysis: An Introduction (pp. 247–318). https://doi.org/10.1007/978-3-642-30062-2_8

Richards, J. A., & Jia, X. (2006). Remote Sensing Digital Image Analysis. In *Remote Sensing Digital Image Analysis*. https://doi.org/10.1007/3-540-29711-1

Ridd, M. K., & Liu, J. (1998). A comparison of four algorithms for change detection in an urban environment. *Remote Sensing of Environment*, *63*(2), 95–100. https://doi.org/10.1016/S0034-4257(97)00112-0

Rim-rukeh, A. (2015). Oil Spill Management in Nigeria: SWOT Analysis of the Joint Investigation Visit (JIV) Process. *Journal of Environmental Protection*, *6*(March), 259–271. https://doi.org/10.4236/jep.2015.63026

Rimal, B., Zhang, L., Keshtkar, H., Wang, N., & Lin, Y. (2017). Monitoring and Modeling of Spatiotemporal Urban Expansion and Land-Use/Land-Cover Change Using Integrated Markov Chain Cellular Automata Model. *ISPRS International Journal of Geo-Information*, *6*(9), 288. https://doi.org/10.3390/ijgi6090288

Roberts, D. A., Barbara, S., Roth, K., & Perroy, R. L. (2011). Spectral and Spatial Methods of Hyperspectral Image Analysis for Estimation of Biophysical and Biochemical Properties of Agricultural Crops. In *Hyperspectral Remote Sensing of Vegetation*. https://doi.org/10.1201/b11222-20

Robertson, D. L., & King, D. J. (2011). Comparison of pixel- and object-based classification in land cover change mapping. *International Journal of Remote Sensing*, *32*(6), 1505–1529. https://doi.org/10.1080/01431160903571791

Robinove, C. J. (1981). The logic of multispectral classification and mapping of land. *Remote Sensing of Environment*, *11*(C), 231–244. https://doi.org/10.1016/0034-4257(81)90022-5

Ross, S., & Bhadauria, H. S. (2015). A Review of Change Detection Techniques of LandCover Using Remote Sensing Data. *IOSR Journal of Computer Engineering Ver. IV*, *17*(3), 2278–2661. https://doi.org/10.9790/0661-17341721

Rowland, A. (2010). *GIS-Based Prediction of Pipeline Third-Party Interference Using Hybrid Multivariate Statistical Analysis, PhD Thesis*. Newcastle University, Newcastle upon Tyne, UK.

Rujoiu-Mare, M.-R., & Mihai, B.-A. (2016). Mapping Land Cover Using Remote Sensing Data and GIS Techniques: A Case Study of Prahova Subcarpathians. *Procedia Environmental Sciences*, *32*, 244–255. https://doi.org/10.1016/j.proenv.2016.03.029

Saha, A. K., Arora, M. K., Csaplovics, E., & Gupta, R. P. (2005). Land Cover Classification Using IRS LISS III Image and DEM in a Rugged Terrain: A Case Study in Himalayas. *Geocarto International*, *20*(2), 33–40. https://doi.org/10.1080/10106040508542343

Sam, K. (2016). *Environmental Management of Oil Contaminated Sites in Nigeria: Improving Policy and Risk-based Framework*. (October), 1–202.

Sam, Kabari, Coulon, F., & Prpich, G. (2017). A multi-attribute methodology for the prioritisation of oil contaminated sites in the Niger Delta. *Science of the Total Environment*, Vol. 579, pp. 1323–1332. https://doi.org/10.1016/j.scitotenv.2016.11.126

Schober, P., & Schwarte, L. A. (2018). Correlation coefficients: Appropriate use and interpretation. *Anesthesia and Analgesia*, *126*(5), 1763–1768. https://doi.org/10.1213/ANE.0000000000002864

Seetha, M., Muralikrishna, Deekshatulu, B. L., Malleswari, B. L., Nagaratna, & Hegde, P. (2008). Artificial Neural Networks and Other Methods of Image Classification. *Theoretical and Applied Information Technology*, 1039–1053.

Seiter, K., Hensen, C., Schröter, J., & Zabel, M. (2004). Organic carbon content in surface sediments - Defining regional provinces. *Deep-Sea Research Part I: Oceanographic Research Papers*, *51*(12), 2001–2026. https://doi.org/10.1016/j.dsr.2004.06.014

Serrano-Calvo, R., Cutler, M. E. J., & Bengough, A. G. (2021). Spectral and growth characteristics of willows and maize in soil contaminated with a layer of crude or refined oil. *Remote Sensing*, *13*(17), 1–25. https://doi.org/10.3390/rs13173376

Setianto, A., & Triandini, T. (2015). Comparison of Kriging and Inverse Distance Weighted (Idw) Interpolation Methods in Lineament Extraction and Analysis. *Journal of Applied Geology*, *5*(1), 21–29. https://doi.org/10.22146/jag.7204

Shadow Governance Intel. (2017). Nigeria's Oil Theft Epidemic. Retrieved June 11, 2019, from oilprice.com website: https://oilprice.com/Energy/Crude-Oil/Nigerias-Oil-Theft-Epidemic.html

Sharma, R., Goyal, A. K., & Dwivedi, R. K. (2016). A review of soft classification approaches on satellite image and accuracy assessment. *Advances in Intelligent Systems and Computing*, *437*, 629–639. https://doi.org/10.1007/978-981-10-0451-3_56

Shelestov, A., Kolotii, A., Skakun, S., Baruth, B., Lozano, R. L., & Yailymov, B. (2017). Biophysical parameters mapping within the SPOT-5 take 5 initiative. *European Journal of Remote Sensing*, *50*(1), 300–309. https://doi.org/10.1080/22797254.2017.1324743

Shier, R. (2004). Statistics: 1.1 Paired t- test. *Pediatrics*, *107*(4), 638–641. https://doi.org/10.1542/peds.107.4.638

Shittu, W. J. (2014). *Mapping oil spill human health risk in rivers state , Niger Delta , Nigeria . PhD thesis , University of Nottingham* . Nottingham.

Shukla, A., & Kot, R. (2016). An Overview of Hyperspectral Remote Sensing and its applications in various Disciplines. *IRA-International Journal of Applied Sciences (ISSN 2455-4499)*, *5*(2), 85. https://doi.org/10.21013/jas.v5.n2.p4

Sims, D. A., & Gamon, J. A. (2002). Relationships between leaf pigment content and spectral reflectance across a wide range of species, leaf structures and developmental stages. *Remote Sensing of Environment*, *81*(2–3), 337–354. https://doi.org/10.1016/S0034-4257(02)00010-X

Singh, B. P., Singh, H. P., & Obeng, E. (2015). *Elephantgrass*. (September 2013).

Statisticssolutions.com. (n.d.). Pearson's Correlation Coefficient. Retrieved September 11, 2021, from https://www.statisticssolutions.com/free-resources/directory-of-statistical-analyses/pearsons-correlation-coefficient/

Steyn, P. (2009). Oil exploration in colonial Nigeria, c. 1903-58. *Journal of Imperial and Commonwealth History*, *37*(2), 249–274. https://doi.org/10.1080/03086530903010376

Stopka, T. J., Krawczyk, C., Gradziel, P., & Geraghty, E. M. (2014). Use of spatial

epidemiology and hot spot analysis to target women eligible for prenatal women, infants, and children services. *American Journal of Public Health*, *104*(SUPPL. 1), 183–189. https://doi.org/10.2105/AJPH.2013.301769

Susantoro, T. M., Wikantika, K., Saepuloh, A., & Harsolumakso, A. H. (2018). Utilization of vegetation indices to interpret the possibility of oil and gas microseepages at ground surface. *IOP Conference Series: Earth and Environmental Science*, *145*(1). https://doi.org/10.1088/1755-1315/145/1/012127

Taiwo, O. B., Olajide, O. A., Soyannwo, O. O., & Makinde, J. M. (2000). Anti-inflammatory, antipyretic and antispasmodic: Properties of Chromolaena odorata. *Pharmaceutical Biology*, *38*(5), 367–370. https://doi.org/10.1076/phbi.38.5.367.5970

Takon, N. (2014). *Environmental damage arising from oil operations in Niger Delta of Nigeria : How not to continually live with their specific impact on population and ecology*. *3*(9), 1878–1893.

Talukdar, S., Singha, P., Mahato, S., Shahfahad, Pal, S., Liou, Y. A., & Rahman, A. (2020). Land-use land-cover classification by machine learning classifiers for satellite observations-A review. *Remote Sensing*, *12*(7). https://doi.org/10.3390/rs12071135

Tamta, K., & Bhadauria, H. S. (2015). Object-Oriented Approach of Landsat Imagery for Flood Mapping. *International Journal of Computer Application*, *122*(16), 6–9.

Tehrany, M. S., Kumar, L., & Drielsma, M. J. (2017). Review of native vegetation condition assessment concepts, methods and future trends. *Journal for Nature Conservation*. https://doi.org/10.1016/j.jnc.2017.08.004

Terzioğlu, S., Başkent, E. Z., & Kadioğullari, A. I. (2009). Monitoring forest structure at landscape level: A case study of Scots pine forest in NE Turkey. *Environmental Monitoring and Assessment*, *152*(1–4), 71–81. https://doi.org/10.1007/s10661-008-0297-3

Thakkar, A. K., Desai, V. R., Patel, A., & Potdar, M. B. (2017). Impact assessment of watershed management programmes on land use/land cover dynamics using remote sensing and GIS. *Remote Sensing Applications: Society and Environment*,

5(October 2016), 1–15. https://doi.org/10.1016/j.rsase.2016.12.001

Thorp, K. R., Wang, G., Bronson, K. F., Badaruddin, M., & Mon, J. (2017). Hyperspectral data mining to identify relevant canopy spectral features for estimating durum wheat growth, nitrogen status, and grain yield. *Computers and Electronics in Agriculture*, *136*, 1–12. https://doi.org/10.1016/j.compag.2017.02.024

Tilahun, A. (2015). Accuracy Assessment of Land Use Land Cover Classification using Google Earth. *American Journal of Environmental Protection*, *4*(4), 193. https://doi.org/10.11648/j.ajep.20150404.14

Tiwari, R. S., Arora, M. K., & Kailash, T. (1999). Soft classification for sub-pixel land cover extraction. *Journal of the Indian Society of Remote Sensing*, *27*(4), 225–234. https://doi.org/10.1007/BF02990835

Tote, C., Delalieux, S., Goossens, M., Williamson, B. J., & Swinnen, E. (2014). Monitoring environmental health using SPOT-VEGETATION-derived and field-measured spectral indices in Karabash, Russia. *International Journal of Remote Sensing*, *35*(August), 2516–2533. https://doi.org/10.1080/01431161.2014.883103

Townshend, J. R., Masek, J. G., Huang, C., Vermote, E. F., Gao, F., Channan, S., … Wolfe, R. E. (2012). Global characterization and monitoring of forest cover using Landsat data: Opportunities and challenges. *International Journal of Digital Earth*, *5*(5), 373–397. https://doi.org/10.1080/17538947.2012.713190

Transon, J., d'Andrimont, R., Maugnard, A., & Defourny, P. (2018). Survey of hyperspectral Earth Observation applications from space in the Sentinel-2 context. *Remote Sensing*, *10*(2), 1–32. https://doi.org/10.3390/rs10020157

Transparency International Defence and Security. (2019). *Military involvement in oil theft in the Niger Delta*. Retrieved from http://ti-defence.org/wp-content/uploads/2019/05/Military-Involvement-Oil-Theft-Niger-Delta_WEB.pdf

TRCC, T. R. and C. C. (n.d.). *Niger Delta Mangrove Citizen Science Project*. Retrieved from www.tropicalconservationcentre.org

Turner, B. L., Skole, D., Sanderson, S., Fischer, G., Fresco, L., & Leemans, R. (1995). Land-Use and Land-Cover Change: science/research plan. *IGBP:* Retrieved from

https://asu.pure.elsevier.com/en/publications/land-use-and-land-cover-change-scienceresearch-plan-2

Turner, W., Spector, S., Gardiner, N., Fladeland, M., Sterling, E., & Steininger, M. (2003). Remote sensing for biodiversity science and conservation. *Trends in Ecology and Evolution*, *18*(6), 306–314. https://doi.org/10.1016/S0169-5347(03)00070-3

Tuttle, M. L. W., Charpentier, R., & Brownfield, M. E. (1999). The Niger Delta Petroleum System: Niger Delta Province, Nigeria, Cameroon, and Equatorial Guinea, Africa. *World Energy Project*, (99-50-H), 64.

Twumasi, Y. A., & Merem, E. C. (2006). GIS and remote sensing applications in the assessment of change within a coastal environment in the niger delta region of Nigeria. *International Journal of Environmental Research and Public Health*, *3*(1), 98–106. https://doi.org/10.3390/ijerph2006030011

Ugochukwu, C. N. C., & Ertel, J. (2008). Negative impacts of oil exploration on biodiversity management in the Niger De area of Nigeria. *Impact Assessment and Project Appraisal*, *26*(2), 139–147. https://doi.org/10.3152/146155108X316397

Umar, A. T., & Hajj Othman, M. S. (2017). Causes and consequences of crude oil pipeline vandalism in the Niger delta region of Nigeria: A confirmatory factor analysis approach. *Cogent Economics & Finance*, *5*(1). https://doi.org/10.1080/23322039.2017.1353199

Umar, H. A., Abdul Khanan, M. F., Ahmad, A., Sani, M. J., Abd Rahman, M. Z., & Abdul Rahman, A. (2019). Spatial database development for oil spills pollution affecting water quality system in Niger Delta. *International Archives of the Photogrammetry, Remote Sensing and Spatial Information Sciences - ISPRS Archives*, *42*(4/W16), 645–657. https://doi.org/10.5194/isprs-archives-XLII-4-W16-645-2019

Umar, H. A., Abdul Khanan, M. F., Ogbonnaya, C., Shiru, M. S., Ahmad, A., & Baba, A. I. (2021). Environmental and socioeconomic impacts of pipeline transport interdiction in Niger Delta, Nigeria. *Heliyon*, *7*(5), e06999. https://doi.org/10.1016/j.heliyon.2021.e06999

UNDP. (2006). *NIGER DELTA HUMAN DEVELOPMENT REPORT*.

Unep. (2011). *Environmental Assessment of Ogoniland*.

Unger, D., Hung, I.-K., Farrish, K., & Dans, D. (2015). Quantifying Land Cover Change Due to Petroleum Exploration and Production in the Haynesville Shale Region Using Remote Sensing. *International Journal of Applied Geospatial Research*, *6*(2), 1–17. https://doi.org/10.4018/ijagr.2015040101

Urban, D. L., & Wallin, D. O. (2002). Introduction to Markov models. *Learning Landscape Ecology: A Practical Guide to Concepts and Techniques*, 35–48. https://doi.org/10.1007/b97339

Uyi, O. O., Ekhator, F., Ikuenobe, C. E., Borokini, T. I., Aigbokhan, E. I., Egbon, I. N., … Omokhua, G. A. (2014). Chromolaena odorata invasion in Nigeria: A case for coordinated biological control. *Management of Biological Invasions*, *5*(4), 377–393. https://doi.org/10.3391/mbi.2014.5.4.09

Vane, C. H., Harrison, I., & Kim, A. W. (2007). Polycyclic aromatic hydrocarbons (PAHs) and polychlorinated biphenyls (PCBs) in sediments from the Mersey Estuary, U.K. *Science of the Total Environment*, *374*(1), 112–126. https://doi.org/10.1016/j.scitotenv.2006.12.036

Vane, Christopher H., Kim, A. W., Moss-Hayes, V., Turner, G., Mills, K., Chenery, S. R., … Brain, M. (2020). Organic pollutants, heavy metals and toxicity in oil spill impacted salt marsh sediment cores, Staten Island, New York City, USA. *Marine Pollution Bulletin*, *151*(January), 110721. https://doi.org/10.1016/j.marpolbul.2019.110721

Vane, Christopher H., Turner, G. H., Chenery, S. R., Richardson, M., Cave, M. C., Terrington, R., … Moss-Hayes, V. (2020). Trends in heavy metals, polychlorinated biphenyls and toxicity from sediment cores of the inner River Thames estuary, London, UK. *Environmental Science: Processes and Impacts*, *22*(2), 364–380. https://doi.org/10.1039/c9em00430k

Varga, K., Szabó, S., Szabó, G., Dévai, G., Tóthmérész, B., Lloyd, R., … Echeverría, C. (2010). Improved land cover mapping using aerial photographs and satellite images. *Annals of the Association of American Geographers*, *00*(1), 241–266.

https://doi.org/10.1080/10106040802677037

Villa, P., Bresciani, M., Braga, F., & Bolpagni, R. (2014). Comparative assessment of broadband vegetation indices over aquatic vegetation. *IEEE Journal of Selected Topics in Applied Earth Observations and Remote Sensing*, *7*(7), 3117–3127. https://doi.org/10.1109/JSTARS.2014.2315718

Walker, P. (2009). *Guidlines fo Post Processing ASD FieldSpec Pro and FieldSpec 3 Spectral Data Files using the FSF MS Excel Template*. 18.

Wang, J., Price, K. P., & Rich, P. M. (2001). Spatial patterns of NDVI in response to precipitation and temperature in the central Great Plains. *International Journal of Remote Sensing*, *22*(18), 3827–3844. https://doi.org/10.1080/01431160010007033

Wang, L., Sousa, W. P., & Gong, P. (2004). Integration of object-based and pixel-based classification for mapping mangroves with IKONOS imagery. *International Journal of Remote Sensing*, *25*(24), 5655–5668. https://doi.org/10.1080/014311602331291215

Wang, Le, & Sousa, W. P. (2009). Distinguishing mangrove species with laboratory measurements of hyperspectral leaf reflectance. *International Journal of Remote Sensing*, *30*(5), 1267–1281. https://doi.org/10.1080/01431160802474014

Wang, W., Li, W., Zhang, C., & Zhang, W. (2018). Improving object-based land use/cover classification from medium resolution imagery by Markov chain geostatistical post-classification. *Land*, *7*(1), 5–8. https://doi.org/10.3390/LAND7010031

Wang, X., Feng, J., & Wang, J. (2009). Petroleum hydrocarbon contamination and impact on soil characteristics from oilfield Momoge Wetland. *Huan jing ke xue= Huanjing kexue*, *30*(8), 2394–2401.

Wang, Z., Li, K., & Xi, M. (2016). Spatial Analysis of Leakage Accidents of Oil Pipeline River Crossing Sections. *The Open Civil Engineering Journal*, *10*(1), 836–846. https://doi.org/10.2174/1874149501610010836

Whanda, S., Adekola, O., Adamu, B., Yahaya, S., & Pandey, P. C. (2016). *Geo-Spatial Analysis of Oil Spill Distribution and Susceptibility in the Niger Delta Region of Nigeria*. (August), 438–456.

Xue, J., & Su, B. (2017). *Significant Remote Sensing Vegetation Indices : A Review of Developments and Applications*. *2017*. https://doi.org/10.1155/2017/1353691

Yan, W. Y., Shaker, A., & El-Ashmawy, N. (2015). Urban land cover classification using airborne LiDAR data: A review. *Remote Sensing of Environment*, *158*, 295–310. https://doi.org/10.1016/j.rse.2014.11.001

Yang, J., Shi, S., Gong, W., Du, L., Sun, J., & Song, S. (2017). The characterization of plant species using first-derivative fluorescence spectra. *Luminescence*, *32*(3), 348–352. https://doi.org/10.1002/bio.3185

Yanow, K. (2018). Remote Sensing Platforms. *Geographic Information Science & Technology Body of Knowledge*, *2018*(Q4). https://doi.org/10.22224/gistbok/2018.4.1

Yoon, G., Cho, S. I., Jeong, S., & Park, J. (2003). Object oriented classification using Landsat images. *In Proceedings of the 24th Asian Conference on Remote Sensing, Busan, South Korea, 3–7 November*, 1–3.

Yu, Q., Epstein, H. E., Engstrom, R., Shiklomanov, N., & Strelestskiy, D. (2015). Land cover and land use changes in the oil and gas regions of Northwestern Siberia under changing climatic conditions. *Environmental Research Letters*, *10*(12), 124020. https://doi.org/10.1088/1748-9326/10/12/124020

Yu, W., Zhou, W., Qian, Y., & Yan, J. (2016). A new approach for land cover classification and change analysis: Integrating backdating and an object-based method. *Remote Sensing of Environment*, *177*, 37–47. https://doi.org/10.1016/j.rse.2016.02.030

Yusuf, K. (2022, September 8). Nigeria lost an estimated $10 billion to large-scale crude theft in seven months. Retrieved September 16, 2022, from www.premiumtimesng.com website: https://www.premiumtimesng.com/news/headlines/552781-analysis-how-broke-nigeria-lost-10-billion-to-crude-oil-theft-in-seven-months.html#.YyTSafoU5Xc.link

Zabbey, N., & Malaquias, M. A. E. (2013). Epifauna diversity and ecology on intertidal flats in the tropical Niger Delta, with remarks on the gastropod species Haminoea

orbignyana. *Marine Biological Association of the United Kingdom. Journal of the Marine Biological Association of the United Kingdom*, *93*(1), 249–257. https://doi.org/http://dx.doi.org/10.1017/S0025315411001615

Zabbey, N., Sam, K., & Onyebuchi, A. T. (2017). Remediation of contaminated lands in the Niger Delta, Nigeria: Prospects and challenges. *Science of the Total Environment*, *586*, 952–965. https://doi.org/10.1016/j.scitotenv.2017.02.075

Zanter, K. (2019). Landsat Collection 1 Level 1 Landsat. In *United States Geological Survey* (Vol. 2).

Zhang, H. K., & Roy, D. P. (2017). Using the 500 m MODIS land cover product to derive a consistent continental scale 30 m Landsat land cover classification. *Remote Sensing of Environment*, *197*, 15–34. https://doi.org/10.1016/j.rse.2017.05.024

Zhong, Y., Wang, X., Wang, S., & Zhang, L. (2021). Advances in spaceborne hyperspectral remote sensing in China. *Geo-Spatial Information Science*, *24*(1), 95–120. https://doi.org/10.1080/10095020.2020.1860653

Zhu, L., Zhao, X., Lai, L., Wang, J., Jiang, L., Ding, J., … Rimmington, G. M. (2013). Soil TPH Concentration Estimation Using Vegetation Indices in an Oil Polluted Area of Eastern China. *PLoS ONE*, *8*(1). https://doi.org/10.1371/journal.pone.0054028

Zitta, N., Musa, A. A., & Muhammed, I. (2022). Sensitivity Analysis of Suspected External Driving Factors Contributing to Land Use Land Cover Dynamics in Jos Plateau. *Nigerian Journal of Environmental Sciences and Technology (NIJEST)*, *6*(1), 58–70.

Appendices

Appendix A Hydrocarbons and soil parameter data

		Microtox	Total Organic Carbon	Petroleum Hydrocarbons (Nonv		
Plot No	Plants Types	EC50 mg L^{-1}	TOC (%)	Resin	Aromatic	Aliphatic
P1	AG,EG, OP	27899	1.58	450	91	550
P2	AG,EG	19561	1.66	2020	332	1915
P3	AG,EG, OP	27309	1.86	1515	168	1340
P4	AG,EG, OP	18922	1.24	<443	<58	<119
P5	AG,EG, OP	23128	2.15	<443	<58	136
P6	AG,EG, OP	36496	1.38	<443	<58	122
P7	AG,EG, MT, OP	40423	0.8	<443	68	144
P8	AG,EG, MT, OP	33671	0.5	<443	<58	134
P9	AG,EG, OP	13278	1.29	987	608	1997
P10	AG,EG, MT, OP	7986	1.27	<443	219	551
P11	AG,EG, MT, OP	20364	1.37	<443	<58	<119
P12	AG,EG, MT, OP	37792	0.96	<443	<58	<119
P13	AG,EG, MT, OP	10975	2.21	930	219	955
P14	MG	4848	13.98	2373	69	327
P15	MG	2525	26.17	1115	<58	<119
P16	MG	3990	13.63	4021	463	1424
P17	MG	2992	17.06	932	145	254
P18	MG	2672	15.74	1137	120	273
P19	MG	19168	1.97	1030	176	820
P20	MG	14248	13.85	25483	12549	30446
P21	MG	29720	0.61	<443	75	254
P22	MG	6455	12.83	2437	196	629

Appendix B The HVIs that correlated better with each soil hydrocarbon parameter and the strongest R values for each plant type/species.

SHP	Awolowo		Elephant		Mango		
	HVIs	R-value	HVIs	R-value	HVIs	R-value	HVIs
TPH	NDVVI844,447	**0.179**	mND 750	**-0.311**	MDATT index	**-0.582**	PRI
EC50	MDATT index	-0.301	NDVVI844,447	**-0.344**	MDATT index	-0.657	NDVVI844
TOC	NDVVI844,447	**0.621**	MDATT index	-0.286	mND 750	**-0.725**	MDATT in

Please Note. The MDATT index sign means the opposite, i.e., A negative sign indicates a positive correlation.

SHP=Soil hydrocarbon parameter

Appendix C Land cover maps

C.1 Land cover persistence map

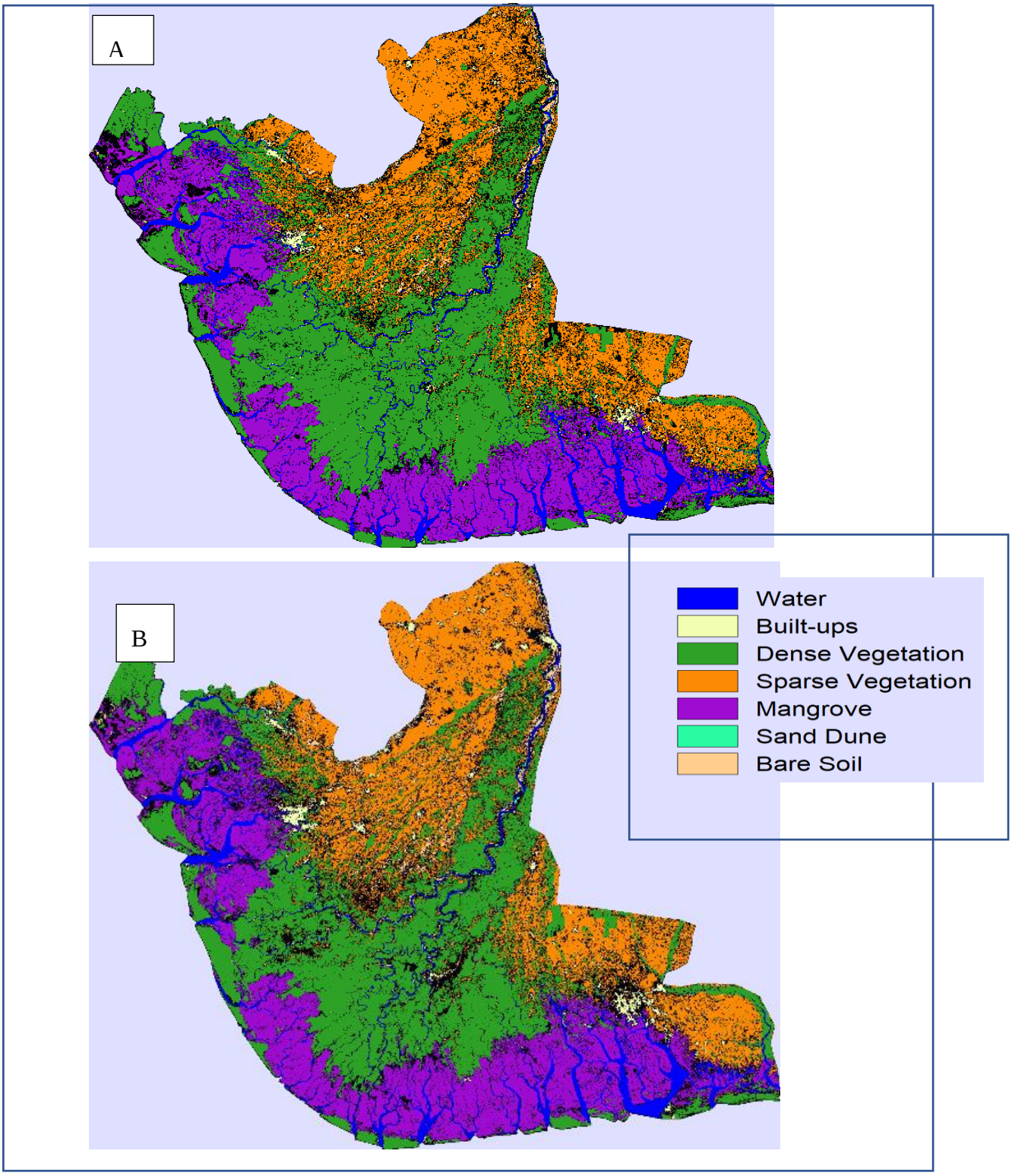

Land cover persistence map (a)1987-2002 and (b) 2002-2016

C.2 Land gains and losses

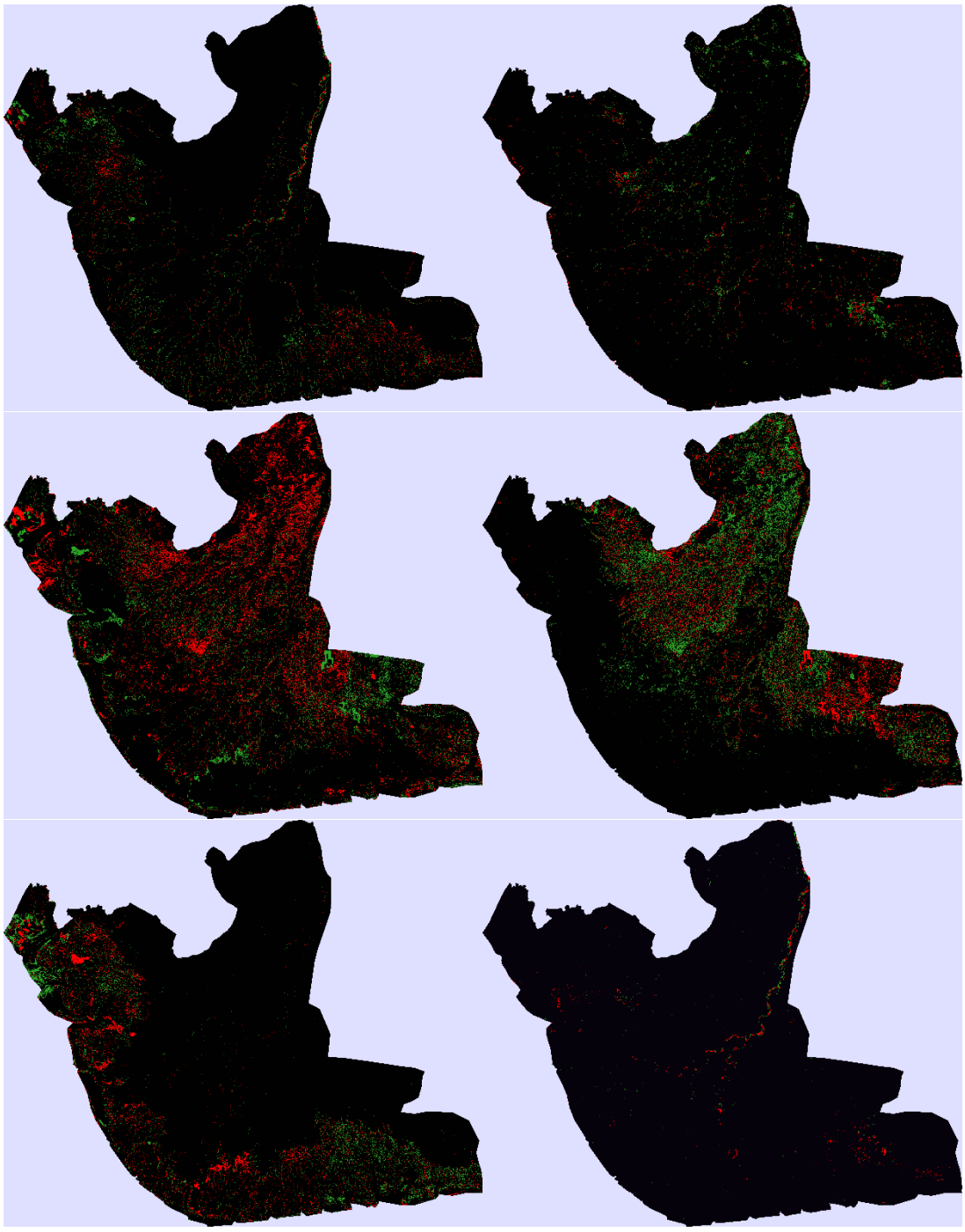

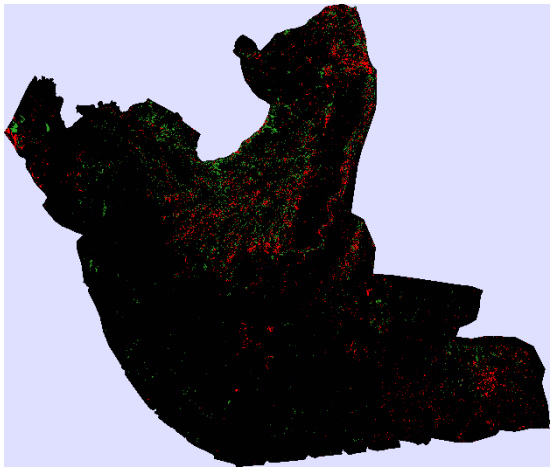

Gains and losses from 1987-2002: (a) water, (b) built ups, (c) dense, (d) sparse, (e) mangrove, (f) sand dune and (g) bare soil.

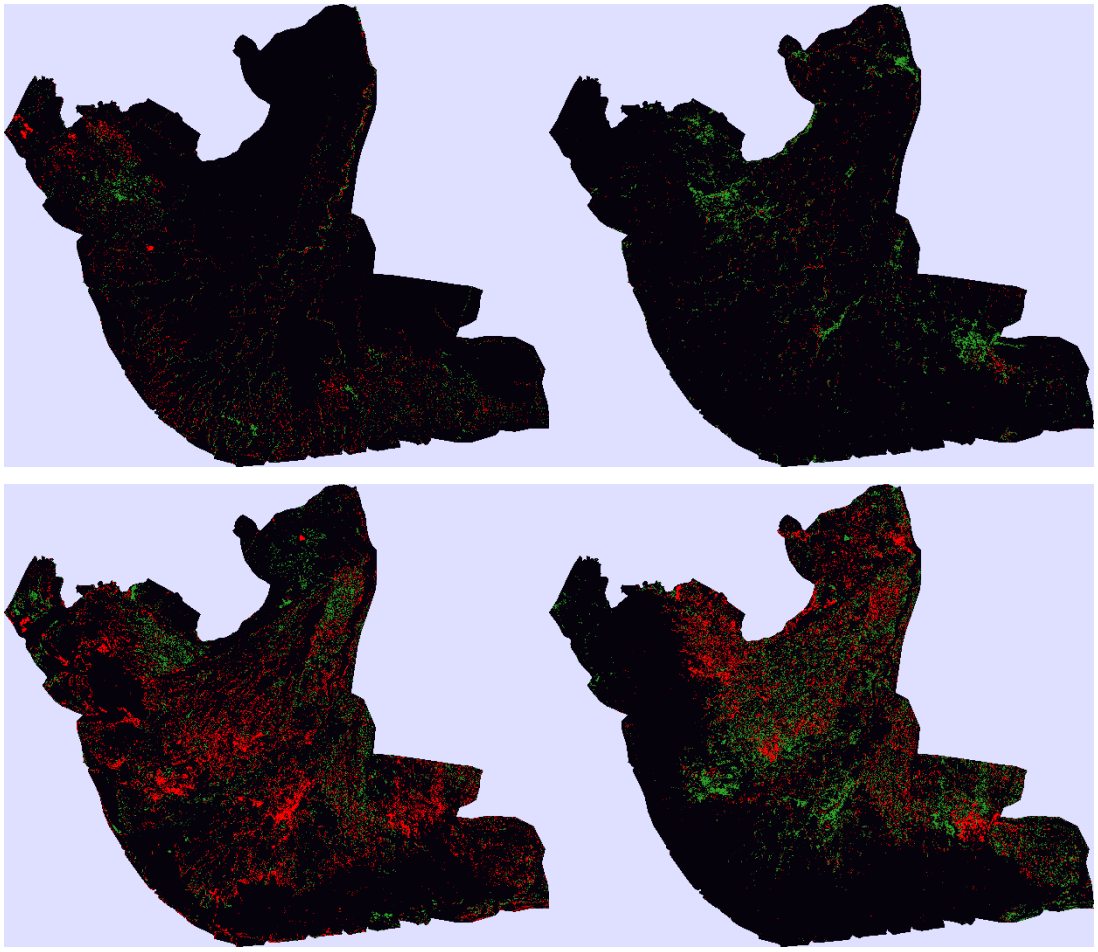

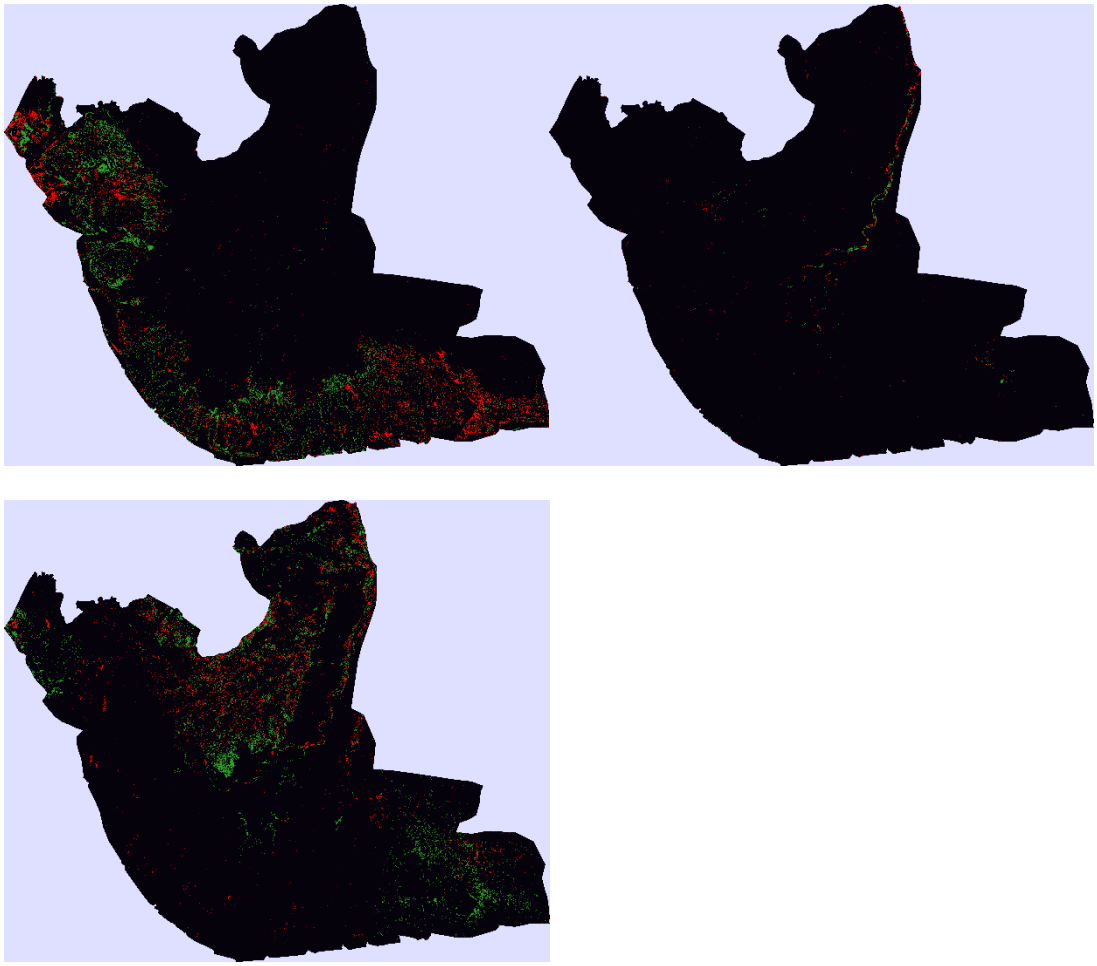

Gains and losses from 2002-2016: (a) water, (b) built ups, (c) dense, (d) sparse, (e) mangrove, (f) sand dune and (g) bare soil